CALTRANS: Impact of the Use of Portland-Limestone Cement on Concrete Performance as Plain or Reinforced Material

Final Report

Keshav Bharadwaj, Oregon State University, Corvallis, OR
Krishna Siva Teja Chopperla, Oregon State University, Corvallis, OR
Antara Choudhary, Oregon State University, Corvallis, OR
Deborah Glosser, Oregon State University, Corvallis, OR
Rita Maria Ghantous, Oregon State University, Corvallis, OR
Gokul Dev Vasudevan, Oregon State University, Corvallis, OR

Dr. Jason H. Ideker, Oregon State University, Corvallis, OR
Dr. O. Burkan Isgor, Oregon State University, Corvallis, OR
Dr. David Trejo, Oregon State University, Corvallis, OR
Dr. W. Jason Weiss, PI, Oregon State University, Corvallis, OR

April 30th, 2021, Revised June 29th, 2021

Table of Contents

List of Tables

List of Figures

While the assembling of this report was a group effort, the significant contributing authors of each section is noted below.

1. Executive summary – Prof. Jason Weiss
2. Background – Prof. Jason Weiss, Prof. Burkan Isgor, Prof. Jason Ideker, Prof. David Trejo
3. Constituent materials and mixtures considered in the experimental plan - Prof. Jason Weiss, Prof. Burkan Isgor, Prof. Jason Ideker, Prof. David Trejo
4. Constituent material characterization – Antara Choudhary, Prof. Jason Weiss, Prof. Burkan Isgor
5. Alkali-silica reactivity – Siva Teja Chopperla, Prof. Jason Ideker
6. Shrinkage and restrained shrinkage cracking – Antara Choudhary, Prof. Jason Weiss, Prof. Burkan Isgor
7. Mechanical properties – Antara Choudhary, Prof. Jason Weiss, Prof. Burkan Isgor
8. Transport properties – Antara Choudhary, Dr. Rita Ghantous, Prof. Jason Weiss, Prof. Burkan Isgor
9. Chloride binding – Nathalene Then, Dr. Rita Ghantous, Prof. Jason Weiss, Prof. Burkan Isgor
10. Resistance to Chloride Ingress in Concrete – Dr. Rita Ghantous, Nathalene Then, Gokul Vasudevan, Prof. Jason Weiss, Prof. Burkan Isgor
11. Corrosion of reinforcing steel – Gokul Dev Vasudevan, Prof. David Trejo
12. Air entrainment – Siva Teja Chopperla, Prof. Jason Ideker
13. External sulfate attack – Siva Teja Chopperla, Prof. Jason Ideker
14. Construction schedule – Gokul Vasudevan, Antara Choudary, Prof. David Trejo
15. Environmental impact – Dr. Sabbie Miller, Siva Teja Chopperla, Prof. Jason Ideker
16. Thermodynamic simulations – Keshav Bharadwaj, Prof. Jason Weiss, Prof. Burkan Isgor
17. Conclusions – Prof. Jason Weiss, Professor Burkan Isgor

The list of study advisory members is also noted below:

- Dr. Paul Tennis (PCA)
- Jacquelyn Wong S (CALTRANS)
- Zihui Li
- Joe R Harline
- Kirk McDonald
- S Lim
- Tom Tietz
- Joe Holland
- Patrick Lo
- Craig Knapp

1 Executive Summary

CALTRANS does not currently allow Portland-Limestone Cements (PLC) to replace Ordinary Portland Cement (OPC) in concrete. PLC has been proposed for consideration in CALTRANS specifications due to potential benefits in reducing greenhouse gas (GHG) emissions. This report outlines a comprehensive plan to provide both experimental and computational analysis results to address whether PLC may replace OPC without loss of mechanical and durability performance of concrete materials and mixtures specific to California. The objective of this study was to provide data for CALTRANS to make informed decisions on whether specification changes to permit use of PLC would be appropriate. Additionally, the research team was asked to assess the impact of added limestone (LS) powder as an alternative to using ASTM C 595/AASHTO M 240 cement.

In general, the following observations were made (as compared to OPC):

- PLC and OPC+LS systems were found to have a greater degree of clinker reaction,
- PLC and OPC+LS systems had similar or improved ASR performance,
- PLC and OPC+LS systems had statistically similar shrinkage (the only exception was the slag cement system, which had 7% to 8% more shrinkage due to greater chemical reaction),
- PLC and OPC+LS systems had average flexural strength consistently within +/- 15% of the parent system. The difference in average flexural strength was between -5% and 13%,
- PLC and OPC+LS had statistically similar set times,
- PLC and OPC+LS systems had statistically similar bound chloride contents for most mixtures. Additional benefits were observed when slag cement was used with PLC.
- PLC and OPC+LS systems had comparable porosity, formation factor, and chloride apparent diffusion coefficient to OPC concrete.
- PLC-based concretes have similar critical chloride thresholds and time to corrosion initiation.
- PLC-based mortars had similar or slightly improved performance when exposed to sulfate,
- PLCs (or OPC +LS) offer the potential for a 10%-12% reduction of GHG emissions.
- PLC and OPC + LS systems allow ettringite to be stabilized, and hemicarbonate/ monocarbonate forms instead of monosulfate, which reduces porosity.

The results indicate that PLCs can be used as a direct 1:1 substitution for OPC in concrete mixtures. It should also be noted that PLC can replace OPC in systems containing supplementary cementitious materials (SCM). Further, when PLCs are used with SCM, there can be a synergistic behavior between the limestone and alumina that improves overall performance. As such, we recommend that specifications that permit the use of OPC (ASTM C 150, AASHTO M 85) could

also permit the use of PLC (ASTM C 595, AASHTO M 240). Specifications could also be developed to permit the use of up to 10% limestone with OPC; however, some details will be needed on the chemical and physical properties of the limestone to ensure its size (packing and reaction) and chemical purity.

2 Background

Portland-limestone cements (PLC) are not currently specified for use by CALTRANS. A plan was developed to determine whether the performance of concrete made with PLC using clinker used for producing Type II/V cement would be adversely impacted as compared to a similar OPC-based concrete in California [1]. These materials were evaluated both experimentally and computationally. The ultimate goal of this work is to provide CALTRANS with data to make informed decisions on the potential specification of PLC and indicate whether any limitations on PLC should be considered.

ASTM C150 (AASHTO M 85) currently allows up to 5% limestone in hydraulic cement. ASTM C595 (AASHTO M 240) allows up to 15% limestone in blended cements. There have been several recent reviews on the use of PLC as a replacement for OPC [2]. This report will not repeat the review of the literature performed in those studies. However, while several studies have been conducted on the use of Type I OPC and PLC [3-6], there are limited studies on the use of PLC made with the clinkers that are typical of those used in California for the production of Type II/V cements.

An anonymous survey was submitted to ask state highway materials engineers whether they permit the use of PLC. Currently, approximately 83% of the State Highway Agencies (SHAs) that responded reported allowing PLC in a wide range of applications (one state did note that it did not allow this in cement bases, and another did not allow this where Type II cement is used). Of the 30 state representatives that responded, only 10% do not permit the use of PLC. Sixty-three percent of the SHA have approximated that PLC is used less than 10% of the time; however, 7% of the states suggesting it is used more than 65% of the time. Over 80% of the response reported an interest (moderate to great) in learning more about the results of the CALTRANS study when it is completed.

Furthermore, there are limited studies using the Type II/V clinkers used to make PLC with SCM. This research addresses the need to provide CALTRANS with data to make informed decisions on the potential specification of PLC or OPC + LS as an alternative to OPC.

3 Constituent Materials and Mixtures Considered in the Experimental Plan

Mixture proportions investigated in this project have been developed based on the CALTRANS specifications and after consultations with the study advisory committee (SAC), consisting of CALTRANS members and industry. The constituent materials were also selected based on a discussion with CALTRANS and industry. Samples were made using OPC and PLC cements made from the same clinkers. Specifically, this study considered five clinkers (listed as A to E) that result in five OPC cements and six PLC cements (one of the clinkers was used with two limestone addition levels). Additional mixtures were made by adding a ground limestone powder to mixtures as a replacement for cement (these mixtures are listed as OPC + LS). A water-to-cementitious materials ratio (w/cm) of 0.40[1] was selected for all mixtures. While it was initially proposed in the contract that approximately 28 mixtures would be studied with less testing for some test series, 86 different mixture compositions were studied in this project. The samples were produced in the form of pastes (no aggregate), mortar (with sand), and concrete (with sand and coarse aggregate).

Five OPCs and six corresponding PLCs were provided in large quantities by five different cement producers, which have their manufacturing operations established to deliver cements to the California region. These cements have been designated with letters A, B, C, D, and E throughout the report in reference to the sources of the cements. The naming convention for the cementitious materials refers to the parent plant (A through E); whether the mixture is OPC, PLC, or OPC+LS (designated with O, P, or O+LS, respectively); the type of cement (II, V or IIV); and the approximate percentage of LS used (e.g., L10 or 10LS). The details on the constituent materials are provided later in this document (Section 4); however, Table 3.1 provides an example of the cementitious materials nomenclature used in this report.

[1] ACI 211.7 and other guides note that limestone is not an SCM, although it is a cement ingredient when used in a PLC. Therefore, when added limestone is used, this ratio includes limestone as part of the denominator; i.e., w/(cm+ls) = 0.40. For simplicity, this ratio will be designated as w/cm throughout the report.

Table 3.1. Nomenclature of cements used in this study

Parent clinker	Type	OPC	PLC	OPC + Limestone
A	II	A_OII	A_L15	A_OII+10LS
B	II/V	B_OIIV	B_L15	B_OIIV+10LS
C	V	C_OV	C_L10	C_OV+10LS
			C_L15	
D	V	D_OV	D_L15	D_OV+10LS
E	II/V	E_OIIV	E_11	E_OIIV+10LS

The study predominantly uses low CaO fly ash (FA1), slag cement (SL), silica fume (SF), and natural pozzolan (NP) as SCMs. FA1 has a CaO content <10%. Fly ash from another source (FA2) with CaO content between 10%-15% was procured only for ASR testing. Details on these materials are provided in Section 4.

In 2018, members of the OSU team met with CALTRANS and industry members and determined that the following mixtures would be studied in in this project. Mixtures 0 to 5 (denoted as M0 to M5) were identified as general binders, with a sixth mixture specifically added for the ASR study. The specific details of these mixtures are provided in Section 6.

General binders:

M0. No SCM
M1. 25% Fly Ash replacement - (CaO ~ 8.5%), consistent throughout except mixture 6
M2. 20% Fly Ash + 5% Silica Fume
M3. 50% Slag
M4. 25% Fly Ash + 25% Slag
M5. 25% Natural Pozzolan (NP)

Binder for the ASR study:
M6. 25% Fly Ash 2 (CaO ~ 12.5%)

The mixture proportions were sent to the committee for review, and approval for these mixture proportions was received. These mixture proportions are presented later in the Section 6. The aggregate used in the concrete mixture was also characterized, and trial mixtures were evaluated for workability and consistency.

152

4 Constituent Materials Characterization

4.1 Research Objective

This section aims to provide materials characterization for the materials used throughout this study. This includes the chemical compositions and particle size distributions of cementitious materials, and information on the heat of hydration of the clinkers, and the degree of reactivity of the SCM.

4.2 Background/Literature Review

Material characterization was performed to classify the reference binder materials used in the remainder of the study. Commercially available OPCs, PLCs, limestone powders, SCMs were analyzed [7]. Specifically, this section of the report provides background on chemical composition, particle size, hydration heat, and pozzolanic reactivity.

This project examines the use of SCM such as fly ash, slag, silica fume. CALTRANS widely use these to improve long term durability while reducing the carbon footprint of the concrete. The replacement of clinker by SCM contributes to reducing greenhouse gas emissions and energy consumption during cement manufacturing [8, 9].

There is a general agreement in the scientific community that when limestone is used with hydraulic cement at contents up to 15%, it generally has a similar mechanical performance as OPC. Shaker et al. [10] demonstrated that concrete made with CEM II (A-L) has similar mechanical resistance to the one made with OPC CEM I 42.5N. A minor difference in the mechanical performance between CEM I 42.5R and 15% PLC concrete has been observed in the study of Dhir et al. [11]. Chen et al. [12] found that the addition of limestone in a quantities less than 8% increases concrete strength. Meddah et al. [13] reported that the addition of 15% limestone as a partial replacement of OPC had an insignificant effect on the modulus of elasticity (5% reduction compared with OPC). De Weerdt et al. [14] observed that up to 15% of OPC could be replaced by limestone powder without impairing the compressive strength development. When more than 15% of the OPC is replaced by a limestone, a reduction in the mechanical strength has been observed at later ages along with a decrease in the modulus of elasticity [11, 15-18] due to the dilution effect. The similarity between OPC and PLC is particularly true in North America, where limestone is interground (typically) to result in a finer mixture (of the OPC and limestone) that is explicitly designed to have similar performance. Huang et al.[19] proved that the replacement of part of the OPC with limestone in ultra-high performance concrete mixtures (using silica fume) improves the mechanical properties of concrete as well as its hydration.

It should be noted that there can be some benefits of adding limestone to cement such as an increase in the compressive strength and a decrease in porosity [20]. Limestone can participate to some extent in chemical reaction with aluminum-rich phases in OPC and SCM by forming

carboaluminates [6, 21, 22], which can reduce the induction period, setting time and stabilize ettringite which can lead to the reduction in the volume of hydrates and porosity [16, 23-27]. These potential aluminate reactions that cause a decrease in porosity and an increase in compressive strength were the basis for the limitation of limestone addition to 15%. Early studies note that the porosity and strength in PLCs with a 12%-15% limestone content is nearly equal to the porosity and strength for a cement of the same chemistry containing no limestone [20].

Menéndez et al.[28] reported benefits from combining limestone with blast furnace slag and OPC to improve the early and later age compressive strength of mortar or concrete. At early ages (e.g., during the first 48h), the hydration is improved by limestone because the limestone particles can act as nucleation sites for cement hydrates [29-31]. Sun et al. [32] showed that the limestone is preferentially ground to be among the finest particles because it is softer than conventional clinker. This resulted in high performing blends of OPC, limestone, and slag [28].

Bentz et al. [33] demonstrated that high volume fly ash benefited explicitly from the addition of finely ground limestone, which helped it offset the retardation of hydration and delayed setting time. As a result, the use of fine limestone powder in high volume fly ash mixtures may be very promising for ready-mix producer, however, the fineness of the limestone is crucial.

These studies show that there is a general agreement in the literature that the replacement of cement with limestone (when finely ground) can be beneficial for the mechanical properties, hydration, and microstructural properties of cementitious materials when SCM are used. Nevertheless, to the best of the authors' knowledge, most of the studies in the literature focused on type I or II cement. This study aims to determine the impact of the replacement of OPC with limestone in a wider range of cement types on both the mechanical and chemical characteristics of cementitious materials.

4.3 An Overview of the Experimental Characterization Performed for the Cementitious Powders

This section describes testing for chemical composition using x-ray fluorescence, loss on ignition, particle size distribution of the cement, and SCM. Five OPCs, 6 PLCs, the limestone powder, and SCM were evaluated. The heat of hydration was assessed for the mixtures shown in section 4.6 (mixtures 0 to 5) using a fixed w/cm. Finally, the reactivities of the SCM were assessed using the Pozzolanic Reactivity Test described in [34-37].

4.4 Chemical Composition and Loss on Ignition

4.4.1 Experimental Methods

A PANalytical Epsilon 3XLE bench-top energy dispersive X-Ray fluorescence (XRF) spectrometer (Figure 4-1a) was used to analyze the chemical composition of the cement and SCMs used in this study. The XRF samples were prepared in the form of fused beads. For each sample type (cement or SCM), a calibration was performed with known standards to quantify the elements studied [7] accurately. The calibration involved measuring high purity samples with known concentrations and establishing a relationship between the measured intensities and concentrations. The XRF was demonstrated to comply with ASTM C114-18 [38] standards for chemical analysis of hydraulic cement.

Before the XRF analysis, the loss on ignition (LOI) was obtained for each sample by heating 3 g of the samples in a furnace up to 970 °C for 3 hours in accordance with ASTM C114-18 [38]. It should be noted that the LOI at 750°C±50°C was the same as the LOI at 970°C as there was no mass loss between 750°C and 970°C. The mass loss observed in the sample after being heated to 970 °C gives the LOI of the cement or fly ash. The cement beads were prepared by combining 1g of cement and 5g of flux in LeNeo Fluxer for 20 minutes. While the cement was fused in its original state, a slightly different procedure was used for the SCM. To prepare the SCM beads, 0.55g of the SCM (obtained after the LOI test) was combined with 5.5 g of flux (consisting of 49.75% lithium metaborate, 49.75% lithium tetraborate, and 0.50% lithium iodide) in a platinum flat bottomed crucible. The reduced SCM and flux were mixed gently but thoroughly using a spatula and then transferred to LeNeo Fluxer for fusion at a temperature of 1450 °C.

The device uses a predetermined fusing program for general oxides for 25 minutes. The clear cement/SCM beads after fusion were further analyzed in the XRF spectrometer, shown in Figure 4-1.

(a)

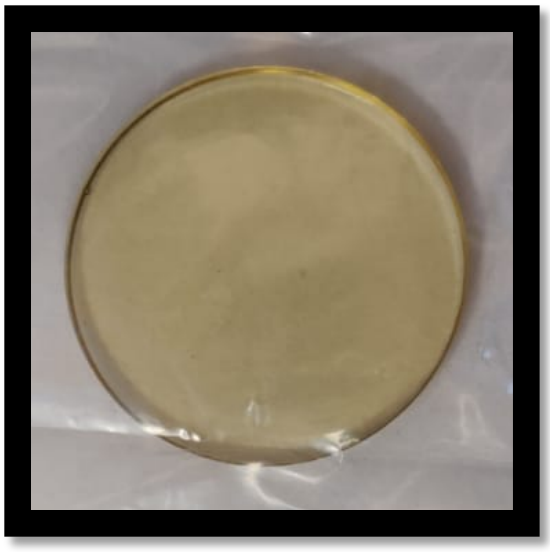

(b)

Figure 4-1. (a) PANalytical Epsilon 3XLE XRF spectrometer (b) a cement bead

4.4.2 Typical Experimental Measurement and Interpretation

The chemical composition obtained from the XRF spectrometer provides the mass of each elemental oxide (in g) per 100g of cement/SCM used to make the bead. For the PLC, the limestone content was also measured. The cement's chemical oxide composition was used to classify the parent clinker type based on ASTM C150.

The companies producing the cements A, B, D, and E also sent out samples of the limestone rocks, which are added to the clinker during the grinding phase to produce the OPC and PLCs. The $CaCO_3$ contents of these limestones was determined by grinding the limestone rocks into fine powder and determining the mass of CO_2 released when the powder is heated from 600º-800ºC using Thermo-Gravimetric Analysis (TGA) [38-41] [2]. Stoichiometry dictates that 100 g of calcite - ($CaCO_3$) releases 40 g of CO_2 upon decomposition. The received cements were also analyzed for mass loss between 600º-800ºC using TGA, and their limestone content was determined.

[2] The $CaCO_3$ content of the rocks was also measured using a furnace (mass loss between 550°C to 950°C; see ASTM C114) and the $CaCO_3$ contents obtained from the TGA approach, and the furnace approach were within 1% of each other.

4.4.3 Experimental Results and Discussion

As determined from XRF, the chemical oxide composition and limestone content of all the cements received from Companies A, B, C, D, and E are provided in Table 4.1.

Table 4.1a. Chemical composition of OPCs and PLCs from Company A and B

	Cement Source A		Cement Source B	
%	**A_OII**	**A_L15**	**B_OIIV**	**B_L15**
SiO_2	19.95	18.38	20.54	18.46
Al_2O_3	3.95	3.62	4.05	3.71
Fe_2O_3	2.28	2.07	3.62	3.46
CaO	63.32	61.69	61.72	60.45
MgO	1.43	1.33	2.52	2.28
SO_3	2.55	2.48	1.80	1.71
LOI	2.71	6.42	1.96	6.75
Na_2O	0.21	0.22	0.17	0.13
K_2O	0.48	0.44	0.69	0.63
TiO_2	0.19	0.18	0.22	0.20
P_2O_5	0.10	0.10	0.11	0.10
ZnO	0.01	0.01	0.03	0.03
Mn_2O_3	0.07	0.07	0.07	0.06
Cl	0.003	0.003	0.007	0.004
Limestone	4.31	13.32	1.79	13.11
Clinker Type	II	II	II/V	II/V

Table 4.1b. Chemical composition of OPCs and PLCs from Company C, D, and E

	Cement Source C			Cement Source D		Cement Source E	
%	**C_OV**	**C_L10**	**C_L15**	**D_OV**	**D_L15**	**E_OIIV**	**E_L11**
SiO_2	19.45	18.77	18.36	20.54	18.46	19.98	19.38
Al_2O_3	3.68	3.65	3.50	4.05	3.71	3.72	3.61
Fe_2O_3	3.35	3.18	3.01	3.62	3.46	3.49	3.30
CaO	60.32	59.43	58.37	61.72	60.45	61.97	61.65
MgO	4.45	4.33	4.24	2.52	2.28	1.71	1.73
SO_3	2.73	3.03	2.91	1.80	1.71	2.66	2.70
LOI	2.53	4.37	6.12	1.96	6.75	2.35	4.71
Na_2O	0.22	0.22	0.24	0.17	0.13	0.21	0.23
K_2O	0.36	0.27	0.30	0.69	0.63	0.51	0.46
TiO_2	0.23	0.22	0.20	0.22	0.20	0.22	0.21
P_2O_5	0.06	0.05	0.05	0.11	0.10	0.13	0.13
ZnO	0.02	0.02	0.02	0.03	0.03	0.01	0.01
Mn_2O_3	0.06	0.05	0.05	0.07	0.06	0.05	0.05
Cl	0.006	0.005	0.005	0.007	0.004	0.003	0.006
Limestone	4.2	10	14	3.48	13.71	5	11.11
Clinker Type	V	V	V	V	V	II/V	II/V

The SCMs used to produce cement paste/mortar or concrete based on CALTRANS specifications were also characterized, and the results are shown in Table 4.2.

Table 4.2. Chemical composition of SCMs and limestone

%	Fly Ash 1	Slag	Natural Pozzolan	Silica Fume	Fly Ash 2	Lime-stone	Lassen-ite*	Bassal-ite*	Blended Natural Pozzolan *
SiO_2	51.86	31.58	66.42	95.88	47.15	2.93	67.76	74.13	30.05
Al_2O_3	21.70	12.13	11.98	0.69	16.57	0.79	14.70	13.39	5.89
Fe_2O_3	5.04	0.55	0.86	0.12	5.88	0.41	6.34	0.84	1.46
CaO	8.61	41.34	4.06	0.70	12.54	86.50	2.11	0.91	3.02
MgO	2.58	6.97	0.18	0.26	4.80	5.74	0.84	0.09	0.37
SO_3	0.78	3.75	0.19	0.15	0.60	0.13	1.03	0.09	0.18
LOI	1.42	0.00	4.09	4.30	2.43	42.27	8.71	3.33	8.73
Na_2O	2.58	0.24	3.57	0.16	3.65	0.14	1.85	3.68	1.23
K_2O	1.45	0.28	4.35	0.49	1.72	0.12	1.70	4.69	1.36
TiO_2	1.19	0.47	0.09	0.01	1.17	0.04	0.58	0.09	0.14
P_2O_5	0.23	0.00	0.00	0.05	0.24	0.09	0.19	0.01	0.07
ZnO	0.02	0.00	0.00	0.06	0.01	0.00	0.01	0.00	0.00
Mn_2O_3	0.03	0.19	0.07	0.04	0.09	0.02	0.15	0.07	0.04
Cl	0.01	0.00	0.02	0.01	0.00	0.01	0.01	0.02	0.01

*Note that the chemical compositions of Lassenite, Bassalite, and Blended Natural Pozzolans are mentioned in the table as CALTRANS had provided these materials for testing; however, they are not used anywhere else in the report.

Table 4.1 illustrates that the project has only Type II, Type II/V, and Type V cements, which provide moderate to high sulfate resistance to comply with CALTRANS specifications. Determination of the materials' chemical composition shows that the OPC and PLCs from the same parent company have similar chemical composition when the limestone content is accounted for as expected. The OPCs had limestone contents between 3%-6% (ASTM C 150, AASHTO M 85 permit up to 5% limestone). The PLCs had limestone contents ranging from 10%-15% (which was consistent with the values noted by the producer). Table 4.1 provides the chemical composition of the cement used in this study, while Table 4.2 provides the chemical composition of the SCMs used in this study. This information is valuable to interpret the remainder of the experiments performed in this project and computational modeling.

4.5 Particle Size Analysis

4.5.1 Experimental Methods

Particle size analysis was performed on both the cement and SCMs using a Horiba LA-920 particle size analyzer shown in Figure 4-2. Isopropyl alcohol (IPA) was used as the solvent to disperse the particles in the front of a laser-lamp assembly, which measures the particle size distribution using laser light scattering.

Before each test, the device's solution pathway was rinsed several times with IPA to remove any contaminants following the standard operating procedure. Rinsing and draining cycles were repeated until there was no observed scatter (solid particles scatter the light) on the real-time scatter sensor (frequency-diameter plot) on the software (i.e., the solid impurities had been flushed out and only the solvent remained). An initial alignment function was then performed on the device to realign the laser-lamp assembly axis with the measuring station. After initial alignment, the lamp and laser power raised to a full 100% [42]. The system was reset before every reading to the baseline solution signal.

Approximately 3 to 5 g of powder was added in small increments of 0.5 g through the inlet hole into the solvent below. The solution was then circulated several times to prevent the clumping of powder particles together. The powder was added to the solvent and circulated until the laser's power and the lamp was reduced to be in the range of 80 to 90%, and a visible scatter was observed on the real-time scatter monitor. After this, the actual measurement was performed for 30 seconds, and the particle size distribution was measured.

Figure 4-2. Horiba LA-920 Particle Size Analyzer

4.5.2 Typical Experimental Measurement and Interpretation

A typical particle size distribution is shown in Figure 4-3. The y-axis describes the relative frequency of the volume fraction (%) of particles in a unit volume of measured material detected at a given size (diameter) in Figure 4-3a. In contrast, the y-axis describes the cumulative volume fraction of particles with a size (diameter) lower than a particular size in a unit volume of measured material in Figure 4-3b. The x-axis of these plots is the average size (diameter) of the powder

particles in microns. The particle sizes of evenly ground materials like cements usually follow a normal distribution; however, bimodal distributions are sometimes observed in SCMs. Figure 4-3b also shows the d50 and the d90 values of the particle size distribution, which is defined as the 50th and 90th percentile particle size respectively.

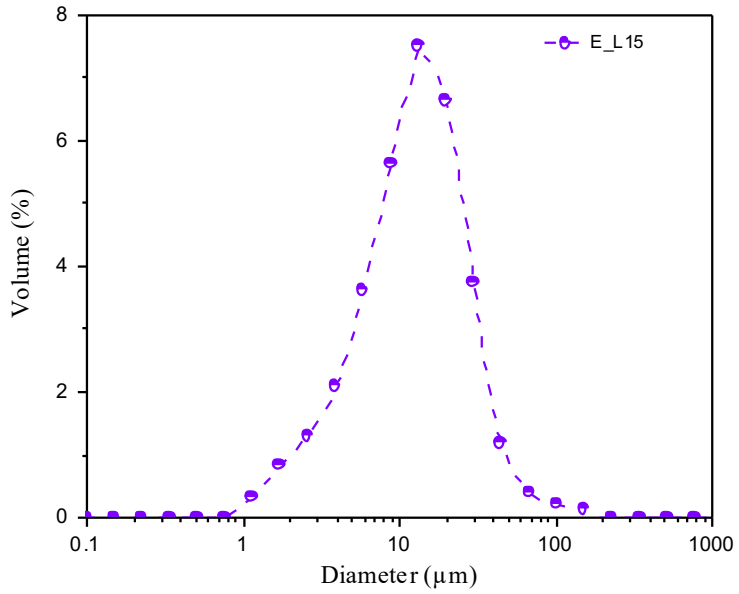

(a)

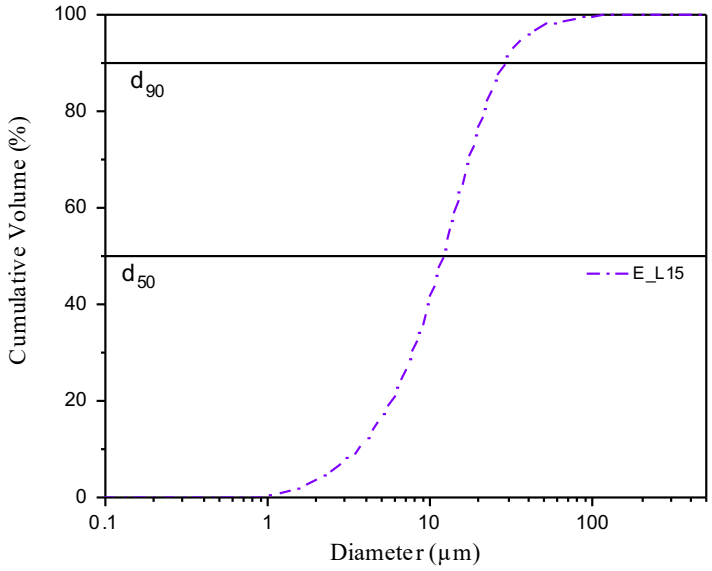

(b)

Figure 4-3. Typical particle size distributions of cements showing (a) volume vs. diameter (b) cumulative volume vs. diameter

4.5.3 Experimental Results and Discussion

The results of particle size analysis of all the cements and SCMs are presented in Figure 4-4 (a)-(d). It should be noted that in general, the OPC and PLC all have a similar particle size distribution with the exception of A_L15, which appears to have a proportion of larger clinker particles, and E_OIIV has a higher concentration of more finely ground particles. As expected, silica fume was the finest and the slag was the coarsest cementitious material,

Table 4.3 summarizes the d50 and d90 values of these materials. The comparison of particle size distributions for the cements shows that when the d_{50} is used as a measure of particle size are similar (+/-5%). Cement A has a coarser particle size distribution than PLC; however, in general, the average particle size of PLC is smaller than the OPC.

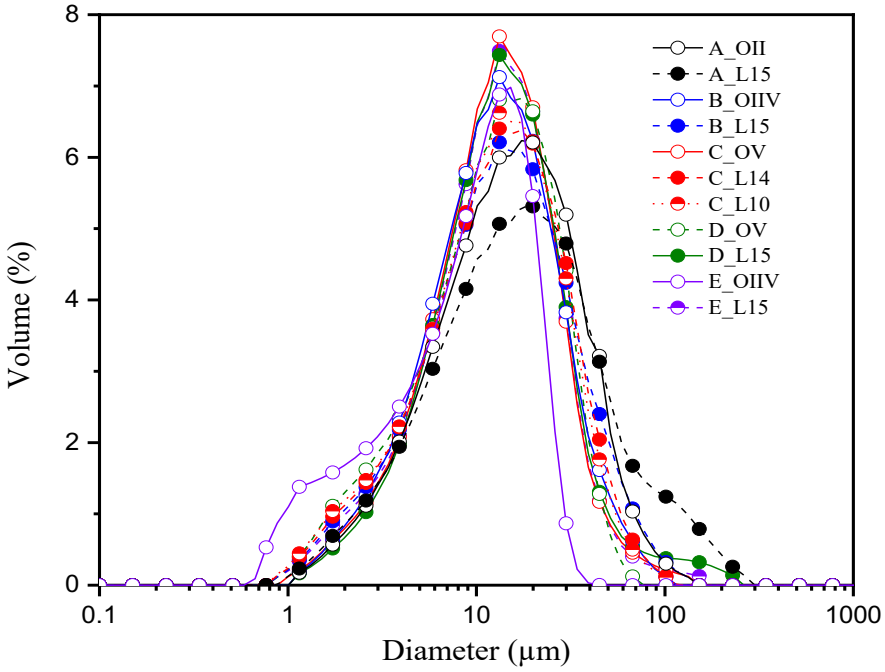

(a)

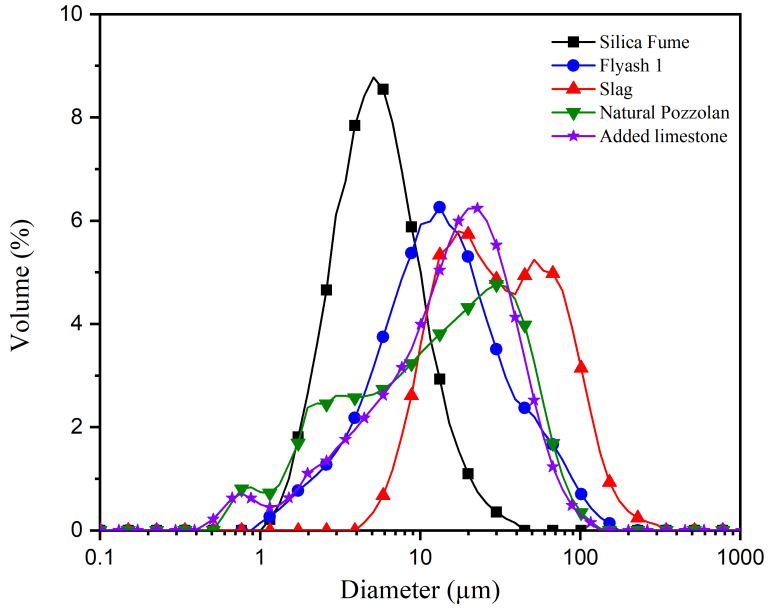
Silica Fume
Flyash 1
Slag
Natural Pozzolan
Added limestone
Volume (%)
Diameter (µm)
0
2
4
6
8
10
0.1
1
10
100
1000

(b)

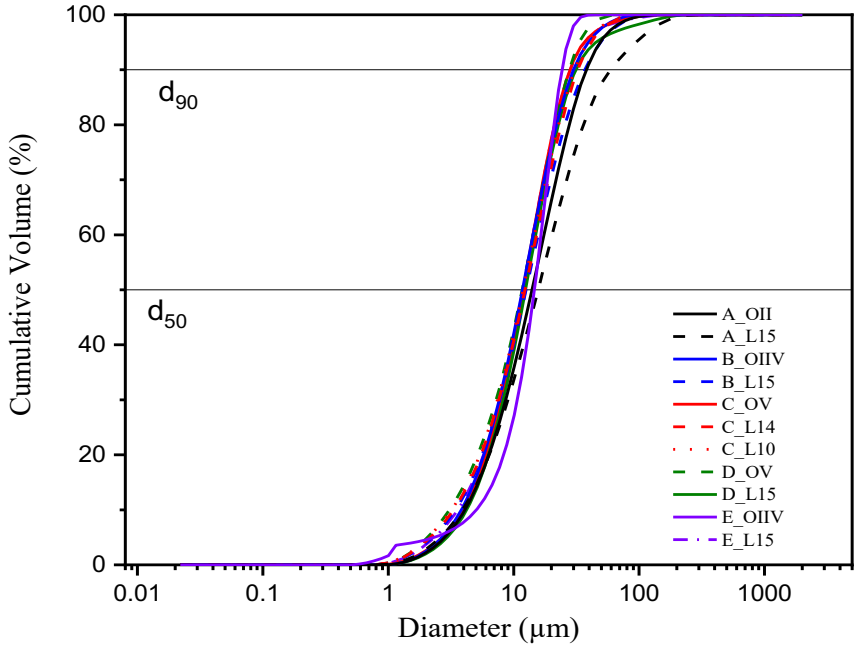
d90
d50
A_OII
A_L15
B_OIIV
B_L15
C_OV
C_L14
C_L10
D_OV
D_L15
E_OIIV
E_L15
Cumulative Volume (%)
Diameter (µm)
0
20
40
60
80
100
0.01
0.1
1
10
100
1000

(c)

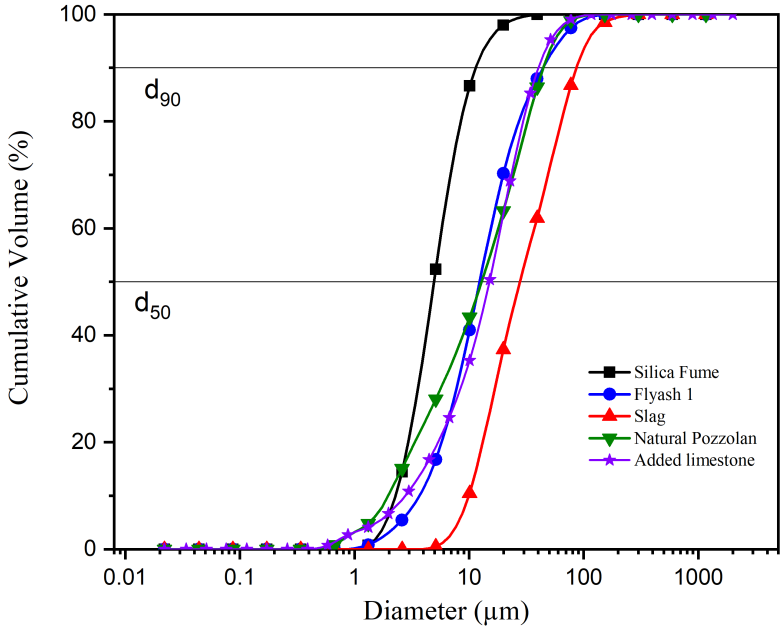

(d)

Figure 4-4. Particle size distributions depicting volume fraction vs particle diameter of (a) Cements (b) SCMs; cumulative volume fraction vs particle diameter of (c) Cements (d) SCMs.

Table 4.3. d_{50} and d_{90} values of tested materials

	d_{50} (µm)	d_{90} (µm)
A_OII	10.52	27.89
A_L15	15.70	59.18
B_OIIV	11.77	29.94
B_L15	12.57	37.06
C_OV	12.53	27.90
C_L10	12.33	32.53
C_L14	11.95	30.75
D_OV	12.45	31.46
D_L15	11.72	27.88
E_OIIV	11.15	30.98
E_L15	11.87	28.40
Fly Ash 1	13.01	44.62
Silica Fume	4.96	11.28
Slag	29.08	87.81
Natural Pozzolan	13.11	44.28
Added Limestone	15.03	40.27

4.6 Heat of Hydration

4.6.1 Experimental Methods

The influence of limestone replacement on the reaction rate was measured using heat release values of the OPC, PLC, OPC+SCM, and PLC+SCM systems. This involved performing cement paste mixtures tests in isothermal calorimeter (TAM Air, TA Instruments shown in Figure 4-5) at 23°C ± 0.1°C for seven days.

Figure 4-5. TAM Air isothermal Calorimeter used for heat flow measurements from samples

The cement paste samples were mixed in a vacuum mixer at 250 revolutions per minute for four minutes and immediately transferred to a glass ampoule. These ampoules were then sealed and lowered into the isothermal calorimeter stabilized at 23°C ±0.1°C. After a short delay (twenty minutes) for baseline correction, the heat values were recorded continuously for seven days. The

paste mixture proportions are described in Table 4.4. The w/cm for all mixtures was kept constant at 0.40.

Table 4.4. Mixture proportions of cement paste mixtures

	Mixture short name example using B_OIIV	Cement[#]	Fly Ash	Slag	Silica fume	Natural Pozzolan	water
M0	B_OIIV	200	----	----	----	----	80
M1	B_OIIV-25FA1	150	50	----	----	----	80
M2	B_OIIV-20FA1-5SF	150	40	----	10	----	80
M3	B_OIIV-50SL	100	----	100	----	----	80
M4	B_OIIV-25FA1-25SL	100	50	50	----	----	80
M5	B_OIIV-25NP	150	----	----	----	50	80

*All the mixture proportion values are in g
Cement: OPC, PLC, OPC + 10% limestone

All the mixtures described in Table 4.4 were performed using all five cements (A, B, C, D, and E) with their respective OPC, PLC, and OPC+10%LS systems. The experimental matrix describing the progress is shown in Table 4.5. Each mixture in Table 4.5 was tested twice, and an average is reported.

353 **Table 4.5. Experimental matrix of heat of reaction tests**

	M0	M1	M2	M3	M4	M5
A_OII	√	√	√	√	√	√
A_L15	√	√	√	√	√	√
A_OII+10LS	√	√	√	√	√	√
B_OIIV	√	√	√	√	√	~
B_L15	√	√	√	√	√	~
B_OIIV+10LS	√	√	√	√	√	~
C_OV	√	√	√	√	√	~
C_L10	√	√	√	√	√	~
C_L14	√	√	√	√	√	~
C_OV+10LS	√	√	√	√	√	~
D_OV	√	√	√	√	√	√
D_L15	√	√	√	√	√	√
D_OV+10LS	√	√	√	√	√	√
E_OIIV	√	√	√	√	√	~
E_11	√	√	√	√	√	~
E_OIIV+10LS	√	√	√	√	√	~

354 √ completed
355 ~ not tested

356

357 ### *4.6.2 Typical Experimental Measurement and Interpretation*

358 Figure 4-6 shows a typical heat release (cumulative heat of hydration) determined using an
359 isothermal calorimeter. The vertical axis represents the total heat released values from each sample
360 normalized by the per unit mass of binder (powder), while the horizontal axis represents the age
361 of the cement paste sample in days. The tests were run for approximately seven days. The systems
362 with higher overall heat release have a greater extent of reaction than the systems with a lower
363 heat release. For the systems shown in Figure 4-6, Binder 1 has undergone exhibits a greater extent
364 of reaction than Binder 2 at the end of seven days. Several factors can influence this mixture to
365 exhibit a greater extent of reaction, such as the proportion of active clinker in the system, the
366 fineness, or the materials' reactivity.

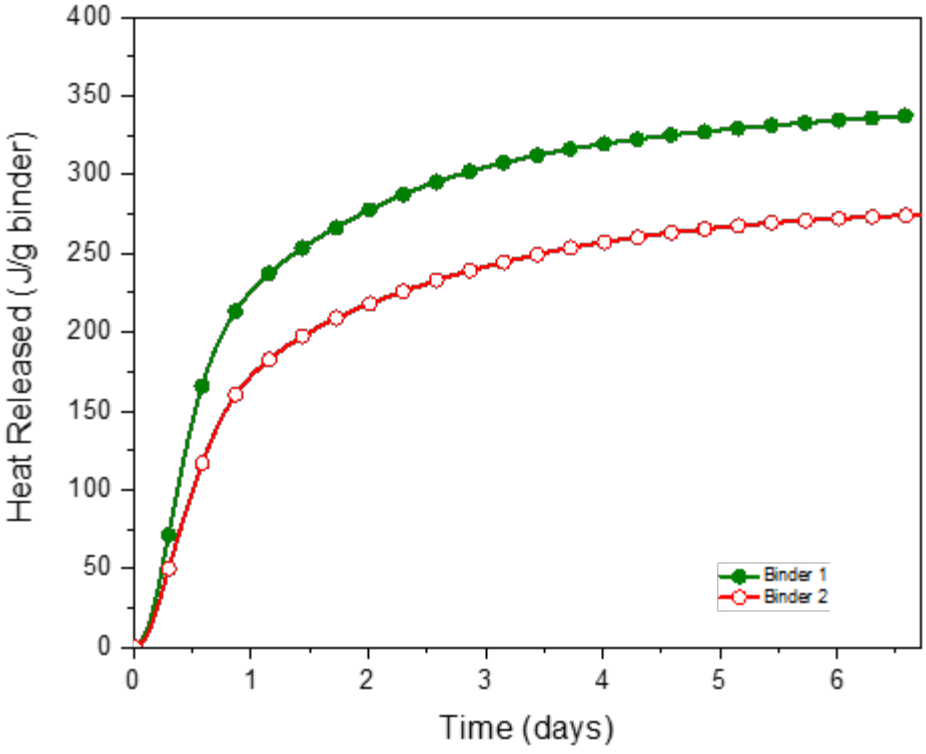

Figure 4-6. Typical Heat of reaction plot

4.6.3 Experimental Results and Discussion

Figure 4-7 (a)-(f) shows the heat of reaction results comparing OPC, PLC, and OPC+10%LS systems for cement A for the different mixture proportions. The heat of reaction results of the remaining cements is provided in Appendix B.

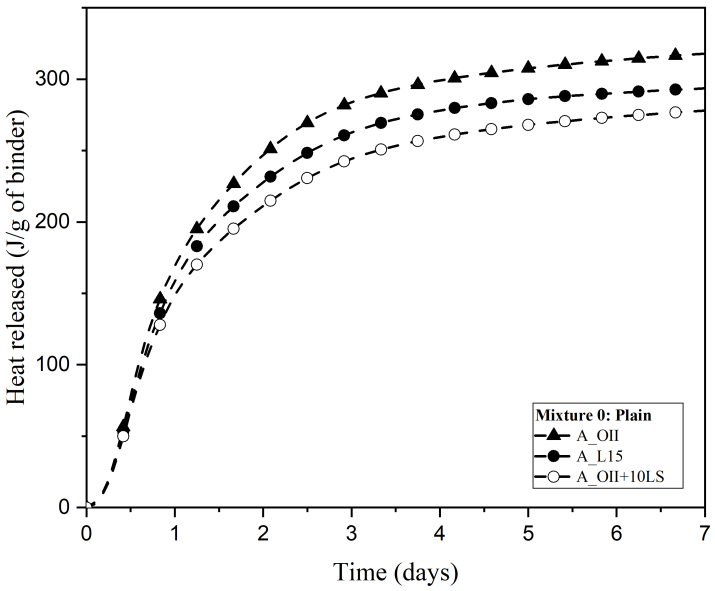
Heat released (J/g of binder)
Time (days)
Mixture 0: Plain
A_OII
A_L15
A_OII+10LS

,

(a)

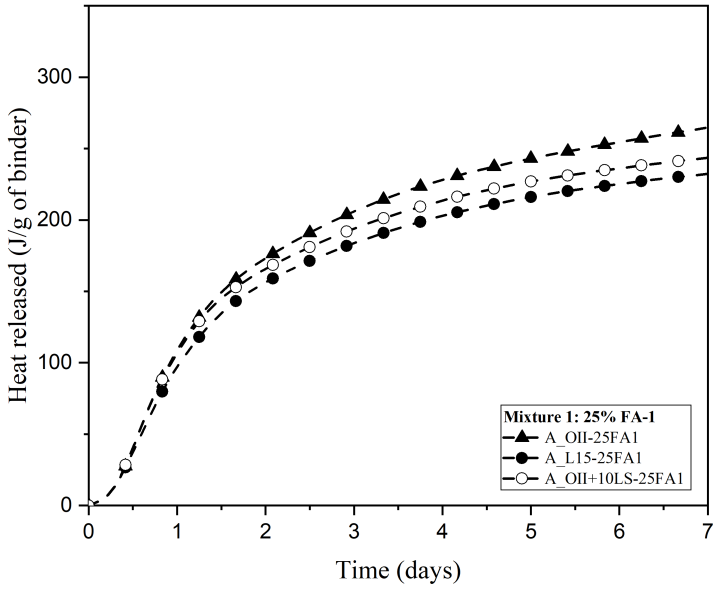
Heat released (J/g of binder)
Time (days)
Mixture 1: 25% FA-1
A_OII-25FA1
A_L15-25FA1
A_OII+10LS-25FA1

(b)

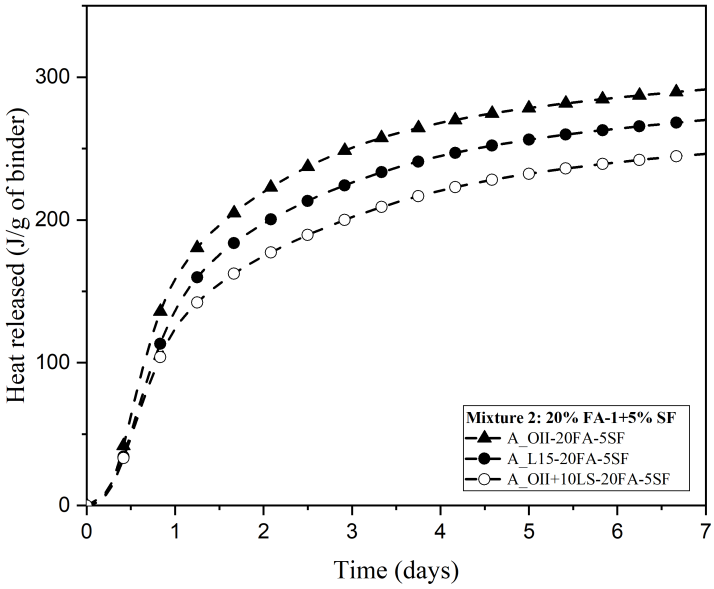
Heat released (J/g of binder)
Time (days)
Mixture 2: 20% FA-1+5% SF
A_OII-20FA-5SF
A_L15-20FA-5SF
A_OII+10LS-20FA-5SF

(c)

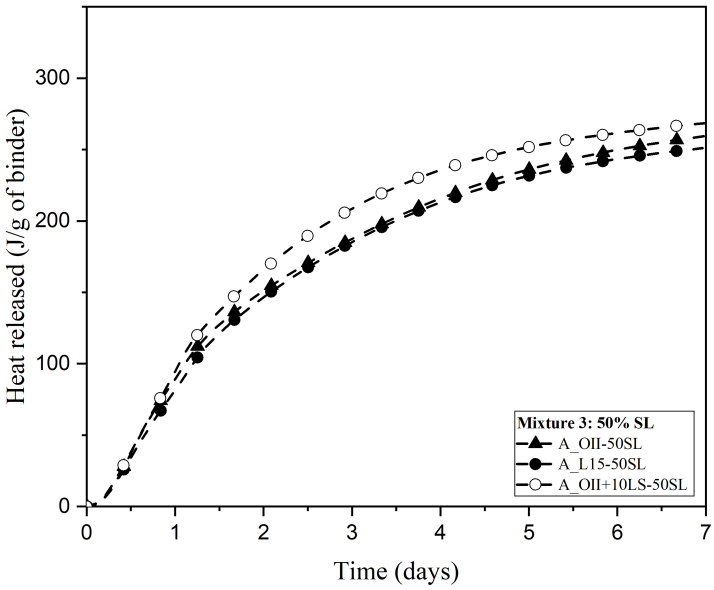
Heat released (J/g of binder)
Time (days)
Mixture 3: 50% SL
A_OII-50SL
A_L15-50SL
A_OII+10LS-50SL

(d)

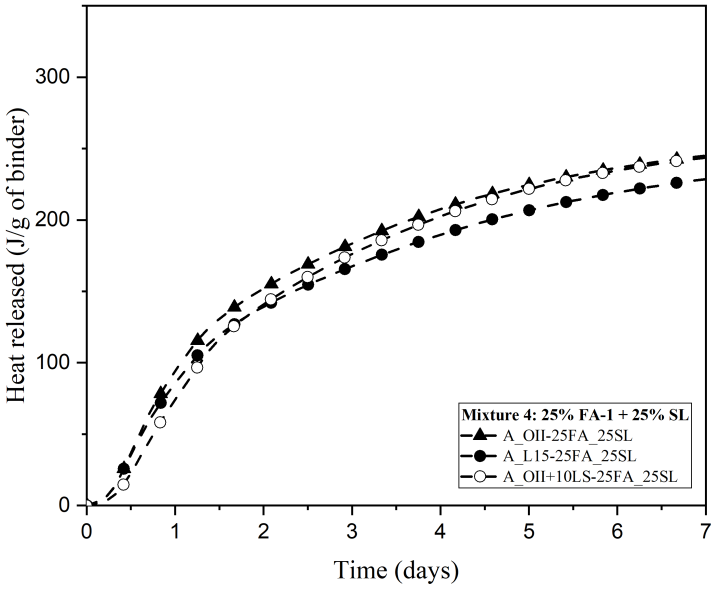

(e)

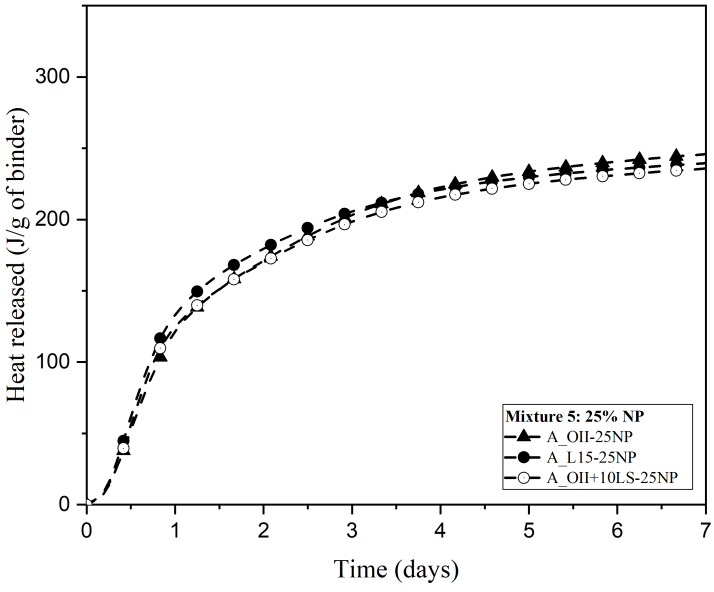

(f)

373 **Figure 4-7. (a-f) Total heat released per unit binder in cement paste measured for seven**
374 **days using Isothermal Calorimeter for Cement A for M0, 1, 2, 3, 4 and 5 respectively**

While Figure 4-7 was performed for Cement A, similar results were obtained for the other cements. The total heat released (when normalized per unit of binder) has approximately ±10% variation when the OPC, PLC, and OPC+LS systems are compared. In general, a slightly lower heat release occurs with the PLC (1 to 8%) and OPC+LS (3 to 15%) systems, indicating less overall reactivity consistent with dilution. This decrease is consistent with a reduction in clinker content in the PLC and OPC+10LS systems. This was not found to be statistically significant for the PLC mixtures; however, it was statistically significant for the OPC + LS mixtures.

When the verticals axis's normalization was done by clinker content, the PLC and OPC+10LS have a higher heat of reaction, illustrating that more of the cement clicker reacts in those systems. The reaction of fly ash, being primarily pozzolanic, can be seen at later ages as this requires more time for the reaction to occur. The reaction between the hydraulic slag and the limestone present in the system is responsible for additional heat release in PLC and OPC+10LS systems in M3 and 4.

4.7 The Reactivity of SCMs

4.7.1 Experimental Methods

A reactivity test is used to quantify the maximum degree of reactivity (DOR*) of the SCMs [35-37, 43]. The DOR* of an SCM is the maximum % amount of the SCM that reacts with calcium hydroxide (CH) in a pozzolanic reaction. The test method uses a combination of experimentally determined CH consumption, as quantified by TGA, and heat release obtained from isothermal calorimetry (IC). These values are superimposed on a plot with thermodynamically calculated CH consumption and heat release lines for reference SiO_2 and Al_2O_3 systems at equilibrium at different theoretical maximum reactivities. To obtain reference lines, thermodynamic modeling was performed using GEMS3K software [44-47] and the CemData v.18.01 database [48]. Depending on the relative position of the point represented by CH consumption and heat release with respect to the theoretical lines, the DOR* can be quantified. This test provides a methodology for measuring the amount of reactive versus non-reactive components of a pozzolan..

The blends for measuring reactivity were made by dry mixing reagent-grade CH and the SCM in a 3:1 mass ratio [34, 37]. The powder was then mixed with 0.5 M potassium hydroxide (KOH) solution while keeping the liquid-to-powder mass ratio constant at 0.9. For each test, 38 g of materials were mixed for 4 minutes in a plastic container using a spatula. After mixing, approximately 7 g of the paste was immediately sealed in a glass ampoule. The ampoules were transferred to an isothermal calorimeter (TAM Air, TA Instruments) that had been preconditioned at 50°C ± 2°C for 24 hours. Following signal stabilization, about 45 minutes after the ampoule was placed in the calorimeter. The heat flow was recorded for a total of 240 hours.

After 240 hours of IC testing, the ampoules were removed from the calorimeter, and 20 mg of the removed sample was analyzed using TGA (Q50, TA Instruments). The TGA involved heating the sample from 23°C to 1000°C in a nitrogen-purged atmosphere at a rate of 10°C/min. TGA was performed within 12 hours of removing the samples from the isothermal calorimeter. The mass loss between 350°C to 450°C corresponds to the decomposition of CH. The decomposition of CH was used to calculate CH remaining in the system after 240 hours (21). CH decomposition occurs between 350-450°C [38, 39, 43]. Testing and analysis followed the method described in Appendix A. CH consumption versus heat release was plotted for each SCM. Each SCM's reactivity was determined using thermodynamically calculated reference lines for the SiO_2 and Al_2O_3 reactions with 0.5 M KOH at 50°C. This method provides the maximum degree of reactivity (DOR*) at equilibrium.

4.7.2 Analysis Results and Discussion

The SCMs used in the project Fly Ash 1 (FA-1), Slag, Silica Fume, Natural Pozzolan, and Fly Ash 2 (FA-2) were all tested for their maximum degree of reactivity (DOR*) and results were plotted against the reference reaction lines depicting the reaction of pure silica and alumina with 0.5 M KOH in Figure 4-8. The DOR* are summarized in Table 4.6.

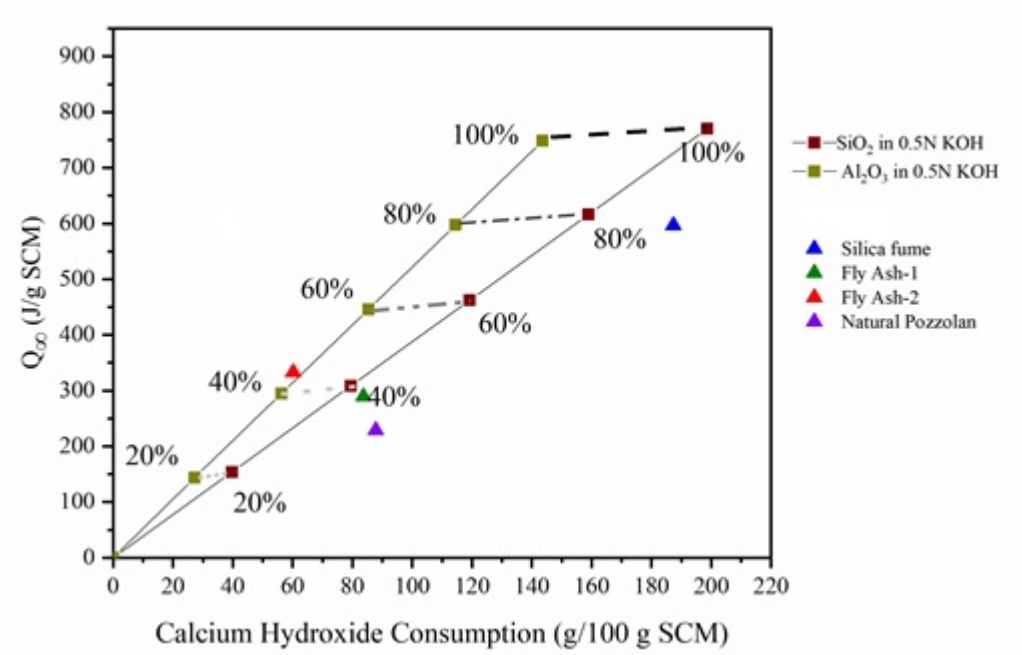

Figure 4-8. Maximum degree of pozzolanic reactivity (DOR*) results for CALTRANS SCMs

Table 4.6. SCM Heat (Q_∞), CH, and DOR values

	CH consumed (g/g 100 SCM)	Q_∞ (J/g SCM)	DOR*
Silica fume	189.2	599.8	76.15%
Fly Ash-1	83.7	289.4	37.15%
Fly Ash-2	60.2	332.9	44.67%
Natural Pozzolan	87.8	228.7	28.19%

The DOR* of SCM corresponds to the maximum degree of pozzolanic reactivity shown by the SCM under relatively idealistic conditions.

The silica fume, a fine powder composed of almost pure reactive silica dioxide, has a reactivity of 76%. The natural pozzolan contains reactive silica-based SCM shows a DOR* of 28%. Fly Ash 1, and Fly Ash 2 were observed to have a similar DOR* of 37 and 45%; however, their position with respect to the reference SiO_2 and Al_2O_3 reaction is impacted by the fact that Fly Ash 2 has higher CaO content than Fly Ash 1. Note that the PRT was developed to determine the reactivity of pozzolanic materials (materials which primarily contains SiO2 and Al2O3) and since slag is a mostly a hydraulic material containing significant CaO the PRT in its current form cannot be directly used for measuring the reactivity of slag. Although, the PRT has been extended to quantify the reactivity of slags in recent work, but this is beyond the scope of this report.

4.8 Significant Findings

This section of the report has provided information on the loss of ignition, chemical composition, oxide composition, the particle size of the raw materials, and the SCMs reactivity. The results are useful for providing reference values for use in the remainder of the study. In general, a similar particle size analysis exists for the OPC and PLC. The heat of hydration was found to be with +/- 10% when the OPC, PLC, and OPC+LS systems were compared based on total cumulative heat; however, the PLC and OPC+LS systems were found to have a greater degree of reaction. The degree of reactivity (DOR*) was determined for each of the SCM used, with the silica fume generally having a value of over 75%, with the other SCMs having values in the range of 28 to 45%.

5 Alkali-Silica Reactivity

Alkali-silica reaction (ASR) in concrete was first studied by Thomas E. Stanton of the California State Division of Highways during the 1930s and published in a study in 1940 [49]. ASR is a chemical reaction between amorphous silica found in some aggregates and alkali hydroxides in the concrete pore solution. Cement is the primary source of alkalis. The other sources of alkali can be SCMs, deicers, aggregates, chemical admixtures, and seawater. Given sufficient moisture, the reaction product, ASR gel, swells, and exerts pressure on the surrounding concrete leading to cracking.

Since the discovery of ASR, significant research has been done on understanding the mechanism of ASR and the expansion caused by it, developing test methods to evaluate ASR, and developing strategies to mitigate the distress caused by the reaction in concrete. Rajabipour et al. [50] summarized the current understanding of reaction mechanisms and the current knowledge of ASR mitigation.

The use of SCMs in sufficient quantities and lithium compounds have been found to be the most effective ways to mitigate ASR so far. Thomas summarized the effect of the use of SCMs on ASR expansion [51]. The quantity of SCM required to mitigate ASR depends on the SCM composition mainly calcium oxide, silica, and alkali content [51]. It also depends on the reactivity level of aggregate and the amount of alkalis available from the cement and other sources. SCMs mitigate ASR mainly by lowering the pore solution alkalinity through binding the alkalis by C-S-H hydrates [52, 53]. The replacement level of cement with SCM needs to be increased to control ASR expansion with an increase in its calcium content, increase in alkalis available, increase in aggregate reactivity, and decrease in SCM's silica content. Also, SCMs rich in alumina are considered to be effective in controlling ASR expansion as aluminum in pore solution was found to lower the reactive silica dissolution rate from aggregates [54, 55].

Using a sufficient amount of certain lithium compounds, especially $LiNO_3$, as an admixture in new concrete has also been found to be a viable way to mitigate ASR [56]. Folliard et al. [56] published a report summarizing the proposed mechanisms on how lithium compounds work and guidelines for using lithium compounds to mitigate or prevent ASR. The main conclusions from the report were: (i) the effectiveness of lithium admixtures is a function of its dosage (in terms of lithium-to-alkali molar ratio) in the mixture and of the petrographic nature of the reactive aggregate to the control, (ii) required lithium-to-alkali molar ratio to mitigate ASR vary significantly for different aggregates (as low as 0.56 to >1.11), (iii) it was recommended to use SCMs along with lithium admixture to reduce the cost using lithium compounds and to produce low-permeability concrete to provide better durability, and, (iv) the most recommended method to assess the effectiveness of lithium admixture was ASTM C1293, with a 2-year duration. Due to lithium's cost, however, it is becoming less and less frequently used in concrete construction.

As California has siliceous aggregate sources that show the potential for ASR and damage, SCMs are included as a prescriptive specification to address ASR concerns. In two recent studies, PLC generally showed a synergistic benefit when used with SCM [5, 57]; however, the influence of PLC on mitigation of ASR has not been extensively evaluated.

5.1 Research Objective

The main objective in this part of the project is to extensively study the influence of PLC usage in conjunction with SCMs on the expansion due to ASR. Ultimately, the results of this task will inform CALTRANS if their current mitigation options for a range of alkali-silica reactivity levels can be utilized as-is, increased, or decreased when combined with a PLC.

5.2 Background/Literature Review

There are several test methods to detect the alkali-silica reactivity of aggregates. These range from tests on aggregates, mortar, and concrete, to petrographic examination of aggregates and concrete. There are also modifications to these tests that allow for the use of SCMs in the mixture to test their efficacy in mitigating the reactivity of the aggregates.

The most commonly used laboratory test methods to evaluate the effectiveness of the usage of SCMs to mitigate or control ASR are accelerated mortar bar test - AMBT (ASTM C1567 [58]) and concrete prism test - CPT (ASTM C1293 [59]). AMBT involves immersion of mortar bars of dimensions 25 x 25 x 285 mm cast with the reactive fine aggregate (crushed, if the reactive aggregate is a coarse aggregate) in 1N NaOH solution at 80^{o}C for 14 days. CPT involves storing concrete bars of dimensions 75 x 75 x 285 mm over water at 38^{o}C for a year (with no mitigation measures) or two years (mixtures with mitigation measures). Thomas et al. discussed these tests in detail, and the authors also discussed how the AMBT and CPT methods are different in testing the effectiveness of SCMs controlling ASR expansion [60]. It was concluded that none of the current ASTM methods to evaluate the mitigation measures for ASR are ideal methods due to their limitations. The AMBT is mostly criticized for its severe test conditions, which results in a loss in reliability. The CPT is mainly criticized for its long test duration and its inability to test job mixtures (e.g., capture low-alkali loading mixtures). The authors also concluded that the CPT method is the most reliable ASTM method available currently, and the use of AMBT is possible to determine the required minimum amount of SCM to control ASR expansion as there is a low risk of damaging expansion in the field when the combination of materials pass the AMBT performance criteria [60]. The miniature concrete prism test – MCPT (AASHTO T 380 [61]) is a newer test method, which is also of interest as the preliminary results regarding the prediction of the field performance show promising results in shorter duration (up to 84 days) when compared to the CPT method [62, 63].

Laker and Smartz used PLC with 10-12% interground limestone to evaluate alkali-silica reactivity. ASTM C 1567 was used in the study. They observed that PLC performed similarly to PC in terms of expansions [64].

Thomas et al. [65] tested PLC with 12% interground limestone for its resistance to ASR and compared the results to PC. AMBT (ASTM C1260), CPT, and accelerated concrete prism test (ACPT) were done using alkali-silica reactive Spratt aggregate. ACPT is similar to ASTM C1293, with the exception of storage temperature is 60°C. The authors observed no consistent difference in expansion results produced with PLC compared with OPC [65]. Figure 5-1 shows the reported expansion results of AMBT at 14 days, CPT at one year, and ACPT at three months.

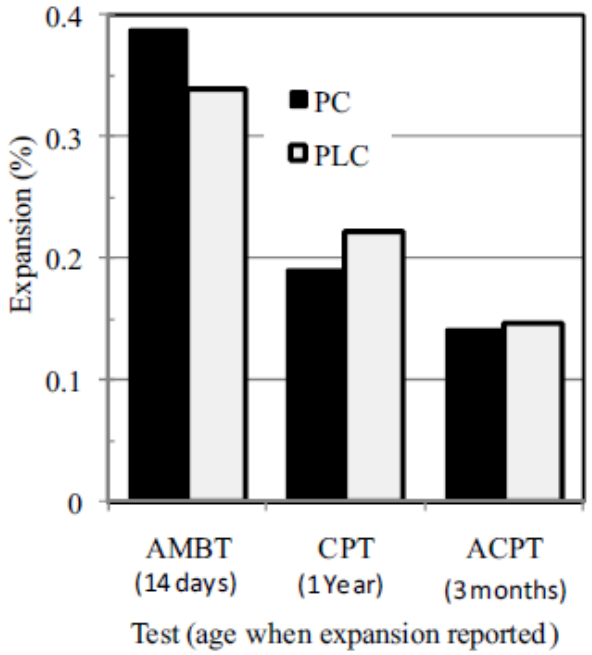

Figure 5-1. Expansion results of mortar and concrete prisms [65]

Hooton et al. [66] compared the performance of three cements with different levels of limestone – 3.5%, 10%, and 15% and labeled as GU (OPC), PLC10, and PLC15, respectively. Both the AMBT and CPT methods were done for various mixes. Figure 5-2 shows the reported AMBT expansions.

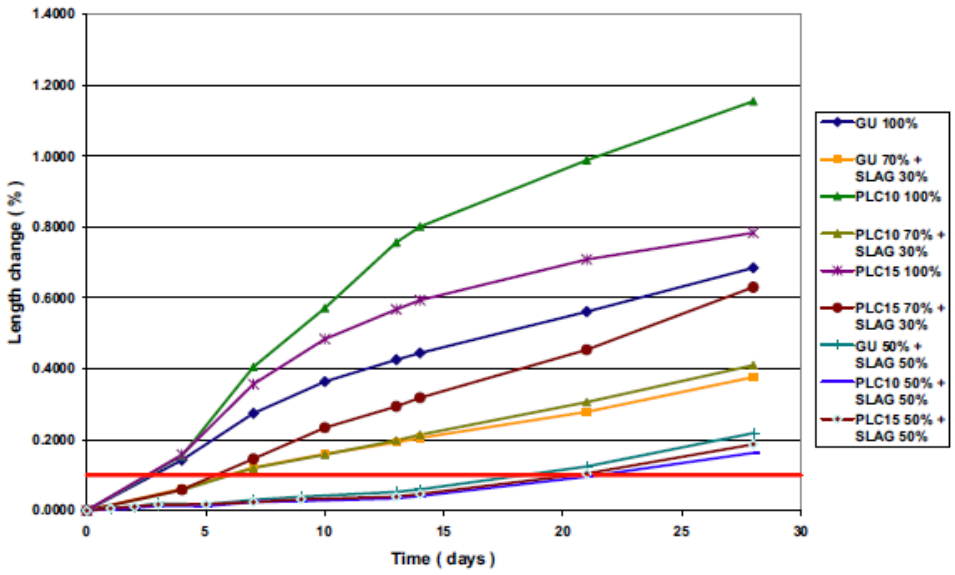

Figure 5-2. AMBT (ASTM C1567) expansions [66]

When no slag was used, none of the mixtures passed the AMBT test, and PLC10 and PLC15 had higher expansions than GU. Even replacing the cements with 30% slag was not sufficient. When 50% of the cements were replaced with slag, all the cements passed the AMBT test. It was observed that both the PLC10 and PLC15 cements had less expansion than the GU cement [66]. Figure 5-3 shows the reported CPT expansions.

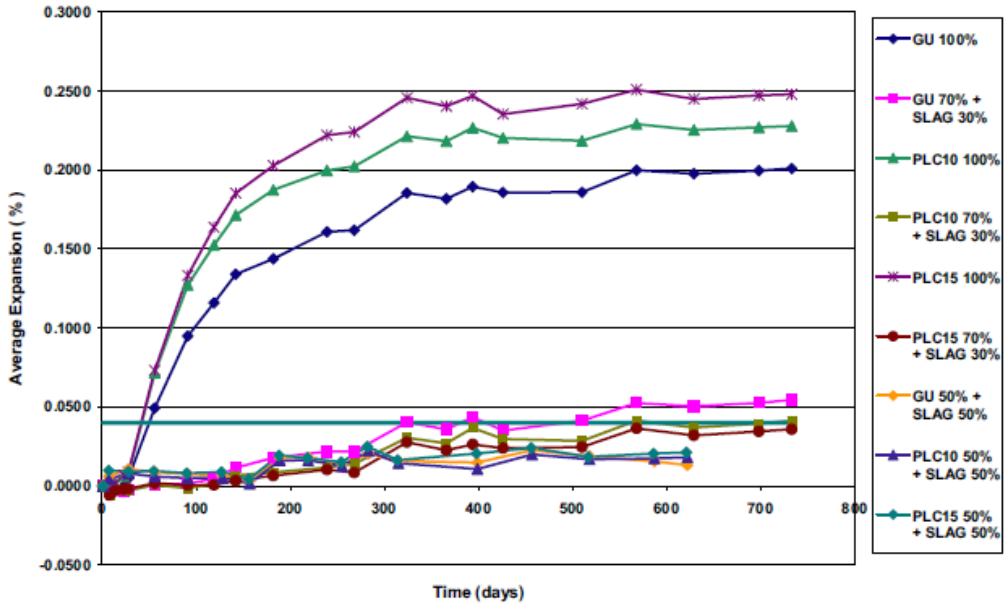

Figure 5-3. CPT (ASTM C1293) expansions [66]

From the CPT results - GU, PLC10, PLC15, GU Slag 30%, and PLC10 Slag, 30% failed the test. Whereas, PLC15 Slag 30%, GU Slag 50%, PLC10 Slag 50%, and PLC15 Slag 50% passed the test with less than 0.04% expansion even after two years. It was observed that expansions were in an increasing order with the limestone content when no SCM was used or in the case of the cements replaced with 50% slag. This was not observed in the case of cements replaced with 30% slag [66].

From this literature review, concrete with PLCs and no SCMs expanded more than their respective 100% OPC. Whereas in the case of mixtures containing SCMs, no consistent difference in expansion results produced with PLC compared with OPC. Therefore, there is a need for study to evaluate the performance of PLCs in the presence of various types of SCMs to verify appropriate SCM contents for ASR prevention.

5.3 Experimental Test Matrix

To evaluate the cements' relative ASR performance in this study, the ASTM C441 [67] test that uses borosilicate glass as fine aggregate was conducted. The testing was divided into two phases. As part of ASTM C441 – phase I, all the received cements were tested. As part of phase II, cement + SCMs were tested. The cements or mixtures tested as part of ASTM C441 - phase II and ASTM C1567 with Bishop fine aggregate are summarized in Table 5.1. The concrete mixtures with SCMs that were tested according to AASHTO T 380 are shown in Table 5.2.

Table 5.1. Experimental matrix for ASTM C441 phase-II and ASTM C1567 testing

Cement	Mixture #	SCM proportions	ASTM C441 phase-II	ASTM C1567	
				F1 fine aggregate	F2 fine aggregate
A_OII	1	25FA1	x	x	-
	2	20FA1-5SF	x	-	-
	3	50SL	x	-	-
	4	25FA1-25SL	x	-	-
	5	25NP	-	x	-
	6	25FA2	x	-	-
A_L15	1	25FA1	x	x	-
	2	20FA1-5SF	x	-	-
	3	50SL	x	-	-
	4	25FA1-25SL	x	-	-
	5	25NP	-	x	-
	6	25FA2	x	-	-
B_OIIV	1	25FA1	x	x	x
	2	20FA1-5SF	x	x	x

	3	**50SL**	x	x	x
	4	**25FA1-25SL**	x	x	x
	5	**25NP**	-	x	-
	6	**25FA2**	x	x	x
B_L15	**1**	**25FA1**	x	x	x
	2	**20FA1-5SF**	x	x	x
	3	**50SL**	x	x	x
	4	**25FA1-25SL**	x	x	x
	5	**25NP**	-	x	-
	6	**25FA2**	x	x	x
B_OIIV+10LS	**1**	**25FA1**	-	x	x
	2	**20FA1-5SF**	-	x	x
	3	**50SL**	-	x	x
	4	**25FA1-25SL**	-	x	x
	5	**25NP**	-	x	-
	6	**25FA2**	-	x	x
C_OV	**1**	**25FA1**	x	-	-
	2	**20FA1-5SF**	x	-	-
	3	**50SL**	-	x	-
	6	**25FA2**	-	-	x
C_L10	**1**	**25FA1**	x	-	-
	2	**20FA1-5SF**	x	-	-
	3	**50SL**	-	x	-
	6	**25FA2**	-	-	x
D_OV	**5**	**25NP**	-	-	x
D_L15	**5**	**25NP**	-	-	x
E_OIIV	**1**	**25FA1**	-	x	-
E_L11	**1**	**25FA1**	-	x	-

566

Table 5.2. Experimental matrix for AASHTO T 380 testing

Cement	Mixture #	SCM proportions	AASHTO T 380	
			F1 fine aggregate	F2 fine aggregate
B_OIIV	1	25FA1	x	-
	2	20FA1-5SF	x	-
	3	50SL	x	-
	4	25FA1-25SL	x	-
	5	25NP	-	x
	6	30FA2	x	x
B_L15	1	25FA1	x	x
	2	20FA1-5SF	x	-
	3	50SL	x	-
	4	25FA1-25SL	x	-
	5	25NP	-	x
	6	30FA2	x	x
B_OIIV+10LS	1	25FA1	x	-
	2	20FA1-5SF	-	-
	3	50SL	x	-
	4	25FA1-25SL	-	-
	5	25NP	-	-
	6	30FA2	x	-

5.4 ASTM C441 - Phase I

5.4.1 Experimental Methods

ASTM C441 [67] is a test method that involves casting mortar bars (25 x 25 x 285 mm) using borosilicate glass with a standard gradation as fine aggregate. This test method is used to assess the relative effectiveness of a potential SCM source to reduce expansion caused by ASR. For this part of the project, ASTM C441 was used to compare PLCs' performance to their respective OPCs as well as PLCs plus SCMs. As the fine aggregate used in this method is borosilicate glass, which is not used in the field mixtures, the test method only indicates the relative performance of the cement with respect to alkali-silica reaction. It does not predict a combination of cementitious material to prevent ASR for a potentially reactive aggregate.

The test method involved casting three mortar bars per mixture. The mortar bars are stored in a vertical position in an air-tight container over water at 38^{o}C. Each container accommodated two mixtures (six bars) per ASTM C441, as shown in Figure 5-4. The total testing period for the method was 14 days. The water to cementitious ratios used for the mixtures were based on the flow test (ASTM C1437) to produce a flow between 100 and 115 as per ASTM C441.

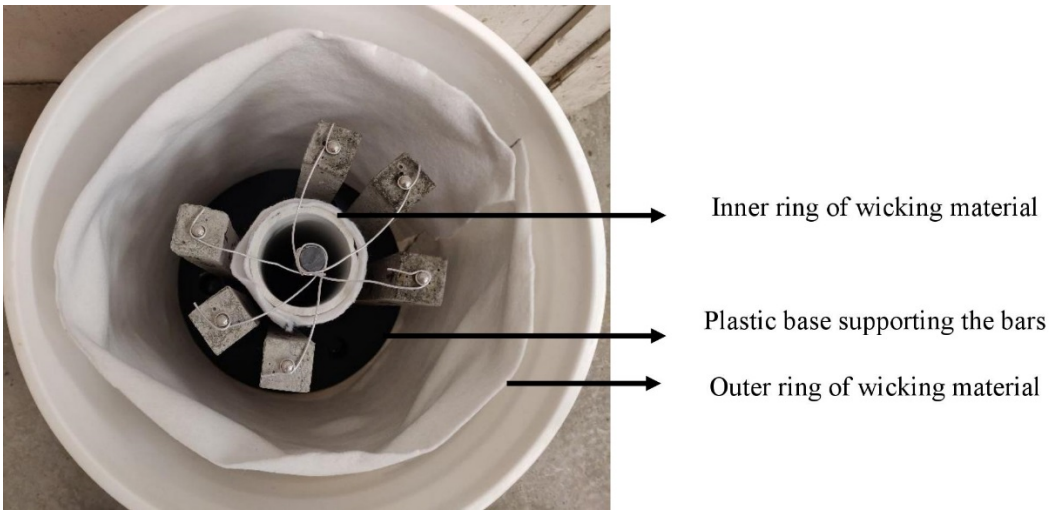

Figure 5-4. Top view of the ASTM C441 set up used

All the received cements were tested using ASTM C441. The test set-up was initially validated using a control set of mortar bars cast with high-alkali cement (0.96% Na_2O_e). The water to cement ratio for all the mixtures were either 0.54 or 0.55 to produce a flow between 100 and 115 according to ASTM C441.

5.4.2 Typical Experimental Measurement and Interpretation

The length and mass measurements were made after demolding (initial measurements) and on the fourteenth day (final measurements). The length measurements were made using a length comparator with an accuracy of 0.0001 in. The measured lengths were used to calculate the expansion of the bars. Then the average expansions of the mixture were calculated and reported.

5.4.3 Experimental Results

Figure 5-5 shows the average 14-day expansion results of the bars with all the cements received from CALTRANS and were tested according to ASTM C441. The expansions of the PLCs were compared to their respective parent OPCs. The percentage reduction in average expansion for each PLC compared to the parent OPC was also reported in the figure.

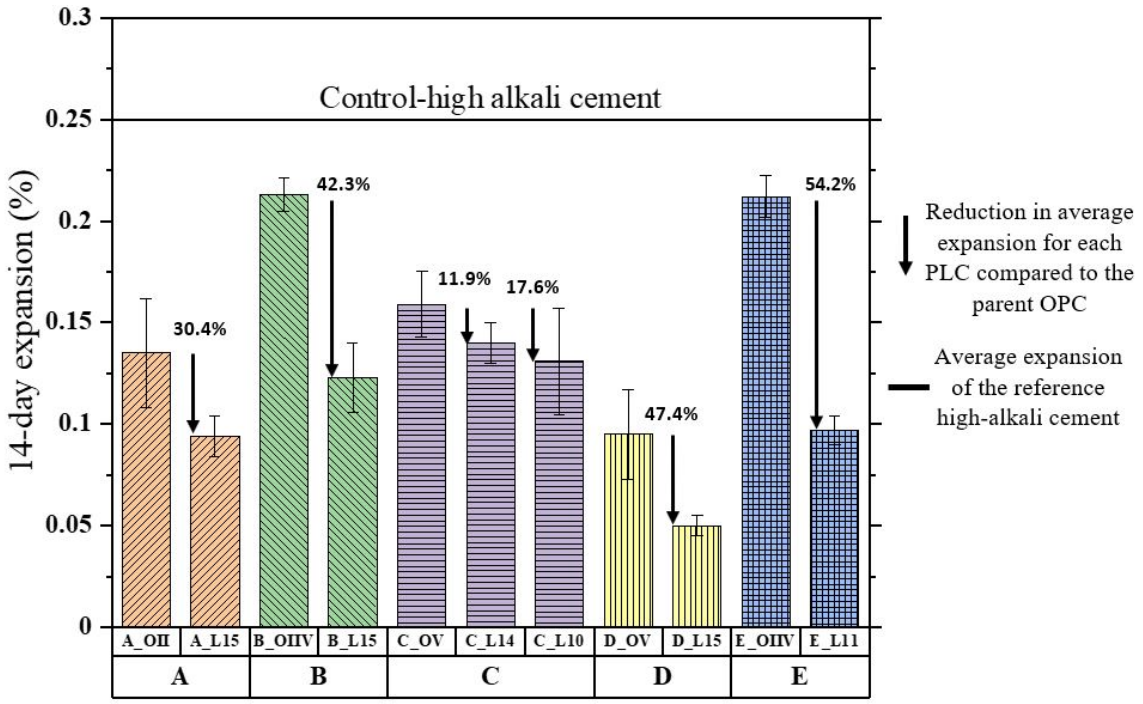

600

601 **Figure 5-5. ASTM C441 - phase I 14-d expansion results of received PLCs and OPCs**

602 Table 5.3 shows the results of ASTM C441 average 14-day expansion, standard deviation of the
603 expansions, maximum allowed according to the standard, and percentage reduction in expansions
604 of the PLCs compared to the parent OPCs.

605 **Table 5.3. ASTM C441 – phase I results**

Mixtures – C441 phase I	Average 14-d expansion (%)	Standard deviation of the expansion (%)	% SD allowance max. (according to ASTM C441)	% reduction in % expansion compared to parent OPC
Control	0.250	0.0359	0.0375	~
A_OII	0.135	0.0270	0.0216	~
A_L15	0.094	0.0100	0.0141	30.4
B_OIIV	0.213	0.0080	0.0319	~
B_L15	0.123	0.0170	0.0184	42.3
C_OV	0.159	0.0160	0.0238	~
C_L14	0.140	0.0101	0.0210	11.9
C_L10	0.131	0.0261	0.0196	17.6
D_OV	0.095	0.0220	0.0142	~
D_L15	0.050	0.0050	0.0075	47.4
E_OIIV	0.212	0.0103	0.0318	~
E_L11	0.097	0.0070	0.0145	54.2

606

607 ### *5.4.4 Discussion of the Results*

608 From Figure 5-5, it is evident that the PLCs performed better than their respective OPCs. All the
609 cements expanded less than the control-high alkali cement, likely due to their lower alkali content
610 than the control high alkali cement. Cement B_IIOV expanded the highest among the CALTRANS
611 cements, likely due to its high alkali content among the received cements. It was observed that all
612 the mixtures except A_OII, C_L10, and D_OV had met the maximum allowed standard deviation
613 limit in ASTM C441. It should be noted that the precision and bias statement for ASTM C441
614 was done with high alkali cement (0.95 to 1.05% Na_2O_e) and not for cements with finely ground
615 limestone.

616 ### *5.4.5 Significant Findings*

617 The main take away from the Phase I ASTM C441 testing is that the PLCs performed better than
618 their respective OPCs in reducing ASR associated expansion. PLCs with similar amounts of finely
619 ground limestone also performed comparably to each other (i.e., the OPC and OPC+LS had similar
620 performance). As a result, this allowed us to move forward with a smaller number of PLCs in
621 Phase II to focus on the evaluation of SCMs in conjunction with PLCs.

5.5 ASTM C441 – Phase 2

5.5.1 Experimental Methods

The experimental method is the same as described for the ASTM C441 – Phase I. ASTM C441 – Phase II involves testing the mixtures with SCMs. This test aims to determine if the PLCs perform equal or better than their respective OPCs when a portion of the PLC is replaced with SCMs.

5.5.2 Typical Experimental Measurement and Interpretation

The length and mass measurements were made after demolding (initial measurements) and on the fourteenth day (final measurements). The length measurements were made using a length comparator. The measured lengths were used to calculate the expansion of the bars. Then the average expansions of the mixture were calculated and reported.

5.5.3 Experimental Results

Figure 5-6 to Figure 5-10 show the results of ASTM C441 - phase II. For an even comparison, efforts were made to maintain the same water to binder ratio for a PLC and its parent OPC. Please note that HA stands for high-alkali cement (0.96% Na_2O_e) and was used as a control per ASTM C441.

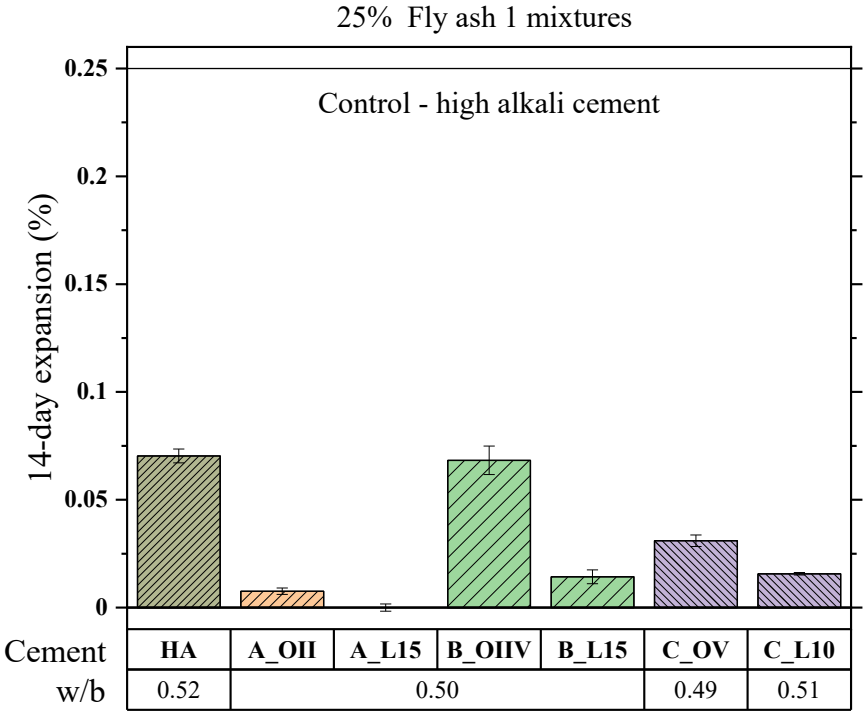

Figure 5-6. ASTM C441 results for 25% FA1 mixtures

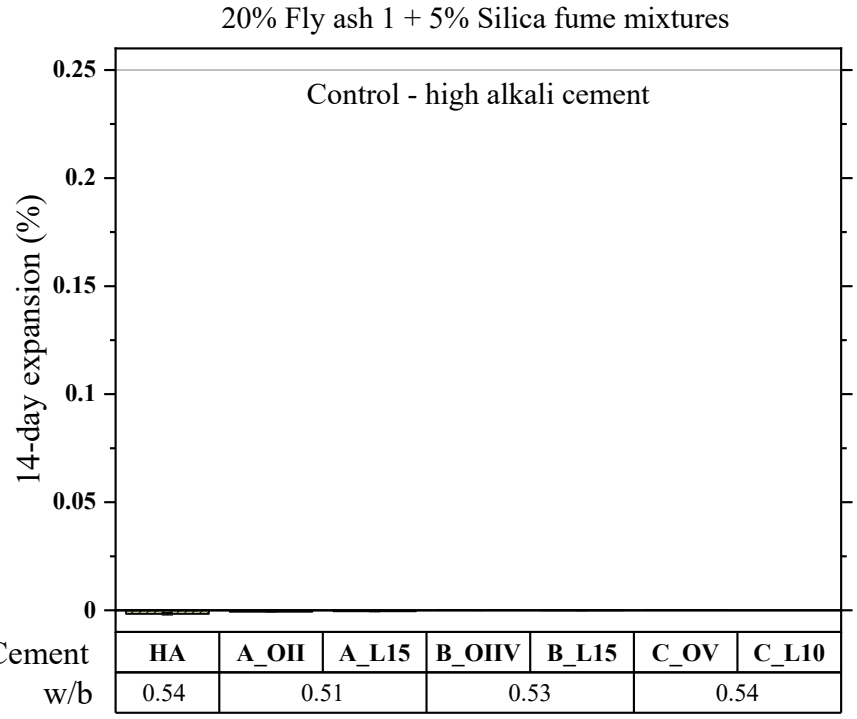

Figure 5-7. ASTM C441 results for 20% FA1 + 5% silica fume mixtures

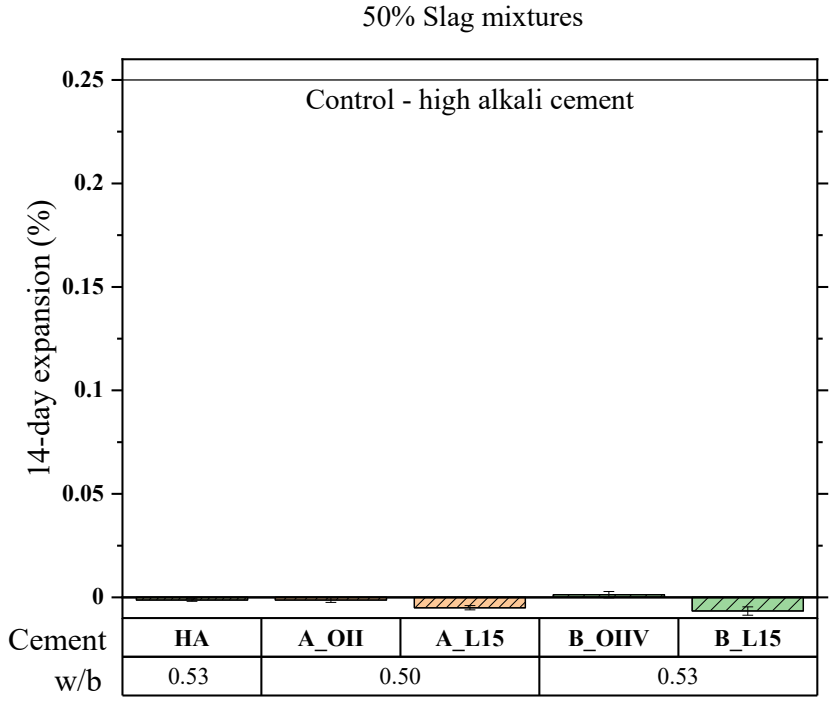

Figure 5-8. ASTM C441 results for 50% slag mixtures

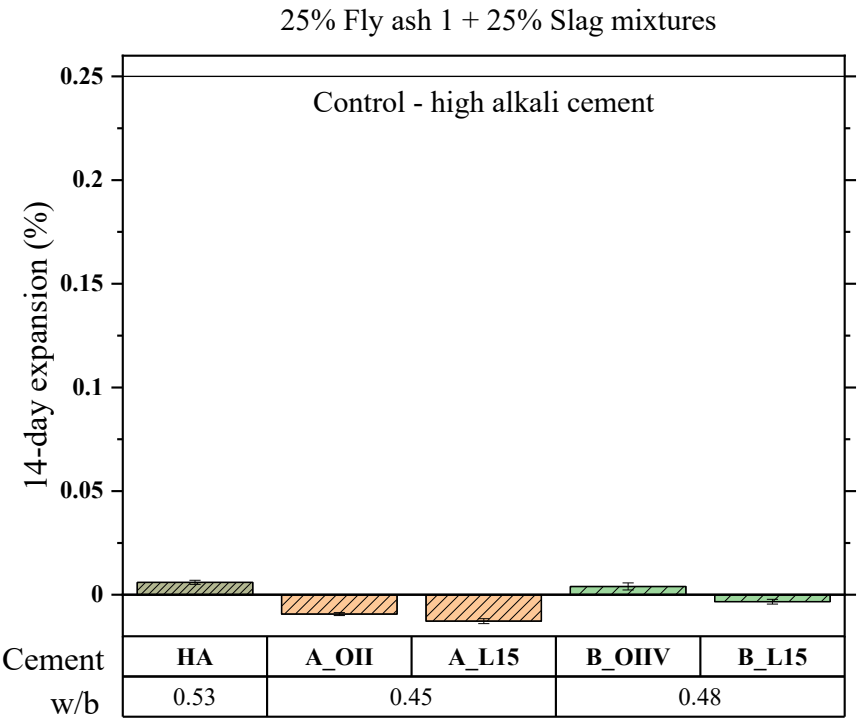

643

644 **Figure 5-9. ASTM C441 results for 25% FA1 + 25% slag mixtures**

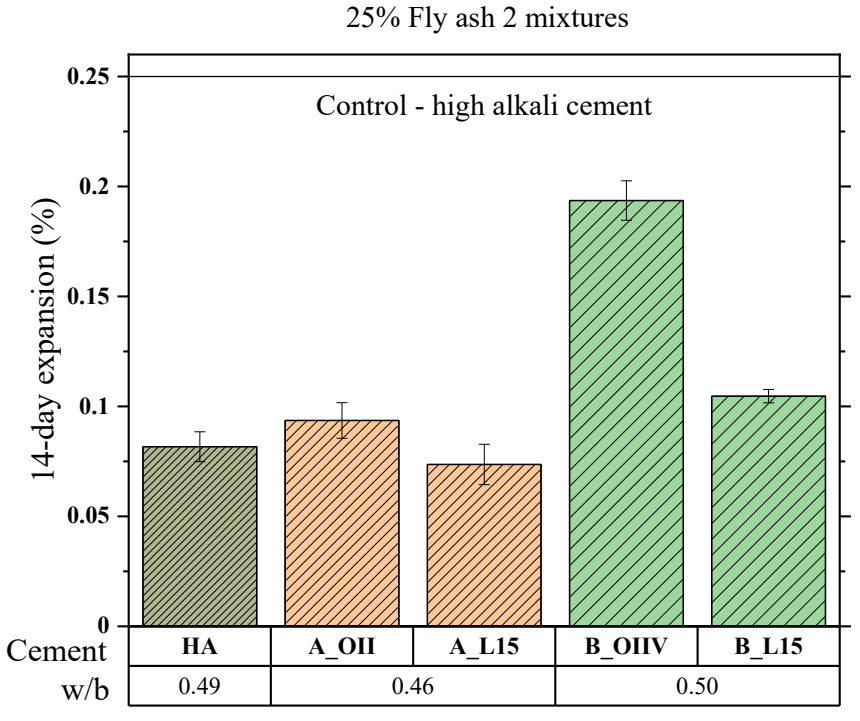

645

646 **Figure 5-10. ASTM C441 results for 25% FA2 mixtures**

5.5.4 Discussion of the Results

In all the cases, the expansions of the mixtures (with SCMs) were less than the control – high alkali cement (with no SCM). It was observed that all the PLCs performed better than their respective OPCs in the presence of SCMs.

5.5.5 Significant Findings

The main takeaway from the ASTM C441 testing is that all the PLCs performed better than their respective OPCs in the presence of SCMs. Further, there was generally good agreement among the PLCs. This allowed for the selection of a smaller number of PLCs to test in Phase 2 of the project, as decided at the November 2019 project meeting.

5.6 ASTM C1260 – Phase 2

5.6.1 Experimental Methods

ASTM 1260 [58] is a standard test method for detecting potential alkali reactivity of aggregates in mortar bars. Mortar bars of dimensions 25 x 25 x 285 mm are prepared according to ASTM C1260. It involves immersion of mortar bars in 1N NaOH solution at 80°C for 14 days. Each test container contains four bars soaked in 1N NaOH solution, as shown in Figure 5-11. To test coarse aggregates, they are crushed to meet the required gradation stated in the standard.

Figure 5-11. ASTM C1260 mortar bars immersed in 1N NaOH solution in a test container; note that the length of each prism is 285 mm for scale.

5.6.2 Typical Experimental Measurement and Interpretation

The length and mass measurements were made before immersing the bars in sodium hydroxide solution (initial measurements) and various days after immersion until fourteen days. The length measurements were made using a length comparator. The measured lengths were used to calculate the expansion of the bars. Then the average expansions of the mixture were calculated and reported. Based on the average 14-day expansion of the mixture, the aggregate reactivity was determined according to ASTM C1778 [68].

5.6.3 Experimental Results

A selection of reactive aggregates from four potential sources was collected. Table 5.4 shows the results of the ASTM C1260 [58] testing. Table 5.5 shows the estimated major constituents in the reactive fine aggregates determined using petrographic analysis according to ASTM C295 done by an independent testing firm.

Table 5.4. ASTM C1260 results

No.	Type of aggregate	Source	ASTM C1260 14-day average expansion (%)	ASTM C1778 classification
1	**Fine (F1)**	S1	0.54	R3 Very highly-reactive
2	**Fine (F2)**	S2	0.47	R3 Very highly-reactive
3	**Coarse (C1)**	S2	0.33	R2 Highly-reactive
4	**Coarse (C2)**	S3	0.24	R1 Moderately-reactive

680 **Table 5.5. Estimated major constituents in the reactive fine aggregates by petrographic**
681 **examination**

Constituent	Approximate % by weight
Fine aggregate – 1 (F1)	
Granitic Rock	44.7
Quartz	17.6
Feldspar	16.3
Diorite	8.8
Volcanic Rock	6.4
Fine aggregate – 2 (F2)	
Intermediate Volcanic Rock	59.2
Intermediate Volcanic Rock (Oxidized)	12.1
Felsic Volcanic Rock	12.6
Feldspar	4.4
Quartz	2.3
Granitic Rock	1.7

682

683 F1 aggregate was primarily comprised of granitic rock, diorite, and volcanic rock as well as quartz
684 and feldspar mineral grains. The strained quartz and volcanic glass contained within the aggregate
685 were identified as being potentially susceptible to ASR. F2 aggregate was primarily comprised of
686 volcanic rock fragments of intermediate to felsic composition, with minor to trace amounts of
687 granitic rock fragments and individual mineral grains including quartz, feldspar, pyroxene,
688 amphibole, biotite, and opaques. The volcanic rock fragments predominate throughout the various
689 size fractions. The microcrystalline quartz and/or volcanic glass were identified as the greatest
690 potential contributors to ASR.

691 ### *5.6.4 Discussion of the Results*

692 Fine aggregates – F1 and F2, which both are very-highly reactive fine aggregate, were selected to
693 use and study for this project.

694 ### *5.6.5 Significant Findings*

695 It was decided between OSU and CALTRANS Project Leaders to use the two fine aggregates
696 investigated for the remainder of the reactive aggregate assessment.

697 ## 5.7 ASTM C1567 – Phase 2

698 ### *5.7.1 Experimental Methods*

699 ASTM C1567 [58] is used to evaluate the effectiveness of SCMs to mitigate or control ASR
700 expansion. The sample preparation procedure and the testing procedure for ASTM C1567 is the

same as for ASTM C1260. The only difference is that a portion of the OPC is replaced with the desired amount, by mass, of SCM or a combination of SCM (e.g., fly ash + silica fume) to be evaluated.

5.7.2 Typical Experimental Measurement and Interpretation

The experimental measurement and interpretation are the same as for ASTM C1260. If the average 14-day expansion of a mixture is less than 0.10%, it is considered that the SCM dosage effectively mitigates deleterious ASR expansion.

5.7.3 Experimental Results

Figure 5-12 and Figure 5-13 show the results of ASTM C1567 for all the mixtures tested with F1 aggregate. Figure 5-14 shows the results of ASTM C1567 for all the mixtures tested with F2 aggregate.

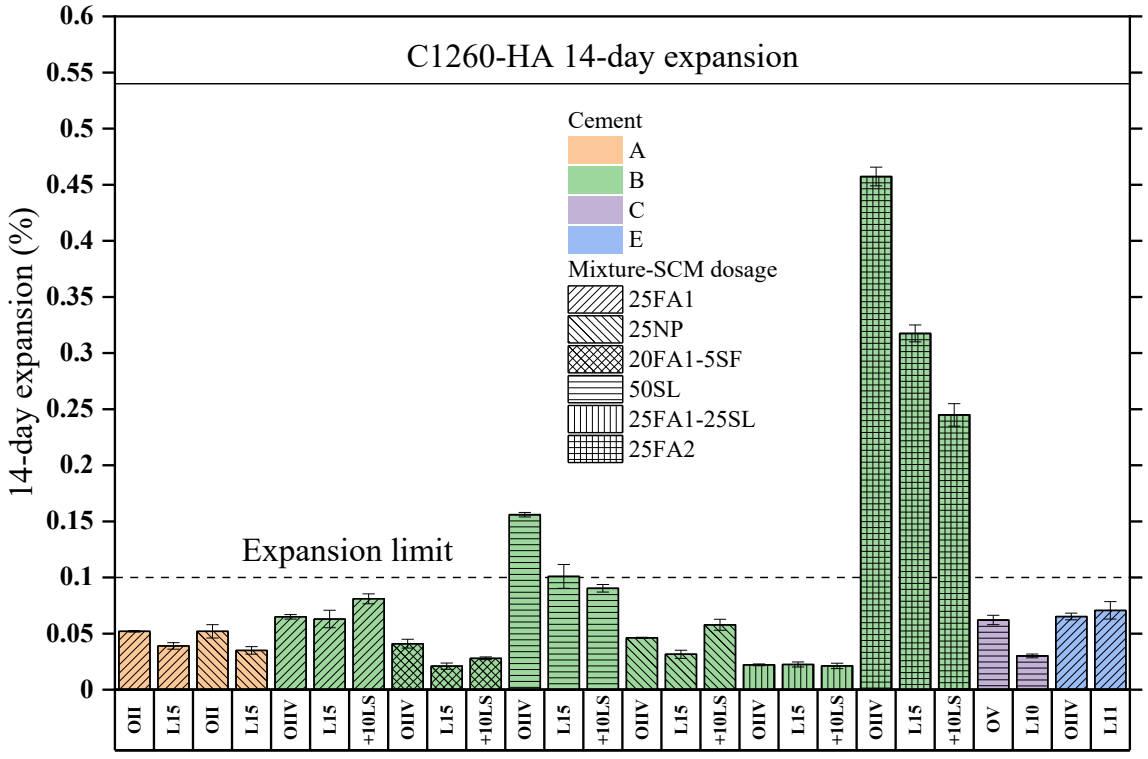

Figure 5-12. ASTM C1567 results comparing the expansions of OPCs, PLCs, and OPC + 10% LS systems with F1 aggregate (very-highly reactive as per ASTM C1778)

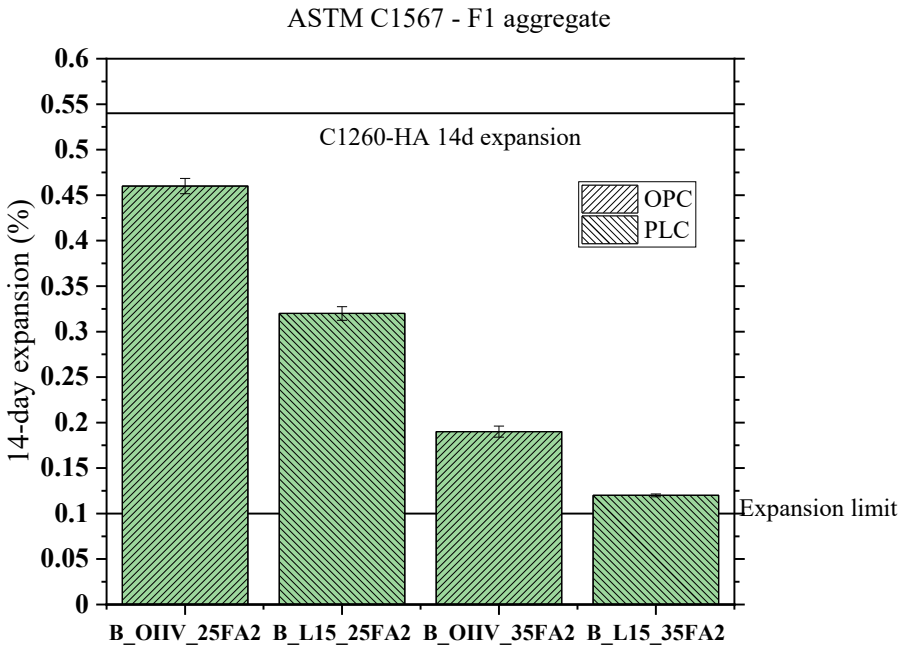

716

717 **Figure 5-13. Comparison of ASTM C1567 expansions of mixtures with F1 aggregate and**
718 **cements B_OIIV and B_L15 with 25% and 35% FA2.**

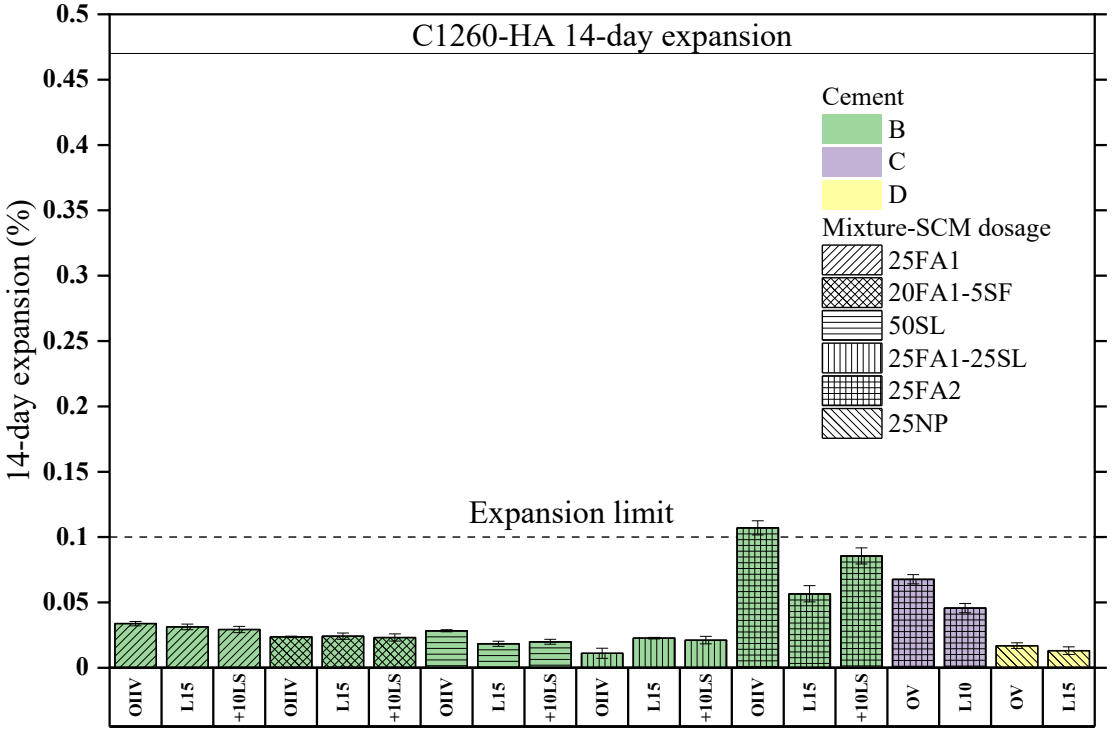

719

720 **Figure 5-14. ASTM C1567 results comparing the expansions of OPCs, PLCs, and OPC +**
721 **10% limestone systems with F2 aggregate (very-highly reactive as per ASTM C1778)**

5.7.4 Discussion of the Results

Figure 5-12 shows that the use of SCMs significantly reduced the expansion of the mortar bars. PLCs performed equal or better than the parent OPCs. All the mixtures expanded less than expansion limit of 0.10% except the 50% slag (B_OIIV_50SL, B_L15_50SL) and 25% FA2 (B_OIIV_25FA2, B_L15_25FA2, B_OIIV_25FA2 + 10LS) mixtures that included cement B. The blended OPC + 10% limestone systems expanded equal or more than the PLCs except in the 50% slag mixture and 25% FA2 mixtures of cement B. In most cases, OPC + 10% LS mixtures performed equal or better than their parent OPCs, and their expansions were lower than the expansion limit in the cases where they had more expansion than the parent OPCs.

Figure 5-13 shows that increasing the replacement level of FA2 from 25% to 35% decreased the expansions considerably. However, even at 35% FA2, the mortar bars failed the ASTM C1567 test. Nevertheless, it should be noted that B_L15 performed better than B_OIIV with both 25% and 35% FA2.

Figure 5-14 observed that the use of SCMs significantly reduced the expansion of the mortar bars. All the mixtures expanded less than the expansion limit of 0.10% except B_OIIV_25FA2. Similar to the case for F1 aggregate, 25FA2 mixtures expanded the most among the SCM mixtures. The PLCs and the blended OPC + 10% limestone systems expanded equal or less than the parent OPCs with an exception of B_OIIV_25FA1-25SL mixture. It was observed that B_OIIV_25FA1-25SL expanded slightly less than its limestone cements. However, the expansions of all the three mixtures of B_25FA1-25SL were very low, and the difference in the expansions was negligible compared to the expansion limit.

Among all the mixtures with SCMs, the mixtures with FA2 expanded the most. This could be due to its higher alkali content (4.0% Na_2O_e) and CaO (12.5%) content compared to FA1 (3.5% Na_2O_e and 8.6% CaO). In addition, it should be noted that one of the other important factors for controlling ASR related expansion is using SCMs that are high in alumina. FA2 (16.6% Al_2O_3) has a considerably lower Al_2O_3 content compared to FA1 (21.7% Al_2O_3), and this likely accounts for the higher expansion observed at the same replacement level of 25%. If this ash were to be used with this very highly reactive fine aggregate, a higher replacement level would be needed and could be verified through ASTM C1567 testing. It may also be effective in a ternary blend with 5% silica fume or metakaolin while retaining the 25% replacement level. However, further performance-based testing would be needed to determine that amount.

According to CALTRANS specifications, fly ash complying with AASHTO M 295, Class F, and **either** of the following shall be used:

- Available alkali as Na_2O + 0.658 K_2O must not exceed 1.5 percent when tested under ASTM C311.

- Total alkali as $Na_2O + 0.658\ K_2O$ must not exceed 5.0 percent when tested under AASHTO T 105.

Both FA1 and FA2 have total alkali content less than 5.0% Na_2O_e, thus complying with the second requirement. The available alkali (ASTM C311) of the ashes are not determined as part of this project. There exists a linear correlation between total equivalent alkali and available alkali (ASTM C311), as shown in Figure 5-15. The data in Figure 5-15 were collected from literature [69, 70] to determine the correlation between available alkali and total alkali for Class F fly ashes. The calculated available alkali (ASTM C311) for FA1 and FA2 according to the equation in Figure 5-15 were 1.4% Na_2O_e (<1.5% limit) and 1.7% Na_2O_e (>1.5% limit), respectively. This indicates that FA2 contributed higher alkali compared to FA1.

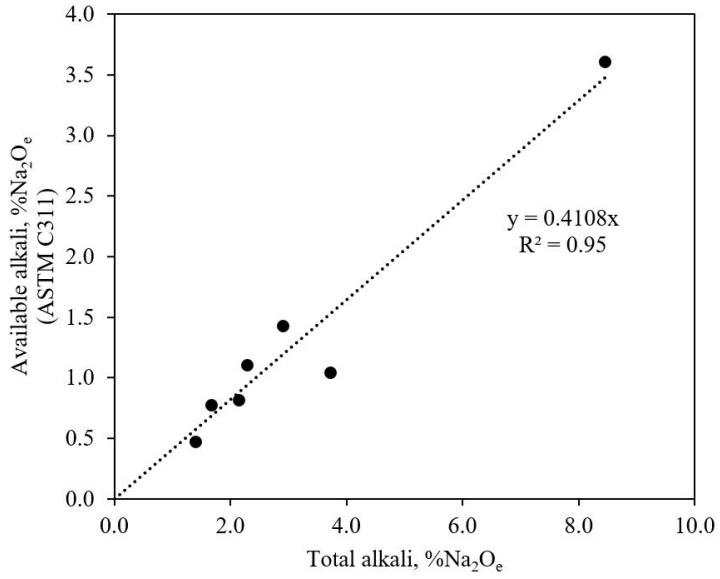

Figure 5-15. Correlation between available alkali (ASTM C311) and total alkali of Class F fly ashes (Data from [69] and [70]).

To further confirm the contribution of alkalis from FA2 to pore solution, cement pastes were cast in 50 mm (diameter) x 100 mm (length) cylinder molds and were sealed cured for 28 days at 23°C. After the curing period, the cylinders were demolded, and the specimens were squeezed in a pore press to extract the pore solutions. The extracted pore solutions were filtered and analyzed using ICP-OES to determine their ion compositions. Figure 5-16 shows the sum of sodium and potassium ion concentrations in the pore solutions of hardened cement pastes (for the materials in this project) that were sealed cured at 23°C for 28 days.

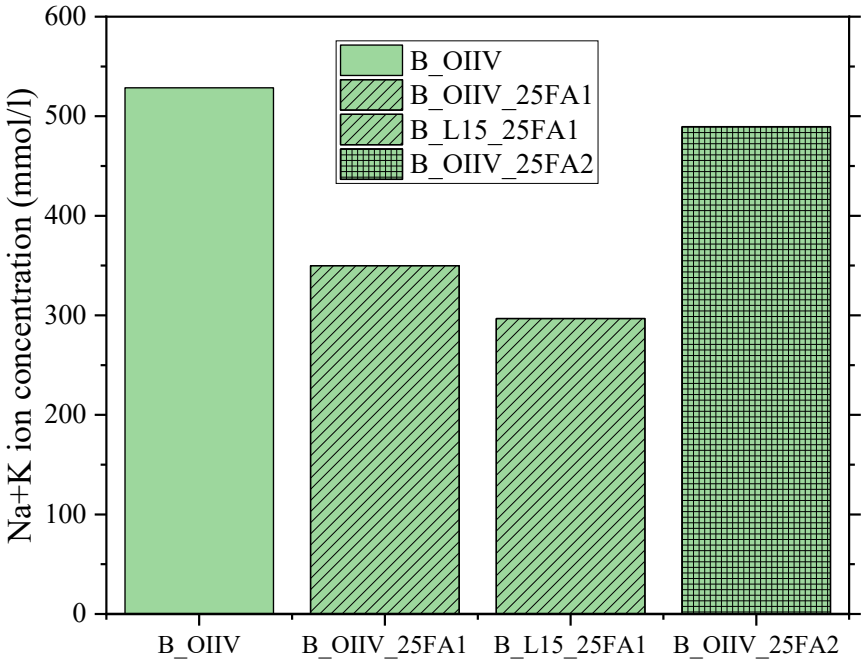

Figure 5-16. Sum of sodium and potassium ion concentrations in the pore solutions of hardened cement pastes that were sealed cured at 23ºC for 28 days for the materials in this project

It was observed that pore solution alkalinity of B_OIIV_25FA2 is higher than B_OIIV_25FA1 giving further evidence that FA2 provides more alkalis to pore solution than it binds, and it has higher available alkali than FA1.

5.7.5 Significant Findings

The main take away from the C1567 testing is that the PLCs perform similar to or better than their parent OPCs. In addition, it was observed that the presence of all SCMs reduced expansions compared to the control for all the mixtures. This resulted in the majority of the mixtures (39 of 45) being below the 0.10% expansion limit with the six exceptions, as noted in section 5.7.4.

5.8 AASHTO T 380 (Miniature Concrete Prism Test)

5.8.1 Experimental Methods

The miniature concrete prism test (MCPT) is a recently developed test method by Latifee and Rangaraju [71] to overcome the limitations of the AMBT and the CPT. The method was recently standardized by AASTHO, and it is available as AASHTO T 380. The MCPT involved casting concrete bars of dimensions 50mm x 50mm x 285mm with w/cm of 0.45 according to AASHTO T 380. F1 and F2 reactive aggregates were used as fine aggregate, and a non-reactive limestone aggregate was used as a coarse aggregate in the study. The coarse aggregate consisted of 9.5 mm

sieve retained rock (57.5% by mass) and 4.8 mm sieve retained rock (42.5% by mass). The alkali content of the mixture was boosted to 1.25% of the cement mass according to the standard. The concrete bars were immersed in 1N sodium hydroxide solution (as shown in Figure 5-17) and stored at 60ºC for a period of 56 days, and the expansions were monitored periodically.

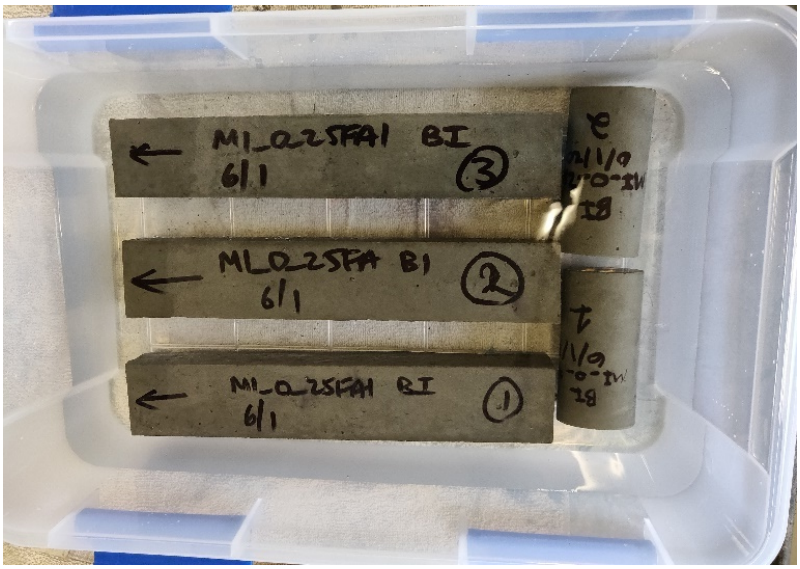

Figure 5-17. Top view of the MCPT specimens immersed in 1N NaOH solution

5.8.2 Typical Experimental Measurement and Interpretation

The length and mass measurements were made before immersing the bars in sodium hydroxide solution (initial measurements) and various days after immersion until 84 days. The length measurements were made using a length comparator. The measured lengths were used to calculate the expansion of the bars. Then the average expansions of the mixture were calculated and reported. The criteria for determining the efficacy of SCMs in preventing ASR expansion according to AASHTO T 380 are:

- ineffective if the 56-day average expansion greater than 0.025%
- effective if the 56-day average expansion is less than 0.020%
- uncertain if the 56-day average expansion is in between 0.020% and 0.025%

5.8.3 Experimental Results

Figure 5-18 and Figure 5-19 show the AASHTO T 380 expansion results at 56 days for the mixtures with F1 and F2 aggregates, respectively.

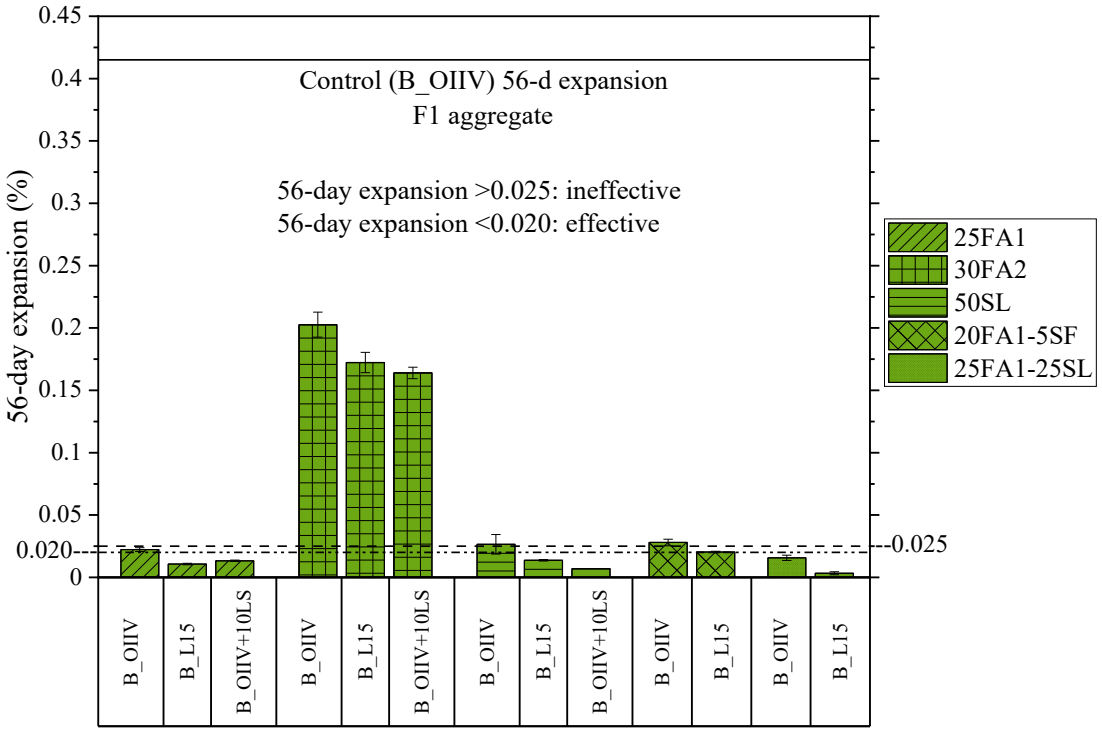

816

817 **Figure 5-18. 56-day AASHTO T 380 expansion results of the mixtures with F1 aggregate**
818 **and portland cement B**

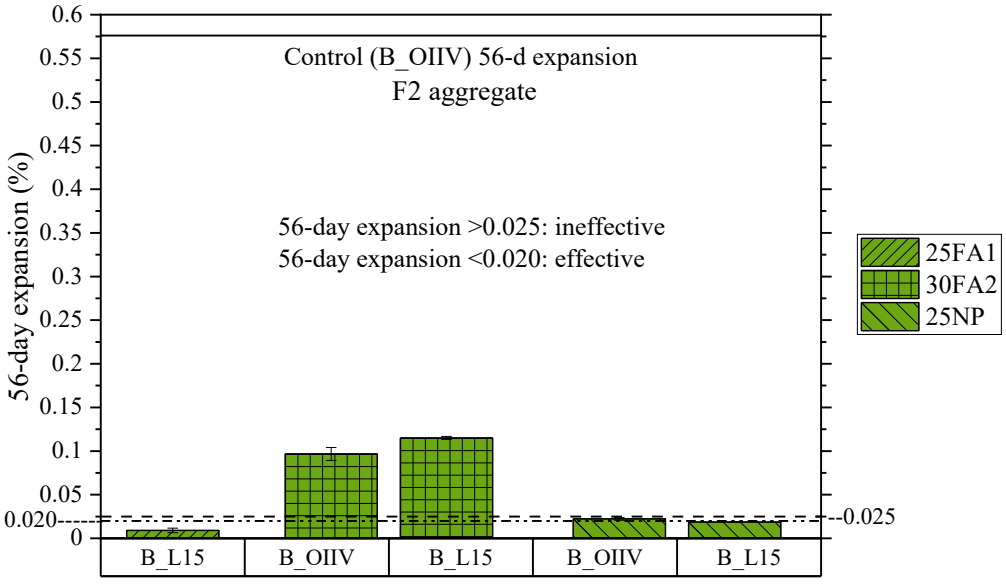

819

820 **Figure 5-19. 56-day AASHTO T 380 expansion results of the mixtures with F2 aggregate**

821

5.8.4 Discussion of the Results

Figure 5-18 shows that the use of SCMs significantly reduced the expansions compared to the control mixture with F1 aggregate. All the concrete mixtures with PLCs (interground and added limestone) expanded lower than the mixtures with the parent OPCs. The percentage reduction in the expansions of the mixtures with PLCs ranged from 15% to 79% with respect to their parent OPC mixture in combinations with SCMs. In the case of the mixtures with 50% slag, the outcome of the test method (effective or ineffective) varied based on the presence of OPC or PLC in the mixture. Similar to the observation made from the ASTM C1567 results, the mixtures with 25FA1-25SL expanded the least, and the mixtures with FA2 expanded the most among the SCM combinations tested and failed in AASHTO T 380.

From Figure 5-19, it was observed that the concrete mixtures with F2 aggregate and SCMs performed better than the control mixture as expected. It was observed that the B_L15-30FA2 mixture expanded slightly more than the B_OIIV-30FA2 mixture. However, both the mixtures with 30FA2 failed the test due its higher alkali content and lower alumina content. Either a higher replacement of FA2 or a ternary blend of FA2+(SCM) would be needed to reduce expansions below the expansion limit. It was observed that B_L15-25NP mixture expanded 14% less than B_OIIV-25NP mixture.

5.8.5 Significant Findings

The main take away from AASHTO T 380 testing is that the PLCs perform similar to or better than their parent OPCs. The only exception observed was the mixture with 30FA2 and F2 aggregate, where the PLC mixture expanded slightly higher than the OPC mixtures; however, both the mixtures failed the test.

5.9 ASTM C1293 (Concrete Prism Test)

5.9.1 Experimental Methods

ASTM C1293 is a standard test method for detecting potential alkali reactivity of aggregates in concrete bars and determining the efficiency of SCMs to prevent ASR. In this study, ASTM C1293 test was used to determine the aggregate reactivity level of F1 and F2 aggregates. Concrete bars of dimensions 75 x 75 x 285 mm are prepared according to ASTM C1293. A non-reactive limestone aggregate was used as a coarse aggregate in the study. The coarse aggregate consisted of 12.5 mm sieve retained rock (33.3% by mass), 9.5 mm sieve retained rock (33.3% by mass) and 4.8 mm sieve retained rock (33.3% by mass). The alkali content of the mixture was boosted to 1.25% of the cement mass according to the standard. It involved storage of concrete bars in sealed buckets over water at 38^{o}C for a period of one year. Each test container contained three bars.

5.9.2 Typical Experimental Measurement and Interpretation

The length and mass measurements were made before storing the bars in sealed buckets (initial measurements) and periodically after that as mentioned in ASTM C1293. The length measurements were made using a length comparator. The measured lengths were used to calculate the expansion of the bars. Then the average expansions of the mixture were calculated and reported. The criteria for determining the alkali reactivity of aggregates according to ASTM C1778 is

- Non-reactive if the 1-year average expansion is less than 0.04%
- Moderately reactive if the 1-year average expansion is less than 0.12% and greater than or equal to 0.04%
- Highly reactive if the 1-year average expansion is less than 0.24% and greater than or equal to 0.12%
- Very highly reactive if the 1-year average expansion is greater than or equal to 0.24%

5.9.3 Experimental Results

Figure 5-20 shows the expansion results of all the four mixtures tested according to ASTM C1293.

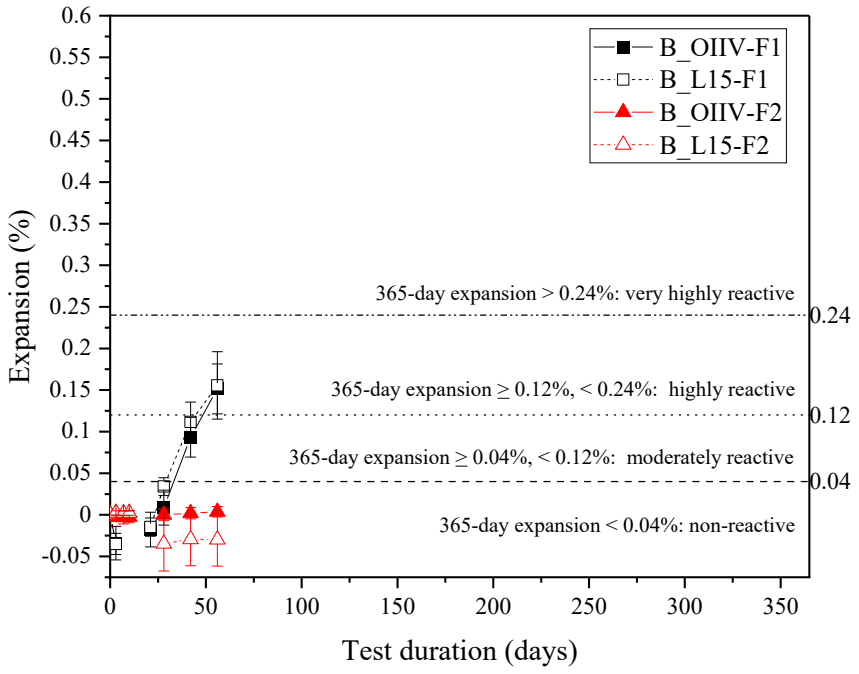

Figure 5-20. ASTM C1293 expansion results (Note: the total test duration is 365 days)

5.9.4 Discussion of the Results

The total test duration of ASTM C1293 method to classify the reactivity of aggregates is 365 days. The mixtures have been monitored for only 56-days at the time of writing the report. The reactivity of F1 and F2 aggregates will be determined according to ASTM C1778 after 365 days of monitoring the specimens.

5.9.5 Significant Findings

While testing for ASTM C1293 is still in progress and a final conclusion cannot be drawn, at the time report has been issued, it can be noticed that the PLC behaves similarly to the OPC system for both the reactive aggregates. As such, the preliminary indication suggests that the aggregate reactivity level is expected to be similar for both the OPC and PLC systems.

6 Shrinkage and Restrained Shrinkage Cracking

Drying shrinkage occurs primarily due to the capillary pressure that develops as fluid leaves the cement paste pores. The Kelvin-Laplace-Young equation [72] states that as the size of a pore is reduced, the capillary pressure that would develop increases, which would result in increased shrinkage. Many state highway agencies have been concerned that the increased fineness of PLC may make mixtures made using PLC more susceptible to shrinkage and shrinkage cracking than those made with OPC [73, 74]. This portion of the research investigated the shrinkage for paste made using OPC, PLC, and OPC+ LS for both plain mixtures (M0) and systems containing SCM (M1 to M5).

6.1 Research Objective

This portion of the research's primary objective was to determine whether the replacement of OPC with PLC or OPC with OPC + LS in conjunction with SCMs impacts cement paste shrinkage. This will be evaluated using ASTM C157. Ultimately, this research will inform CALTRANS whether PLC can be used as an equivalent replacement of OPC without impacting the shrinkage and cracking performance. This would enable language to be added to the specifications, if deemed necessary, stating what aspects would need to be measured through trial batches using the actual mixture design and raw materials if PLC is used.

6.2 Background/Literature Review

Some state highway agencies are concerned that the increased fineness associated with the PLC's manufacture may mixtures made using PLC more susceptible to shrinkage and shrinkage cracking [5, 57, 75, 76]. Previous studies on PLC shrinkage have also provided mixed results related to the PLC shrinkage compared to an OPC made from the same clinker. Adams and Race [77] reported that limestone addition increased the drying shrinkage of type I and type II cements. However, this study is nearly 20 years old, and as a result, the PLC that was used had been made using a fundamentally different approach than the current approach. Some studies have reported that the addition of limestone does not affect or reduces overall shrinkage in concrete. Alunno-Rossetti and Curcio [15] produced comparable concrete mixtures using two sets of OPC and PLC (produced at two different plants) and observed their creep and shrinkage behavior for one year. They noted that OPCs and their respective PLCs exhibited essentially the same shrinkage rate and total drying shrinkage for one year. Stubstad et al. [75] measured shrinkage and shrinkage cracking of mixtures with up to 5% limestone and observed less shrinkage in the OPC cements. Dhir et al. [11] compared OPC concrete with comparable PLC concretes (310 kg/m^3 and w/cm = 0.60) and reported marginal reduction in shrinkage for concretes produced with ground limestone (15% to 45%). Cost [78] and Smartz and Lankar [3] reported similar shrinkage in OPC and PLC systems (however, detailed data was not provided). As a result, it appears that, in general, the OPC and PLC have similar shrinkage; however, this can be dependent on the fineness of the cement and

limestone. Bucher et al. [73, 74] measured autogenous shrinkage, unrestrained shrinkage, and restrained drying shrinkage of mortars produced using three cements (with an OPC with 0%, a PLC with 5%, and a PLC with 10% LS) as shown in Figure 6-1. The tests concluded that both autogenous and unrestrained shrinkage in mortar samples were slightly less with increasing limestone content. Bucher et al. [73, 74] examined the addition of limestone of different fineness to OPC as a replacement to evaluate the shrinkage cracking. Bucher et al. [73, 74]observed that the coarser limestone had a slower rate of stress development and a longer time to develop the first restrained shrinkage crack. However, it should be noted that the study by Bucher et al. [73, 74] was not on PLC that was designed to be 'equivalent' OPC in terms of strength development. They also noted that the coarser limestone had a slower rate of stress development, and thus addition of limestone also increased the time to cracking slightly compared to OPC mortar (Figure 6-2). Piasta and Sikora [79] examined the shrinkage of concrete with limestone cements combined with SCMs and concluded that SCMS were useful in reducing shrinkage. Similar observations have been reported by Barrett et al. [2, 76] (Figure 6-3). Bentz et al. [80] attributed the reduced shrinkage in PLC mortars to the differences in particle size distributions of constituents.

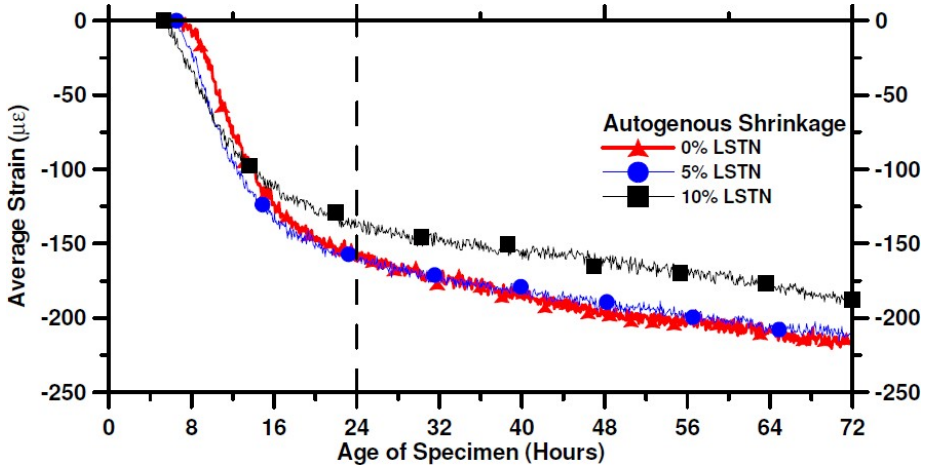

(a)

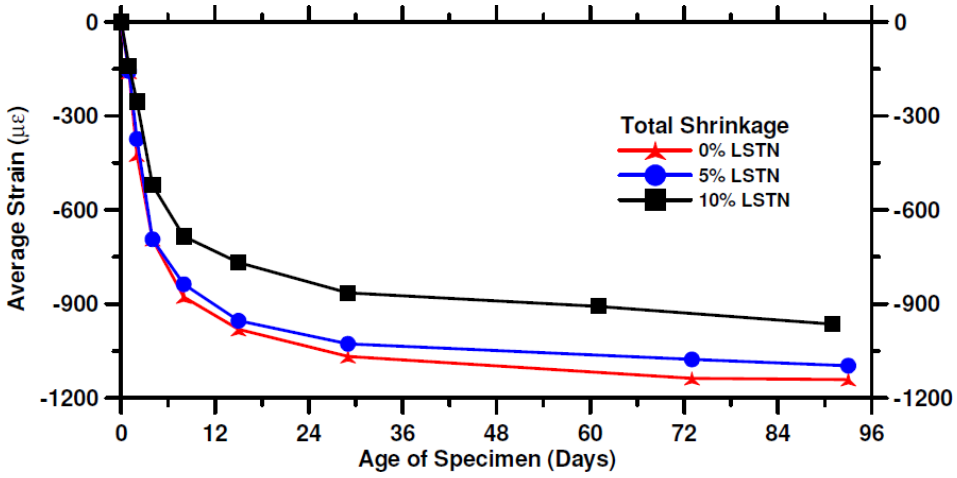

(b)

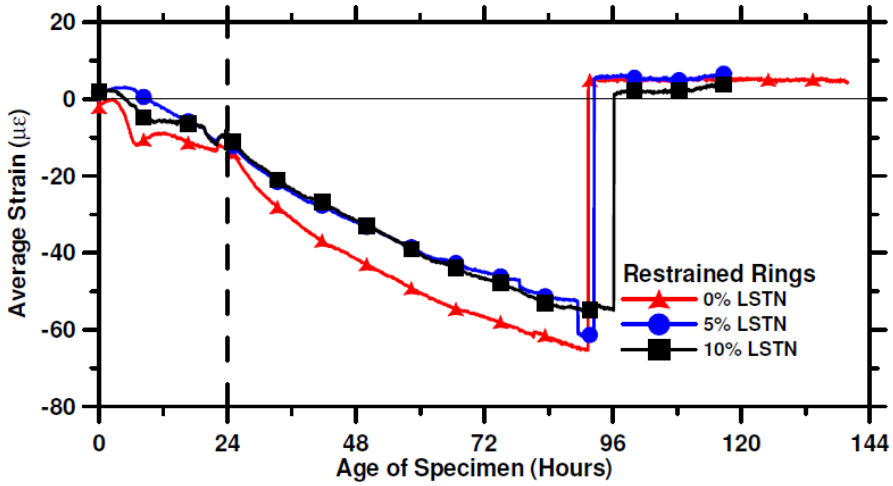

(c)

935 **Figure 6-1. (a) Autogenous, (b) unrestrained, and (c) restrained shrinkage (ASTM C1581)**
936 **for cements with 0%, 5% and 10% LS [73]**

937

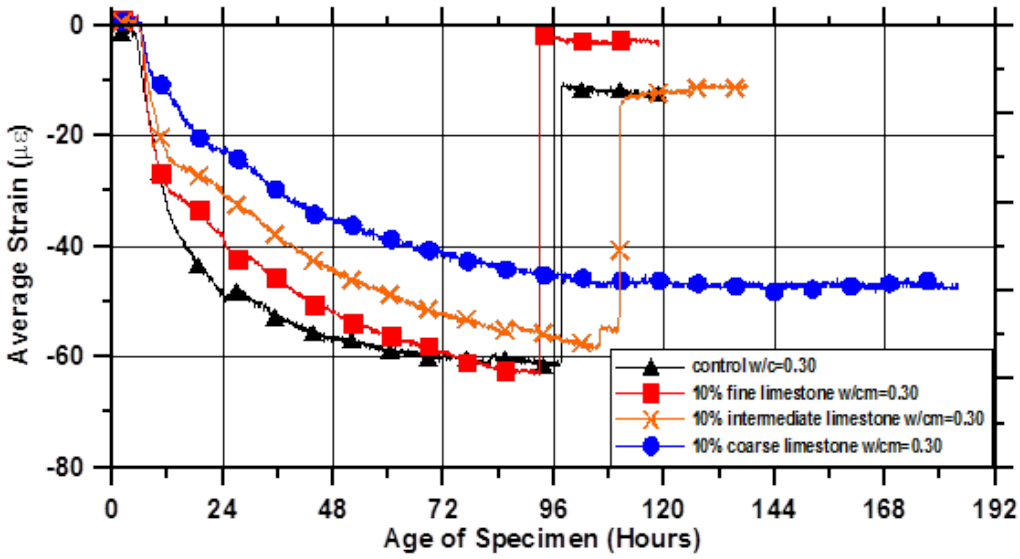

938

939 **Figure 6-2. The influence of the fineness of limestone on the restrained shrinkage stress**
940 **development in OPC + 10% LS systems [74]**

941

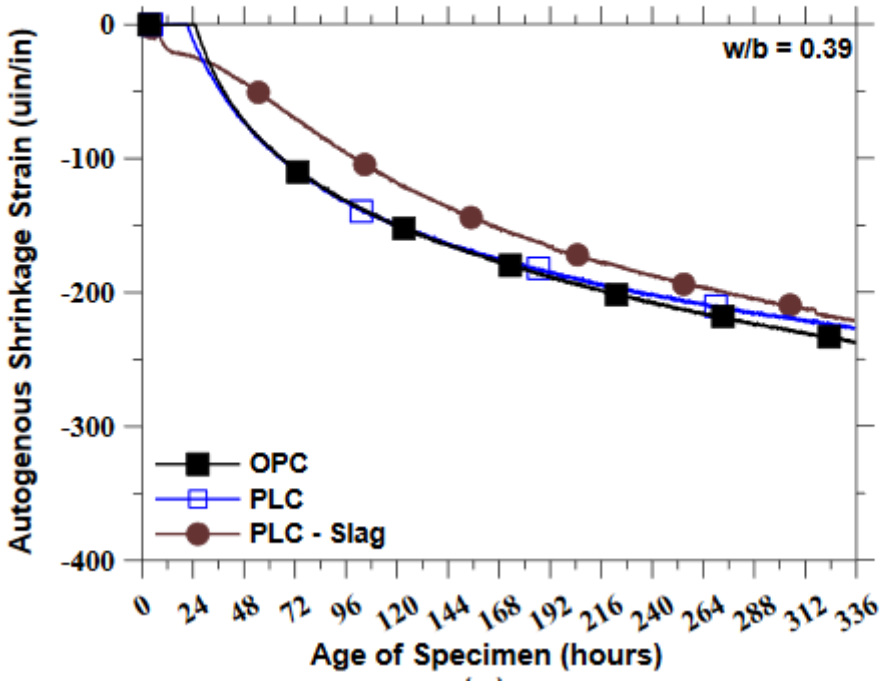

(a)

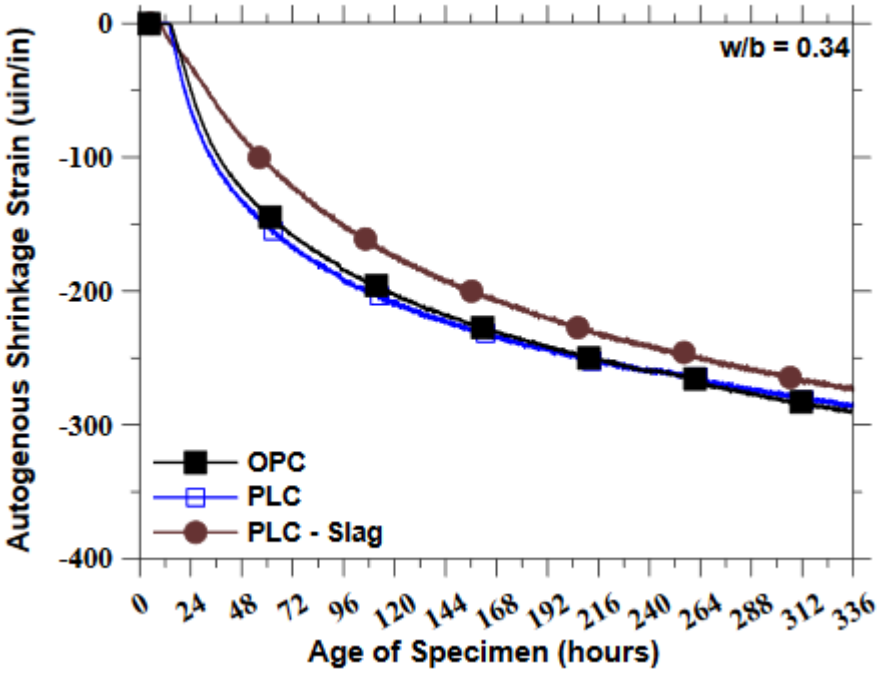

(b)

Figure 6-3. Autogenous shrinkage measurements for OPC, PLC, and PLC-slag systems with: (a) w/b 0.39; and (b) w/b 0.34 [76]

Barrett et al. [76] studied commercial OPC and PLC systems that were 'equivalent' (manufactured to meet ASTM C595 based on the principle of similar 28-day strengths) and reported no significant change in drying shrinkage or restrained shrinkage cracking (Figure 6-4) with the one exception of a PLC cement that was ground to a fineness level that was much finer (30% more than that typically observed).

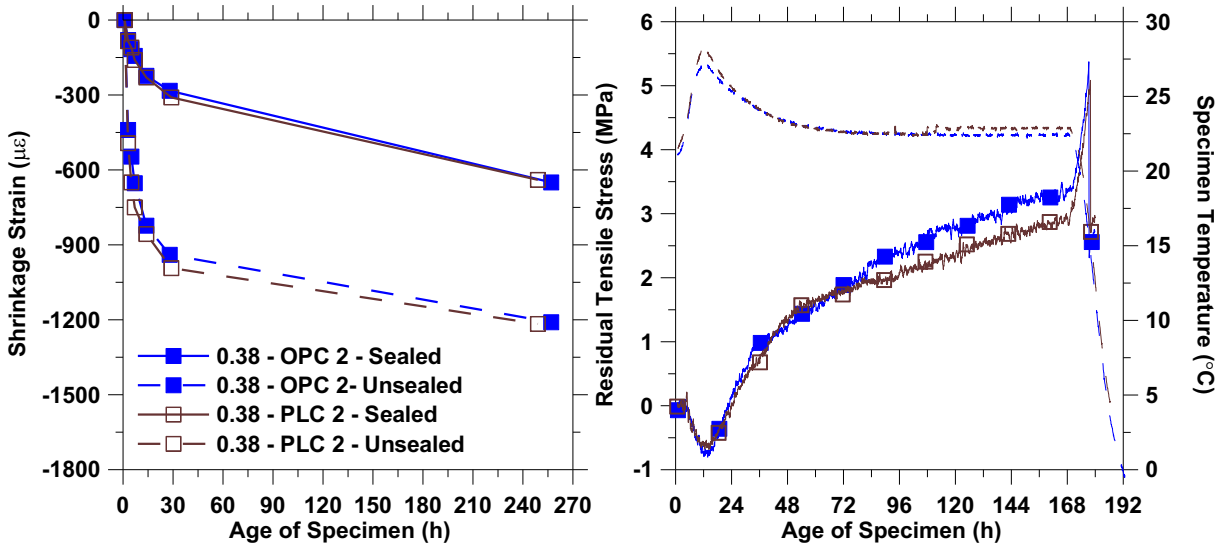

(a) (b)

Figure 6-4. (a) Free shrinkage of sealed and unsealed OPC and PLC concrete and (b) Stress Developed for OPC and PLC when restrained from shrinking freely. [76]

6.3 Experimental Test Matrix

To evaluate the relative performance of all cements in this study, drying shrinkage testing was performed following the ASTM C 157 [81] (as used by CALTRANS). The shrinkage tests were performed on mortar prisms (25 x 25 x 285 mm). Two samples were tested for each mixture. The mixtures for the test using the proportions provided in Table 6.1 based on the SCM replacement levels (by mass) provided in Section 3.

The test matrix comprising 80 mortar mixtures, which were cast and tested for drying shrinkage tests, is shown in Table 6.2.

Table 6.1. Mixture proportions for mixtures evaluated for shrinkage

		Mass given in (kg/m^3)					
Material	**S.G.**	**M0**	**M1**	**M2**	**M3**	**M4**	**M5**
Cement or cement+powder*	3.15	696.9	498.8	492.8	339.0	328.2	503.9
Fly Ash	2.34	0	166	131	0	164	0
Silica Fume	2.20	0	0	33	0	0	0
Slag	2.83	0	0	0	339	164	0
Natural Pozzolan	2.36	0	0	0	0	0	168
#23 Sand (SSD)	2.67	1335	1335	1335	1335	1335	1335
Water	1	279	266	263	271	263	269

* OPC, PLC or OPC+10LS

Table 6.2. Test matrix for drying shrinkage tests on mortar specimens

	M0	**M1**	**M2**	**M3**	**M4**	**M5**
A_OII	√	√	√	√	√	√
A_L15	√	√	√	√	√	√
A_OII+10LS	√	√	√	√	√	√
B_OIIV	√	√	√	√	√	~
B_L15	√	√	√	√	√	~
B_OIIV+10LS	√	√	√	√	√	~
C_OV	√	√	√	√	√	~
C_L10	√	√	√	√	√	~
C_L14	√	√	√	√	√	~
C_OV+10LS	√	√	√	√	√	~
D_OV	√	√	√	√	√	√
D_L15	√	√	√	√	√	√
D_OV+10LS	√	√	√	√	√	√
E_OIIV	√	√	√	√	√	~
E_11	√	√	√	√	√	~
E_OIIV+10LS	√	√	√	√	√	~

6.4 Experimental Methods

Drying shrinkage tests were performed on mortar specimens using the mixture proportions shown in Table 6.1. The mortar mixtures were prepared using concrete sand. The mixtures were prepared with a batch size of 0.002 m^3. The samples were mixed in a Hobart (N50 5-Quart) mixer. The cementitious powders were dry mixed for 15 seconds at low agitation (60 rotation per minute), and then water was added to the mixing bowl, and the paste was mixed for 30 seconds. The sand

was added in the next 30 seconds of mixing. After sand addition, the agitation speed was increased to intermediate (120 rotations per minute), and the mortar was mixed at this speed for 30 seconds and then stopped for a quick scraping of the bowl and the attachments. Following this, the mixture was mixed for another 1 minute at intermediate agitation before it was poured into molds. Three mixtures with the same mixture design but different cements (OPC, PLC, and OPC+10%LS respectively) of the same parent clinker were cast on the same day to enable direct comparison of the samples.

The mortar mixture was placed in two prism-shaped molds (25 x 25 x 285 mm.). Metal pins (gauge studs) were cast in the ends of the beams to facilitate length change measurements using a comparator. Figure 6-5 illustrates the comparator that was used for shrinkage measurements. In addition to the shrinkage prisms, six cylinders (50 mm diameter x 40 mm length) were also cast for testing the mixture's mechanical properties as described in section 7.

Figure 6-5. Drying shrinkage Comparator where a) illustrates the reference bar's measurement and b) shows the sample's measurement.

The drying shrinkage measurements were performed using ASTM C157 (AASHTO T 160) on the mortar prisms. Fresh mortar samples were stored under wet burlap at 23 ± 2°C for 24 hours. The samples were then demolded and placed in water at 23 ± 2°C for 30 minutes, after which initial length measurements were recorded. After the initial length measurements, the samples were again stored in water up to 3 days from casting time. The specimens were then removed from the water, and their length was measured. They were stored in the drying chamber up to 28 days from casting. The length change measurements were performed at every 1, 3, 5, 7, 14, and 28 days.

6.5 Typical Experimental Measurement and Interpretation

Figure 6-6 depicts a typical drying shrinkage plot. The y-axis depicts the drying shrinkage strain in micro-strain (με). The x-axis represents the duration of exposure to drying (in days) at which the shrinkage measurements were made. The typical values of drying shrinkage strains observed in mortar beams is between 1000-1500 με. Each plot compares the shrinkage measurements of (i) OPC (ii) PLC and (iii) OPC+ limestone bars with the same parent clinker corresponding to one particular mixture described in the graph legend.

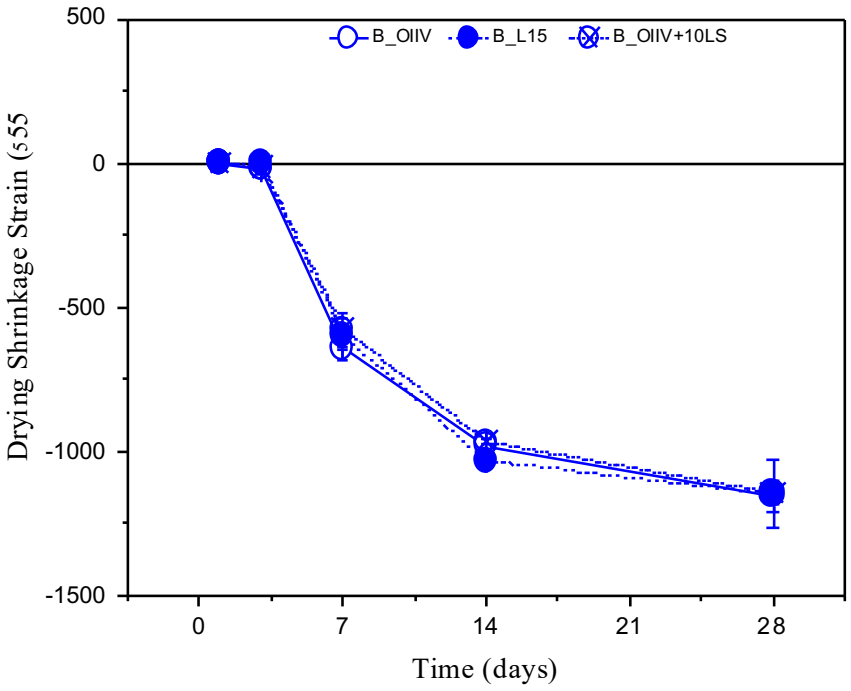

Figure 6-6. Typical plot of drying shrinkage results of (Cement B-Mixture 4)

6.6 Experimental Results

Drying shrinkage results are shown for cement D for the different mixture proportions are provided in Figure 6-7(a-f). The drying shrinkage results of the remaining cements are provided in Appendix C.

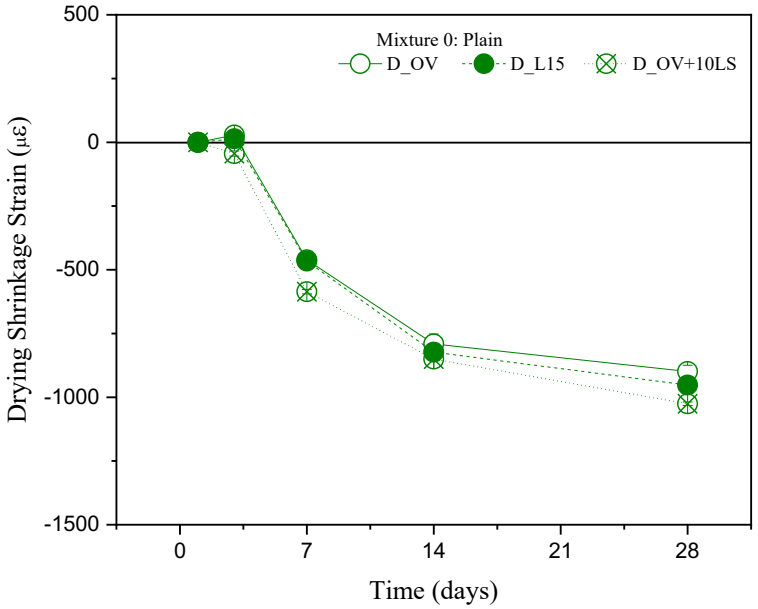

(a)

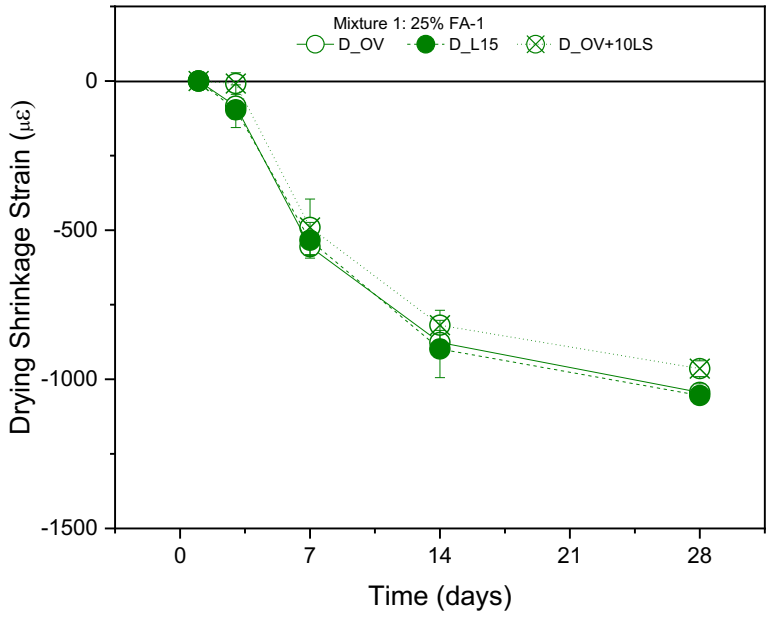

(b)

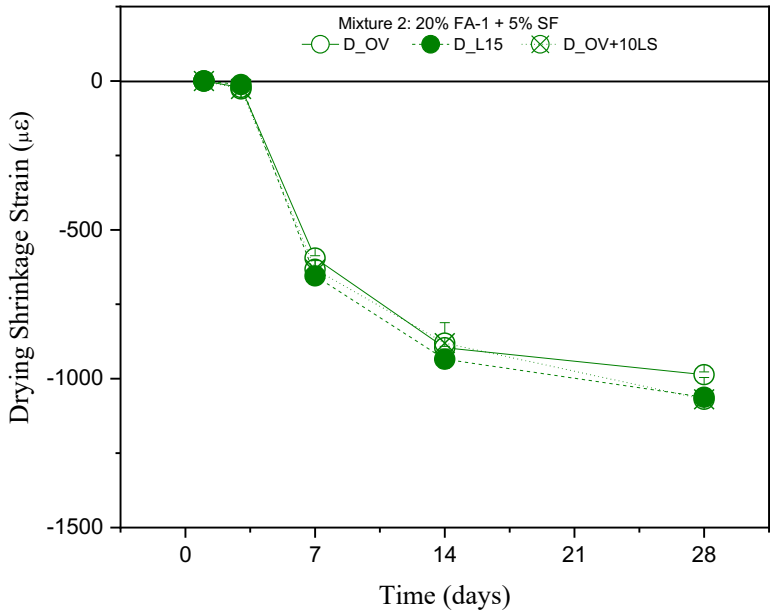
Mixture 2: 20% FA-1 + 5% SF
D_OV
D_L15
D_OV+10LS
Drying Shrinkage Strain (με)
0
-500
-1000
-1500
0
7
14
21
28
Time (days)

(c)

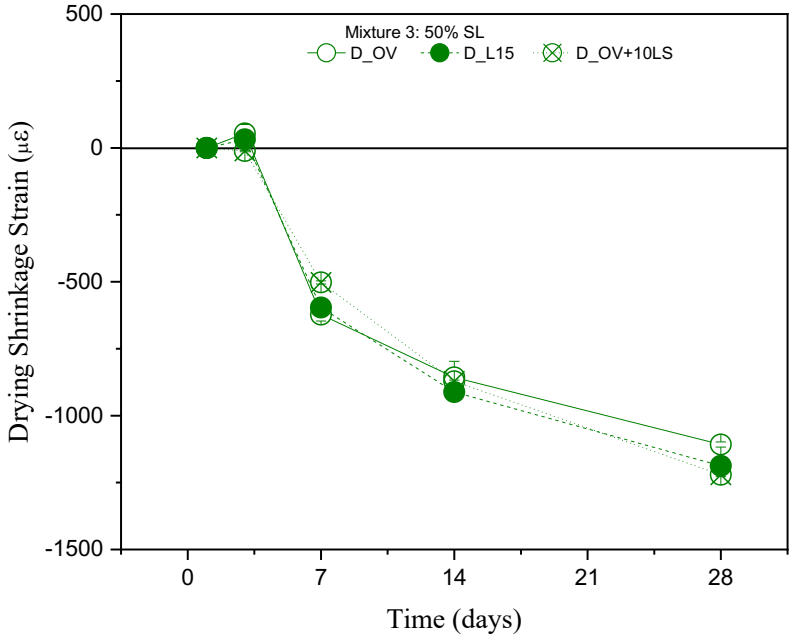
Mixture 3: 50% SL
D_OV
D_L15
D_OV+10LS
Drying Shrinkage Strain (με)
500
0
-500
-1000
-1500
0
7
14
21
28
Time (days)

(d)

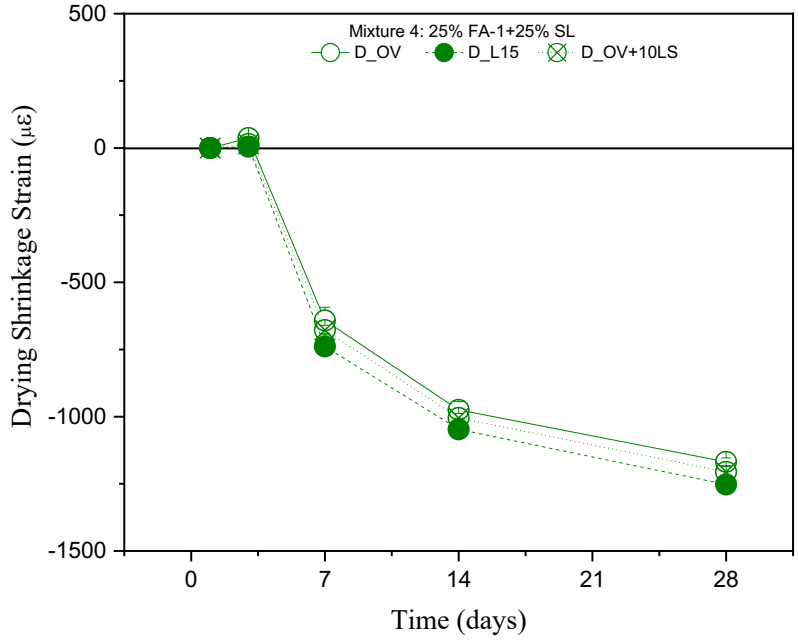

(e)

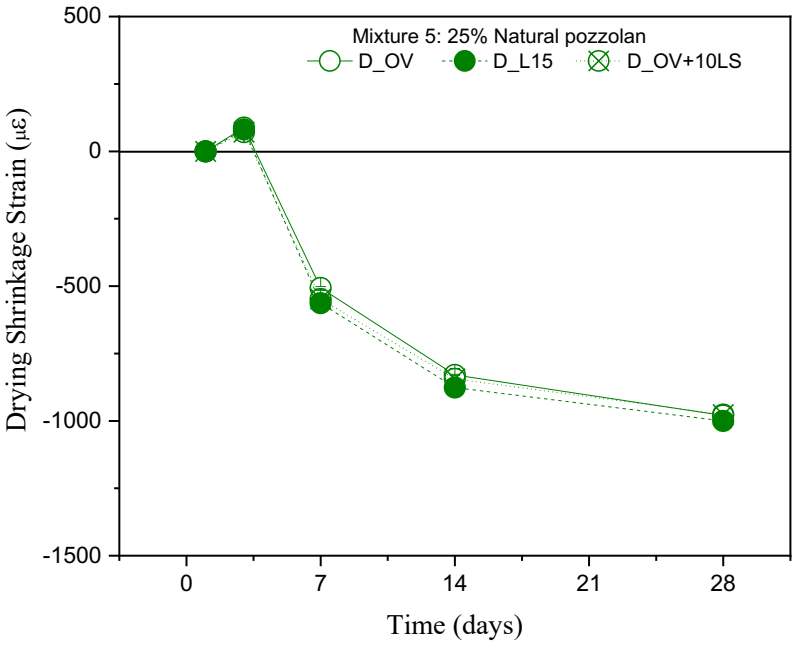

(f)

Figure 6-7. (a)-(f) Drying shrinkage results of Cement D for M0, 1, 2, 3, 4, and 5, respectively

6.7 Discussion of the Results

As clearly seen in Figure 6-7(a) and Figure 6-7(b), for M0 and M1 no discernable difference observed between drying shrinkage strains in OPC and corresponding PLC samples at all ages.

For OPC+10LS samples, the drying shrinkage at early ages were slightly higher than OPC and PLC systems. However, by the age of 28 days, the difference in shrinkage strains was almost non-discernable. Figure 6-7 (c)-(f) shows that OPC, PLC, and OPC + LS systems have no marked difference in drying shrinkage strains. The shrinkage of mixtures 2, 3, and 4 displayed a higher drying shrinkage strain than M1 and M2. The addition of natural pozzolan did not affect the drying shrinkage of mortar samples.

Figure 6-8 illustrates the shrinkage of all 80 mixtures. The Y-axis represents the shrinkage of the PLC or OPC + LS mixtures, while the X-axis represents the OPC systems' shrinkage. A plot that follows the 1:1 solid diagonal line would imply no difference between the OPC and PLC or OPC and OPC + LS. Dashed lines represent a variation of 20% from equivalence. It can be noted that, as expected, the shrinkage increases over time (i.e., moving from Figure 6-7(a) to Figure 6-7(d)).

To determine if the results were statistically significant, t-tests of the shrinkage tests were performed. It was determined that the vast majority of the samples were found to be statistically similar. The only exception for the OPC versus PLC system occurred for M3 and M4 at 14 and 28 days, with the PLC systems' shrinkage being 7-8% higher. Similarly, the OPC's exceptions versus OPC + LS systems for M0 occurred at 3 and 7 days, M2 at 28 days (6% higher), and M4 at 14 and 28 days (3 and 4% higher on average). At this point, it should be remembered that a 1% variation in paste content can result in shrinkage variations of 6 to 10% [73, 74, 82]. Further, M3 and M4 mixtures made using OPC have approximately 10% more shrinkage than M0.

6.8 Significant Findings

Preliminary testing on shrinkage cracking showed no statistically significant difference in cracking performance, consistent with the literature. Due to similar drying shrinkage and the literature, the Study Advisory Committee determined that additional restrained shrinkage cracking testing was not needed.

As a result, variations in shrinkage with replacing OPC with PLC or OPC with OPC + LS do not appear to be a sufficient concern as it would relate to shrinkage cracking.

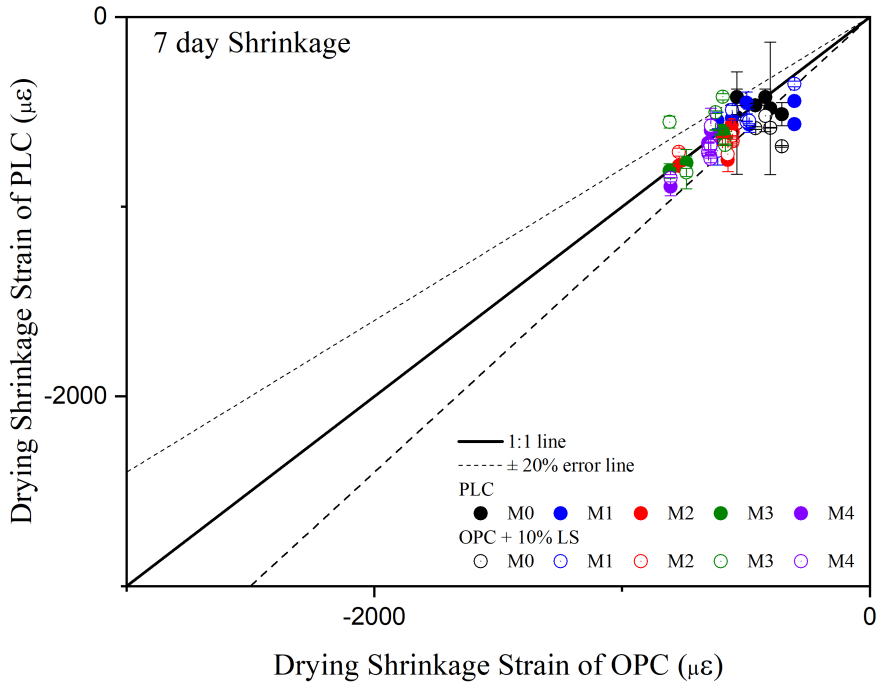
7 day Shrinkage
Drying Shrinkage Strain of PLC (με)
Drying Shrinkage Strain of OPC (με)
0
-2000
-2000
0
1:1 line
± 20% error line
PLC
M0 M1 M2 M3 M4
OPC + 10% LS
M0 M1 M2 M3 M4

(a)

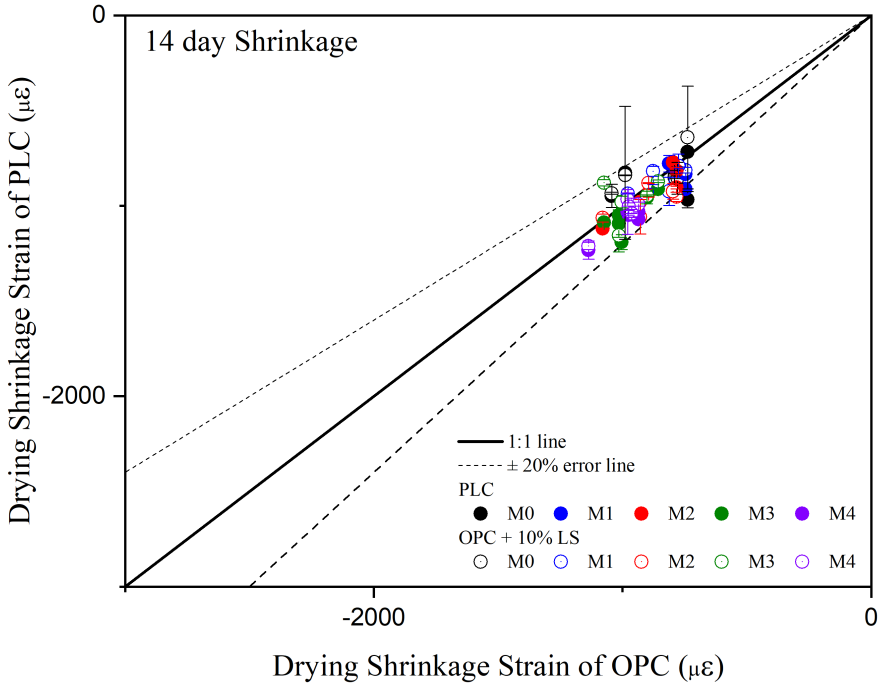
14 day Shrinkage
Drying Shrinkage Strain of PLC (με)
Drying Shrinkage Strain of OPC (με)
0
-2000
-2000
0
1:1 line
± 20% error line
PLC
M0 M1 M2 M3 M4
OPC + 10% LS
M0 M1 M2 M3 M4

(b)

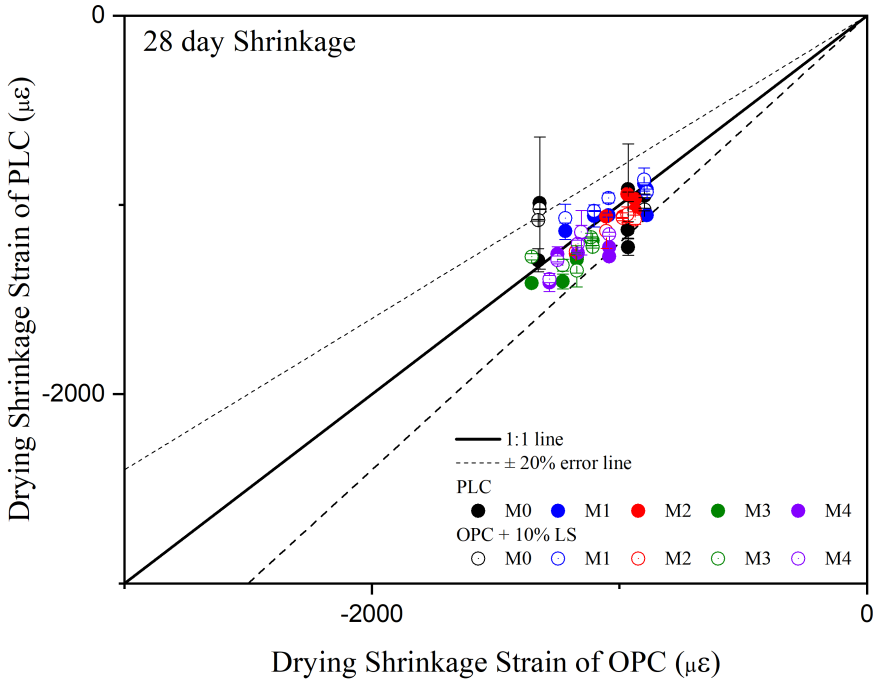

(c)

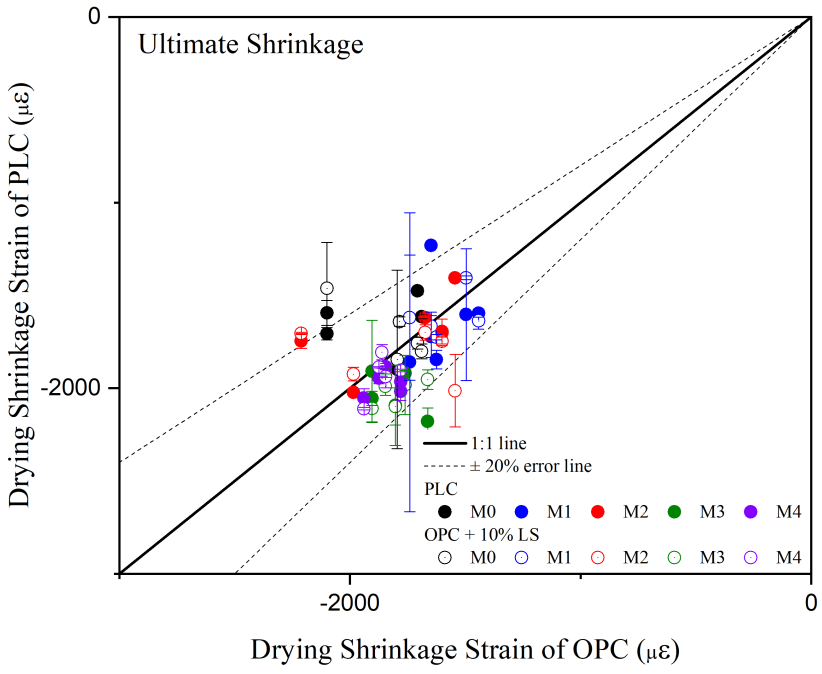

(d)

Figure 6-8. 1:1 Shrinkage Plots OPC vs. PLC and OPC vs. OPC +LS for a) 7 days of drying, b) 14 days of drying, c) 28 days of drying, and d) ultimate drying

7 Mechanical Properties

7.1 Research Objective

Flexural strength development is an essential factor in assessing the performance of PLC. Some have been concerned that replacing 15% of the cement clinker with limestone would result in substantial strength reduction, especially at early ages. However, it should be noted that in North America, ASTM C595/AASTHO M240 cements (PLC) are designed to target a similar 28-day performance. As a result, the fineness of the PLC is generally increased to offset early age strength reduction. This portion of the research investigated the flexural strength for paste made using OPC, PLC, and OPC + LS for both plain systems (M0) and systems containing SCM (M1 to M5).

7.2 Background/Literature review

Dhir et al. [11] showed a slight reduction in mechanical performance between CEM I 42.5R and a similar PLC containing 15% limestone. Chen et al. [12] found that the replacement of clinker with limestone increased in compressive strength of up to 8%. De Weerdt et al. [83] observed that up to 15% of portland cement could be replaced by limestone powder without impairing the compressive strength development. This is pointed out as a reminder that care must be taken when reviewing international literature since many regions do not target similar 28-day performance as has been done in North America for PLC (ASTM C595/AASTHO M240).

North American PLC with a limestone content up to 15% has a similar mechanical performance as ordinary portland cement (OPC) at 28 days [6]. Barrett et al. [2, 76] examined North American PLCs (ASTM C 595/ASTM M240) relating the performance of systems made using OPC with systems made from PLC from the same clinker using primarily Type I and Type III cements. Figure 7-1 shows the study results for the compressive strength, elastic modulus, and flexural strength. In general, it was found that PLCs show an increase in compressive strength at early ages that diminishes with time, resulting in similar compressive strengths at 28 days of age. Systems that had OPC-blended limestone cements had an average reduction in strength of 8.5% at 28 days. This has been attributed to the fact that the cements were not ground finer to account for clinker dilution.

Menéndez et al. [28] showed that when limestone additions occurred in cements containing blast furnace slag, early and later age compressive strength improved. They concluded that during the first 48h, the limestone acts as a nucleation site increasing hydration reactions [16, 23]. They also suggested that after seven days, a synergy occurs with limestone and slag. Barrett et al. [2, 76] demonstrated the benefits of limestone addition in mixtures containing fly ash. Bentz et al. [84] showed substantial improvements in high volume fly ash when limestone was added. Limestone was suggested as a potential method to compensate for high volume fly ash's impact on the retardation of hydration and delayed setting time. It has been suggested that limestone participates

in the hydration reaction by forming carboaluminates. The carboaluminates may reduce the induction period, set time, and stabilize ettringite, leading to the reduction in the volume of hydrates and porosity [24, 25].

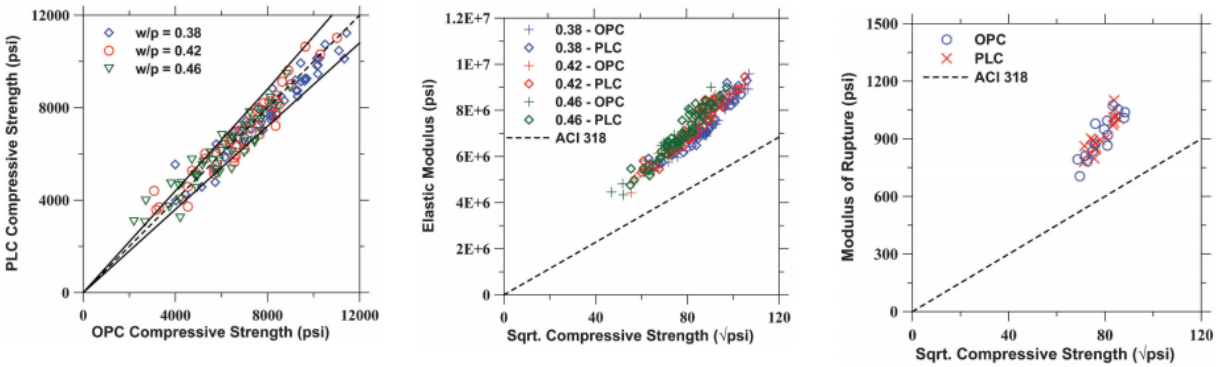

Figure 7-1. A Comparison of the mechanical properties of OPC and PLC: (a) compressive strength, (b) Elastic modulus vs. square root of compressive Strength, and, (c) Flexural Strength vs. Square Root of Compressive Strength [76]

Meddah et al. [13] also showed that 15% replacement of OPC with limestone had a 5% reduction in the modulus of elasticity for concrete produced with PLC when compared with OPC-based concrete. Barrett et al. [76] concluded that the modulus of elasticity and flexural strength of concrete produced with OPC and PLC are similar. Figure 7-1b shows their similarity and compares them to the equations used to estimate these properties by ACI. The modulus estimate is substantially larger (COV of 40%) than any minor variation caused by PLC addition.

When OPC is replaced by a limestone content higher than 15%, a reduction in the mechanical strength at later ages has been observed as well as a decrease in the modulus of elasticity [11, 15-18]. However, it should be noted that these cements are not consistent with the ASTM C 595/AASHTO M 240 specification.

There is a consensus in the literature that the replacement of cement clinker with interground limestone levels up to 15% can benefit the mechanical properties. Most literature focuses on cement type I or III cements with little, if any, work done on type II/V cements. This study aims to determine the impact of PLC on paste's mechanical properties, specifically here focusing on flexural strength.

7.3 Experimental Test Matrix

The Ball on Three Ball (B3B) test was performed to flexural strength testing described in the following section [85-89]. The flexural strength was measured on mortar cylinders (50 mm diameter x 100 mm length) that were sectioned to a nominal thickness of 2.65 mm. Samples were cast along with the shrinkage samples, as discussed in section 6. The mixtures for the test using the proportions provided in Table 6-1 based on the SCM replacement levels (by mass) provided in

Section 3 The test matrix comprises 80 mortar mixtures, which were cast and tested for flexural strength in accordance with Table 6.2.

7.4 Experimental Methods

Fresh mortar samples were mixed using the procedure described in section 6.4. The fresh mortar was cast in plastic cylinders (52 mm diameter and 100 mm length) in two layers. Each layer was consolidated using a tamping rod. The samples were then sealed with duct tape to prevent the loss of any moisture. The sealed samples were stored at 23 ± 1°C for curing. The samples were demolded and prepared for flexural strength using the ball-on-three-ball (B3B) test at 7, 14, 28 and 90 days [89].

At the age of testing, the sealed cylinder samples were demolded and cut with a diamond-tipped saw blade that was water-cooled to produce disc specimens with a nominal thickness of 2.65 mm (the samples were measured after they were broken, and the average of 3 thickness measurements was used as the thickness). The ends of the samples (approximately the last 10 mm) were discarded to avoid end defects. The sliced discs were gently wiped with a towel to remove excess moisture and then tested using the B3B machine (Mark-10 Tester with a Series 5 force gauge). Approximately 6-7 slices were sampled from each cylinder to obtain a representative data set. The B3B test set-up is shown in Figure 7-1. The rate of loading is 0.22 N/sec. The peak load (F) and the thickness of the broken pieces (t) were noted down for each tested disc. The flexural strength (σ) was determined for each disc of radius (R) using the equation provided in Börger's work [85-88] which was modified and adapted for mortar specimens by Fu and Weiss [89]

$$\sigma = \left[c_0 + \frac{(c_1 + c_2\alpha + c_3\alpha^2 + c_4 \cdot \alpha^3)(1 + c_6\beta)}{1 + c_5\alpha}\right]\frac{F}{t^2} \quad \textbf{(7-1)}$$

where, $\alpha = t/R$, $\beta = R_a/R$, $c_0 = -14.671$, $c_1 = 17.988$, $c_2 = 567.22$, $c_3 = -80.945$, $c_4 = -53.486$, $c_5 = 36.01$, and $c_6 = 0.0709$ (for Poisson's ratio = 0.2 for cement mortar).

Figure 7-1. The Experimental Setup for the B3B test: a) without the sample b) showing a mortar disk during testing and c) showing a mortar disk after testing (note the three vertical pins provide no restraint and are only used to locate the sample)

7.5 Typical Experimental Measurement and Interpretation

Figure 7-2 provides a typical plot of flexural strength for the mortars made using PLC and OPC. The strength data was collected at the ages of 7, 14, and 28 days is shown on the X-axis. The Y-axis denotes the flexural strength of PLC and OPC+ limestone samples at different ages normalized by the average flexural strength on OPC samples of the same parent clinker at that age. The reference line drawn at 100% corresponds to the strength of the OPC average sample strength at that age. The points lying above this line signify that the PLC has a higher strength than OPC samples, and the points below correspond to lower strength. Similar to what has been observed by others, at early ages, the PLC system may have slightly lower or similar strength; however, at the age of 28 days, the PLC and OPC mixtures have similar performance.

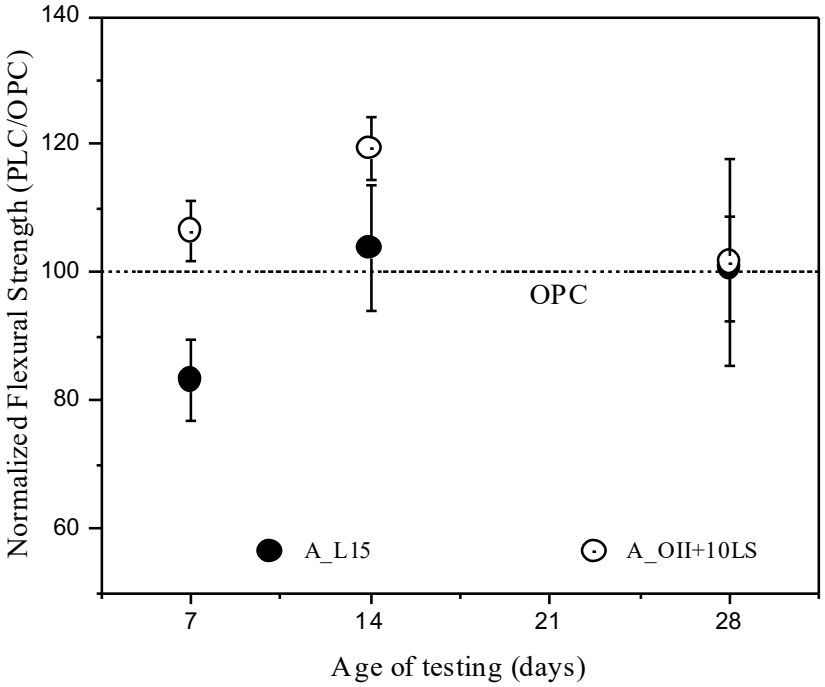

Figure 7-2. Typical plot of normalized flexural strength results of (Cement A-M3)

7.6 Experimental Results

The flexural strength for the series of mixture made using Cement B is provided in Figure 7-3 (a)-(e). Again, the samples made using PLC and OPC + LS are normalized to the flexural strength of the OPC samples. The flexural strength results of the other cements are provided in Appendix D.

The strength at early ages for both the PLC and the OPC+LS were lower than the OPC at early ages for M0, 1, 2 (no SCM, 25% fly ash and 20% fly ash/5% silica fume respectively). A 10% reduction in flexural strength was noted at later ages as well. Mixtures 3-5 did not show this delay (50% slag, and 25% slag/25% fly ash, 25% natural pozzolan, respectively).

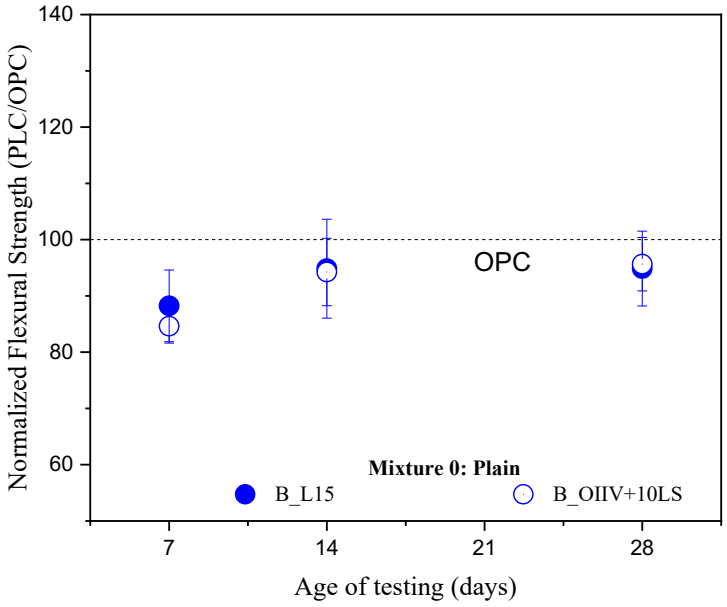

(a)

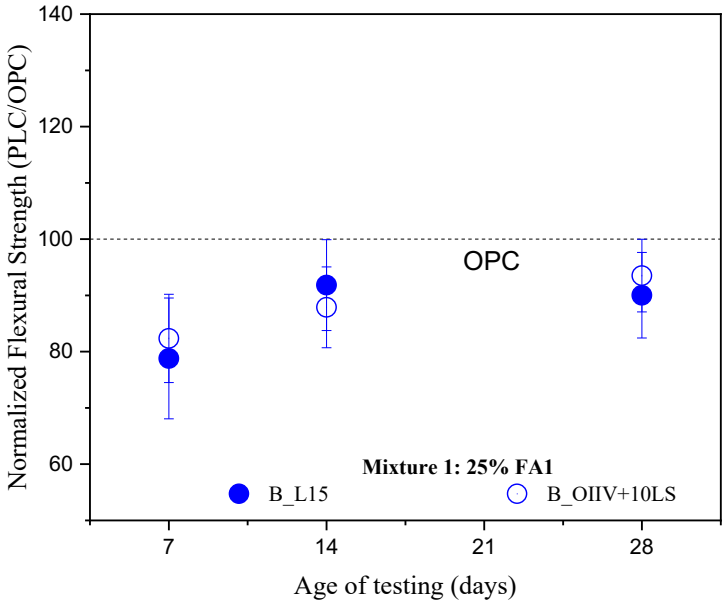

(b)

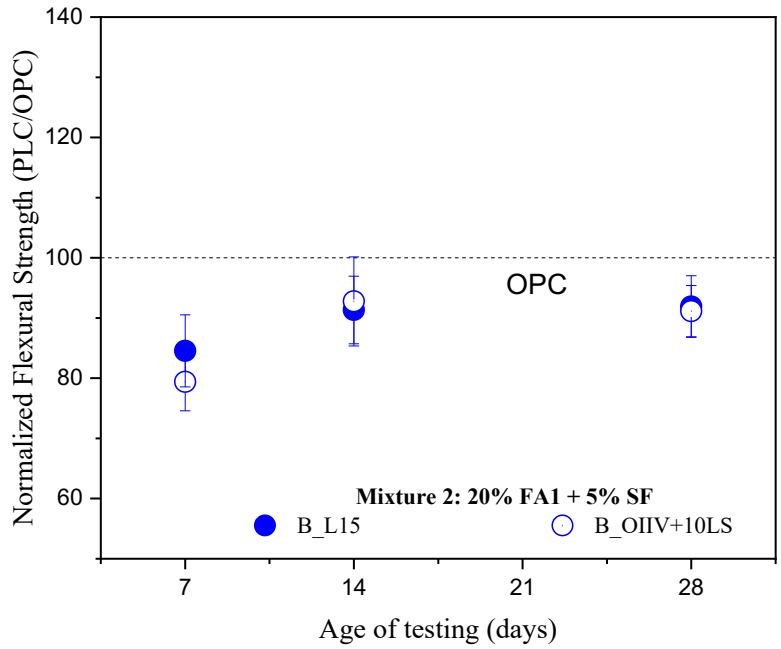
Normalized Flexural Strength (PLC/OPC)
140
120
100
80
60
OPC
Mixture 2: 20% FA1 + 5% SF
B_L15
B_OIIV+10LS
7
14
21
28
Age of testing (days)

(c)

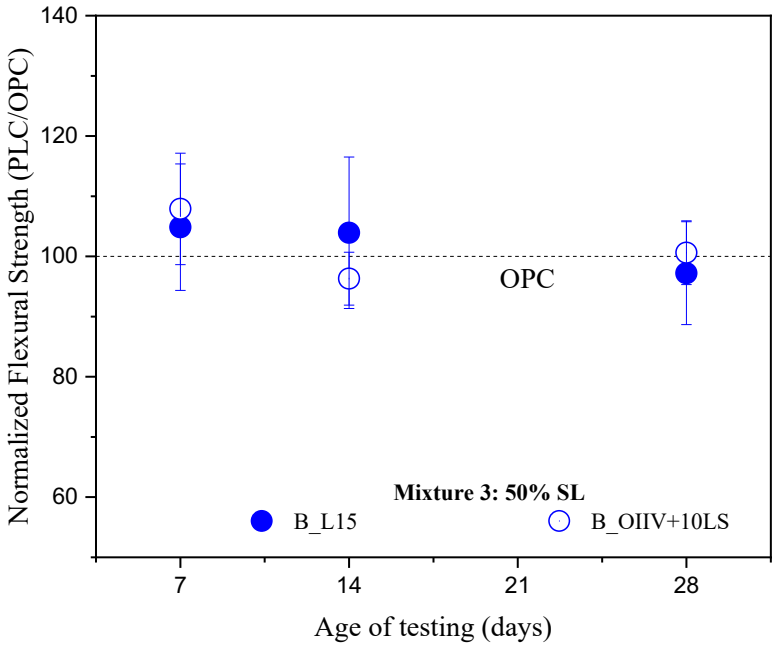
Normalized Flexural Strength (PLC/OPC)
140
120
100
80
60
OPC
Mixture 3: 50% SL
B_L15
B_OIIV+10LS
7
14
21
28
Age of testing (days)

(d)

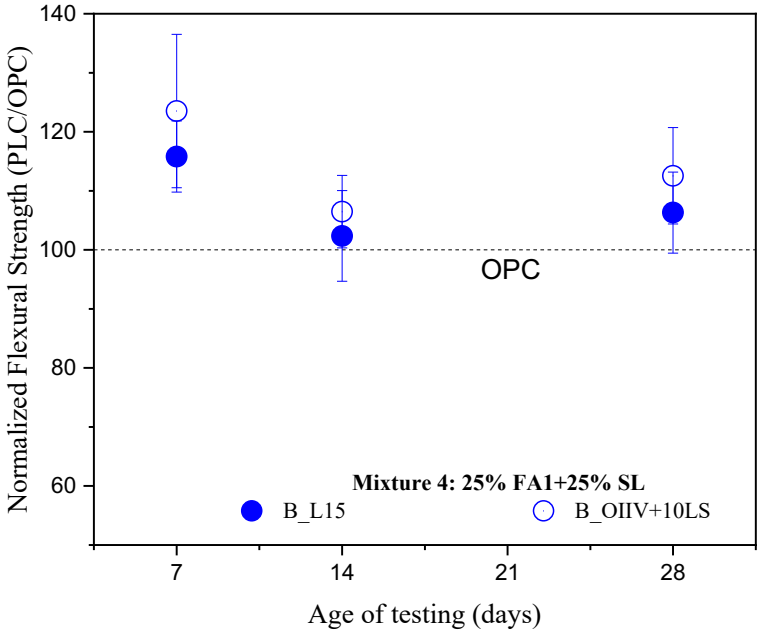

(e)

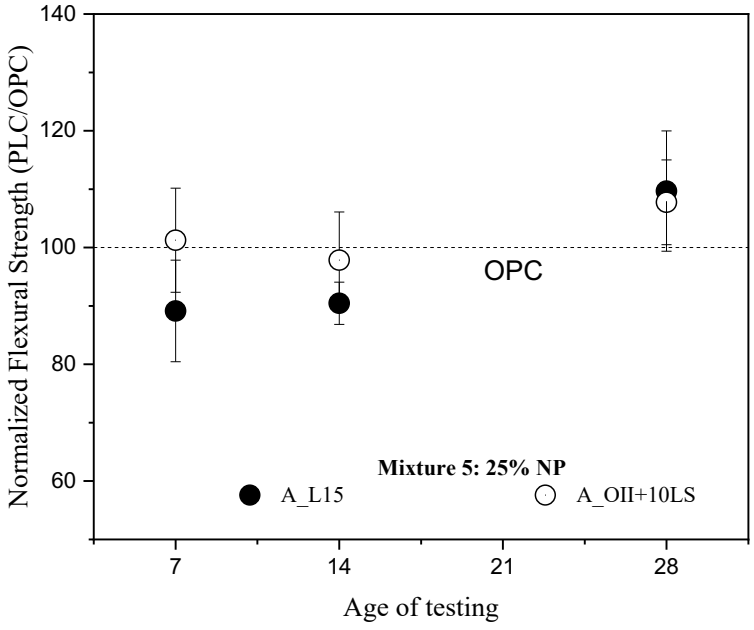

(f)

1156 **Figure 7-3. (a)-(f) Flexural strength results using B3B test for Cement B for M0, 1, 2, 3, 4,**
1157 **and 5 respectively**

7.7 Discussion of the Results

In general, for all the cement clinkers studied, the PLC and OPC +LS mortar samples had a flexural strength that was less than 5% lower than the OPC mixtures. The following section describes the trends for cements A through E.

M0 (plain) demonstrated PLC strength that was 10% lower at seven days and 5% lower at the other ages, while the OPC + LS was 18.5% lower at seven days, 10% lower at 14 days, and 5% at other ages. M1 (25%FA) had a PLC and OPC +LS strength was approximately 15% lower at early ages, and this difference reduced over time. M2 (25% FA +SF) was at most 8% lower. M3 (slag) and M4 (silica fume and slag) were found to have statistically similar strengths in comparing OPC, PLC, and OPC + LS. M5 (natural pozzolan) was found to have statistically similar strengths in comparing OPC, PLC, and OPC + LS with one exception in that the PLC was on average 14% less at 90 days. Figures 7-4 show that the addition of limestone reduces flexural strength at an early age for plain systems (M0) and fly ash systems (M1). Still, the effect of limestone replacement and clinker reduction is almost inconsequential when considering sample to sample variability by 14, 28, and 90 days (Figure 7-4 b, c, d). Thermodynamic models (Part II of the report) and physical testing will correlate the strength with porosity. Initial results indicate that M0, M1, and M2 have a slight increase in porosity for the PLC and OPC + LS systems than the OPC systems.

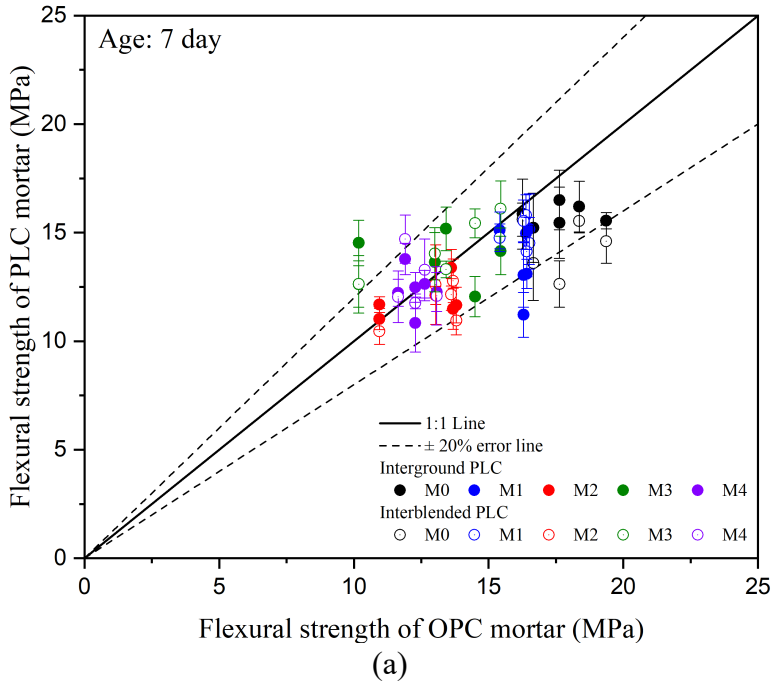

(a)

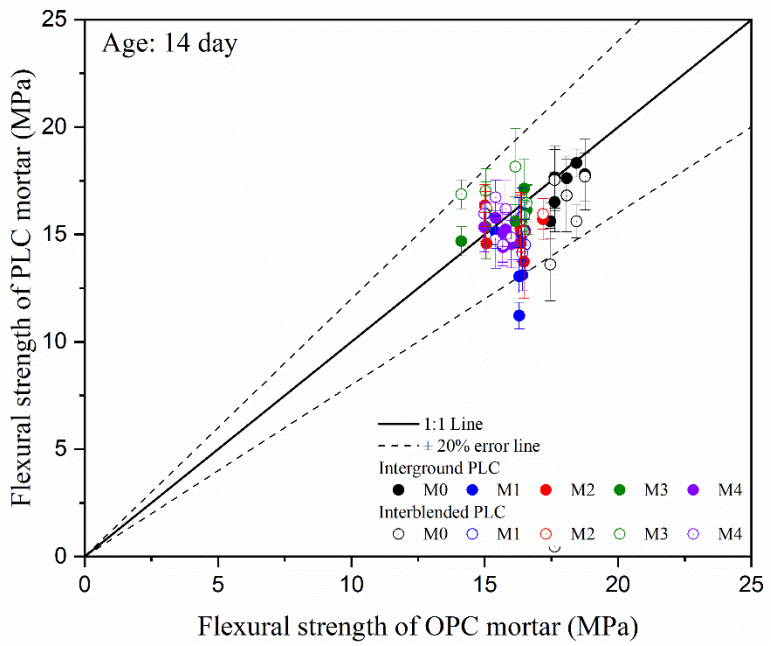
Age: 14 day
Flexural strength of PLC mortar (MPa)
Flexural strength of OPC mortar (MPa)
0
5
10
15
20
25
1:1 Line
± 20% error line
Interground PLC
M0 M1 M2 M3 M4
Interblended PLC
M0 M1 M2 M3 M4

(b)

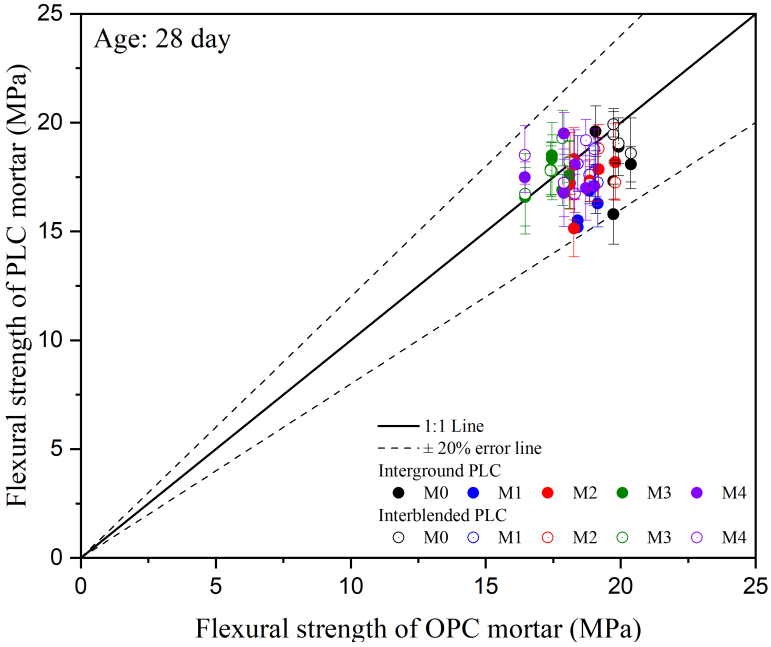
Age: 28 day
Flexural strength of PLC mortar (MPa)
Flexural strength of OPC mortar (MPa)
0
5
10
15
20
25
1:1 Line
± 20% error line
Interground PLC
M0 M1 M2 M3 M4
Interblended PLC
M0 M1 M2 M3 M4

(c)

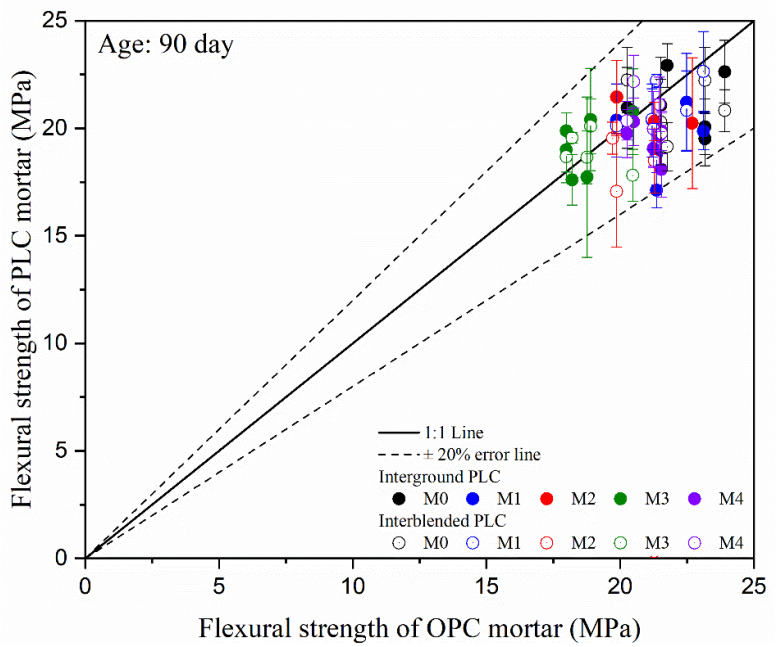

(d)

Figure 7-4. (a)-(d) Flexural strength results using B3B test for M0-M4.

7.8 Significant Findings

This study examined the performance of PLC made with clinkers that are typically used for Type II/V OPC that contain SCM. Eighty different mixtures were prepared to evaluate the influence of the PLC flexural strength. The flexural strength in the PLC and OPC + LS mixtures was on average less than 5% lower than the OPC mixtures. However, the flexural strength was up to 13% greater for PLC when combined with slag. Overall, the flexural strength was consistently within the +/- 20% range compared with the parent system. In conclusion, PLC can be used as an alternative to OPC for systems made with type II/V clinker with and without SCM.

8 Transport Properties

8.1 Research Objective

The durability of concrete is impacted by its ability to resist ingress of fluids and ions. This chapter examines the transport properties of mortars made using OPC, PLC, and OPC+LS systems. The objective is to determine the influence of PLC and OPC+LS on the pore structure of concrete and provide data to inform CALTRANS on the potential replacement OPC related to fluid transport.

Transport in cementitious systems is generally categorized as 1) absorption of fluids, 2) hydraulic permeation, 3) diffusion of ions. Several test methods exist to determine these factors; however, recent work has shown that these critical factors can be related to a measurable property called the formation factor (F, AASHTO PP-84). The formation factor is generally measured using electrical testing (e.g., resistivity) and is inversely related to the product of the total porosity and the connectivity of the pores. This chapter will measure the formation factor of OPC, PLC, and OPC+LS mortars and related properties. Similar properties for concrete mixtures are presented separately in Chapter 10 as part of the discussion on chloride ingress in concrete.

8.2 Background/Literature review

As previously mentioned, the transport properties of concrete are often evaluated using electrical measurements (e.g., RCPT (ASTM C1202), electrical conductivity, or electrical resistivity (ASTM C1876, AASHTO TP-119)). In an earlier study, Stubstad et al. [1] compared OPC and PLC and noted that PLC performed better than OPC in the ASTM C1202 test (for rapid chloride penetrability). Barrett et al. [31] measured the bulk resistivity of PLCs and found that while the results were generally similar to the OPC, some PLC mixtures performed better than the OPC, and some did not perform as well. Barrett et al. did conclude that the results were within ± 25% of the reference OPC mixtures and stated that more information was needed on the role of pore solution resistivity to understand the variations [37]. It is worth noting that the bulk resistivity of PLC systems containing fly ash exhibited an improvement of up to one order of magnitude compared to OPC systems. Hooton et al. [5] and Lakar and Smart [64] also reported similar performance between the OPC and PLC systems when electrical properties are measured,

Elgahud et al. [41] reported results from a wide variety of tests over the last 30 years and found that, in general, limestone addition increased the rate of chloride diffusion and ingress. However, it should be noted that care needs to be taken in these systems as the design of PLC around the world can vary. It should be noted that North American PLC has been designed to have a similar 28-day compressive strength to that of the OPC and tends to perform differently from around the world. Barrett et al. found that while North American PLC systems have similar volumes of permeable voids as OPC, the chloride diffusion coefficients in these systems could be up to 30% higher than the OPC systems. This trend, however, was substantially reversed when SCMs were

used. The PLC-SCM systems outperformed the OPC-SCM systems. Further, the PLC systems containing fly ash have chloride diffusion coefficients that are up to 90% lower than systems without fly ash.

Others have investigated fluid sorption directly. Barrett et al. [31] measured a series of PLC systems and found that the initial and secondary rates of absorption of the PLCs were within ± 30% of the reference OPCs. Ramazeianipour et al. [22] showed that there was no impact on absorption at low levels of limestone addition. Still, at higher levels of limestone addition, the absorption increased slightly at early ages but decreased at later ages. Tsivilis et al. [32,33,34] reported that for high w/cm (0.7), the PLC had a similar water absorption response as the OPC.

8.3 Experimental Test Matrix

The formation factor is measured using electrical resistivity (AASTHO TP-119) and is inversely related to the product of the total porosity (AASTHO TP-135) and the connectivity of the pores. This chapter describes experiments to determine the porosity and electrical resistivity of mortar samples. These samples were cast along with the shrinkage bars (section 6), and flexural strength (section 7) using the proportions provided in Table 6.1 are based on the SCM replacement levels (by mass) provided in Table 6.2. The test matrix comprises 80 mortar mixtures.

8.4 Experimental Methods

Fresh mortar samples were mixed and cast using the procedure described in Section 6. The sealed samples were stored at 23 ± 1°C for curing. The samples were demolded and prepared for porosity (AASHTO TP 135-20 [90]) and resistivity (AASHTO TP-119-20 [91]) testing at the age of 90 days.

8.4.1 Porosity

Porosity was measured following AASHTO T 135-20 [90] using two samples per mixture. The ends were cut using a saw. The samples were surface dried before vacuum saturation at a pressure of 6 Torr for four hours. During the third hour of vacuum saturation, standard pore solution (13250 g water, 102.6 g NaOH, 143.9 g KOH, and 27 g $Ca(OH)_2$) was introduced into the bucket via an external tube to saturate the pores with the standard pore solution. After the samples had been exposed to the solution under vacuum for an hour, they were removed from the vacuum and stored in the solution for three days. After this storage, each specimen was removed from the solution, and its saturated mass was recorded in the SSD condition. The apparent mass of the specimen underwater was also measured. The sample was then dried in oven conditioned at 105°C, and the mass of sample after five days of drying (i.e., a stabilized mass) was recorded. The specimen porosity was determined using:

$$\phi_s = \frac{m_s - m_a}{m_s - m_d} \quad \textbf{(8-1)}$$

where, $\phi_s$is the porosity of the specimen, m_s is the saturated surface-dry mass of the specimen in air, m_a is the apparent mass of the saturated specimen in water, and m_d is the oven-dry mass of the specimen in air

8.4.2 Electrical Resistivity Test

Electrical resistivity was measured following AASHTO TP 119-15. the resistivity was measured after the samples were saturated in the standard pore solution for three days. The resistance was measured along with temperature, and sample geometry. The resistivity of the specimen was calculated using:

$$\rho_s = R \cdot \frac{A}{L} \quad \textbf{(8-2)}$$

Where, ρ_s is the resistivity of specimen, R is the resistance of the specimen (Ω), A is specimen cross-sectional area (m^2), L = average specimen length (m). Temperature corrections were made using the Arrhenius approach following the guidance of Coyle et al. [92] with an activation energy of 15 kJ/mol.

8.4.3 Formation Factor and Pore Connectivity

The formation factor was calculated using

$$F = \frac{\rho_s}{\rho_{ps}} \quad \textbf{(8-3)}$$

where, F is the formation factor and ρ_{ps} is the resistivity of standard pore solution (Ω-m), assumed to be 0.127 Ω-m.

The connectivity of each sample was calculated using.

$$\beta = \frac{1}{\phi_s \cdot F} \quad \textbf{(8-4)}$$

where, β is the measure of connectivity of pores.

8.5 Typical Experimental Measurement and Interpretation

Figure 8-1 provides a typical plot of the measured porosity for the mortars made using PLC and OPC+10LS normalized by the porosity of OPC mortars. The Y-axis denotes the porosity of PLC and OPC+ limestone samples at 90 days normalized by the average porosity of the OPC samples of the same parent clinker at that age. The reference line drawn at 100% corresponds to the porosity of the OPC average sample at that age. The points lying above this line signify that the PLC mortar has a higher porosity than OPC mortar, and the points below correspond to lower porosity. Similar plots were developed for the measured electrical resistivity.

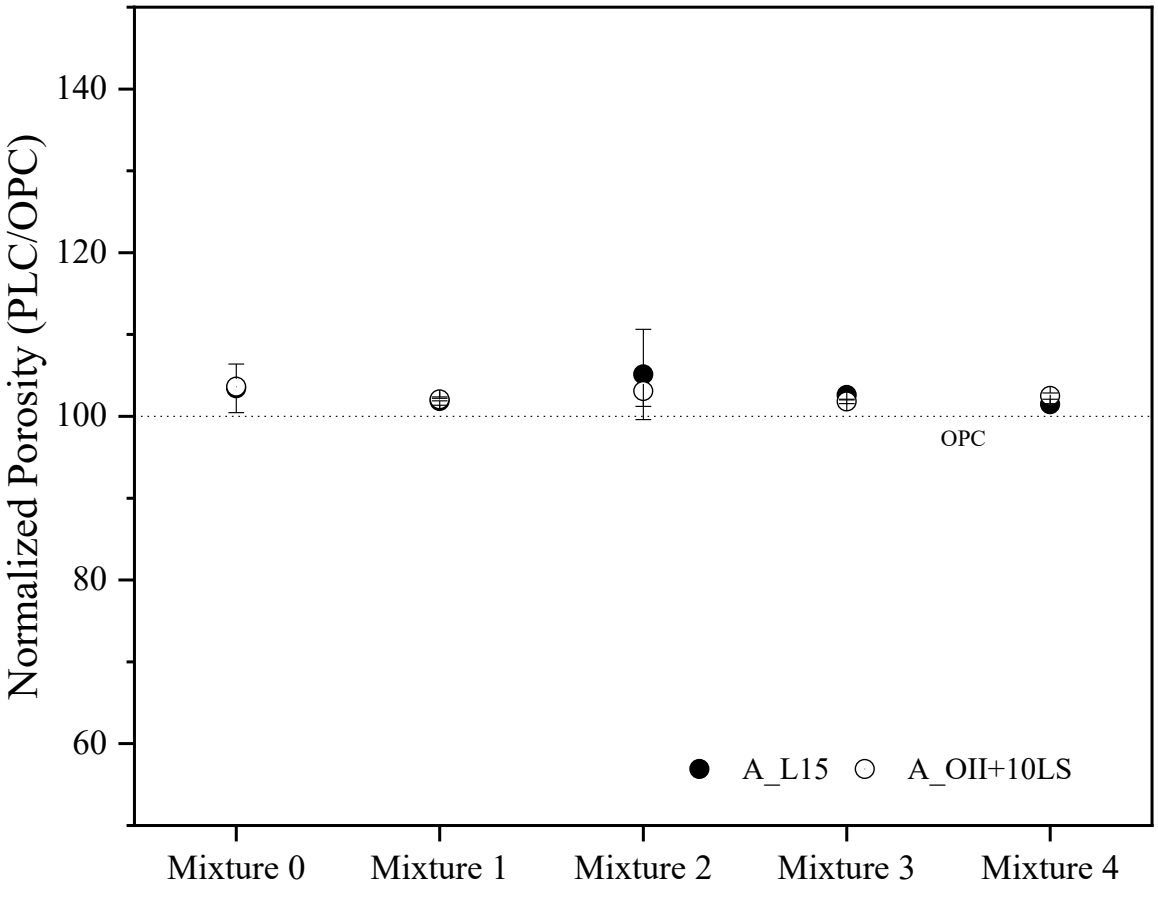

Figure 8-1. Typical plot of normalized porosity results of Cement A for all mixtures

Figure 8-2 is a typical 1:1 consolidated plot of porosity of PLC and OPC+10LS mortars as compared to the porosity of OPC mortars. The x-axis denotes the OPC porosity and the y-axis denotes the PLC and OPC+LS samples at 90 days for M0-M4. The solid 1:1 reference line corresponds to an equivalent porosity of the OPC and PLC samples. Points lying above this line signify that the PLC mortar has a higher porosity than OPC mortar, and the points below correspond to lower porosity. ±20% and ±40% error lines are also provided. Similar plots were made to represent other properties.

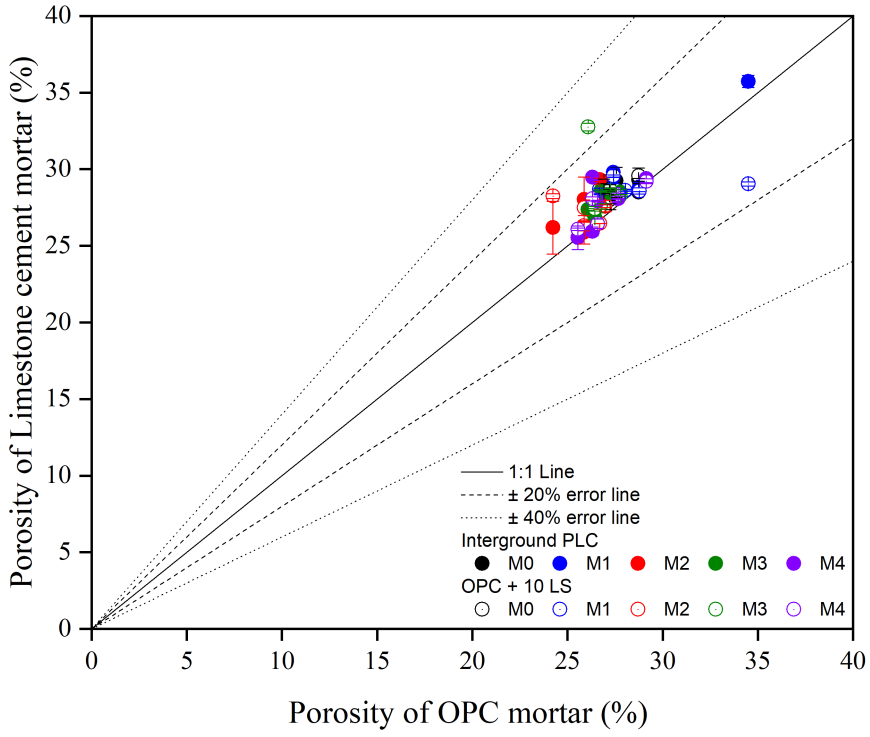

Figure 8-2. Typical plot of porosity results comparing porosities of PLC mixtures with OPC mixtures

8.6 Experimental Results

The porosity and resistivity are provided in Figure 8-3 for mortars made using Cement E while the porosity and resistivity results of the other cements are provided in Appendix E. The 90-day porosity of the PLC and OPC+10LS mortars for all the mixtures are shown in Figure 8-4. The 90-day resistivity of the PLC and OPC+10LS mortars for all the mixtures are shown in Figure 8-4

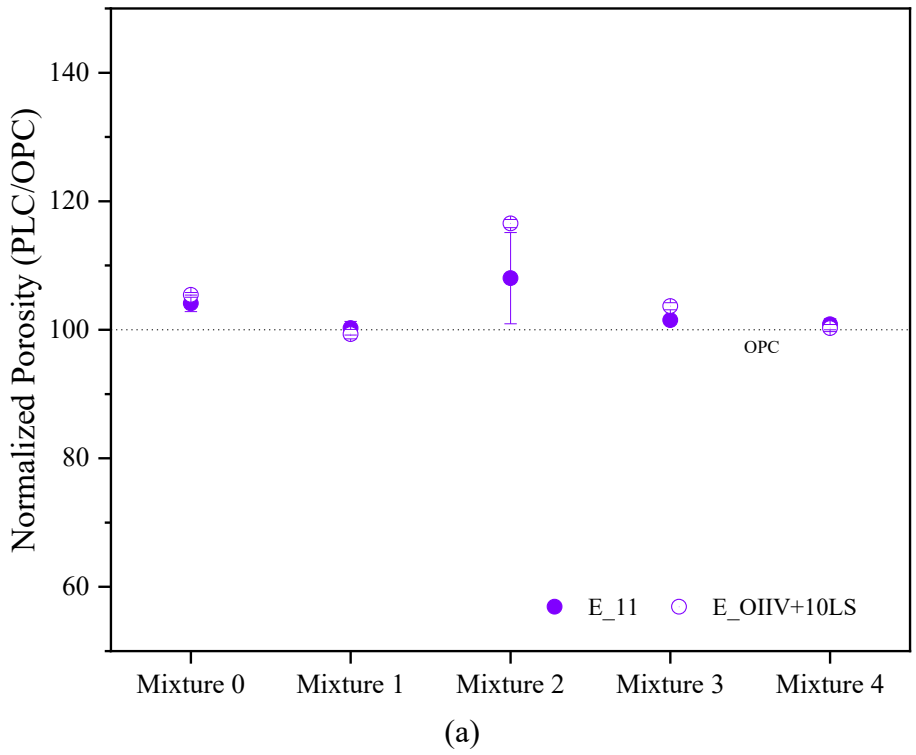

Figure 8-3. (a) Normalized porosity, and (b) Normalized electrical resistivity results for all the mixtures made using Cement E

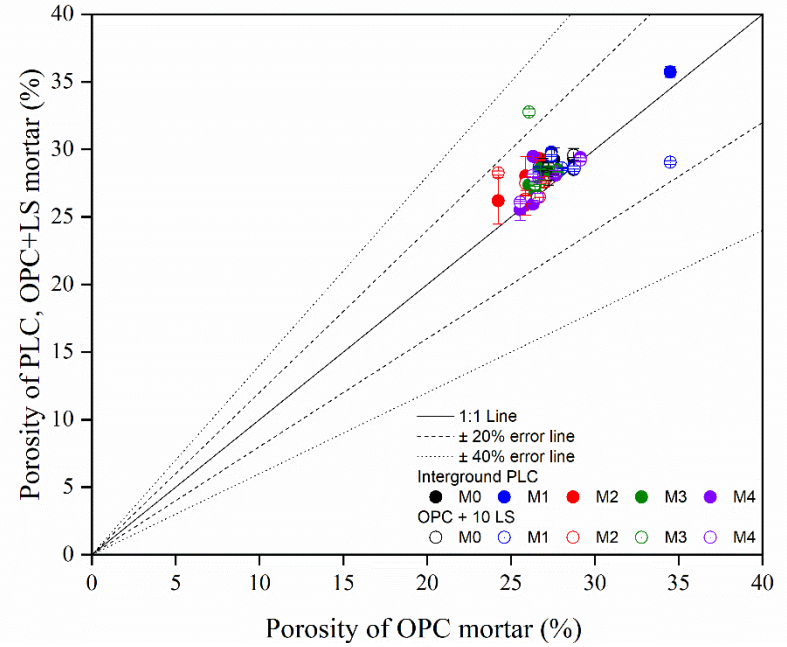

Figure 8-4. Porosity of PLC and OPC + 10 LS mortar compared to porosity of OPC mortars after 90 days

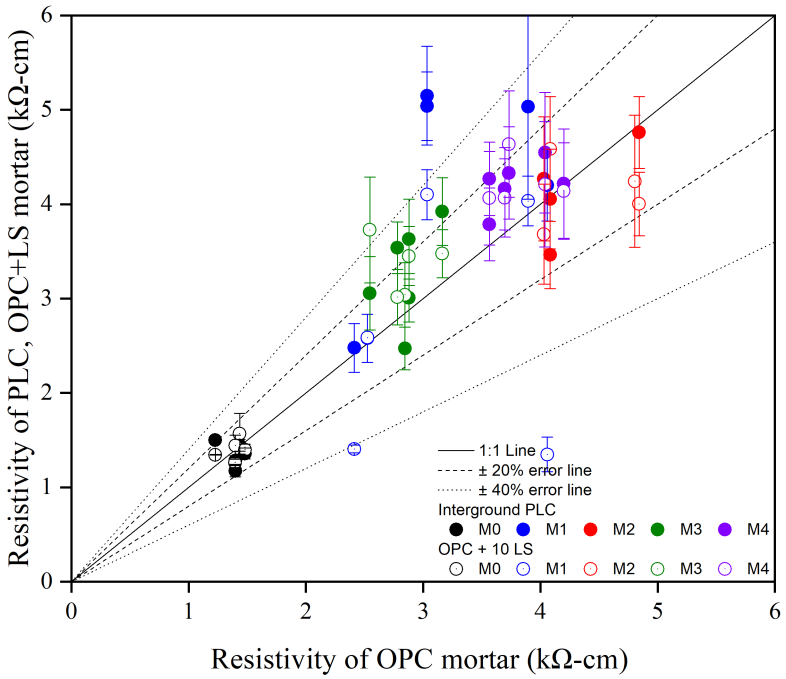

Figure 8-5. Resistivity of PLC and OPC + 10 LS mortar compared to pore connectivity of OPC mortars after 90 days

8.7 Discussion of the Results

The porosity of the PLC and OPC + 10LS mortar samples are observed to be consistently 5% higher than the porosity observed in OPC mortar samples (Figure 8-4). This occurred in both the plain systems and the systems containing SCM. The resistivity of the PLC and OPC + 10LS mortar samples is observed to be greater than the OPC samples (Figure 8-5). This occurred in both the plain systems and the systems containing SCM. Mixtures with SCMs have a greater resistivity than plain systems. The electrical resistivity of PLC mortar samples was 10%-30% higher than the OPC. The OPC+10LS mortars also had a higher resistivity than the OPC samples, barring a few outliers (suspected of having undergone inadequate blending during mixing). In general, it can be concluded that PLC and OPC+LS systems had an improved electrical resistivity.

The formation factor and pore connectivity were calculated (using equation (8-3) and (8-4) respectively) for the mixtures tested and are shown in Figure 8-6. Mixtures containing SCMs had a higher formation factor and lower pore connectivity than plain samples. The PLC + SCM mortar samples generally performed better than the OPC +SCM systems with a lower pore connectivity (approximately 10%) due to pore refinement. The OPC+10LS + SCM mortar samples also display a greater spread in results due potentially to the cement not being ground as finely and the LS also being coarser.

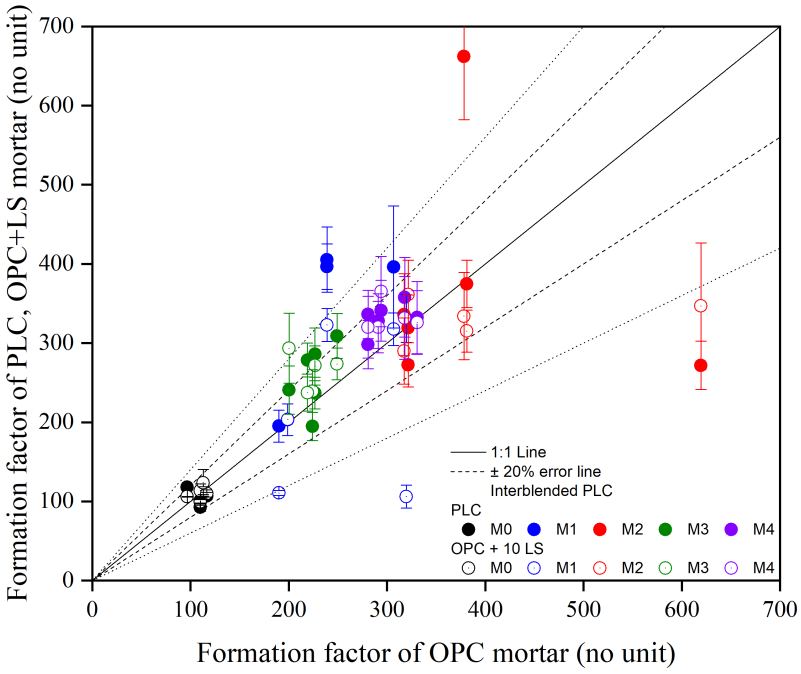

(a)

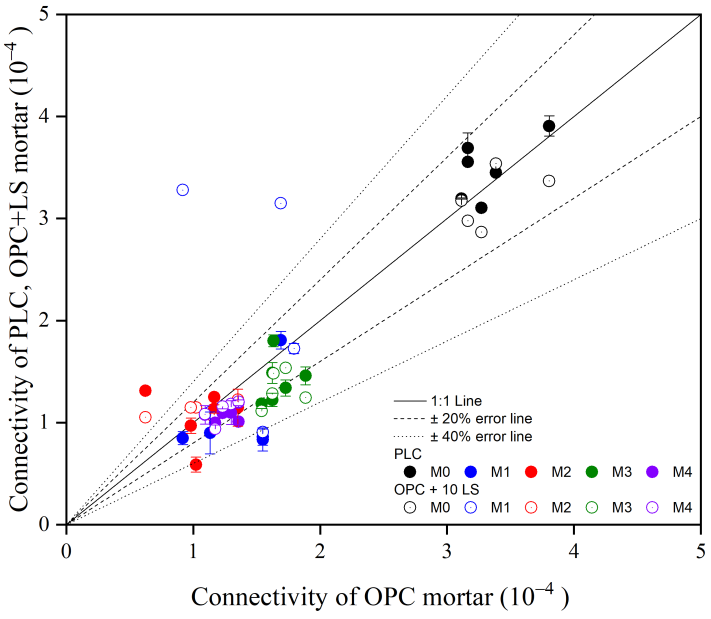

(b)

Figure 8-6. (a) Formation factor and (b) Pore connectivity of PLC and OPC + 10 LS mortar compared to pore connectivity of OPC mortars after 90 days

8.8 Significant Findings

This section examined the transport properties of OPC, PLC, and OPC+LS mortars. Porosity and electrical resistivity were measured. The formation factor and pore connectivity were computed. In general, the PLC and OPC +LS mortar samples displayed 5% greater porosity than samples made with OPC. However, the resistivity of PLC and OPC+LS mortar samples were 10% and 5% greater than OPC samples on average, respectively due to a reduction in pore connectivity.

9 Chloride Binding

Chlorides from seawater or deicing salts [93-97] can enter the concrete's pore structure and cause steel reinforcement corrosion. While a portion of these ions are transported through the pores, a portion of the chlorides are bound chemically or physically adsorbed on the pore walls. Changes have been made to ACI 318-19 to quantify the allowable chloride content in concrete mixtures in terms of total cementitious material content, not simply the cement content as was the case in prior code additions. Despite this advancement, questions remain regarding chlorides and concrete containing limestone. Specifically, there is uncertainty regarding whether the limestone portion of a PLC would contribute to the binding chlorides, and therefore, whether PLC and OPC+LS be treated differently than other cementitious systems. This portion of the research is intended to answer these questions by investigating chloride binding for mortar made using OPC, PLC, and OPC+ LS for both plain mixtures (M0) and SCM systems (M1 to M5).

9.1 Research Objectives

The primary objective is to determine whether the replacement of OPC with PLC or OPC with OPC + LS in conjunction with SCMs impacts chloride binding in concrete. Ultimately, this research will inform CALTRANS whether PLC can be used as an equivalent replacement of OPC without impacting the chloride binding performance. The work will also determine the variation in the chloride binding of pastes made using five sources of ASTM Type II/V OPCs (A, B, C, D, E). The work will also determine SCM's impact (fly ash, silica fume, slag) on the binding capacity of mixtures with limestone.

9.2 Background/Literature Review

Reports published in 2010 and 2011 discussed the durability of concrete made with PLC [98]. It was concluded that PLC containing up to 15% limestone does not negatively impact the chloride ingress in PLC-based systems. PLC can refine pore size distribution due to particle size, increase strength, and develop chemical reactions that produce carbo-aluminate phases, reducing porosity. Unfortunately, however, none of the work specifically examined the chloride binding in mixtures made using PLC.

Chlorides are typically introduced to hardened concrete from seawater or deicing salts [93-97]. A portion of the chloride remains in the pore solution and can move inside the concrete's pore structure, while a portion is chemically and physically bound. Chloride binding isotherms are typically developed for a concrete mixture as a plot of the free chloride content against the bound chloride content. These binding isotherms can be used in service life predictions and select appropriate cementitious materials to increase the durability of concrete structures [99]. Therefore, it is critical to characterize the effect of limestone on the chloride binding of concrete.

9.2.1 Binding Mechanisms

The two mechanisms involved in chloride binding are chemical binding (through Friedel's salt, Kuzel's salt, and calcium oxychloride) and physical adsorption (e.g., on C-S-H). Chemical binding can mainly be attributed to AFm and alumina-containing unhydrated phases such as C_3A and C_4AF [96, 100, 101].

In an OPC-based mixture, AFm chemically reacts with chlorides to transform into Kuzel's salt ($3CaO{\cdot}Al_2O_3{\cdot}0.5CaSO_4{\cdot}0.5CaCl_2{\cdot}10H_2O$) at low chloride concentrations (<0.1M) and Friedel's salt ($3CaO{\cdot}Al_2O_3{\cdot}CaCl_2{\cdot}10H_2O$) at higher concentrations (>0.1M) [96, 100, 102]. AFt becomes unstable at higher chloride concentrations (>2M) and partially decomposes to form AFm and Friedel's salt. The aluminate phases in C_3A and C_4AF may also chemically bind chlorides to form Friedel's salt [97, 100, 103]. Balonis et al. [101] suggest that a typical portland cement contains sulfates and/or carbonates, and as a result, initially formed AFm is a monosulfoaluminate type (Ms) and converts to OH-AFm (hydroxy AFm) at 25°C or monocarboaluminate (Mc) [53]. Depending on the phases' stability, the sulfate, hydroxyl, and carbonate anions can be displaced by chloride ions to form chloride AFm, which is essentially Friedel's salt [104, 105]. *Physical binding* can be attributed to the physical adsorption of chlorides on the surface of the C-S-H, C-A-H, and C-A-S-H phases [96]. The phenomenon occurs due to the electrostatic Van der Waals forces between charged particles, in this case, between chloride ions and the surface of these phases.

9.2.2 Limestone in Chloride Binding

Limestone may react with calcium aluminate hydrates (C-A-H) in SCM blends to form carboaluminate hydrates, (monocarboaluminate (Mc, $Ca_4Al_2(CO_3)(OH)_{12}{\cdot}5H_2O$) and hemicarboaluminate (Hc, $Ca_4Al_2(CO_3)_{0.5}(OH)_{13}{\cdot}5.5H_2O$) [106]). Ms, Mc, and Hc are all part of the monosulfate (AFm) family and can chemically bind chloride ions to form Friedel's salt (Fs, $Ca_4Al_2Cl_2(OH)_{12}{\cdot}4H_2O$) [106-108]. Ipavec et al. [109] found that the chloride binding capacity of limestone cements is strongly dependent on the external solution's pH. The chloride binding capacity decreases at pH~13.5 but remains unchanged at pH~12.8.

9.2.3 Binding Isotherms

Chloride binding isotherms relate the free (C_f) and bound (C_b) chlorides in concrete at a constant temperature [96]. The binding isotherm is dependent on the chemical composition of the system, including the total aluminate content, limestone content, the type and amount of SCMs used in the mixture, and the pH of the pore solution. The isotherms are typically represented quantitatively using either the Langmuir equation (equation (9-1)) or the Freundlich equation (equation (9-2)).

$$C_b = \frac{\alpha C_f}{\left(1 + \beta C_f\right)} \quad \textbf{(9-1)}$$

$$C_b = \alpha C_f^{\beta} \quad \textbf{(9-2)}$$

where α and β coefficients need to be determined experimentally.

Tang and Nilsson [102] found that the Langmuir isotherm is a good fit at low chloride concentrations (<0.05 M) and the Freundlich isotherm is a good fit at high chloride concentrations (>0.01 M). The Freundlich isotherm will be used in this work to fit the chloride binding data, as the chosen chloride concentrations start from 0.1 M.

9.2.4 Factors Affecting Chloride Binding

Several factors affect chloride binding capacity. Increased chloride binding is observed when cement paste is exposed to $CaCl_2$ solution compared to NaCl. This can be attributed to NaCl having to react first with $Ca(OH)_2$ to form $CaCl_2$ before reacting with the hydrated aluminate phases [110, 111]. If available, $Ca(OH)_2$ will then react with the $CaCl_2$ solution to form calcium oxychloride ($3Ca(OH)_2 \cdot CaCl_2 \cdot 12H_2O$) [95, 96, 103, 105, 112-118] at the correct temperature.

The pH of the pore solution is also an important factor. Delagrave et al. conducted chloride binding tests for cement powder immersed in saturated lime solutions ($Ca(OH)_2$+NaCl) (pH~12.5) and in alkaline solutions (NaOH+KOH+NaCl) (pH~13.5) [119]. They observed a higher amount of bound chlorides when immersed in the lime saturated solution, indicating that a lower pH of the external solution will cause an increase in bound chlorides [113, 119]. Zibara also observed an increase in the pH (13-14) of the storage solution reduced chloride binding [96]. Song et al. studied the influence of pH of hydration products on chloride binding and found that the pH of the external solution increased with time, likely because of the leaching out of alkalis such as K+ and Na+ from the cement matrix [37].

Bu and Weiss investigated the influence of alkali content on the microstructure, chloride binding, and electrical resistivity of concrete by fully saturating concrete specimens in NaOH solution [120]. They found that a higher alkali content in the external solution can decrease the resistivity of the pore solution, causing a reduction of bound chlorides. The higher alkali content also resulted in a denser microstructure, a higher formation factor, an increase in bulk resistivity, and a lower diffusion rate. They concluded that high alkali content in a cementitious system could improve its resistance to chloride ingress [38]; however, the alkali can impact other aspects of the concrete negatively (e.g., ASR). Ipavec et al. found that the presence of limestone decreased chloride binding at a pH~13.5 and did not significantly affect binding at pH~12.8 [109].

In simulated solution tests, saturated lime solution ($Ca(OH)_2$), sodium hydroxide (NaOH), potassium hydroxide (KOH), and sodium sulfate ($NaSO_4$) can be added to chloride solutions to increase the pH. A saturated lime solution has a pH ~12.4, and in the presence of $CaCl_2$, it will

form calcium oxychlorides, complicating the quantification of chloride binding. Sodium, hydroxide, and potassium ions in NaOH and KOH are alkali and contribute to the solution's alkalinity. However, sulfates in $NaSO_4$ are bound first to C_3A before chlorides, and this interrupts chloride binding. Hence, it is advisable to use NaOH and/or KOH to increase the pH of a chloride solution to maintain a pH like that in a concrete matrix.

The aluminate content in the cementitious matrix is another important factor in chloride binding. Increasing the amounts of C_3A was initially found to increase chloride binding [1, 5]. Later it was discovered that it is not only the C_3A but the total aluminate content (C_3A+C_4AF) that increases chloride binding [14, 25]. Aluminates can come from SCMs as well. The binding capacity is dependent on the alumina content of the binder. This is due to the increase of C-A-H and C-A-S-H, which provide a larger surface area for the physical adsorption of chlorides when compared to OPC. For example, silica fume, which contains less alumina than OPC, decreases chloride binding. Slag, which contains more alumina than OPC, increases chloride binding. Fly ash, which typically has the largest alumina content than slag and silica fume, strongly increases binding capacity [96, 109, 121].

9.3 Experimental Test Matrix

Chloride binding testing was performed to evaluate the relative performance of all cements in this study. The binding test will be described in the following section 9.5. The mortars described in section 9.4.1 were tested after flexural strength testing. These samples included mortars made from Type II/V OPCs from five different clinkers, namely A, B, C, D, and E. The samples exposed to sodium chloride (NaCl) as concrete in marine environments are constantly exposed to seawater. The chloride binding isotherms for each of the clinkers were compared to determine if there is variation among the chlorides bound by OPC. The same was done for PLC and OPC+10LS systems. The binding isotherm was measured for OPC, PLC, and OPC+10LS systems made using supplementary cementitious materials (SCMs), namely fly ash, silica fume, and slag. Finally, exposure to calcium chloride ($CaCl_2$) on the chloride binding capacity of PLCs was investigated. Only cement D was exposed to $CaCl_2$. The effect of $CaCl_2$ exposure was studied because it is commonly used as a deicing salt, and this work would provide useful insight into the chloride binding capacity in limestone cements.

The test matrix, comprising 80 mortar mixtures, is provided in Table 6.2.

9.4 Experimental Methods

9.4.1 Mortar samples

The w/cm of mortar pastes was 0.40. The mixing procedure is described in Section 6.4. The mortar samples were cast into cylindrical molds measuring 4 inches (101.6 mm) in diameter and 8 inches

(203.2 mm) in height. The cylinders were sealed, cured at 23°C for 91 days, demolded, then sliced into discs of 2.65 mm width. The discs were tested for tensile strength using the ball-on-three-ball (B3B) test [89], then double-bagged to prevent carbonation. The discs were crushed into smaller pieces using a mortar and pestle and passed through a 3/8-inch (9.5 mm) sieve. The crushed samples were stored in double plastic bags to avoid carbonation before chloride immersion.

9.4.2 Simulated pore solution

A simulated pore solution was prepared to maintain the pH of concrete (~13.5) in the chloride solutions. 102.6 g NaOH and 143.9 g KOH were mixed with 13,250 g DI water according to ASTM C1876-08 and stored in a 5-gallon bucket. The simulated pore solution was mixed with varying concentrations of NaCl and $CaCl_2$ salts to prepare chloride solutions.

9.4.3 Chloride solutions

Sodium chloride was dissolved in simulated pore solution to prepare NaCl concentrations of 0.1 M, 0.5 M, 1 M, 2 M, 3 M, and 5 M, respectively. Granular calcium chloride dihydrate ($CaCl_2 \cdot 2H_2O$, EMD Millipore Inc., reagent grade) was dissolved in simulated pore solution to prepare $CaCl_2$ solutions with concentrations of 0.1M, 0.5M, 1 M, 2 M, and 3 M, respectively (Note the 5M concentration was not prepared due to the formation of Calcium Oxychloride). All cement mixtures were immersed in NaCl solutions, while only cement D mixtures were immersed in $CaCl_2$ solutions.

9.5 Typical Experimental Measurement and Interpretation

9.5.1 Determination of bound chlorides

Approximately 5 g of crushed mortar sample was weighed and stored in a capped centrifuge tube (15 ml, VWR Inc.) with 5 ml chloride solutions (NaCl and $CaCl_2$) of varying concentrations sealed at 23±1°C for 30 days to reach equilibrium. 50µl of the equilibrated solutions was extracted using a pipette, and the chloride concentrations were determined by an automatic titration device shown in Figure 9-1. The bound chloride content was calculated using (Equation (9-3).

$$C_b = \frac{(c_0 - c_1) \cdot V_{sol} \cdot M_{Cl}}{m_{powder}} \quad \textbf{(9-3)}$$

where C_b is the bound chloride content (mg/g powder), and c_0 and c_1 are the initial and final Cl^- concentrations of the exposure solution (M), respectively, V_{sol} is the volume of the solution (ml), M_{Cl} is the molar mass of chloride, and m_{powder} is the mass of the powder (g). The curves were fitted using the Freundlich isotherm.

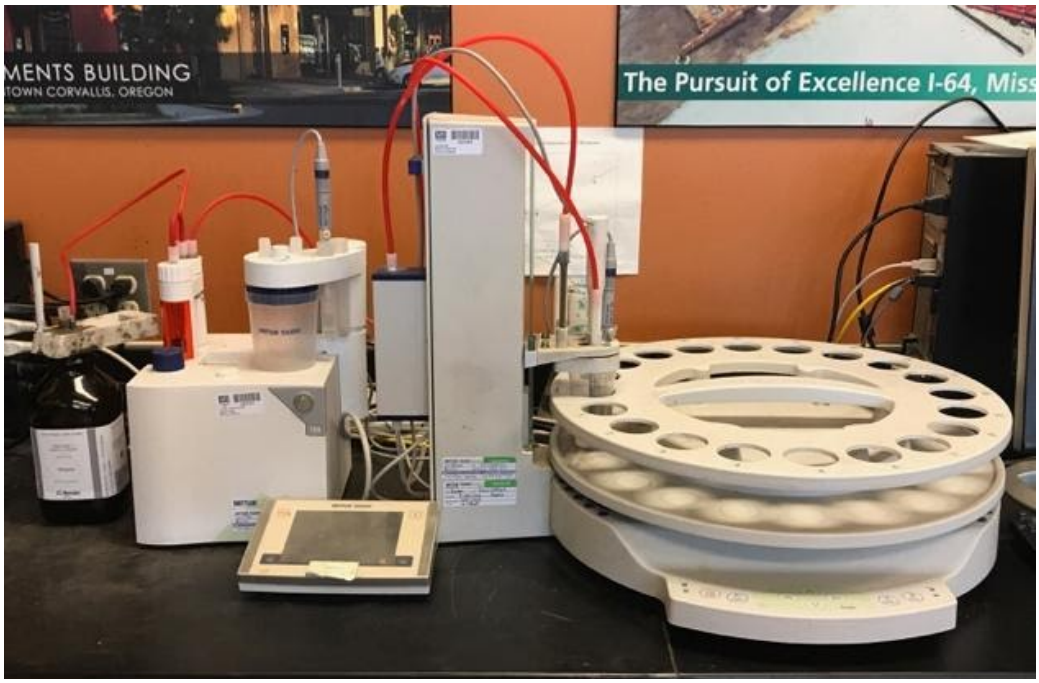

Figure 9-1. Automatic titration device used for determination of bound chlorides

9.5.2 Statistical analysis

Statistical analyses were performed to determine if there is a statistical difference between the chlorides bound by OPC, and PLC, OPC and OPC+10LS, and between mixtures with no SCMs (M0) and mixtures with SCMs (M1-M5). Because the data set contained several groups of data, the analysis of variance (ANOVA) was performed to determine the statistical significance between the means of the different data groups [122]. When one comparison test is conducted, the error rate of 0.05 is used. There will be many comparison tests in such a large set of data, which means the error rate must be adjusted accordingly (familywise error rate, FWER). The means were calculated from the bound chloride data among the different cements A-E. Tukey's honestly significant test (HSD) was performed for the ANOVA tests to correct for FWER.

For the comparison between M0 and M5, t-tests were performed instead, and a Bonferroni correction was used to correct for the FWER. The t-test is used here because the comparisons were for each pair only, so multiple comparisons were unnecessary.

9.6 Experimental Results

This chapter provides information on the binding of chloride ions in hydrated cement pastes made using OPC, PLC, and OPC+LS. In Appendix F, Tables E-OPC, E-PLC, E-OPC+10LS, and E-$CaCl_2$ provide results of the experimentally measured values for the bound chloride, comparing systems with varying limestone content (OPC, PLC, OPC+10LS) as determined using the procedure described in section 9.5.1. Specifically, Table E-OPC illustrates the bound chlorides by

OPC for the five different cement clinkers tested (A to E) with six sodium chloride (NaCl) concentrations (from 0 to 5 M) mixed with simulated pore solution to maintain concrete pH~13. Mixtures were prepared without supplementary cementitious materials (SCMs) and with SCMs as indicated through the mixture designations M0 to M5. M0 was prepared without SCM replacement, M1 was prepared with 25% fly ash, M2 was prepared with 20% fly ash and 5% silica fume, M3 was prepared with 50% slag, M4 was prepared with 25% slag, and 25% fly ash and M5 was prepared with 25% natural pozzolan. Similarly, experimental data is provided in Table E-PLC for the PLC clinker systems, Table E-OPC+10LS for the OPC plus LS systems, and in Table E-$CaCl_2$ for the cement clinker D systems that utilized calcium chloride ($CaCl_2$) as the salt solution as opposed to sodium chloride (NaCl).

As the chloride concentration increases, so does the binding, consistent with the trends commonly observed in the literature [96, 113]. A rise in molarity from 0.1M to 5M corresponds with an increase in free chloride concentration. This increase in free chloride concentration resulted in an increase in binding from ~0.9 to 13 mg Cl/g powder. This increase in binding with concentration can be seen in Figure 9-2, which shows the binding isotherm of M0 with clinker A. In general, the binding does not change significantly based on the parent cement clinker. The full set of binding isotherms of M0-M5 for cements A-E comparing isotherms with varying limestone content (OPC, PLC, OPC+10LS) can be found in Appendix F.

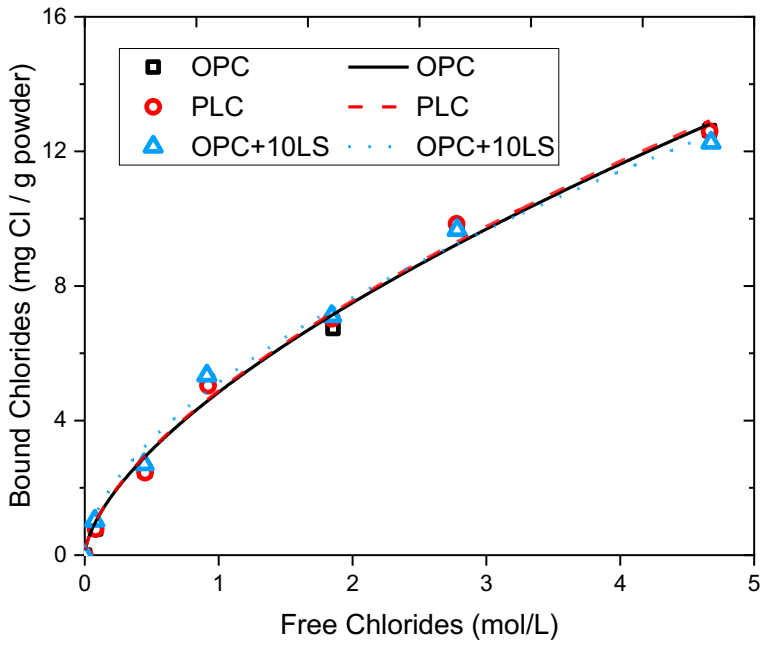

Figure 9-2. Binding isotherms for cement A (M0) (a) OPC, (b) PLC, (c) OPC+10LS

It can also be seen that when SCMs are added, as shown in Figure 9-3 for cement A, binding curves are slightly different for mixtures 0 to 4 in OPC, PLC, and OPC+10LS systems. Fitted parameters for the Freundlich isotherm are also provided in Appendix F.

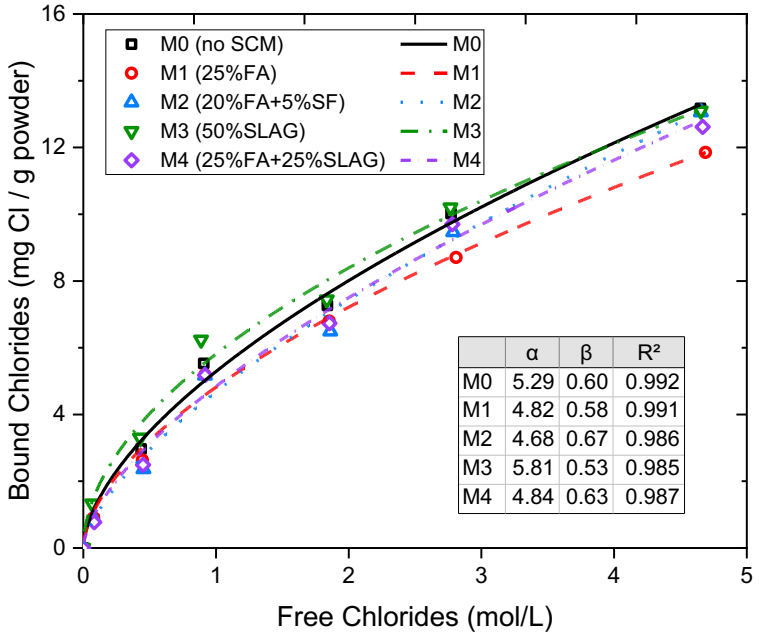

	α	β	R²
M0	5.29	0.60	0.992
M1	4.82	0.58	0.991
M2	4.68	0.67	0.986
M3	5.81	0.53	0.985
M4	4.84	0.63	0.987

(a)

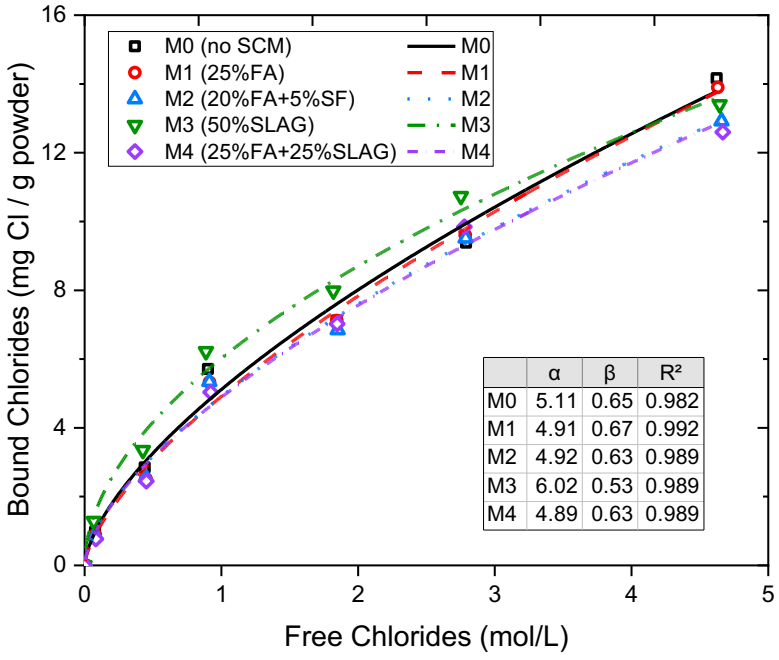

	α	β	R²
M0	5.11	0.65	0.982
M1	4.91	0.67	0.992
M2	4.92	0.63	0.989
M3	6.02	0.53	0.989
M4	4.89	0.63	0.989

(b)

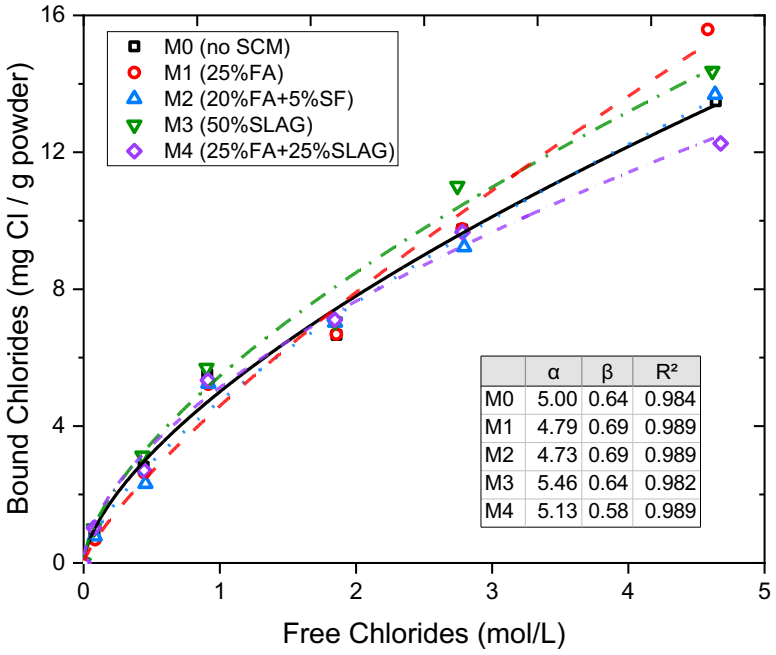

(c)

Figure 9-3. Binding isotherms for cement A (a) OPC, (b) PLC, (c) OPC+10LS

9.7 Discussion of results

9.7.1 Difference in binding of OPC, PLC, and OPC+10LS

The statistically significant difference between the binding isotherms of varying limestone content (OPC, PLC, OPC+10LS) and varying SCM content (M0-M5) was determined through statistical analysis (t-tests and Bonferroni; ANOVA and Tukey's HSD).

No statistical difference was found between the chloride binding of cement pastes made using clinkers A, B, C, D, or E. A statistical difference between bound chlorides of OPC vs. PLC at only one chloride concentration was investigated. A decision was made to require multiple indicators to conclude that there is a statistical difference between the entire system's bound chlorides. As such, the single indicators will not be considered statistically meaningful. No statistical difference was found between the chlorides bound by OPC, PLC, and OPC+10LS. It can be recommended that, based on chloride binding, these binders can be used as a direct substitute for one another.

9.7.2 Difference in binding of M0 and M1-M5

The majority of the SCM showed no statistical difference, except the mixture that contains 50% slag, or M4, which contains 25% slag and 25% fly ash. The slag mixtures tend to increase binding.

There was no statistical difference (as determined through Tukey's HSD procedure) between bound chloride in all the mixtures except M3. As such, all data (except M3) was used to obtain an overall Freundlich fit (α=4.79 and β=0.62), as shown in Figure 9-4. The error ranges shown represent one standard deviation and two standard deviations.

The implications of potentially using one single binding isotherm can be quite large. Considering the papers by Azad [123], the binding isotherm is combined with the formation factor to predict the apparent diffusion coefficient, using the approach described in Section 10.3.3. The use of a single series of alpha and beta terms could enable service life based on the apparent diffusion to be directly related to the formation factor.

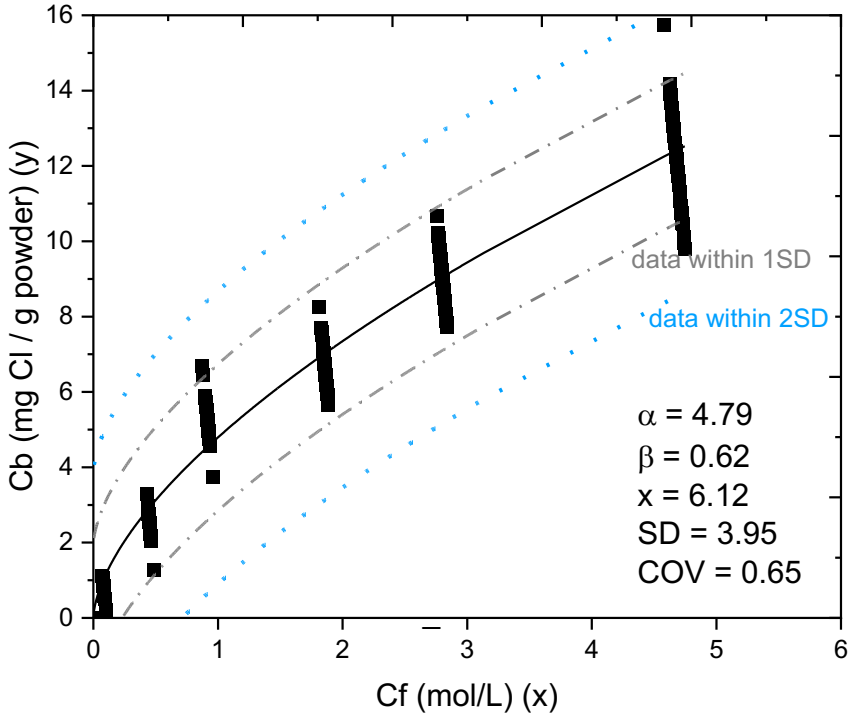

Figure 9-4. Freundlich fit for all data except for slag mixtures

9.7.3 Difference in binding of NaCl and $CaCl_2$

The difference in chloride binding between NaCl and $CaCl_2$ salts at 23°C is shown in Figure 9-5 for the plain (M0) and fly ash system (M1). An increase in binding capacity was observed when chlorides are exposed to $CaCl_2$ salt compared to NaCl. This has also been observed in earlier literature [113, 124, 125]. Similar observations can be made for the other mixtures, as shown in Appendix F.

The increase in chloride binding is not likely to be caused by calcium oxychloride formation due to the temperatures involved. Qiao et al. [126] compared systems with 0% and 40% fly ash,

respectively, and observed that the amount of Friedel's salt formed reaches a plateau at >2.0M for 0% fly ash; however, the plateau starts later at >2.5M for 40% fly ash. This was attributed to the reaction of all available aluminate phases with $CaCl_2$ solutions to form Friedel's salt at high chloride concentrations [113]. The result is that cementitious systems with higher alumina content produce more Friedel's salt at higher chloride concentrations, which changes the slope and inflection point of the binding isotherm. This is a possible explanation for the increase in bound chloride content for limestone and SCM blends exposed to $CaCl_2$ solutions.

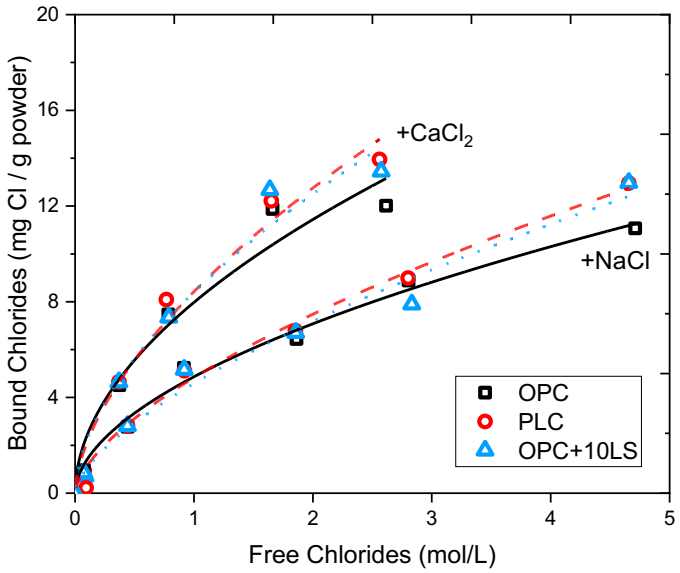

(a)

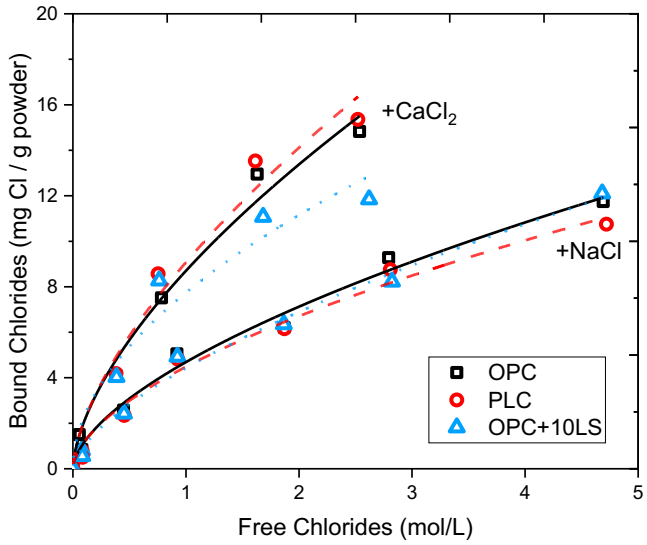

(b)

Figure 9-5. Chloride binding isotherms for cement D of M0 and M2 exposed to $CaCl_2$ salts in simulated pore solution

9.8 Significant Findings

The following conclusions can be drawn. No statistically significant difference was observed in the bound chloride contents of mixtures comparing OPC (i.e., ASTM C 150/AASHTO M 85), PLC (i.e., ASTM C 595/AASHTO M 240), and OPC+LS (provided that a specific size and quality of limestone is used). No statistically significant difference was observed in the bound chloride contents for mixtures comparing OPC, PLC, and OPC+LS with SCM (i.e., fly ash, silica fume, natural pozzolan) in more than one salt concentration. Mixtures containing PLC and OPC + LS mixtures made with ground granulated blast furnace slag outperformed the OPC+Slag systems.

The variation in chloride binding observed between all the commercial OPC mixtures made using different commercially available Type II and V cements is 9% at a chloride concentration of 0.1M and 3% at a 5M. As such, it appears feasible that a single binding isotherm can be used to satisfy the behavior of all Type II and V mixtures. Fly ash, silica fume, and natural pozzolans do not affect the chloride binding capacity in cementitious systems containing up to 15% interground limestone. Slag increased the bound chloride content by 21% at a chloride concentration of 0.1M and 6% at 5M. The chloride binding was 30% higher for $CaCl_2$ than NaCl at 0.1M chloride concentration and 40% higher from 0.5M to 3M.

It should also be noted that for the calculation of the allowable chloride content for new mixtures and comparison with set limits by ACI 318, limestone should be included in the total binder content. In other words, the entire OPC+SCM, PLC+SCM content or OPC+SCM+LS content be considered as binder. Note that as per ASTM C 595 and AASHTO M 240, the chloride content for a PLC is reported as part of the finished cement, which is in line with this suggestion.

10 Resistance to Chloride Ingress in Concrete

10.1 Research Objectives

This work compares the resistance of concrete made using OPC, PLC and OPC+LS to chloride ingress. This chapter builds on concepts from chapters 8 and 9 to predict performance.

10.2 Experimental Test Matrix

Concrete samples were prepared using the mixture proportions in Table 10.1. Cylindrical concrete samples were prepared (101.6 mm diameter and 203.2 mm height), demolded 24 hours after the casting, and were kept in a moist room for 90 days. The samples were stored at relative humidity of 50 ± 5% and temperature of 23 ± 5 °C for 90 days, then tested according to the experimental plan.

Table 10.1. Mixture proportions of concrete samples

		Mass (kg/m^3)					
Material	**S.G.**	**M0**	**M1**	**M2**	**M3**	**M4**	**M5**
Cement*	3.15	504.3	378.2	378.2	252.1	252.1	378.2
Fly Ash	2.34	0	126.1	100.9	0	126.1	0
Silica Fume	2.20	0	0	25.2	0	0	0
Slag	2.83	0	0	0	252.1	126.1	0
Natural Pozzolan	2.36	0	0	0	0	0	126.1
#23 Sand	2.67	732.1	732.1	732.1	732.1	732.1	732.1
#8 Coarse aggregate	2.48	813.4	813.4	813.4	813.4	813.4	813.4
Water	1.00	201.7	201.7	201.7	201.7	201.7	201.7

*Cement: OPC, PLC, OPC + LS

10.3 Experimental Methods

Table 10.2 summarizes the experimental characterizations performed on the concrete samples. One concrete sample was used for porosity measurements and formation factor. A second concrete sample was measured for acid soluble chloride profile.

Table 10.2. Experimental characterizations performed on concrete samples

Cement	**Mixture**	**Porosity**	**Formation factor**	**Acid-Soluble Chloride Profile**	
				ASTM C1152-04	**Calculated ***
	M1	✓	✓	--	✓

A (OPC, PLC)	**M2**	✓	✓	--	✓
	M3	✓	✓	--	✓
	M4	✓	✓	--	✓
C (OPC, PLC)	**M1**	✓	✓	--	✓
	M2	✓	✓	--	✓
	M3	✓	✓	--	✓
	M4	✓	✓	--	✓
E (OPC, PLC, OPC+10% limestone)	**M0**	OPC, PLC	OPC, PLC	OPC, PLC	OPC, PLC
	M1	✓	✓	OPC, PLC	✓
	M2	✓	✓	OPC, PLC	✓
	M3	✓	✓	OPC, PLC	✓
	M4	✓	✓	--	✓
	M5	✓	✓	--	--

✓ means all cement types were tested,
-- means experiments were not performed,
Calculated using the formation factor values and porosity

10.3.1 Porosity, Resistivity, and Apparent Formation Factor

Porosity was measured using AASHTO TP135-20 [90] (section 8.4.1); however, these concrete samples were saturated using a saturated lime solution (2g/L $Ca(OH)_2$). The uniaxial resistance was measured using AASHTO TP 119 [91] after 7 and 14 days of immersion in the simulated pore solution (Option A). The resistivity of the concrete sample (ρ_s) was calculated as described in chapter 8, section 8.4.2. The resistivity of the simulated pore solution (ρ_{ps}) was measured using the VWR B40PCID meter after 7- and 14-days duration of samples immersion (Table 10.3). The formation factor after 7 days and 14 days of immersion in solution was then calculated according to equation (8-3).

Table 10.3. Resistivity of pore solution after 7 and 14 days of immersion

Bucket number	Resistivity of pore solution after 7 days of samples' immersion (Ω·m)	Resistivity of pore solution after 14 days of samples' immersion (Ω·m)
Average	***0.115***	***0.116***
Standard Deviation	***0.001***	***0.001***

10.3.2 Experimental determination of acid soluble chloride profile and chloride apparent diffusion coefficient

The apparent diffusion coefficient (D_a) (using acid soluble chlorides) was determined experimentally using ASTM C1556-11a [127]. At an age of 6 months (section 10.2), the concrete samples were cut, sealed, and immersed in an aqueous sodium chloride solution (NaCl) with a concentration of 165 ± 1 g NaCl per 1 liter of solution for a duration of at least 35 days. At the end of the immersion period in NaCl solution, powder was collected from 8 different layers by grinding off materials in layers parallel to the surface that was in contact with NaCl solution. In this study, the powder was collected at 0.5, 2, 4, 6, 8.5, 11.5, 14.5, and 18 mm from the exposed surface. Following ASTM C1152-04 [128], the ground powders were exposed to nitric acid before titration in order to determine the acid-soluble chloride contents at different depths in the concrete sample.

The total apparent surface chloride content (C_{s-a}) and apparent diffusion coefficient (D_a) are obtained by fitting the data to Eq.10-1 using the approach described in ASTM C1556 as illustrated in Figure 10-1.

$$\frac{C_t(x,t) - C_0}{C_{s-a} - C_0} = erfc\left[\frac{x}{2\sqrt{D_a.t}}\right] \quad \textbf{(10-1)}$$

where, C_0 is the initial chloride concentration of the concrete before exposure to the NaCl solution, $C_t(x,t)$ is the chloride concentration at a given depth in the concrete specimen and a given exposure duration to NaCl solution, x (m) is the depth of the powder in the concrete sample, t is the time (s) at which the samples were extracted for chloride profiles testing [127].

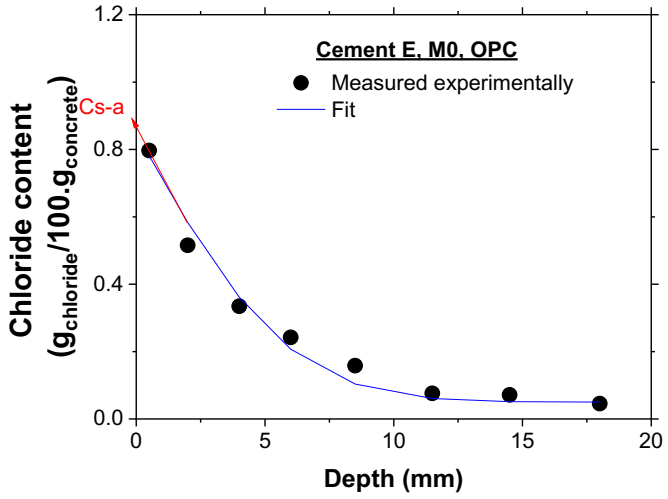

Figure 10-1. Acid-soluble chloride profile, experimental data to determine C_{s-a} and D_a

10.3.3 Theoretical determination of acid soluble chloride profile and D_a

As an alternative to the fitting approach described in 10.3.2, Azad et al. [99] defined equation (10-2) to relate the formation factor, porosity and chloride binding parameters to the D_a of concrete and $C_{s\text{-}a}$.

$$D_a = \frac{D_0}{\phi F\left(1 + \frac{1.25}{\phi}\alpha\beta C_{exp}^{\beta-1}\right)} \quad \textbf{(10-2)}$$

where, D_0 is the self-diffusion coefficient of chloride ion in water (1.38×10^{-9} m^2/s), ϕ is the porosity of the concrete sample, F is the measured formation factor of concrete, α and β are the Freundlich binding parameters for concrete samples, C_{exp} is the free chloride concentration on the surface that is in equilibrium with the chloride concentration of the exposure solution (100kg chloride per $1m^3$ NaCl solution).

The Freundlich binding parameters (α, β) were experimentally determined on all the mortar samples as described in chapter 9, section9.5. Equation (10-3) is used to scale these to concrete based on the assumption that the paste is the only portion of the system that binds chloride. The free chloride remains the same for both mortar and concrete.

$$C_{b-c} = C_b.\left(W_{f-m}\right)^{-1}.W_{f-c} \quad \textbf{(10-3)}$$

where, $C_{b\text{-}c}$ is the bound chlorides in concrete ($mg/g_{concrete}$), C_b is the bound chlorides in mortar (mg/g_{mortar}), $W_{f\text{-}m}$ is the mass fraction of cement paste in mortar (g_{paste}/g_{mortar}), $W_{f\text{-}c}$ is the paste content by mass in concrete ($g_{paste}/g_{concrete}$). The results from this scaling are shown in Figure 10-2.

The Freundlich model was then used to fit the data points calculated in Figure 10-2 (b) to determine the Freundlich binding parameter for the concrete samples.

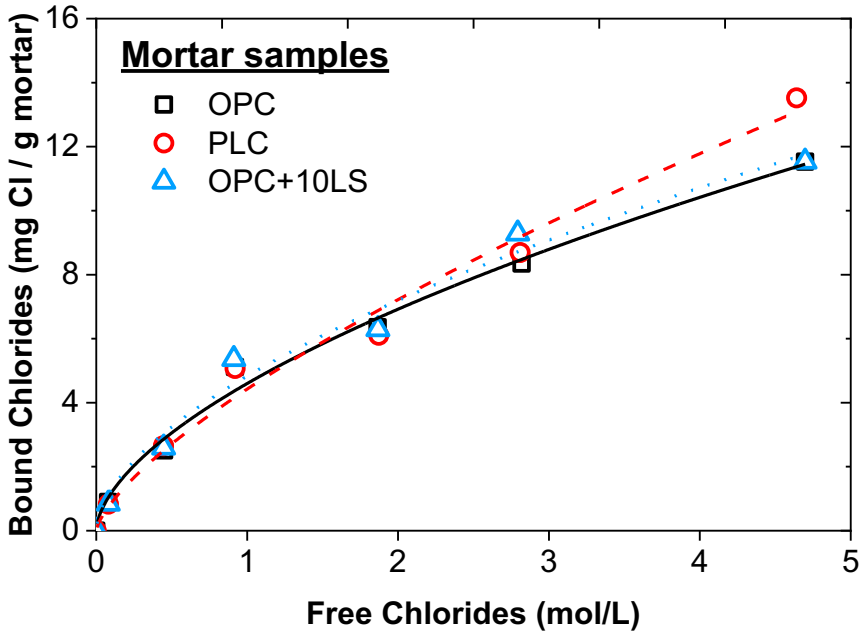

(a)

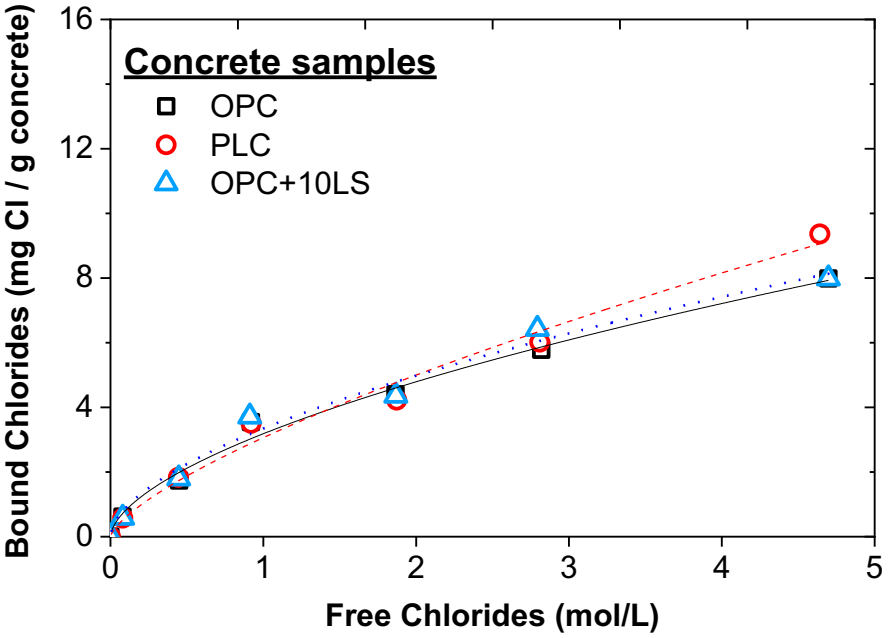

(b)

Figure 10-2. Freundlich binding isotherm: (a) determined experimentally on mortar samples, (b) scaled to concrete samples

In order to determine the acid soluble chloride profile theoretically using equation (10-1), $C_{s\text{-}a}$ needs to be calculated as shown in equation (10-4).

$$C_{s-a} = \phi C_{exp} + C_{s-b} \quad \textbf{(10-4)}$$

where, $\phi$is the porosity, C_{exp} is the free chloride content on the surface, $C_{s\text{-}b}$ is the bound chloride content on the surface. In 165g NaCl/liter of solution there is 2.8 moles of free chloride per liter of solution. Consequently, $C_{s\text{-}b}$ is the bound chloride that corresponds to 2.8 mol/liter of free chloride in the binding isotherm of concrete.

10.4 Experimental results

10.4.1 Porosity

Figure 10-3 shows the porosity of the OPC vs the PLC or OPC + LS concrete samples. In general, the OPC and PLC and OPC + LS system were similar with the exception of a mixture made using OLC +LS which showed a higher porosity than the corresponding OPC sample. This likely reflects insufficient consolidation. For this reason, results from this sample will not be presented in the next sections of this report. Further, this suggests that when LS is added separately special attention is needed to ensure that the sample can be properly consolidated.

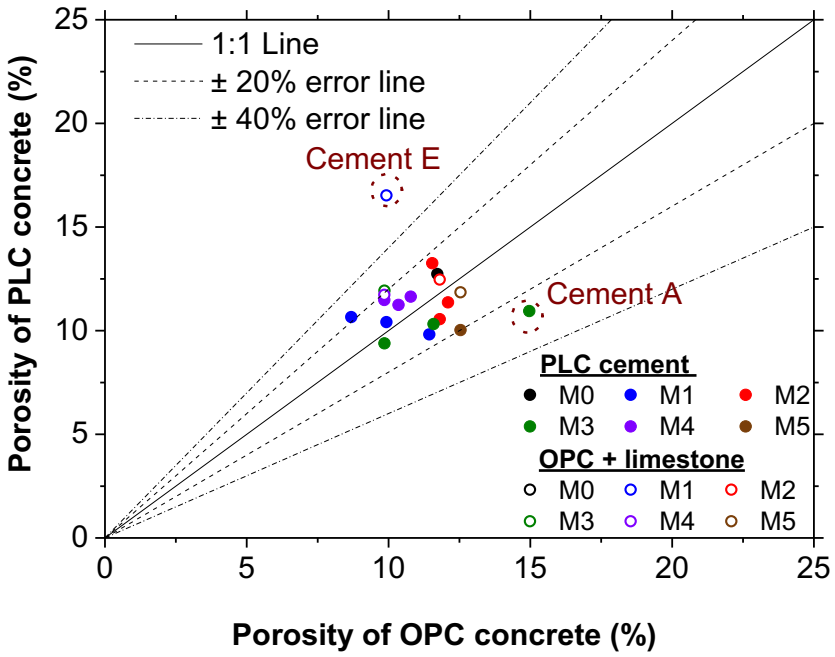

Figure 10-3. Porosity of concrete samples

The formation factor calculated after 7 days of samples' immersion were similar to those calculated after 14 days of samples' immersion in the simulated pore solution. Therefore, in this study, the results obtained after 14 days of samples' immersion are presented and used for the calculations of the chloride profiles.

Figure 10-4 is a plot of formation factor of all concrete made using OPC, PLC and OPC + LS. The points lying above this line signify that the PLC has a higher formation factor than OPC, and the points below correspond to lower formation factor. The plots also show ±20% and ±40% variation lines.

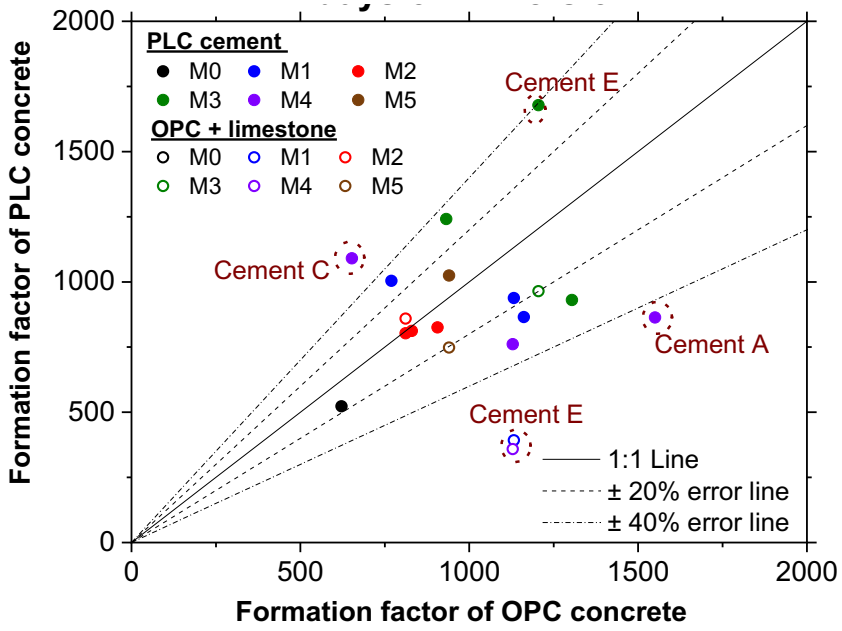

Figure 10-4. Formation factor of OPC, PLC and OPC+LS concrete samples. Circles show data outside the 40% error lines.

10.4.2 Experimental determination of acid soluble chloride profile and chloride apparent diffusion coefficient (ASTM C 1556)

The experimentally determined chloride profiles are shown in Figure 10-5. It can be noticed that for M1-M3 the profiles are nearly identical when comparing OPC and PLC. The only mixture that appears to indicate an increase in ingress is M0. Since there appeared to be an issue with concrete sample preparation, Figure 10-6 was developed to show the theoretical acid-soluble chloride profile obtained from the porosity, formation factor and binding parameters of both M0-OPC and M0-PLC concrete samples. Based on Figure 10-5 and Figure 10-6, it can be noted that both OPC and PLC samples have nearly identical chloride profiles.

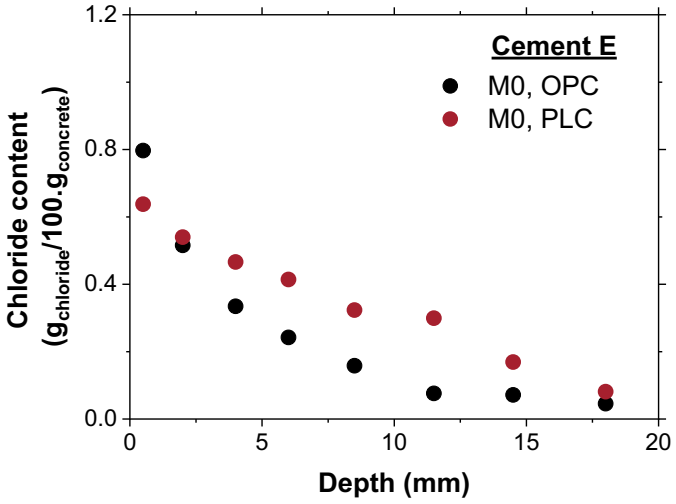
Cement E
M0, OPC
M0, PLC
Chloride content
(g_chloride/100.g_concrete)
Depth (mm)
0.0
0.4
0.8
1.2
0
5
10
15
20

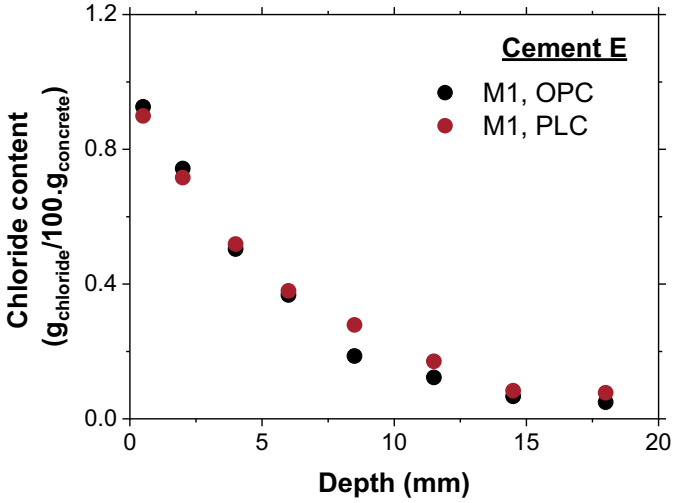
Cement E
M1, OPC
M1, PLC
Chloride content
(g_chloride/100.g_concrete)
Depth (mm)
0.0
0.4
0.8
1.2
0
5
10
15
20

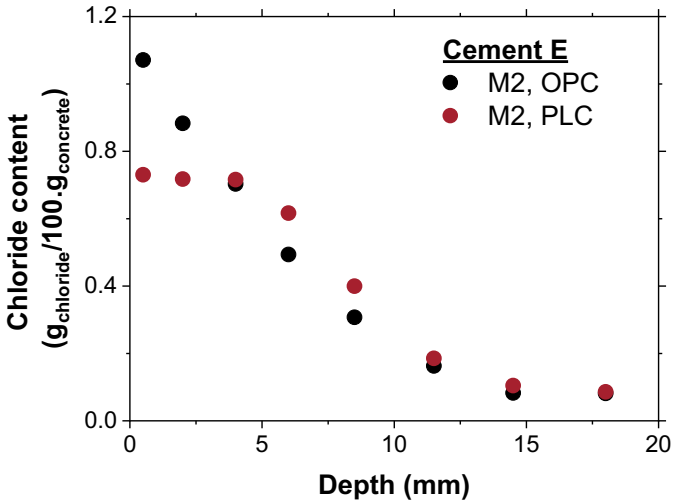
Cement E
M2, OPC
M2, PLC
Chloride content
(g_chloride/100.g_concrete)
Depth (mm)
0.0
0.4
0.8
1.2
0
5
10
15
20

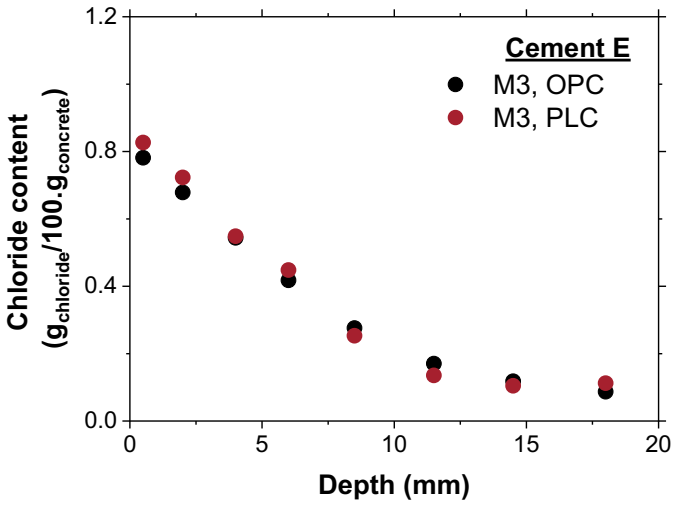

1719 **Figure 10-5. Acid-soluble chloride profiles obtained from experimental data for both OPC**
1720 **and PLC concrete samples**

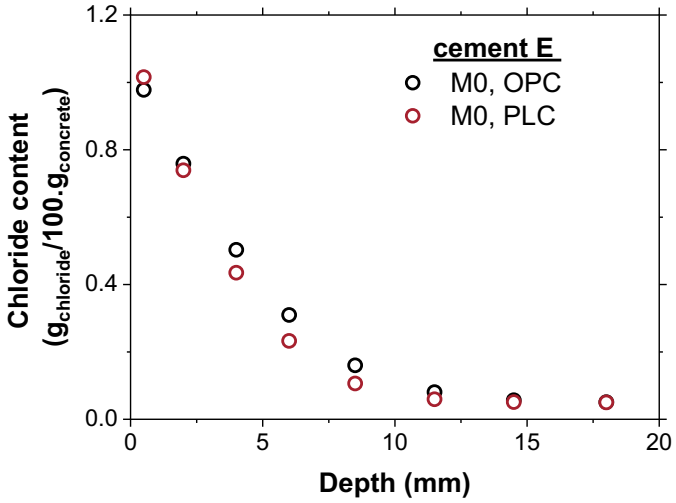

1721

1722 **Figure 10-6. Acid-soluble chloride profiles obtained theoretically for both M0, OPC and**
1723 **M0, PLC concrete samples**

1724

1725 The experimentally determined chloride apparent diffusion coefficient values of PLC concrete
1726 with respect to OPC concrete are illustrated in Figure 10-7. Figure 10-8 shows the experimental
1727 values of the total apparent surface chloride content in PLC samples with respect to OPC. It can
1728 be seen that for these mixtures, PLC and OPC are comparable with the exception of mixture 0
1729 which, as we have understood from the SAC, is not used in environments where corrosion is a
1730 primary concern.

1731

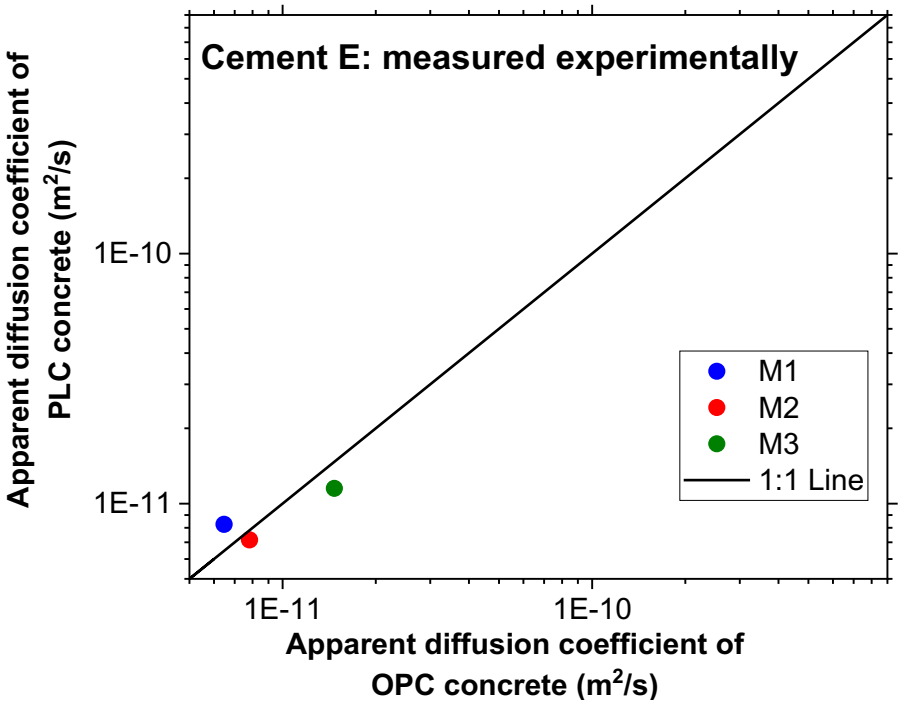

1732

1733 **Figure 10-7. Experimental values of D_a for OPC and PLC concrete samples**

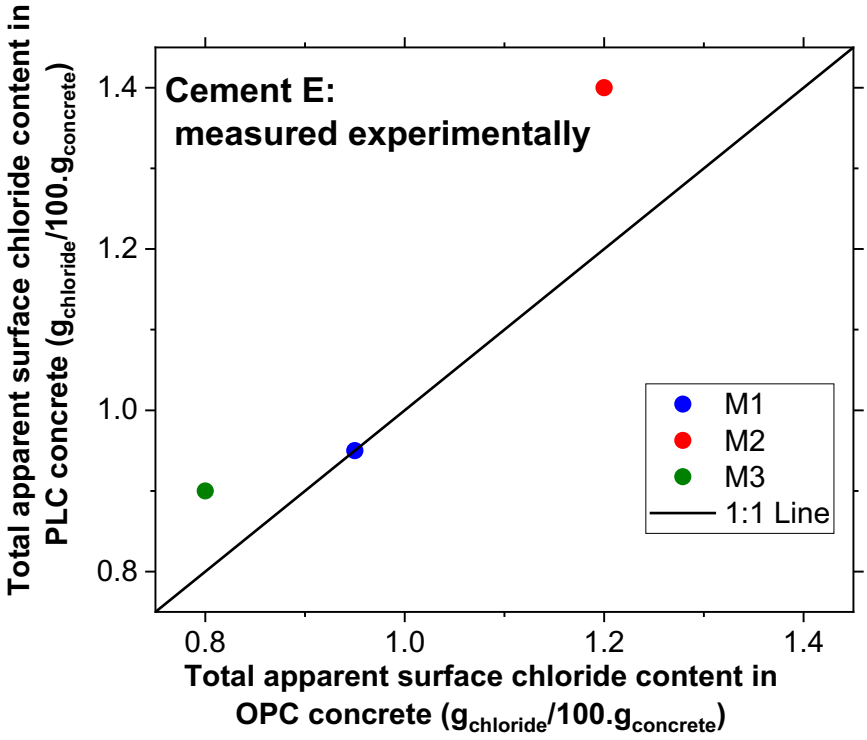

1734

1735 **Figure 10-8. Experimental values of C_{s-a} for OPC and PLC concrete samples**

Table 10.4. Experimental values of C_{s-a} and D_a for OPC and PLC concrete samples

Cement E	Da (m^2/s)		C_{s-a} ($g_{chloride}/100g_{concrete}$)	
	OPC	PLC	OPC	PLC
M1	6.47E-12	8.26E-12	0.95	0.95
M2	7.82E-12	7.16E-12	1.2	1.4
M3	1.47E-11	1.15E-11	0.8	0.9

10.4.3 Theoretical determination of acid soluble chloride profile and chloride apparent diffusion coefficient parameters

Table 10.5 summarizes the Freundlich binding parameters of concrete samples (obtained from equation 10-3 using the data in chapter 9).

Table 10.5. Freundlich binding parameters of concrete samples

Cement		A			C			E		
Sample		OPC	PLC	OPC +LS	OPC	PLC	OPC +LS	OPC	PLC	OPC +LS
M0	α_c	3.66	3.54	3.46	3.23	3.3	3.2	3.18	3.06	3.34
	β_c	0.6	0.65	0.64	0.61	0.6	0.59	0.59	0.71	0.57
	R^2	0.994	0.986	0.987	0.988	0.989	0.986	0.989	0.982	0.979
M1	α_c	3.42	3.49	3.39	3.26	3.19	3.13	3.14	3.29	2.94
	β_c	0.58	0.67	0.69	0.53	0.61	0.58	0.66	0.56	0.59
	R^2	0.993	0.993	0.991	0.968	0.987	0.991	0.985	0.978	0.991
M2	α_c	3.34	3.51	3.37	3.15	3.01	3.33	3.01	3.16	3.42
	β_c	0.67	0.63	0.69	0.56	0.65	0.58	0.58	0.55	0.66
	R^2	0.989	0.991	0.991	0.97	0.988	0.971	0.98	0.96	0.987
M3	α_c	4.08	4.23	3.83	4.23	3.77	3.71	4.28	3.73	3.97
	β_c	0.53	0.53	0.64	0.5	0.59	0.57	0.44	0.63	0.6
	R^2	0.988	0.991	0.986	0.985	0.988	0.979	0.968	0.982	0.989
M4	α_c	3.46	3.49	3.66	3.85	3.77	4.01	3.87	3.83	3.64
	β_c	0.63	0.63	0.58	0.54	0.63	0.58	0.59	0.57	0.63
	R^2	0.99	0.991	0.992	0.994	0.99	0.97	0.991	0.966	0.993

Figure 10-9 (a) illustrates the apparent diffusion coefficient based on the formation factor and porosity calculated using equation (10-2). The total apparent surface chloride content (C_{s-a}) calculated using equation (10-4) is shown in Figure 10-9 (b). It can be noted that both C_{s-a} and D_a values determined on OPC samples are comparable to those determined on the corresponding PLC samples.

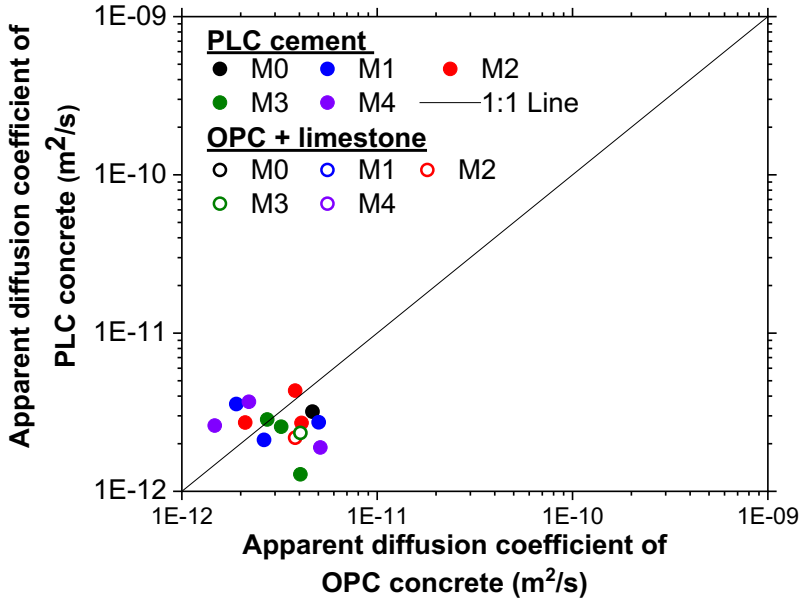

(a)

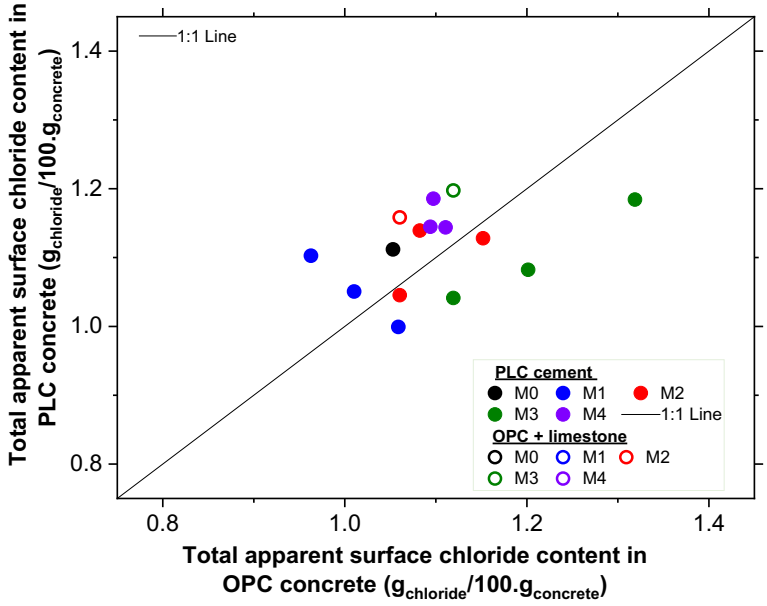

(b)

Figure 10-9. (a) Calculated values of D_a based on the porosity and formation factor measurements for OPC and PLC concrete samples, (b) Calculated values of C_{s-a} based on porosity and formation factor measurements for OPC and PLC concrete samples

10.5 Discussion of Results

The porosity, chloride binding, and formation factor of PLC concrete samples are similar to their OPC counterparts. Samples containing SCM in the mixture design show a higher formation factor. This is due to the refinement of the microstructure induced by SCMs addition.

The acid soluble chloride profiles were calculated for all the mixtures listed in Table 10.1 using equation (10-1) with the parameters from section 10.4.3, the porosities and formation factor for an exposure duration to chloride solution of 20 years (Co = 0.05 ($g_{chloride}/100g_{concrete}$)). These acid soluble profiles for all the mixtures are shown in Appendix G. No significant difference can be noted between the acid soluble profiles of both PLC and OPC samples. The chloride content at 20 years and 50 mm depth (a typical rebar level) are shown in Figure 10-10. The chloride content for all these mixtures at 50mm depth after 20 years of exposure to salt solution range between 2.7 g/100g cement and 5.4g/100g cement. Based on these results, it can be seen that the chloride content in PLC samples is either comparable to or slightly lower than that of the OPC samples.

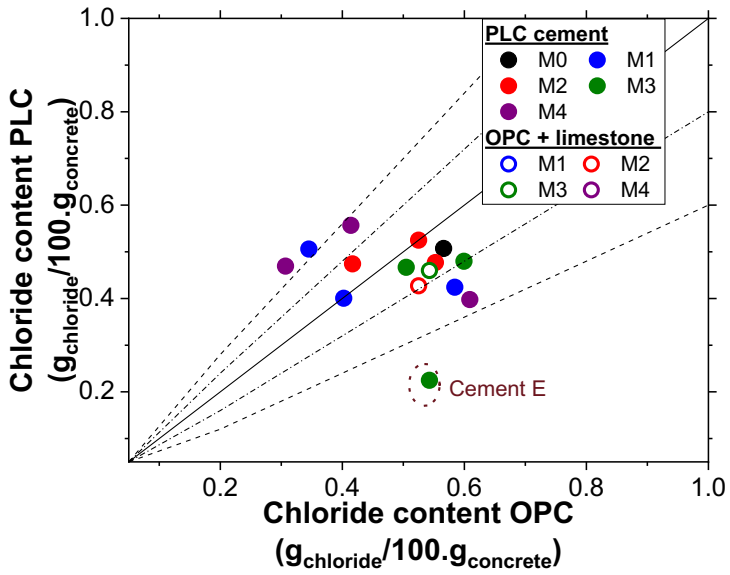

Figure 10-10. Comparison between the chloride content of OPC and PLC concrete at 50 mm depth determined at an exposure period 20 years

10.6 Significant Findings

Based on the collected measurements, it can be concluded that the porosity, formation factor, and chloride apparent diffusion coefficient of PLC concrete are comparable to those obtained on OPC concrete.

11 Corrosion of Reinforcing Steel

The critical chloride threshold (Cl_{crit}) is defined as the concentration of chlorides at the steel-concrete interface that is required to initiate corrosion. Cl_{crit} draws its prominence from the fact that it is a critical parameter to estimate the service life of a reinforced concrete structure. Steel-cementitious system with a high Cl_{crit} value is expected to have a longer service life when compared to the systems with a low Cl_{crit} values. As prominent as this parameter may be, it is surprising that there is very little agreement on Cl_{crit} values. Even though several test setups have been used in the past to assess Cl_{crit} [129], these tests each have limitations and drawbacks and all result in different Cl_{crit} values; this has led to little consensus on realistic Cl_{crit} values. A new test method, the OC_{crit} method, has been developed to quantify the Cl_{crit} of steel-cementitious systems [130, 131]. This method was developed at Oregon State University with an objective to establish a standardized, reliable, and timely test to quantify the amount of chlorides necessary to initiate corrosion. Past studies have shown that the OC_{crit} could yield results faster and more reliably than other accelerated corrosion tests [130, 131].

11.1 Research Objectives

In this chapter, the corrosion performance of reinforcing steel embedded in OPC, PLC, and OPC+LS is evaluated using the OC_{crit} method and the modified ASTM G109 method. The primary objective is to determine whether the replacement of OPC with PLC or OPC + LS in combination with SCMs impacts the corrosion performance of reinforcing steel embedded in these systems. A standardized, fast, and reliable test method can help the SHAs assess these products, in a timely manner, and will provide data to ensure the use of these materials results in acceptable long-term performance [129]. In this study, the OC_{crit} method is used to assess the Cl_{crit} of OPC and PLC cementitious systems with and without SCM replacements. The experimental program in this study assesses the corrosion performance of PLC as opposed to OPC cementitious systems. The specimens were also evaluated using the modified ASTM G109 test method to compare the Cl_{crit} values and time to activation with that of the OC_{crit} specimens. It should be noted that both these test methods have different criteria for corrosion activation and hence may not indicate the same corrosion activity.

11.2 Background/Literature Review

Corrosion is an electrochemical process that involves an anode, a cathode, an electrolyte, and an electrical connection between the anode and cathode for the transfer of electrons. Reactions take place on the surface of both the anodic and cathodic sites whereas mass loss takes place exclusively at the anodic site. The pore water in mortar or concrete acts as the electrolyte making the cementitious system behave as a conducting medium. Cathodic and anodic reaction sites may be located on the same reinforcement (microcell) or on different reinforcing bars (macrocell).

The oxidation and reduction reactions that take place at the anodic and cathodic sites respectively are referred to as half-cell reactions. At the anode, iron is oxidized and goes into solution as ferrous ions, as follows:

$$Fe \rightarrow Fe^{2+} + 2e^{-} \quad \textbf{(11-1)}$$

Depending on the availability of oxygen and the pH of the environment, the following reduction reaction takes place at the cathode:

$$2H_2O + O_2 + 4e^{-} \rightarrow 4OH^{-} \quad \textbf{(11-2)}$$

The ferrous ions that are produced and in solution at the anodic site react with hydroxyl ions to form ferrous hydroxide.

$$Fe^{2+} + 2OH^{-} \rightarrow Fe(OH)_2 \quad \textbf{(11-3)}$$

Ferrous hydroxide can be further oxidized to form hydrated ferric oxide (red brown rust) and hydrated magnetite (green rust). Hydrated ferric oxide and hydrated magnetite can further dehydrate to produce red rust, ferric oxide, Fe_2O_3, and black magnetite, Fe_3O_4. In highly alkaline concrete pore solution environments, ferrous hydroxide can also oxidize to gamma ferric oxyhydroxide (*2γ-FeOOH)*. The reactions follow:

$$4Fe(OH)_2 + O_2 \rightarrow 2Fe_2O_3 \cdot H_2O + 2H_2O \quad \textbf{(11-4)}$$

$$6Fe(OH)_2 + O_2 \rightarrow 2Fe_3O_4 \cdot H_2O + 4H_2O \quad \textbf{(11-5)}$$

$$2Fe(OH)_2 + \frac{1}{2}O_2 \rightarrow 2\gamma - FeOOH + H_2O \quad \textbf{(11-6)}$$

The products from the above reactions can form a passive layer around the steel reinforcing bar and the extent to which each product can protect the steel is still a topic of interest. This stability of this protective passive film can be affected by two environmental exposure conditions: 1) chlorides and 2) carbonation. Both phenomena can break down the passive layer and initiate corrosion of the reinforcement. The corrosion products generally have a larger volume than the base steel reinforcement which can result in internal pressure on the concrete cover, leading to development of tensile stresses. These tensile stresses can lead to cracking, spalling, and deterioration of structural capacity. Loss of steel ductility, reduction in bond strength between the steel reinforcement and concrete, and loss of cross-sectional area of the steel reinforcement are also other consequences of corrosion [132]. In the presence of chlorides, oxygen and moisture, the

passive layer between the steel reinforcement and the concrete is disrupted and localize corrosion initiates. Calcium chloroaluminate (Freidel's Salt) is formed when the chloride ions form a complex with hydration products [133]. If the total concentration of chlorides exceeds the binding capacity of cementitious system, the remaining (e.g., free) chlorides can induce corrosion. The study presented in the current chapter focuses on the chloride-induced corrosion of reinforcing steel.

Corrosion studies on PLCs are crucial because the performance of embedded steel reinforcing bar in a PLC cementitious system when exposed to these environments will ultimately determine the service life of these structures. The type and characteristics of the cementitious cover surrounding the reinforcing bar directly influences the time to corrosion initiation and the propagation of this corrosion. As such, there is a need to assess the corrosion behavior of steel-embedded in PLC cementitious systems. Limited research has been performed on chloride-induced steel corrosion in concrete containing PLC [134-136]. These past studies demonstrate that, up to a certain replacement level of interground limestone filler, PLCs can reduce the corrosion rate of embedded steel. They also report that cement content and fineness have a significant impact on the corrosion behavior. One study reports that mortars with OPC exhibit better durability than mortars containing limestone cement [136]. Because of this, corrosion studies are needed to determine the potential influence of PLCs on the corrosion of steel reinforcement corrosion when exposed to chlorides.

PLC systems, in combination with SCMs such as fly ash, have shown promising results, gaining more credibility as an eco-friendly material. Concrete specimens with PLC have been reported to produce higher compressive strengths than OPC when fly ash is incorporated into the mixture [137]. However, limited research has been performed on the corrosion performance of these systems. This research investigates that gap in knowledge.

11.3 Experimental Test Matrix

The performance of OPC and PLC with select SCM combinations, as shown in Table 11-1, were evaluated. The results include the average chloride concentration in the mortar cover, Cl_{test}, and the times to corrosion initiation. For each SCM combination, specimens were cast with portland cement E_OIIV and PLC E_L11. Comparisons of the corrosion behavior of the steel reinforcement embedded in these systems is then made. Note that the Cl_{test} is the average chloride concentration of the mortar cover and this is not the Cl_{crit}. Trejo and Vaddey (2020) developed a correlation between the Cl_{test} and Cl_{crit} as follows [131]:

$$\frac{Cl_{crit}}{Cl_{test}} = 0.147 + 0.844 \cdot {}^{w}/_{cm} + 0.083Cl_{exp} - 0.014pH_{exp} + 0.004t_{exp} \qquad \textbf{(11-7)}$$

where w/cm is the water to cementitious materials ratio, Cl_{exp} is the concentration of the chloride exposure solution, pH_{exp} is the pH of the exposure solution, and t_{exp} is the time for the specimen to initiate corrosion. Note that Cl_{test} and Cl_{crit} are expressed as percent by cement mass, Cl_{exp} is expressed as percent, and t_{exp} is expressed in days. For this testing, the Cl_{exp} was 2% for all testing, the pH_{exp} was 12.5 for all testing, and the w/cm was 0.4 for all specimens. Using this information, equation (11-7) can be reduced as follows:

$$\frac{Cl_{crit}}{Cl_{test}} = 0.457 + 0.004t_{exp} \quad \textbf{(11-8)}$$

In addition to the cases identified in Table 11.1, OPCs and PLCs from two other clinker sources, namely C_OV, C_L10, A_O11, and A_L15, were also evaluated using the modified ASTM G109 method. For the modified ASTM G109 testing, all cements were evaluated with a 25% fly ash replacement.

11.4 Experimental Methods

11.4.1 OC_{crit} method

A water to cementitious material ratio (w/cm) of 0.4 was used for all the cases. Once the specimens were cast, they were cured in a moist room with 100% RH for 56 days. At the end of the curing period, the anodic specimens were transferred in to a 2% Cl^- solution saturated with calcium hydroxide ($Ca(OH)_2$). The cathodic specimens were stored in a container with saturated $Ca(OH)_2$ solution. The open circuit potential (OCP) of the anodic specimens were measured using a Cu-$CuSO_4$ on all weekdays since the start of exposure. Previous work indicated that microcell current (I_{macro}) and linear polarization resistance (R_p) testing exhibited large scatter [130] when compared to OCP measurements. Because of this, OCP was selected to monitor the corrosion initiation in this program. OCP was recorded on a daily basis and a period of 2 consecutive days during which the OCP was more negative than -350 mV was considered to represent initiation of corrosion. Note that the activation criterion is defined based on the OCP measured using a Cu-$CuSO_4$ electrode and will differ for other standard electrodes. The setup for this test method is illustrated in Figure 11-1.

Table 11.1. Experimental program for OCcrit study

No.	Cement type	SCM addition
1	E_OIIV	Control
2		25FA1
3		20FA1-5SF
4		50SL
5		25FA1-25SL
6	E_L11	25FA1
7		20FA1-5SF
8		50SL
9		25FA1-25SL

Once the specimens have activated, the cover was broken from the test specimen and tested for both water and acid soluble chlorides using the AASHTO TP 260 method. In addition to determining the average chloride concentration of the cover, this testing also provides information on the ratio of free to bound chlorides. Chlorides are present in concrete in two forms: 1) free chlorides that are dissolved in the pore solution and 2) bound chlorides that are physically and chemically bound to the cement hydrates. The free chlorides are responsible for initiating the corrosion process. There are two types of mechanisms by which chloride binding occurs. In the first mechanism, chloride ions are physically adsorbed onto the surface of cement hydrates, especially C-S-H. In the second mechanism, which chemically occurs, chlorides react with monosulfate (AFm) compounds resulting in chloride containing AFm compounds such as Freidel's salt ($C_3A.CaCl_2.10H_2O$). The ratio of water to acid soluble chlorides (WSC/ASC) indicates the relative quantity of bound chlorides in the specimens. If the WSC/ASC ratio is close to unity, there are large concentrations of free chlorides in the pore solution and this indicates a lower binding capacity.

Studies have suggested that the chloride binding capacity of specimens depend on the aluminum content of the binder. Specimens blended with fly ash, slag, or metakaolin have been reported to exhibit increased chloride binding capacities when compared to specimens that were blended with silica fume [138]. This was reported to be attributed to the higher aluminum content of the supplementary cementitious materials. A higher CSH content generally leads to an increased chloride binding [95].

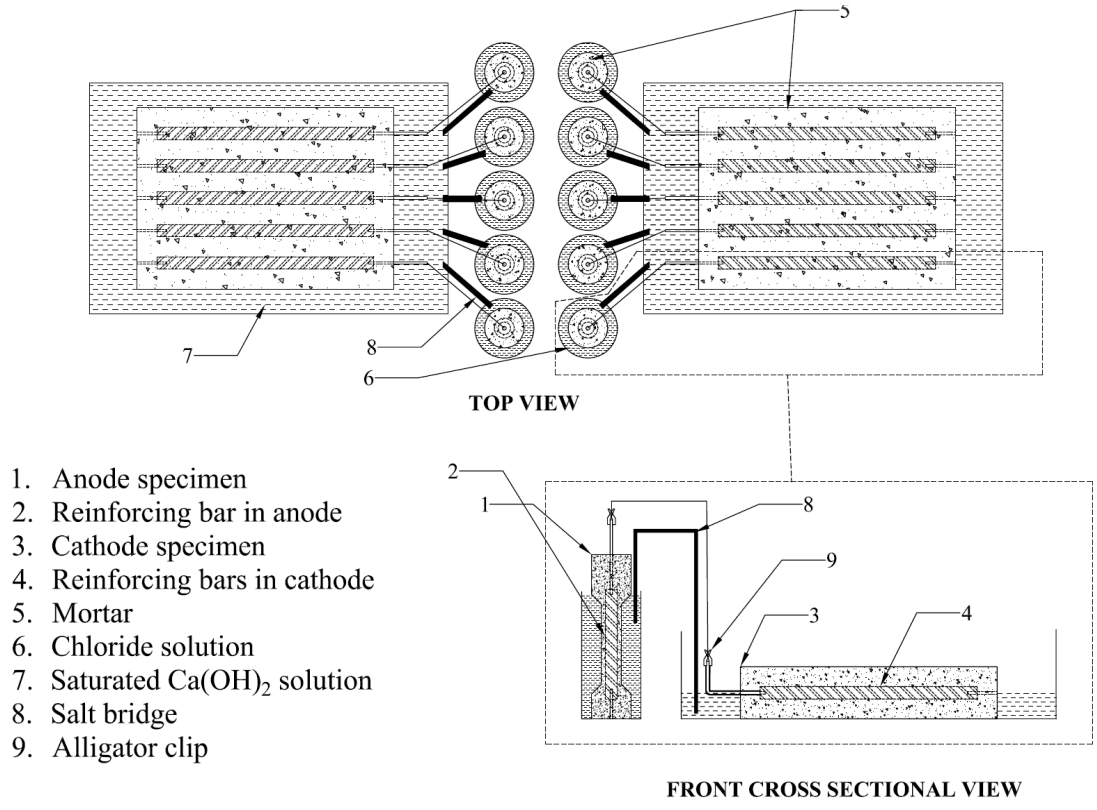

Figure 11-1. Setup for the OC_{crit} test method.

11.4.2 Modified ASTM G109 method

ASTM G109 method is based on the macrocell corrosion process and is commonly used to study corrosion of steel reinforcing bars embedded in concrete [139, 140]. In this method, concrete prisms are cast with one anodic reinforcement bar and two cathodic reinforcement bars (cathode to anode ratio of 2). The corrosion is monitored by: 1) monitoring the OCP of the anodic reinforcing bar and 2) measuring the macrocell current between the anodic and cathodic reinforcing bars. The original method was devised to check the effectiveness of corrosion inhibitors. This method, however, has been used extensively to assess and compare corrosion of reinforcing bars embedded in different cementitious systems. In this study, the ASTM G109 method is used to compare the performance of OPC concrete with PLC or OPC+LS concrete and no corrosion inhibitors were used in this study. Additionally, instead of constructing a dam to store the ponding solution as suggested in ASTM G109, the ponding solution was stored above the cover surrounding the anodic rebar as shown in Figure 11-2.

In this program, concrete specimens were subjected to 56 days of curing in a moist room with 100% RH. Post curing, the specimens were then dried for two weeks in an environment with a 50% RH. The cured specimens were then epoxy-coated on all sides except the top and bottom surfaces. The ponding salt solution was prepared by dissolving 3 parts of sodium chloride to 97

parts of water. The ponding solution, atop the specimen, was applied for two weeks and then vacuumed off where the specimen was dry for the following two weeks (i.e., biweekly wet-dry cycles). The macrocell current and the OCP were measured once every four weeks, starting from the second week of ponding. I_{macro}, the macro-current flowing from the anode to the cathode, was measured using a 100Ω resistor. One end of the resistor was connected to the insulating wire protruding from the copper wire of the cathodic rebars and the other end of the resistor was connected to the anodic rebar. The voltage (V) across the 100Ω resistor was measured by attaching both terminals of the voltmeter to the opposite ends of the resistor. The macro-cell corrosion current density, I_{macro}, was then estimated as V/(R*A), where V represents the voltage across the resistor, R is the resistance (i.e., 100Ω), and A is the curved surface area of the anodic reinforcing bar exposed to the chlorides. The steel reinforcement located between the epoxied ends of the anodic reinforcing bar is considered as the exposed reinforcing steel. The value of 'A' is 0.01 m^2 (15.5 in^2). The setup for this test method is illustrated in Figure 11-2.

The test was carried out until the average integrated charge, based on the macrocell current, reached 150 coulombs, C. At the conclusion of testing, the bars were visually inspected for corrosion and the acid soluble chloride content was measured at the depth corresponding to the top of the reinforcement bar.

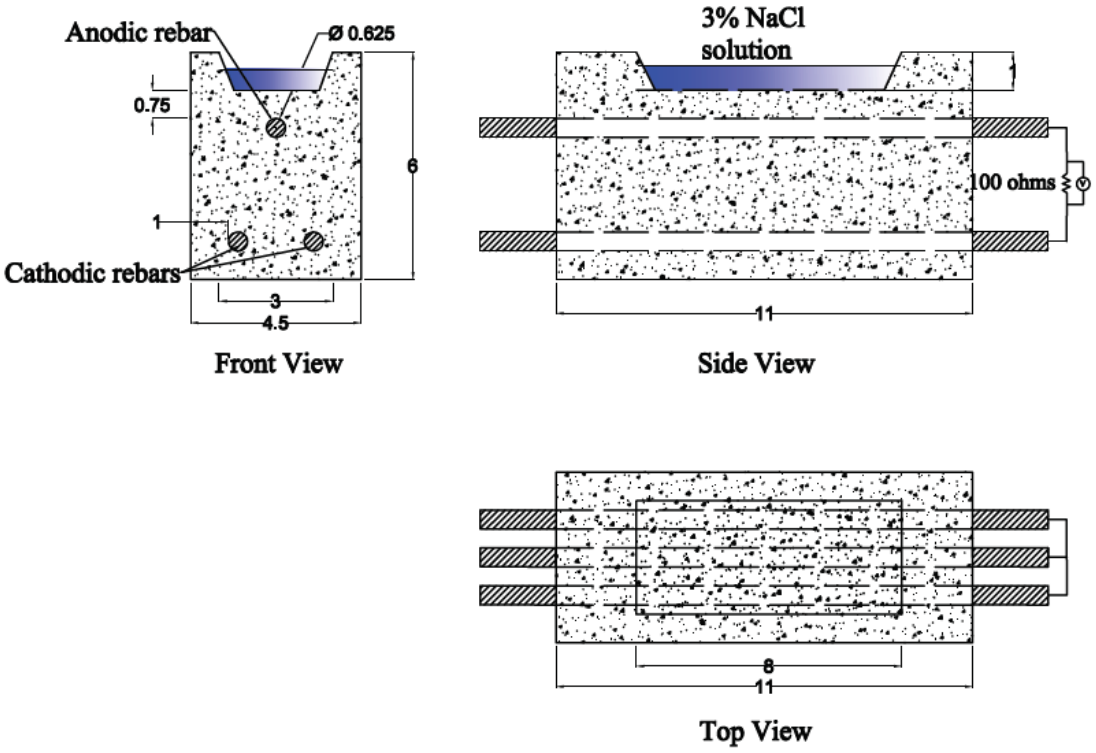

Figure 11-2.Setup for the modified ASTM G109 test method.

11.5 Experimental Results

11.5.1 OC_{crit} method

The OC_{crit} method provides a reliable and fast way to estimate the critical chloride threshold of steel reinforcement embedded in cementitious systems. In this test, the specimens are exposed to 2% chloride solutions and the OCP is assessed every day with a digital multimeter. The specimens are considered "activated," that is corrosion has initiated, when the OCP is less than -350 mV for 2 consecutive days. Once the specimens have activated, they are removed from the chloride solution and the thin cover surrounding the reinforcing bar is removed and tested for average chloride concentration. Figure 11-3 shows the OCP for anodic specimens cast with E_OIIV. In this research these are considered as the control group and are henceforth used as a benchmark to compare and contrast the corrosion performance of the cements and the SCMs in the remaining experimental program. It can be seen in the figure that the activation time range from 22 to 63 days with a mean activation time of 39.8 days. Figure 11-4 shows the OCP for all mortar specimens cast with 25% FA1 for both E_OIIV and E_L11. It can be seen that both cases exhibit similar mean activation times of 55.3 and 49.4 days, respectively. In Figure 11-5, the OCP values of specimens made with 20% FA1 and 5% silica fume are shown. It can be seen that specimens with E_OIIV exhibit a much higher mean activation time when compared to those of E_L11. Figure 11-6 shows the OCP of specimens made with 25% FA1 and 25% slag. It can be seen that both E_OIIV and E_L11 specimens have similar mean activation times of 28.5 and 25.6 days, respectively. Figure 11-7 shows a similar trend for specimens cast with 50% slag for both and E_OIIV and E_L11 cements. Note that the specimens with 50% slag activated much earlier when compared to the other specimens. Figure 11-8 summarizes the time to activation for OC_{crit} specimens. It can be observed that both E_OIIV and E_L11 specimens with 25% FA1have a higher mean time to activation when compared to the control specimens. Time to corrosion initiation and critical chloride threshold are critical factors in determining overall service life. The OCcrit test method was developed to quantify critical chloride threshold values. The test was not developed to determine the transport rates of chlorides into a cementitious system. The reporting of times to corrosion was presented to provide the reader with a general idea of test times. The time to corrosion has not been correlated with critical chloride threshold; specimens with shorter test times could exhibit higher critical chloride values and alternatively, longer test times could result in lower critical chloride test values. Chloride transport rate is independent of critical chloride threshold value.

The C_{test} of the specimens was measured by extracting the thin cover surrounding the reinforcing bar. It is subsequently pulverized, sieved, and then tested based on AASHTO T 260 for both water and acid soluble chlorides. Figure 11-9 shows the results for average water-soluble chlorides. It can be seen that, except for the 25% fly ash and 50% slag mixtures, both E_OIIV and E_L11 specimens had approximately similar quantities of C_{test}. Figure 11-10 shows the results for average

acid-soluble chlorides for the same set of specimens. This figure shows the same trend observed in Figure 11-9. The ratios between the water-soluble and acid-soluble chloride values are shown in Figure 11-11. For the control specimens, this ratio is 0.72. It can be seen that E_OIIV and E_L11 specimens with 25% FA1 has the lowest WSC/ASC values, indicating higher binding capacities. This could be attributed to the high concentration of alumina in FA1 (21.7%). A higher concentration of alumina leads to the formation of Friedel's salt that helps bind the free chlorides and slows down the transport of chlorides to the surface of the rebar. This also helps explain the higher mean activation times of OC_{crit} specimens made with 25% FA1.

Figure 11-12 shows the Cl_{crit} for "partner" specimens. These "partner" specimens were used to calculate the Cl_{crit} of specimens because testing the cover mortar of the OC_{crit} specimens only provides information on the average chloride concentration of the mortar cover. It can be seen that most of the specimens have a Cl_{crit} of about 0.4% by weight of binder. Specimens E_OIIV-25FA1 and E_L11-50SL have higher Cl_{crit} values of 0.59% and 0.63%, respectively.

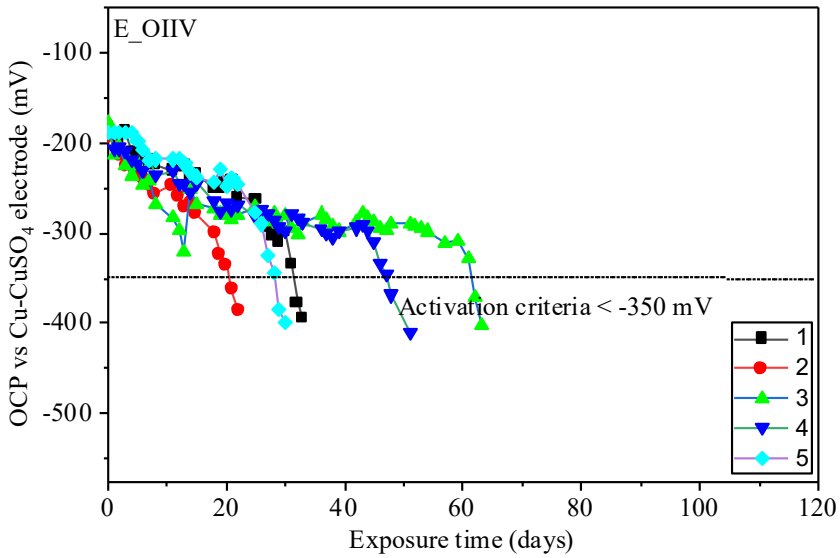

Figure 11-3. Open circuit potential of anode specimens made with E_OIIV

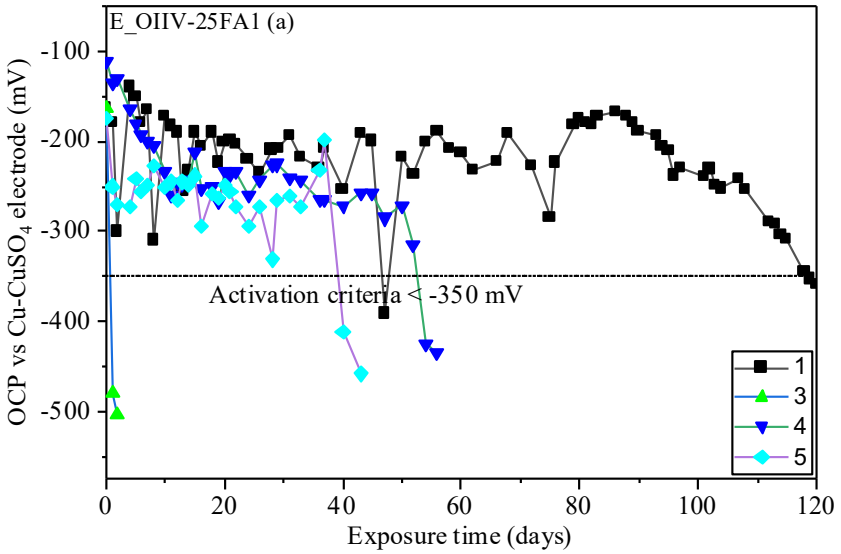

(a)

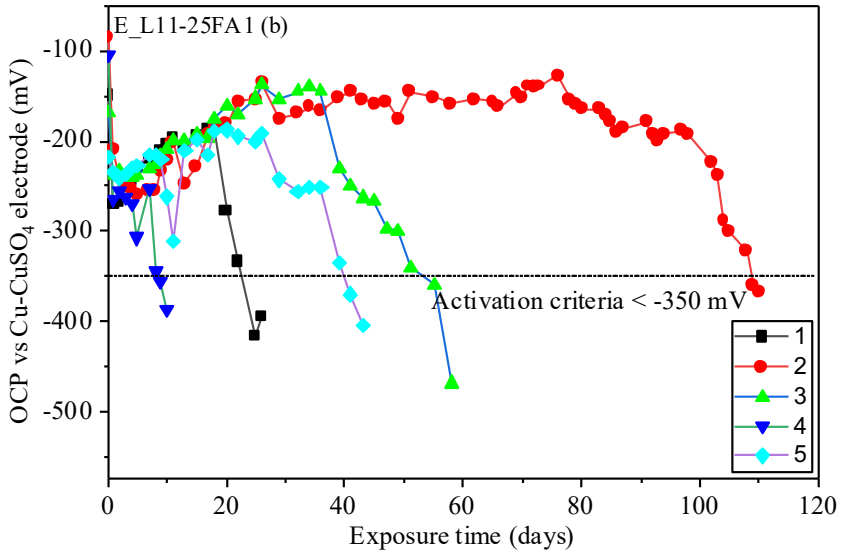

(b)

2004 **Figure 11-4. (a) Open circuit potential of anode specimens made with E_OIIV-25FA1 and**
2005 **(b) Open circuit potential of anode specimens made with E_L11-25FA1**

2006

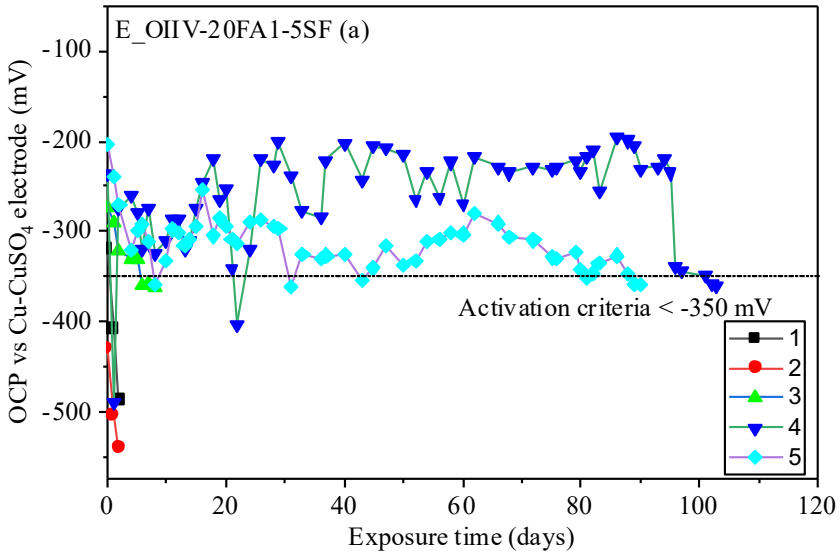

(a)

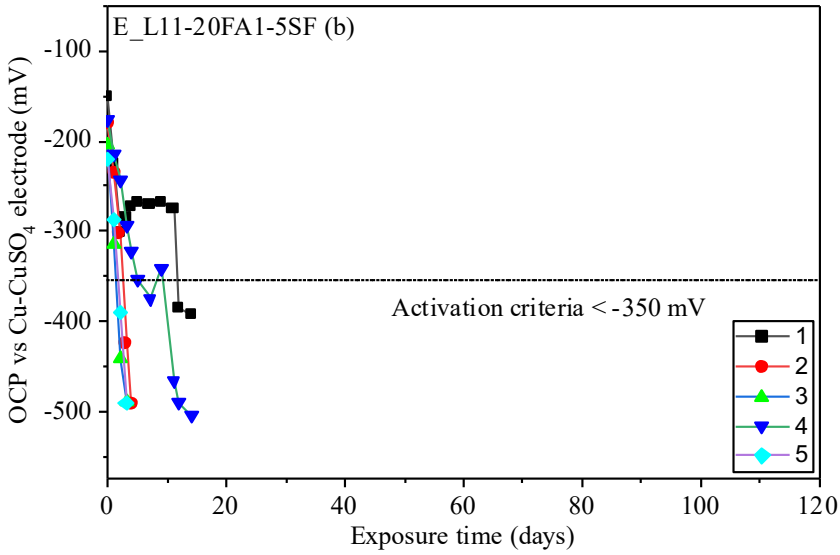

(b)

2007 **Figure 11-5. (a) Open circuit potential of anode specimens made with E_OIIV-20FA1-5SF**
2008 **and (b) Open circuit potential of anode specimens made with E_L11-20FA1-5SF**

2009

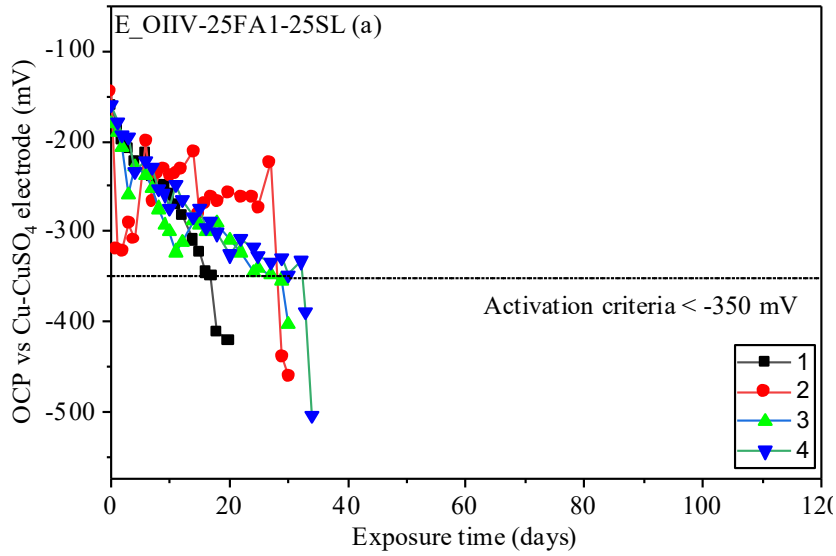

(a)

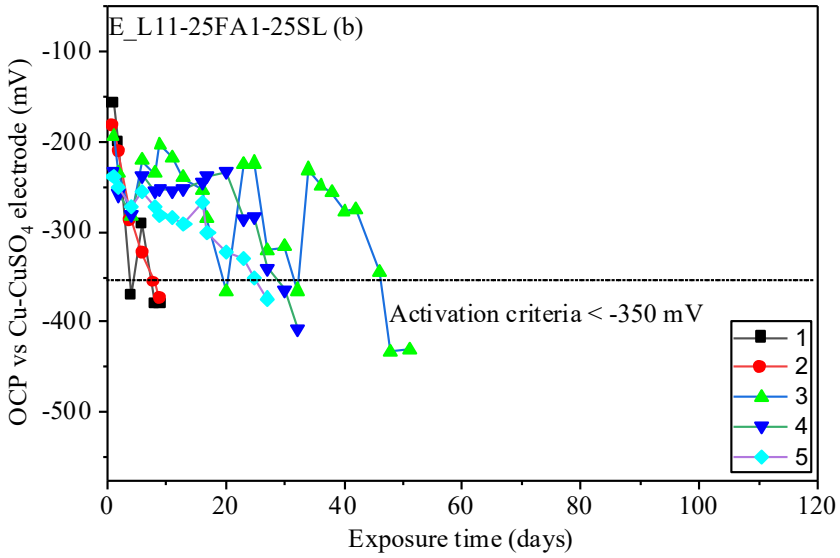

(b)

Figure 11-6. (a) Open circuit potential of anode specimens made with E_OIIV-25FA1-25SL and (b) Open circuit potential of anode specimens made with E_L11-25FA1-25SL

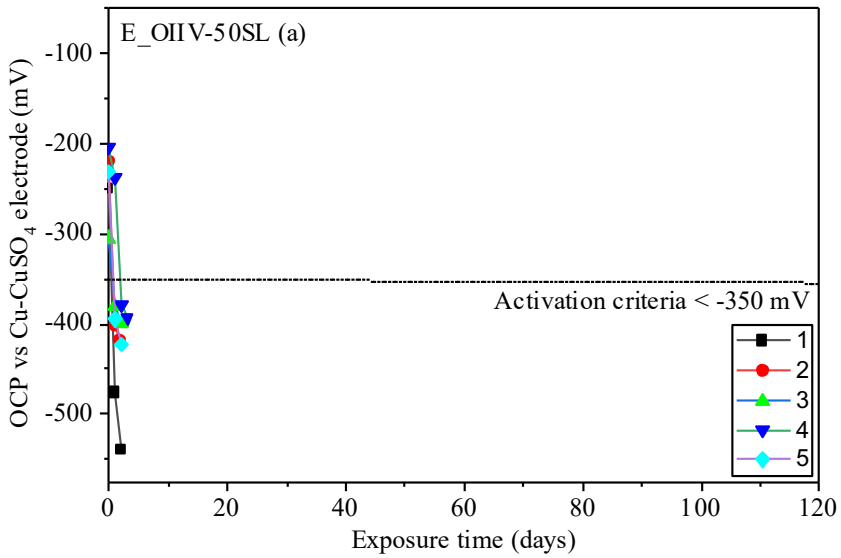

(a)

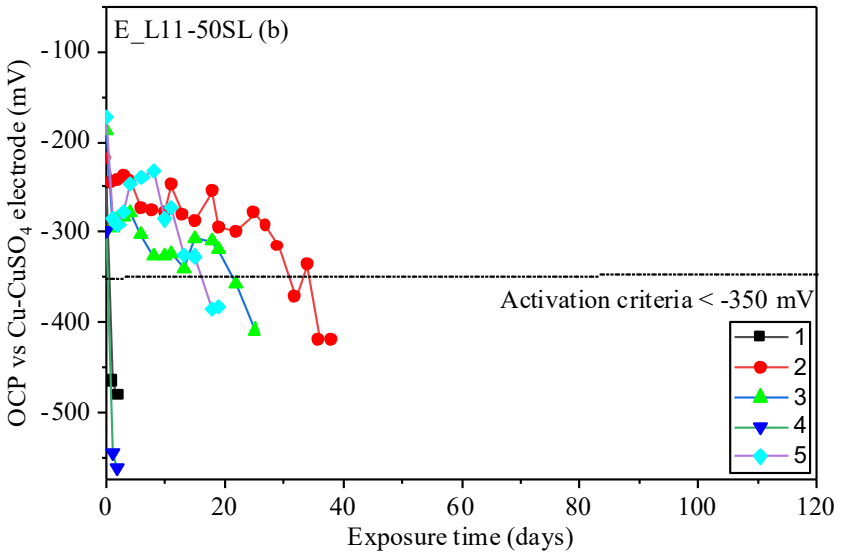

(b)

2013 **Figure 11-7. (a) Open circuit potential of anode specimens made with E_OIIV-50SL and (b)**
2014 **Open circuit potential of anode specimens made with E_L11-50SL**

2015

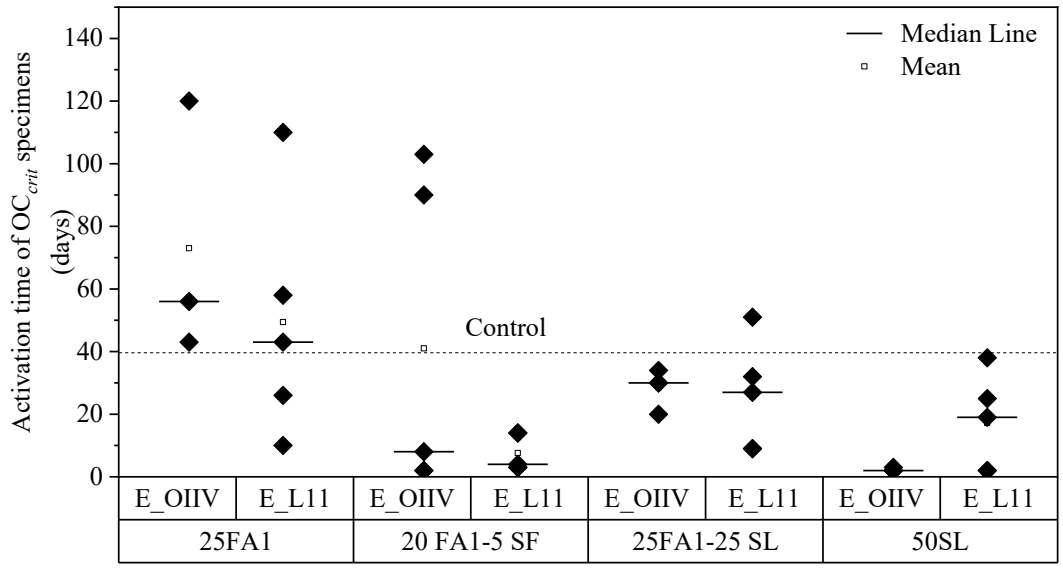

2016

2017 **Figure 11-8.Time to activation of OC$_{crit}$ specimens**

2018

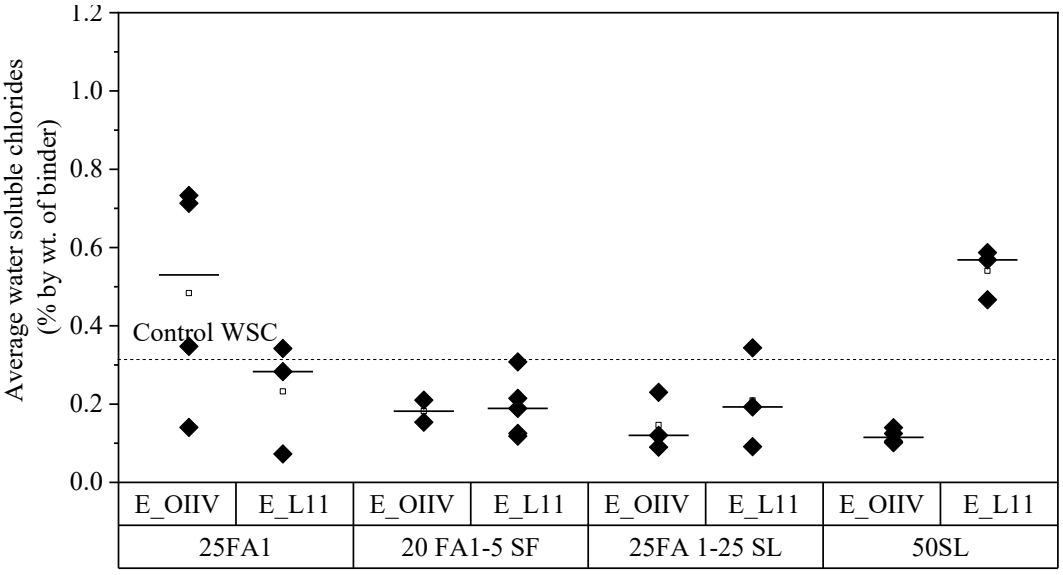

2019

2020 **Figure 11-9. Average chloride concentration of activated specimens based on AASHTO T**
2021 **260 water-soluble method.**

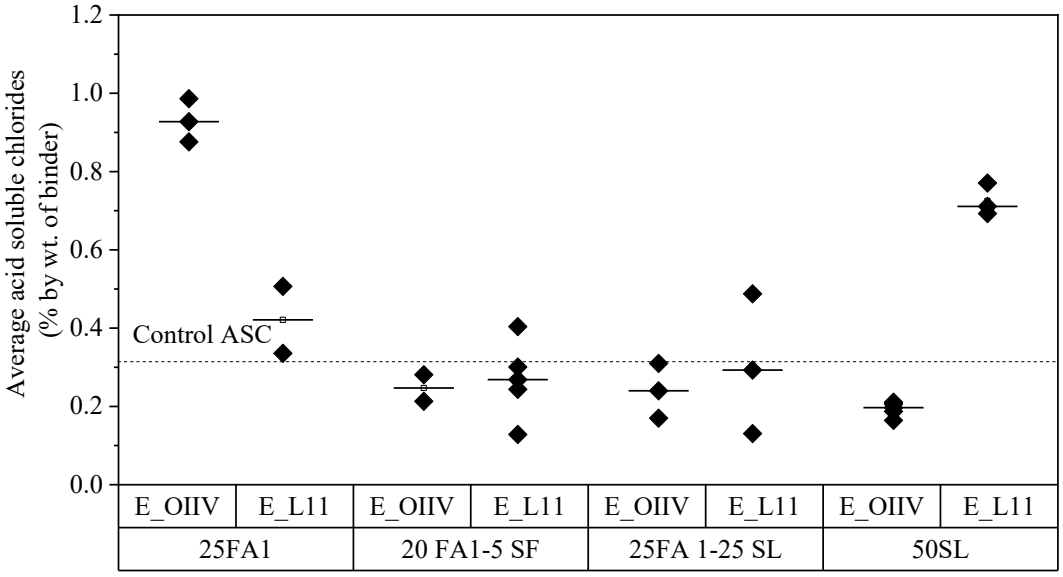

Figure 11-10. Average chloride concentration of activated specimens based on AASHTO T 260 acid-soluble method

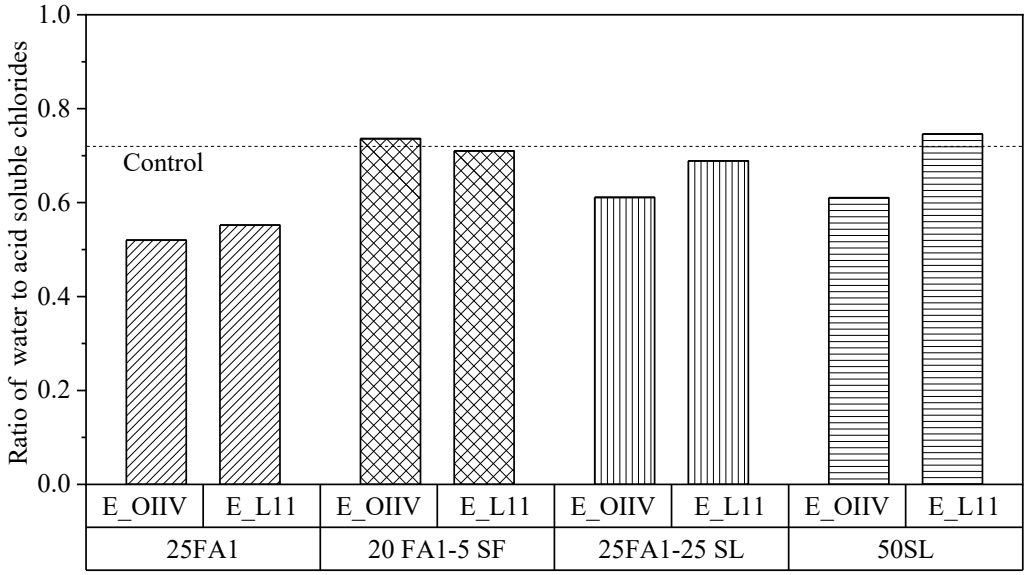

Figure 11-11. Ratio of water to acid soluble chlorides of activated specimens

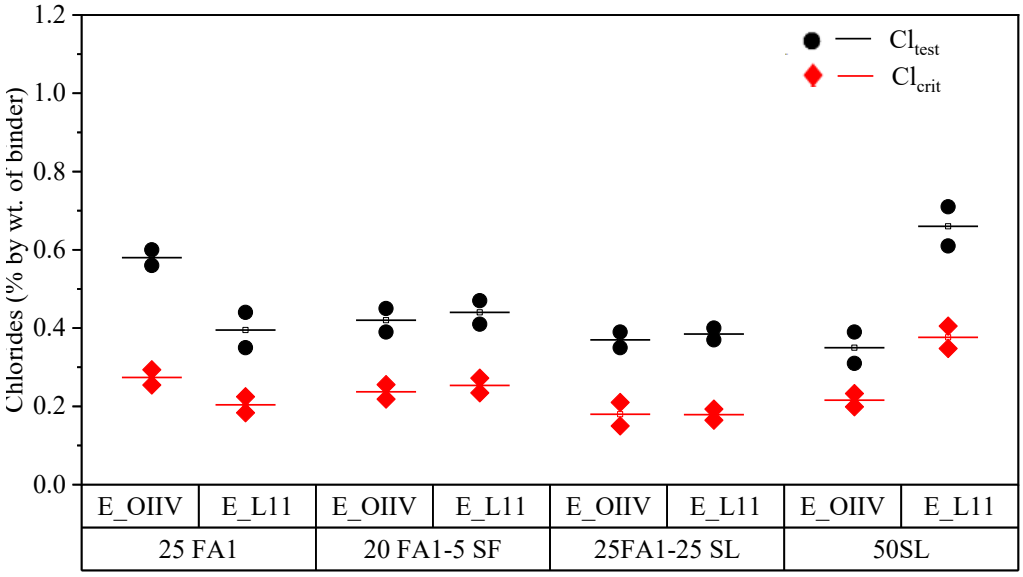

Figure 11-12. Critical and average chloride concentration

11.5.2 Modified ASTM G109 method

Figure 11-13 shows the total charge passed for the modified G109 specimens. It can be seen that specimens with interground limestone exhibit higher charge passed for all three cement sources, throughout the exposure cycles. However, it also should be noted at earlier exposure ages there is significant overlap between the error bars. This indicates that the difference in total charge passed may not be statistically significant. Note that each cycle represents two weeks of exposure to the ponding solution followed by two weeks of drying. Figure 11-14 shows the critical chloride concentration for the same set of specimens. Once the specimens reach the activation criteria, samples are extracted from the top surface of the anodic reinforcement bar and were tested for acid-soluble chlorides following the AASHTO TP-260 standard. It can be seen that 25% FA1 specimens with OPC+10LS have a higher critical chloride concentration when compared to the rest of the specimens. The E_L11 mixtures evaluated with the OC_{crit} test (initiation in 40 days) and modified G109 test (initiation in 7 months) exhibited similar Cl_{crit} values. Comparison of OPC and PLC Cl_{crit} for each clinker source reveals that there is no statistically significant difference.

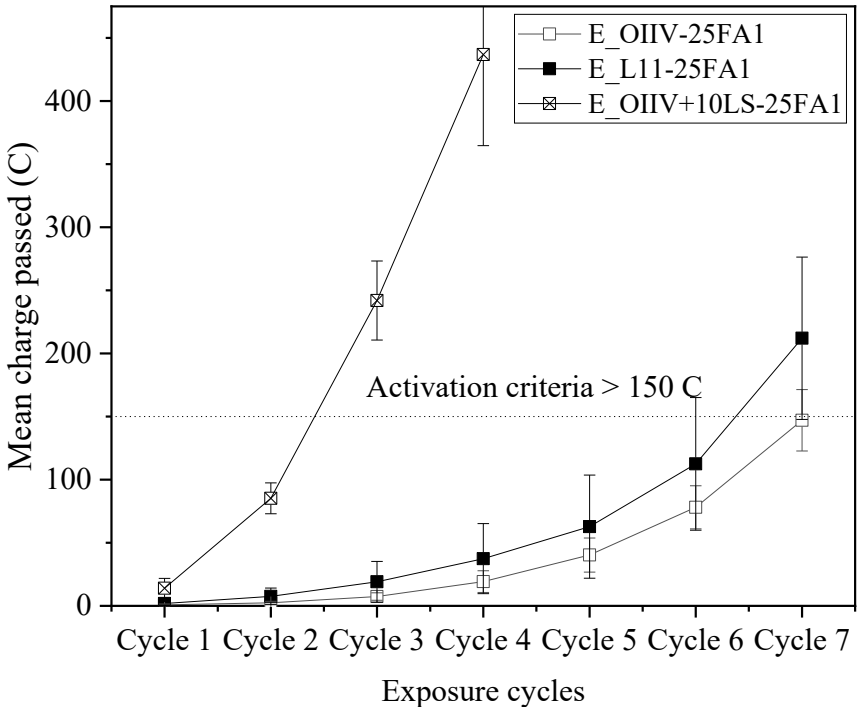
E_OIIV-25FA1
E_L11-25FA1
E_OIIV+10LS-25FA1
Mean charge passed (C)
400
300
200
100
0
Activation criteria > 150 C
Cycle 1 Cycle 2 Cycle 3 Cycle 4 Cycle 5 Cycle 6 Cycle 7
Exposure cycles

(a)

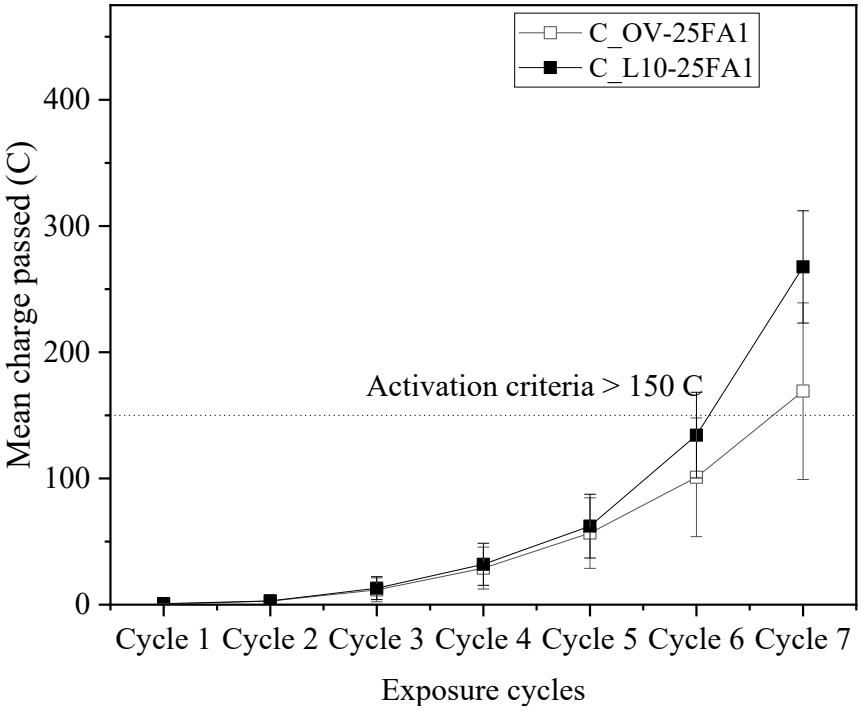
C_OV-25FA1
C_L10-25FA1
Mean charge passed (C)
400
300
200
100
0
Activation criteria > 150 C
Cycle 1 Cycle 2 Cycle 3 Cycle 4 Cycle 5 Cycle 6 Cycle 7
Exposure cycles

(b)

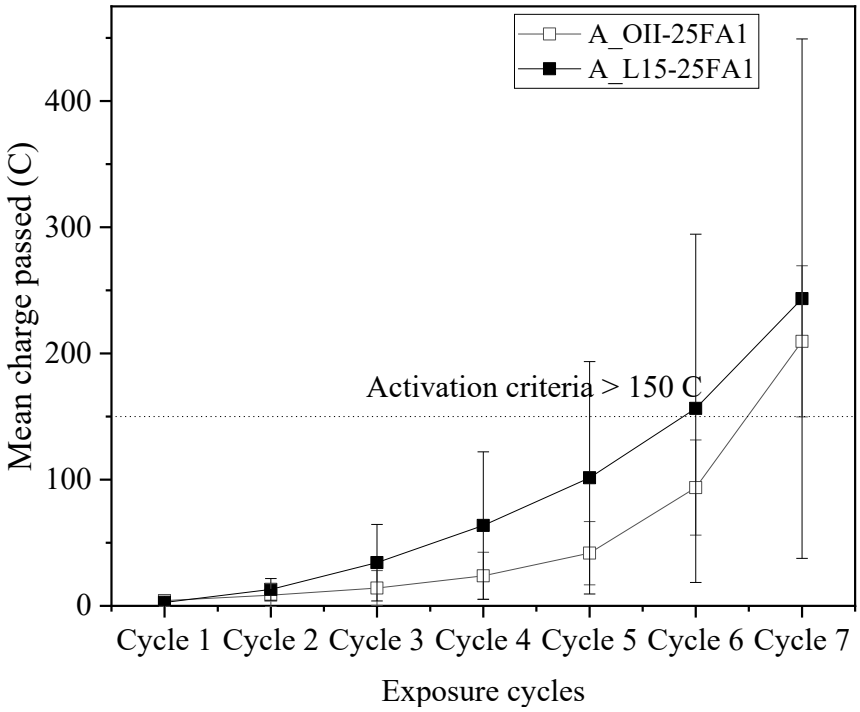

(c)

2049 **Figure 11-13. Total integrated charge passed for modified ASTM G109 specimens**

2050

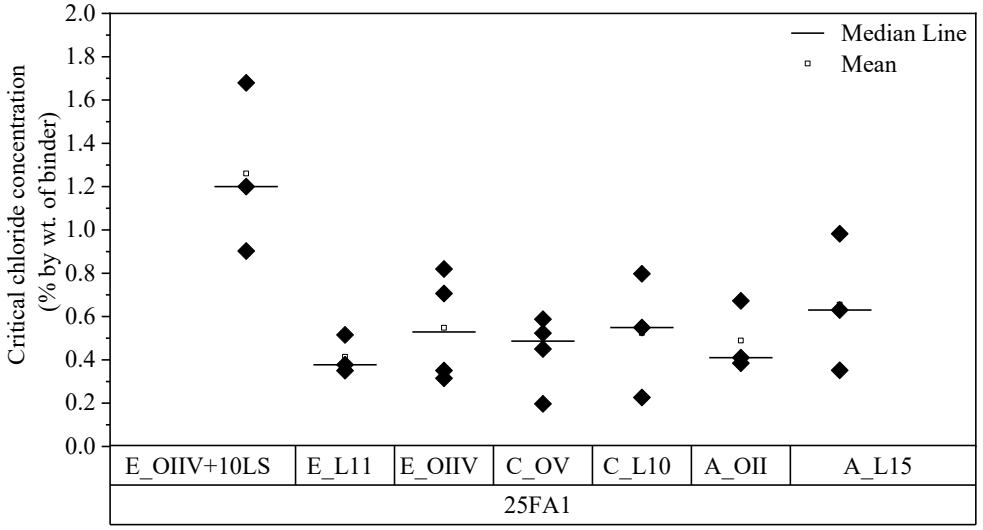

2051

2052 **Figure 11-14. Critical chloride threshold of modified ASTM G109 specimens**

11.6 Significant Findings

In this research, OPC and PLC specimens, in combination with SCMs, were evaluated for corrosion performance using the OC_{crit} and modified ASTM G109 methods. The following conclusions can be drawn from the results that were shown in the earlier section:

The findings from OC_{crit} testing indicates that OPC and PLC systems have comparable times to corrosion initiation. Both OPC and PLC systems with 25% FA1 exhibit longer times to corrosion initiation than the control systems without fly ash. Both systems also exhibit higher Cl_{crit} values when compared to the control specimens. For specimens with 50% slag, the research indicates that the OPC specimens exhibited a mean time to corrosion initiation of 2.2 days.

The Cl_{crit} of most of the specimens observed in the study is around 0.4% by weight of binder, with the exception of E_OIIV-25FA1 and E_L11-50SL. Both E_OIIV-25FA1 and E_L11-50SL exhibited higher mean Cl_{crit} values. This indicates that concrete containing just PLC will likely exhibit similar times to corrosion as systems containing only OPC. This also indicates that PLC systems with fly ash will likely exhibit longer times to corrosion than systems containing only OPC. Although the time to corrosion initiation of the specimens containing 50% slag was short, the mean Cl_{crit} values for the PLC is higher than the control, indicating longer times to corrosion initiation (assuming all other factors are the same).

The findings from the modified ASTM G109 test indicate that OPC and PLC specimens exhibit similar total charge passed until the time of activation and most of the specimens were observed to activate after 7 cycles. Even though PLC specimens have a higher mean charge passed, it is deemed insignificant due to the large error bars.

12 Air Entrainment

Concrete is air-entrained to improve its freezing and thawing (FT) resistance. Air-entraining concrete is done by adding an air-entraining admixture (AEA) during concrete mixing. In ready-mixed concrete and precast this is typically done with a liquid admixture. Powdered air entrainers are also available, therefore, there is the possibility to intergrind or interblend this with the cement. The air-entraining admixture stabilizes air bubbles formed during the mixing process. The surface charge on the bubbles prevents the coalescence of bubbles and causes adherence to cement and aggregate particles. The interior of the entrained air bubbles is inherently hydrophobic so that under normal temperature and pressure conditions, the bubbles are vapor filled. However, during a freezing event the increased pressure from the expansion of freezing pore solution forces the liquid into the air bubbles. The air bubbles in hardened concrete provide extra space for the freezing pore solution to expand, thus relieving the pressure and preventing damage. Therefore, air-entrainment is recommended for all concretes exposed to freezing and thawing and as well as deicing chemicals to improve concrete durability. Air-entrainment also has other benefits such as reducing bleeding and increasing plasticity in the fresh state. In general, both minimum and maximum limits of air-entrainment are provided to offer freezing and thawing resistance and prevent compressive strength reduction [141].

12.1 Research Objective

The objective of this part of the project is to investigate if the same amount of air-entrainment (by % volume) can be achieved with PLCs as with OPCs by using liquid air-entraining admixtures.

12.2 Background and Literature Review

The cyclic freezing and thawing test - ASTM C666 is commonly used to evaluate the FT resistance by determining the durability factor. Thomas et al. [98] evaluated and compared the FT resistance of concretes made with OPCs and PLCs (with 12% interground LS) using ASTM C666. The concrete specimens were made with and without SCMs. The target air content was 5-7%. The measured air content in fresh concrete is shown in Table 12.1.

Table 12.1. Comparison of measured air contents for OPC and PLC mixtures; note that the target air content was 5-7% [98]

Cement	**OPC**	**PLC**	**OPC**	**PLC**	**OPC**	**PLC**	**OPC**	**PLC**
w/cm	**0.40**		**0.45**		**0.45**		**0.45**	
SCM	No SCM		No SCM		35% slag		20% fly ash	
Measured air (%)	6.2	5.4	6.2	5.3	6.0	5.6	5.2	5.0

As observed from Table 12.1, the measured amount of air content for the PLC mixtures was slightly lower than the OPC mixtures. The authors mentioned that the PLC mixtures required slightly higher AEA than the OPC mixtures (this is consistent with mixtures that have a higher surface area of the cementitious materials). However, it is important to note that all the mixtures had achieved the target air content. The mixtures were tested using ASTM C666 (Procedure A) to compare the FT resistance of OPC and PLC mixtures. The ASTM C666 results are presented in Figure 12-1. Personal communications have noted that about 3 million cubic yards of concrete have been made and placed using PLC with air entraining admixtures without any issues related to the PLC cement.

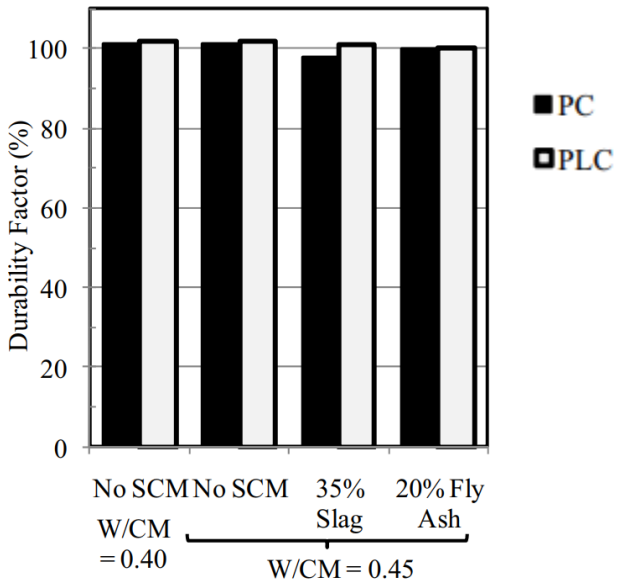

Figure 12-1. Durability factor of the mixtures tested using ASTM C666 (Procedure A) [98]

All of the concrete mixtures performed well in cyclic FT environment per ASTM C666 with durability factors ranging from 98 to 102%. No significant difference in FT performance of OPC and PLC mixtures was observed.

12.3 Experimental Test Matrix

Two sets of concrete mixtures were cast to compare the air-entrainment of OPC and PLC mixtures. Two different fine aggregates (F1 and F2) were used for each set of mixtures. High purity limestone was used as coarse aggregate. The coarse aggregate used has proportions following ASTM C1293 as the same mixtures were used for making concrete prism test specimens for alkali-silica reactivity (ASR) testing. Air entrainment was done after the ASR prisms were cast. More information on the concrete prism test can be found in section 5.9. Equal proportions of coarse aggregate particles retained on 12.5mm, 9.5mm, and 4.75mm sieves were used for all the mixtures.

Cements B_OIIV and B_L15 were used for this task. The AEA used for this task was BASF Master AE90.

12.4 Experimental Methods

The pressure method following ASTM C231/C231M was used to measure the air content in fresh concrete. For each mixture, the batch amounts were calculated to determine air contents at three different AEA dosages starting with 0 ml/100 kg cement (i.e., no added air). After measuring the air content of fresh concrete when no AEA was added, the first dose of AEA was added to the concrete to obtain an air content of 3.5±1% and mixed the concrete for two minutes. After measuring the air content of concrete for the second AEA dosage, more AEA was added to obtain 6.5±1% air content. During this mixing and testing, the concrete that was used to measure air content was not re-used.

12.5 Typical Experimental Measurement and Interpretation

The measured air content of fresh concrete is reported in terms of the percentage of total concrete volume. At each dosage of AEA, only one measurement of air content was made.

12.6 Experimental Results

The measured air contents at different dosages of the AEA for both sets of concrete mixtures are listed in Table 12.2 and Table 12.3. The manufacturer's recommended AEA dosage range was 16 – 260 ml/100 kg cement.

Table 12.2. The measured air contents of the mixtures with F1 fine aggregate

B_OIIV – F1		B_L15 – F1	
AEA dose (ml/100kg cement)	**Measured air content (%)**	**AEA dose (ml/100kg cement)**	**Measured air content (%)**
0	1.0	0	1.0
48	4.0	48	3.0
79	7.5	79	7.0

Table 12.3. The measured air contents of the mixtures with F2 fine aggregate

B_OIIV – F2		B_L15 – F2	
AEA dose (ml/100kg cement)	**Measured air content (%)**	**AEA dose (ml/100kg cement)**	**Measured air content (%)**
0	1.8	0	1.8
56	2.8	64	3.1
181	3.1	189	4.1

12.7 Discussion of the Results

From Table 12.2 and Table 12.3, it was observed that with the increase in AEA dosage, the amount of measured air increased, as expected. For the mixtures with F1 fine aggregate, it was observed that the PLC concrete had air content equal to or slightly less than the OPC concrete. It should be noted that both the OPC and PLC concretes reached the target air contents and were within a desired range of $\pm$1%. For the mixtures with F2 fine aggregate, it was observed that the target air content was not achieved for the highest AEA dosage for both cements. The reason for this could be a high moisture content (12%) and absorption capacity (4.2%) of the F2 fine aggregate. However, the amount of measured air contents for both the OPC and PLC concrete mixtures were similar at all AEA dosages. From the study by Thomas et al. [98], it was observed that even though PLC concrete had slightly lower (by ~1%) air content than the OPC concrete, the measured durability factor from ASTM C666 testing was very similar for both OPC and PLC concretes. Therefore, the OPC and PLC concrete mixtures made in this project are expected to perform similarly in the cyclic FT environment.

12.8 Significant Findings

There was no significant difference in measured air contents between OPC and PLC concrete mixtures. The OPC and PLC concrete mixtures with similar air contents are expected to perform similarly in the FT environment.

Table 8. Concrete Mix Proportions and Test Results – Study 3

	No SCM		25% SCM		40% SCM		50% SCM	
	PC	PLC	PC	PLC	PC	PLC	PC	PLC
W/CM	0.45	0.44	0.44	0.45	0.44	0.44	0.44	0.44
Plastic air, %	6.8	6.0	6.2	6.6	6.8	6.0	6.8	6.5
Slump, mm	100	80	75	100	95	80	95	95
Slump, in.	3.9	3.1	3.0	3.9	3.7	3.1	3.7	3.7
Hardened air, %	5.3	5.6	4.9	5.4	5.6	5.3	5.6	6.6
Spacing factor, μm	173	187	148	149	164	165	150	147
Spacing factor, in.	0.068	0.074	0.058	0.059	0.065	0.065	0.059	0.058

This study from Thomas and Hooton 2010 (reference #98 in v05) shows that the spacing factor is nearly identical for all mixtures with SCMs whether the binder was portland cement or portland-limestone cement. The spacing factor was slightly higher in the case of 100% portland or portland-limestone cement.

13 External Sulfate Attack

California is known to have sulfate-rich soils. Sulfates from external sources can ingress into concrete and cause damage. The damage due to external sulfate attack (ESA) in concrete is primarily caused by secondary ettringite formation. Calcium sulfate in the form of gypsum in cement reacts with hydrated calcium aluminate to form ettringite ($Ca_6(Al,Fe)_2(SO_4)_3(OH)_{12}.26H_2O$; AFt) during early cement hydration. The ettringite forms early during hydration reacts with remaining anhydrous aluminate to form monosulfoaluminate ($3CaO.(Al,Fe)_2O_3.CaSO_4.12H_2O$; AFm). The sulfates present in hydrated cement are mainly these ettringite and monosulfoaluminate. These two phases are finely intermixed with the C-S-H. When external sulfates are present, sulfates ingress and react with AFm and form AFt. This secondary formation of AFt from AFm can develop stresses in hardened concrete as AFt occupies more than twice the volume of AFm [20]. Sulfate attack can also be from internal sources such as concrete having sulfide-bearing aggregates or delayed ettringite formation due to thermal activation occurring during initial hydration.

The reaction products of sulfates and cement hydrates that induce damage are mainly of three types: AFt, gypsum ($CaSO_4.2H_2O$), and thaumasite ($3CaO.SiO_2.SO_4.CO_3.15H_2O$). AFt formed in pores smaller than 100 nm generates crystallization pressure enough to develop cracks in the cementitious matrix, and the supersaturation of the pore solution is needed in the pores to generate crystallization pressure [142, 143]. Mullauer et al. [144] observed that AFt formed in small pores (10 – 50 nm) generated stresses that overcame the tensile strength of the cementitious matrix. This results in expansion and eventually damage of the matrix.

Gypsum can form when calcium hydroxide reacts with ingressed sulfates, as shown in equation (13-1)

$$CH \text{ (from cement hydration)} + N\underline{S}/M\underline{S} + 2H \rightarrow C\underline{S}H_2 + NH/MH \quad \textbf{(13-1)}$$

Gypsum formation can also contribute to the expansion of cement mortars under exposure to high sulfate concentrations [145]. The formed gypsum can further react with unhydrated calcium aluminate, hydrated calcium aluminate or AFm to form AFt, as shown in equations (13-2), (13-3), and (13-4) [146].

$$C_4AH_{13} + 3C\underline{S}H_2 + 14H \rightarrow C_6A\underline{S}_3H_{32} + CH \quad \textbf{(13-2)}$$

$$C_4A\underline{S}H_{12\text{-}18} + 2C\underline{S}H_2 + (10—16)H \rightarrow C_6A\underline{S}_3H_{32} \quad \textbf{(13-3)}$$

$$C_3A + 3C\underline{S}H_2 + 26H \rightarrow C_6A\underline{S}_3H_{32} \quad \textbf{(13-4)}$$

Thaumasite forms in the presence of limestone (as a filler or aggregate) and when exposed to sulfate solution. Structurally, thaumasite is similar to ettringite. Thaumasite forms as a non-binding calcium carbonate silicate sulfate hydrate and needs specific conditions, such as low temperatures (< 15°C), presence of carbonates or bi-carbonates, and moisture. According to Hobbs who studied thaumasite attack in laboratory and field concretes, the combination of conditions needed for thaumasite attack are a low temperature, wet conditions, exposure to a sulfate source, the prior formation of AFt from classical sulfate attack, presence of limestone in the system (at least 15% to 35% calcium carbonate by mass of cement from laboratory observations) [147]. Thaumasite was also found to be formed at relatively higher temperatures; however, high limestone contents (>15%) and prior damage by secondary AFt formation are needed [148, 149].

The cation associated with sulfate affects the extent of damage caused by sulfate attack. The most common cations that are in compound with sulfate and thus attack concrete are calcium, sodium, and magnesium sulfates. Calcium sulfate is the least aggressive, and magnesium sulfate is the most aggressive in terms of sulfate attack. The higher solubility of sodium and magnesium sulfates the more aggressive the attack and resulting damage. AFt and gypsum are formed from AFm, hydrated aluminates, C_3A, and in severe cases, C-S-H under sodium sulfate attack. Sodium sulfate can also cause physical salt attack. AFt, gypsum, brucite, and silica gel are formed under magnesium sulfate attack. The formation of brucite lowers the pH of the pore solution, and this encourages gypsum formation. These reactions continue until CH and C-S-H are exhausted, resulting in loss of cohesion and softening of the cementitious matrix [150].

To limit the formation of AFt from sulfate attack, low C_3A portland cements or sulfate resistant cements such as ASTM C150 Type II and Type V cements are generally recommended. However, it was observed that usage of low C_3A cements alone might not prevent damage due to sulfate attack if the permeability of the concrete is high or the degradation of concrete is due to physical salt attack [151]. Therefore, SCMs and lower water to binder ratio are also used to improve the sulfate resistance of concrete.

13.1 Research Objective

The main objective in this part of the project is to extensively study the influence of usage of PLC in conjunction with SCMs on the expansion due to ESA. The results of this Task will inform CALTRANS if their current mixtures with SCMs can be utilized as-is when combined with a PLC with up to 15% limestone.

13.2 Background and Literature Review

Using limestone in a cementitious system can impart changes in the capillary porosity due to physical effects such as filler effect, dilution effect, and nucleation effect [152]. These physical effects depend on the fineness, amount, and purity of limestone filler used. The effective water to

cement ratio increases due to the dilution effect when a certain portion of cement is replaced with limestone filler. Therefore, an increase in cement replacement with limestone increases the water to cement ratio of the paste due to the dilution effect, and it is only slightly compensated by the other two effects. These physical effects, in turn, affect the water transport of the cementitious system [153]. Transport properties of concrete can govern the ESA resistance. Some studies [154, 155] reported that high limestone contents (>15%) increased the porosity and pore interconnectivity, thus reducing the ESA resistance. However, the mixtures with limestone contents less than 15% when used in conjunction with appropriate levels of SCMs were observed to perform similar to OPCs [150].

Hooton and Thomas [150] evaluated the sulfate resistance of mortars (in laboratory conditions) and concrete (in simulated field conditions) produced with PLCs with up to 15% limestone. The PLCs were produced with both higher-C_3A (11-12%) and moderate C_3A (8-9%) clinkers. The authors observed that when the expansions were mitigated with appropriate levels of SCMs, there was no influence of limestone on sulfate attack resistance. The concrete samples produced with PLCs and appropriate amounts of SCMs under simulated field conditions (very severe sulfate exposure) performed similar or better than ASTM Type V cements for up to 5 years [150].

Hooton and Thomas [150] also studied sulfate resistance of OPCs and PLCs (with up to 15% limestone) at a low temperature of 5°C. The mortar specimens evaluated with modified ASTM C1012 (5°C) showed that the non-sulfate resistant mixtures are initially damaged by ettringite-based sulfate attack and thaumasite is only observed after significant deterioration. Therefore, by using appropriate amounts of SCMs and low C_3A cements to prevent classical sulfate attack, thaumasite sulfate attack can also be prevented. Also, the authors recommended not to use modified ASTM C1012 (5°C) to evaluate low-temperature sulfate attack as it is overly aggressive and did not provide reliable results relating to the performance of cementitious materials at cold temperature in field exposure. It was observed that the amount of limestone up to 15% in the PLC-SCM blends had little impact on the performance of mortars or concretes in sulfate environment at 5°C when tested in either laboratory or field simulated conditions. Moreover, the authors observed that the concrete containing PLC and SCMs generally perform similar, if not better, than concrete containing ASTM C150 Type II or Type V cement at the same w/cm and in the same sulfate-exposure condition [150].

Figure 13-1 presents the expansion ratio (PLC/OPC) of mortars with plain cements subjected to sodium sulfate solution according to ASTM C1012 at different amounts of limestone in the mixture [156-159]. Similarly, Figure 13-2 presents the expansion ratio (PLC/OPC) of mortars with SCMs subjected to sodium sulfate solution according to ASTM C1012 at different amounts of limestone in the mixture [160-163]. The data in Figure 13-1 and Figure 13-2 include expansion measurements obtained at 6, 12, 18 months of exposure to 50 g/L Na_2SO_4 solution at 23°C.

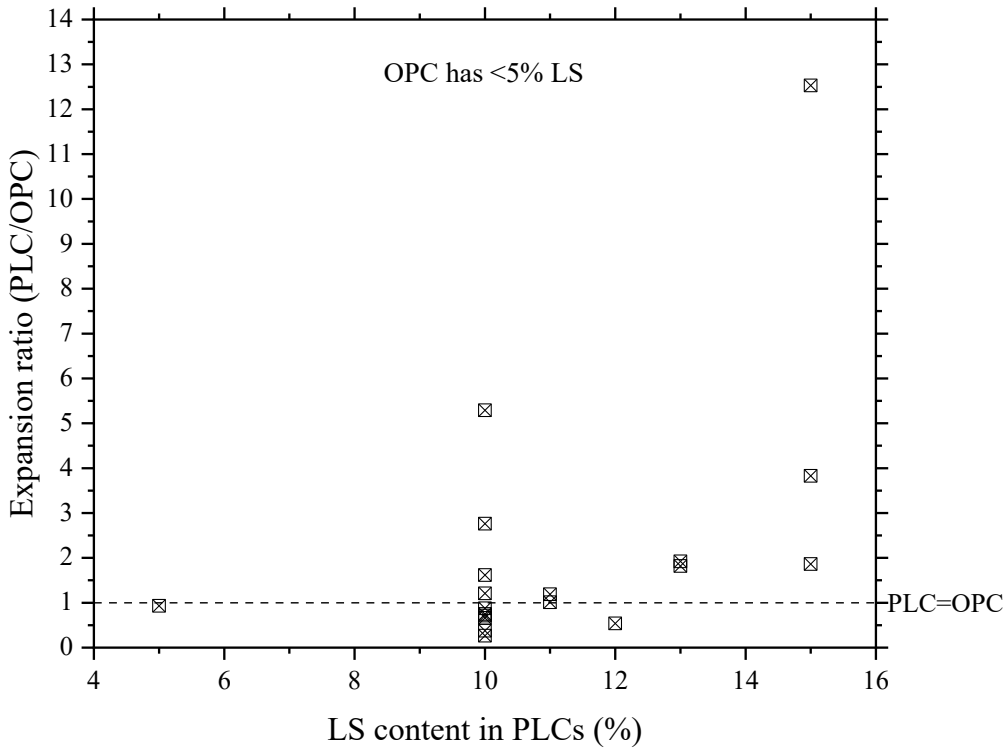

Figure 13-1. External sulfate attack expansion ratio (PLC/OPC) of mortars with plain cements tested according to ASTM C1012 [156, 158, 159, 162]

In the absence of SCMs, the mixtures with PLCs (up to 15% limestone) expanded more than the mixtures with OPC (with <5% limestone) with an expansion ratio as high as 12.5, as shown in Figure 13-1. As discussed earlier, the expansion mainly depends on C_3A content of cement, the fineness and amount of limestone, and how that affects porosity and pore connectivity of the mixtures.

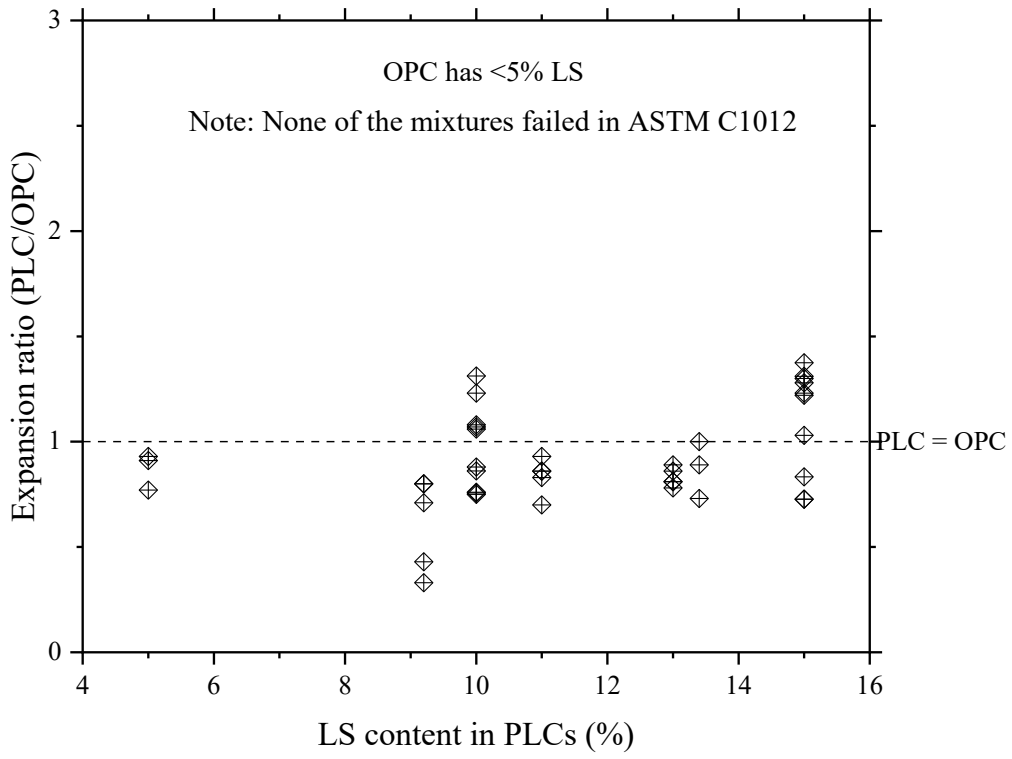

Figure 13-2. External sulfate attack expansion ratio (PLC/OPC) of mortars with SCMs tested according to ASTM C1012 [160-163]

In the presence of SCMs, the expansion ratio (PLC/OPC) did not exceed 1.4, and in most cases, the expansion ratio is less than 1.0, as shown in Figure 13-2. In addition, for the data shown in Figure 13-2, none of the PLC mixtures failed ASTM C1012 even though some of the mixtures with PLCs expanded slightly more than their respective OPCs.

In this project, moderate and high sulfate resistant cements were used to evaluate PLCs (with up to 15% limestone) performance in the presence of SCMs using ASTM C1012. Damage due to thaumasite formation is not expected in the mortars tested in this project as the limestone content is not greater than 15%, low C_3A cements were used, high amounts of SCMs were used, the specimens were stored at room temperature, and completely submerged in sodium sulfate solution.

13.3 Experimental Test Matrix

Two OPCs with different C_3A contents – A_OII and D_OV were selected for this Task to evaluate and compare them to their respective PLC mixtures in conjunction with SCMs according to ASTM C1012. A total of 32 mixtures were cast including the controls (A_OII and D_OV, without SCMs) as shown in Table 13.1.

2297 **Table 13.1. Experimental matrix for ASTM C1012 testing**

Cements	SCM proportions
A_OII A_L15 A_OII+10LS D_OV D_L15 D_OII+10LS	25FA1 20FA1-5SF 50SL 25FA1-25SL 25NP
Controls	A_OII, D_OV

2298

2299 ## 13.4 Experimental Methods

2300 The sulfate resistance of the cements was evaluated in accordance with ASTM C1012. Standard
2301 Ottawa sand was used to cast mortar bars and cubes. Six mortar bars of dimensions 25 x 25 x 285
2302 mm were cast for each mixture to monitor their expansions. Mortar cubes of dimensions 50 x 50
2303 mm were cast to determine their compressive strength. The bars and cubes were cured at 35±3°C
2304 and 100% RH for the first 24 hours after casting. Later, the mortar bars and cubes were cured in a
2305 lime saturated solution at 23°C until they reached a compressive strength of 20 MPa. Then, the
2306 bars were immersed in a 50 g/L of sodium sulfate (Na_2SO_4) solution as shown in Figure 13-3, and
2307 their length change was measured periodically for one year according to ASTM C1012. The
2308 sodium sulfate solution was renewed after every measurement.

2309

2310 **Figure 13-3. ASTM C1012 mortar bars immersed in 50 g/L Na_2SO_4**

13.5 Typical Experimental Measurement and Interpretation

Length and mass measurements were taken before immersing the bars in sodium sulfate solution (as initial measurements) and at various days after immersion until one year. After every measurement, the sodium sulfate solution was renewed. The length measurements were made using a length comparator. The measured lengths were then used to calculate the expansion of the bars. Then the average expansions of six bars per mixture were calculated and reported. According to ACI 318-19, the 6-month ASTM C1012 expansion limit is 0.05%, and the 1-year ASTM C1012 expansion limit is 0.10%. If the average expansion of a particular mixture is more than the expansion limit, the mixture has failed the test. And, it can be interpreted as the cementitious material used in the mixture cannot mitigate external sulfate attack.

13.6 Experimental Results

The expansion results of the mortar bars at six months (26 weeks) and one year (52 weeks) for cement A are provided in Figure 13-4 and Figure 13-5, respectively. Similarly, the expansion results for the mortar bars at six months (26 weeks) and one year (52 weeks) for cement D are provided in Figure 13-6 and Figure 13-7, respectively.

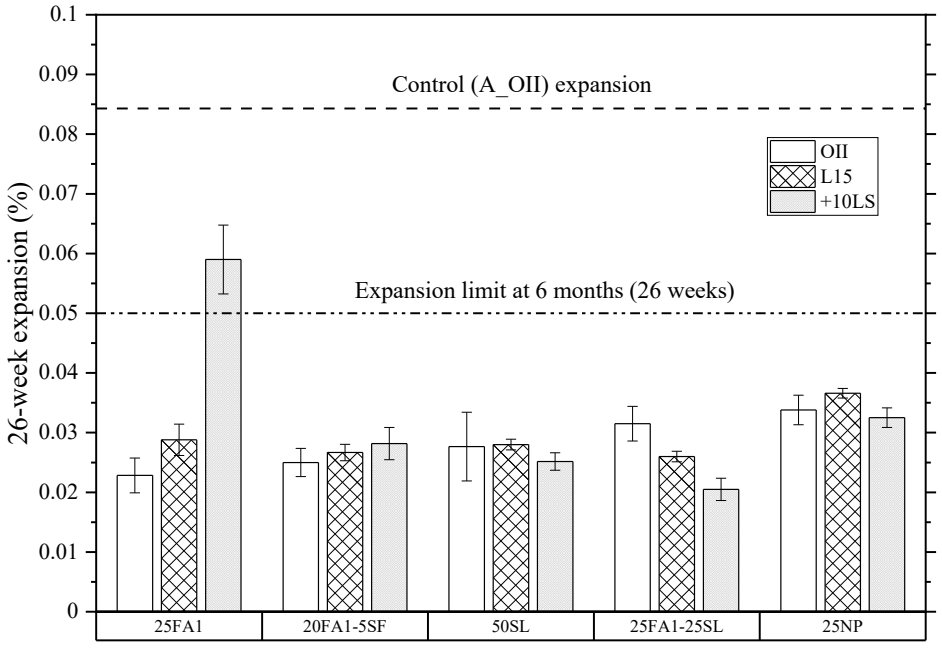

Figure 13-4. 6-month (26 weeks) expansion data of the mortar bars with clinker A

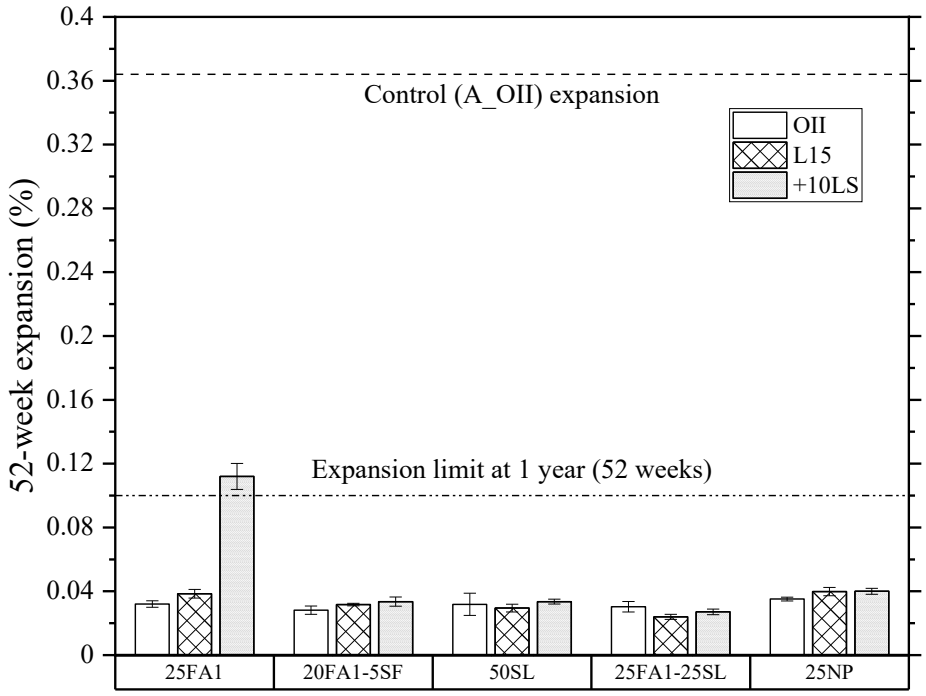

Figure 13-5. 1-year (52 weeks) expansion data of the mortar bars with clinker A

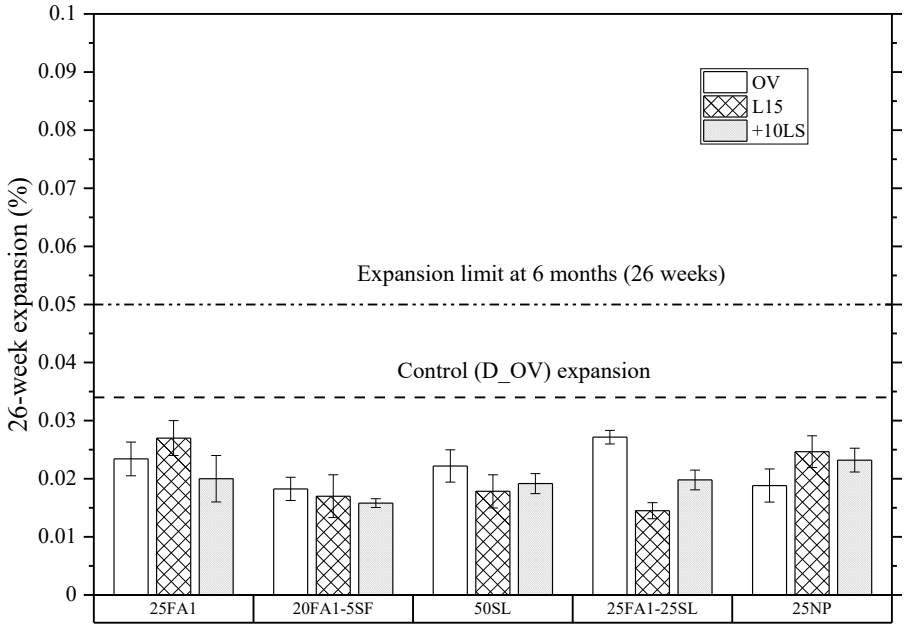

Figure 13-6. 6-month (26 weeks) expansion data of the mortar bars with clinker D

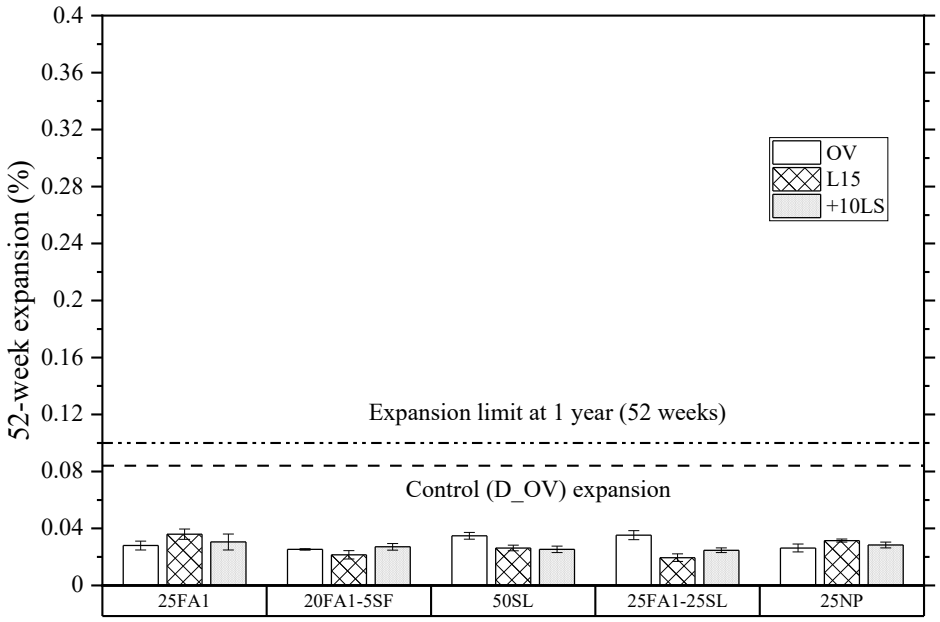

Figure 13-7. 1-year (52 weeks) expansion data of the mortar bars with clinker D

13.7 Discussion of the Results

As seen in Figure 13-4 and Figure 13-5, the mixtures with SCMs reduced the expansion significantly when compared to the control mixture with no SCMs. Except in the case of cement A and 25% FA1, there was no significant difference in both 6-month (26-week) and 1-year (52-week) expansions observed between the A_OII, A_L15, and A_OII +10LS mixtures in the presence of SCMs. In the case of mixtures with 25FA1-25SL, PLC mortars were observed to perform slightly better than the OPC mortar. The mixture - A_OII+10LS _25FA1 was observed to be expanding higher than A_OII_25FA1 and A_L15_25FA1 mixtures. The reason for this is unknown. Potential reasons include incorrect initial length measurements or incorrect material proportions used for mixing. Therefore, the expansion result of A_OII+10LS _25FA1 is considered to be an outlier.

From Figure 13-6 and Figure 13-7, the SCMs' ability to reduce the expansion significantly when compared to the control mixture (D_OV) is evident. There was no significant difference observed in both 6-month (26-week) and 1-year (52-week) expansions between the D_OV, D_L15, and D_OV+10LS mixtures in the presence of SCMs. In the case of mixtures with 25FA1-25SL, PLC mortars were observed to perform slightly better than the OPC mortar, probably due to better pore refinement. Figure 13-8 illustrates the comparison of 6-month expansions of OPC and PLC mortars of both cements A and D (30 mixtures). The Y-axis represents the 6-month expansion of the PLC (interground) and OPC+LS mortars. The X-axis represents the 6-month expansion of the

OPC mortars. The data points along the 1:1 solid line imply that there is no difference in the expansion of the mortars with OPC and PLC. The dashed lines represent a variation of 20% from equivalence.

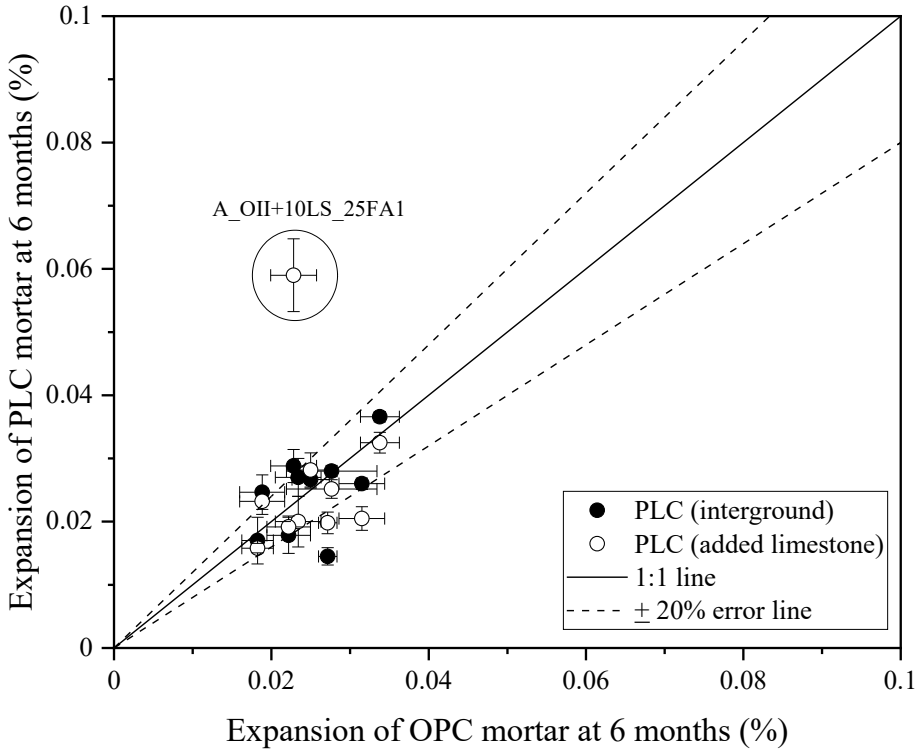

Figure 13-8. ASTM C1012 6-month expansion results: comparison of OPC and PLC mixtures

From Figure 13-8, it was observed that most of the mixtures fall very close to the 1:1 line and within the 20% error lines, implying that there is no significant difference in the expansions observed between the OPC and PLC mortars. The mixture- A_OII+10LS _25FA1 can be clearly identified as an outliner in the plot.

13.8 Significant Findings

The presence of all SCM(s) reduced expansions significantly compared to the control (with no SCM). The main takeaway from this Task is that, overall, the PLCs performed similar to, if not better than, their corresponding OPC mixtures in the presence of SCMs. Therefore, CALTRANS can use their current SCM mixtures as is with ASTM C 150 Type II or V clinker that is then interground or interblended with PLC up to 15% limestone and expect similar external sulfate resistance to ASTM C150 Type II or V cements with no or very low amounts of interground/interblended limestone.

14 Construction Schedule

Certain concrete characteristics can influence the effort required and rate at which the concrete is placed in the field. Two commonly measured characteristics that can influence the constructability and scheduling of concrete construction projects is the workability and setting of the concrete mixtures. Workability, or more specifically slump of the concrete mixtures, is shown in Figure 14-1. This figure shows the slump of concrete mixtures made from the three clinker sources with their respective SCM combinations. The target slump was 4 inches in most cases. It can be seen that the majority of the slump values fall within ±2.5 inches. It should also be noted that slump was measured on the fresh concrete and the heat of hydration data were obtained from a different set of paste samples. This section will focus on the setting times of the concrete mixtures evaluated.

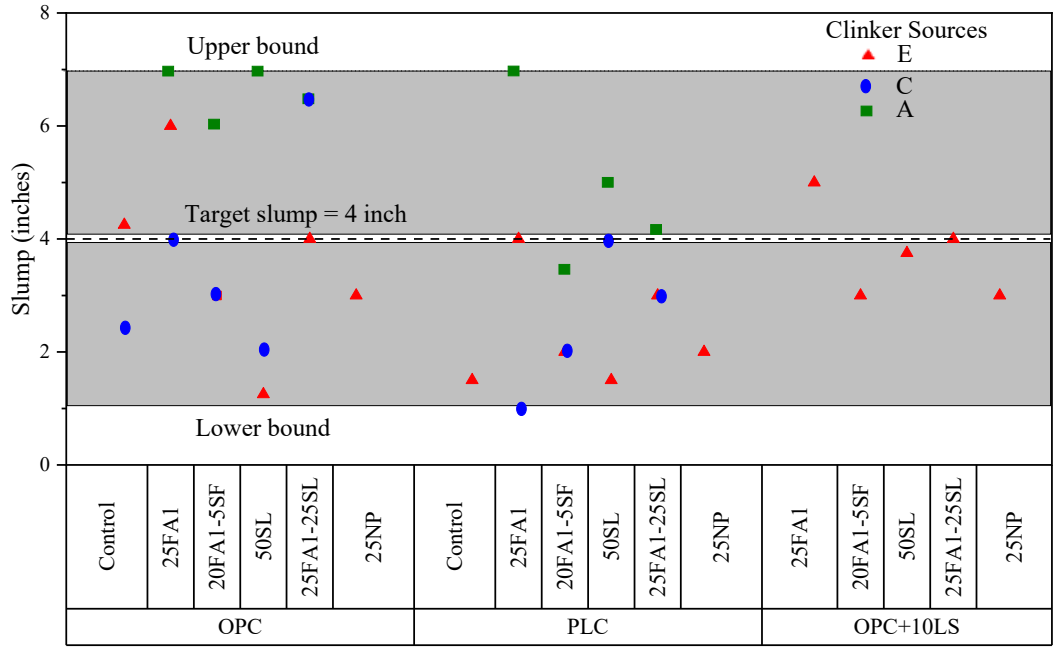

Figure 14-1. Slump values of fresh concrete mixtures.

14.1 Research Objectives

The objective of this section is to quantify the relative time of setting of the different mixtures. This is accomplished using the heat of hydration data as described in Section 4.6 of this report. Testing was performed following ASTM C1753-15. Statistical analyses are used to compare these relative times of setting.

14.2 Background/Literature Review

ASTM C1753-15, *Standard Practice for Evaluating Early Hydration of Hydraulic Cementitious Mixtures Using Thermal Measurements*, was used to evaluate the mixtures in this research [164]. The standard indicates that the thermal profiles can be used to evaluate the hydration behavior of hydraulic cementitious mixtures after the addition of water and this can provide indications concerning setting. Sandberg and Liberman (2007) reported that 21% of the measured main peak temperature correlates with the initial setting time and 42% of the measured main peak temperature correlates with the final set [165]. This research will evaluate the relative initial and final set and will use the 30% and 50% values for comparing the relative initial and final setting times.

14.3 Experimental Test Matrix

All five clinker sources (A, B, C, D, and E) with their respective OPC, PLC, and OPC+10%LS systems were evaluated. In addition, the systems with 25% fly ash, 20% fly ash + 5% silica fume, 50% slag, and 25% fly ash + 25% slag were evaluated for relative setting times. Each mixture included two tests and the average values are reported. The experimental test matrix is shown in Table 4.5.

14.4 Experimental and Analytical Methods

The process stipulated in ASTM C1753-15, *Standard Practice for Evaluating Early Hydration of Hydraulic Cementitious Mixtures Using Thermal Measurements*, was used to evaluate the mixtures in this research. To assess the significance of the potential difference in setting times, t-tests were performed. These tests provide a comparison of the setting times at $t_{30\%}$ and $t_{50\%}$ for the various paste samples. Initially, specimens from all cement sources (A, B, C, D, and E) made with OPC, PLC, and OPC+10LS containing no SCMs were grouped are compared. Following this, comparisons are made between the different mixtures (e.g., PLC from all cements with no SCM and PLC with all cements containing 25% fly ash). A p-value of less than 0.05 indicates that there is a significant difference between the two datasets. Table 14.1 shows the comparisons assessed in this research. Note that comparisons were made for both $t_{30\%}$ and $t_{50\%}$ data.

Table 14.1. Statistical comparisons

Cement Type (Manufacturers)	SCM Addition					
	None (MO)			25% FA, 20% FA+5% SF, 50% Slag, 25% FA + 25% Slag (M1-M4)		
	OPC (A, B, C, D, & E)	PLC (A, B, C, D, & E)	PLC+LS (A, B, C, D, & E)	OPC (A, B, C, D, & E)	PLC (A, B, C, D, & E)	PLC+LS (A, B, C, D, & E)
OPC (A, B, C, D, & E)		X	X	X		
PLC (A, B, C, D, & E)	X		X		X	
PLC+LS (A, B, C, D, & E)	X	X				X

M1=25% FA; M2=20%FA+5%SF; M3=50% slag; M4=25%FA+25% slag.

14.5 Experimental Results

In this chapter, the apparent setting times were measured and compared. Statistical t-tests were performed to compare and contrast these setting times. Both initial ($t_{30\%}$) and final ($t_{50\%}$) setting times were compared. A p-value of less than 0.05 indicates that there is a significant difference between the two datasets. In the first set of t-tests, OPCs, PLCs, and OPC+10LS' were compared within the same mixture (i.e., no SCM, 25% FA, 20% FA+ 5% SF, 50% slag, and 25% FA and 25% slag). This was done for all mixtures (M0 to M4). For example, for mixture M0, the following three comparisons were made:

- OPC and PLC
- PLC and OPC +10LS
- OPC and OPC +10LS

The findings from the two-sample t-tests reveal that, for mixtures M0 to M4, there is no statistically significant difference between the comparison for mixtures without SCMs for both initial and final setting times. The p-values from the t-tests for initial set were: OPC/PLC – 0.95, OPC/OPC+LS – 0.63, and PLC/OPC+LS – 0.51. The p-values from the t-tests for final set were: OPC/PLC – 0.93, OPC/OPC+LS – 0.54, and PLC/OPC+LS – 0.37. This indicates that there is likely no significant difference in setting time between the OPC systems with the inter-grinding or addition of the

limestone. The p-values for all the comparisons were significantly higher than 0.05 threshold by a comfortable margin.

In the second set of t-tests, the OPC, PLC, and OPC+10LS samples of M0 were compared with the OPC, PLC, and OPC+10LS samples of the M1, M2, M3, and M4. shows the p-values for these comparisons (for initial set/for final set). Shaded cells indicate statistically significant values. Comparisons between M0 and M1 reveal that there is no statistically difference between most OPC and PLC mixtures. However, a comparison of the OPC+LS mixtures between mixtures M0 and M1 (25% fly ash addition) indicates a statistically significant difference. The data indicates that when limestone (not interground) and fly ash are included in a mixture, the initial and final setting times can increase. However, it should be noted that the p-values for the other comparisons in this group are relatively close to the p-value threshold of 0.05, indicating the difference between cement types is likely not significant.

For the M0-M2 and M0-M3 comparisons, it can be seen that there are no statistically significant differences for all cases. Comparison of mixtures M0 and M4 indicate the initial and final setting times are statistically significant for all cement types. This indicates that the addition of 25% FA and 25% slag to mixtures leads to longer initial and final setting times. However, note that the initial and final setting times for the mixtures without limestone also exhibited increased setting times and the increase is likely not a result of the limestone additions.

Table 14.2 shows the p-values for these comparisons (for initial set/for final set). Shaded cells indicate statistically significant values. Comparisons between M0 and M1 reveal that there is no statistically difference between most OPC and PLC mixtures. However, a comparison of the OPC+LS mixtures between mixtures M0 and M1 (25% fly ash addition) indicates a statistically significant difference. The data indicates that when limestone (not interground) and fly ash are included in a mixture, the initial and final setting times can increase. However, it should be noted that the p-values for the other comparisons in this group are relatively close to the p-value threshold of 0.05, indicating the difference between cement types is likely not significant.

For the M0-M2 and M0-M3 comparisons, it can be seen that there are no statistically significant differences for all cases. Comparison of mixtures M0 and M4 indicate the initial and final setting times are statistically significant for all cement types. This indicates that the addition of 25% FA and 25% slag to mixtures leads to longer initial and final setting times. However, note that the initial and final setting times for the mixtures without limestone also exhibited increased setting times and the increase is likely not a result of the limestone additions.

Table 14.2. p-values for different mixtures.

Mixture	Cement Type	Mixture M0		
		OPC	PLC	OPC+LS

M1	**OPC**	0.22/0.07		
	PLC		0.10/0.07	
	OPC+LS			0.04/0.03
M2	**OPC**	0.12/0.19		
	PLC		0.08/0.15	
	OPC+LS			0.20/0.36
M3	**OPC**	0.26/0.16		
	PLC		0.14/0.06	
	OPC+LS			0.40/0.41
M4	**OPC**	0.03/0.02		
	PLC		0.08/0.02	
	OPC+LS			0.01/0.02

p-value on the left corresponds to the initial set, p-value on the right corresponds to the final set

14.6 Significant Findings

The fresh characteristics of concrete can influence the constructability of concrete projects. This research evaluated the setting time of concretes containing various cements from different producers with the additions of limestone and various combinations of SCMs. In general, the addition of limestone, whether interground or added to the cement, had no statistically significant influence on the initial or final setting times. Of course, in some cases the addition of SCMs did influence the initial and final setting times.

15 Impact on Greenhouse Gas Emissions

15.1 Background of Sustainability Efforts in the Cement Industry

The production of portland cement clinker produces approximately 6% of the world's anthropogenic CO_{2eq} emissions [166, 167]. The main contribution (~60%) comes from the calcination (heating) process in which limestone ($CaCO_3$) is decomposed into CaO (for cement) and CO_2 (released). Note that while the global values of the contribution from calcinations are typically 50%, the typical values in the state of California are closer to 60% [168]. The other main component (~40%) of the CO_{2eq} emissions comes from the fuel source used to heat the raw materials (limestone and clay) to approximately 1450°C (note that the emissions at this stage are primarily associated with energy resources). Minor emissions come from the grinding of the clinker material and the transportation of materials to and from the cement production facility [166]. The production of OPC is highly efficient (approximately 85% efficient [6, 168, 169]) and the emission of CO_{2eq} from the process is lower than other building materials such as steel, wood and aluminum [170]. The challenge is that we use more cementitious materials than all other building materials combined. Therefore, the overall percent contribution is higher than other building materials.

The portland cement industry and the research community have been focused on reducing CO_{2eq} emissions for many years [166, 169, 171, 172]. Some of the early efforts were to simply optimize the production process, move toward a dry rather than wet production process, increase waste heat recovery and to use alternative fuel sources. There is still work to do in the area of alternative fuel sources and energy where more CO_{2eq} savings can be realized. The use of supplementary cementitious materials (SCMs) such as ground granulated blast furnace slag, fly ash and silica fume – which are all by-products of other industrial processes which would most likely be landfilled – provided a second wave of lowering CO_{2eq} emissions. The third wave of reducing CO_{2eq} emissions the past ~20 years have been on increasing the amount of finely ground limestone as a replacement for a portion of the portland cement. This can be done either as an interground product with the clinker phase of portland cement, or blended product once the portland cement is ground. Most ASTM C 150 Type I, II, III and V cements produced in the United States contain up to 5% finely ground limestone today. The amount of finely ground limestone is increasing beyond 5% to upwards of 15% in the United States. Europe has been using higher amounts of finely ground limestone for many years and certain cements may contain up to 35% FGL [4, 173]. The most recent work (~last 10 years) to reduce CO_{2eq} emissions has centered around LC3 systems where both finely ground limestone and calcined clay are used to replace as much as 50% of the portland cement. Calcined clay does require energy to heat and thus activate the material, though the calcining temperatures (~650°C-800°C) are about ½ that needed to calcine portland cement. Further there is little CO_2 emissions from the calcining process itself as clays typically do not contain $CaCO_3$. The "tool box" for CO_{2eq} reduction in cements has widened and this will provide

even more options in the future as these technologies are further refined and verified for long-term durability (LC3 investigations underway) [174]. While there is much "buzz" about alternative cementitious materials having lower CO_{2eq} footprints most, if not all, of these technologies cannot be produced on the same scale that ordinary portland cement is used. There may be a potential for these materials to be part of a suite of solutions to reduce CO_{2eq} emissions [175]. The impact from this will be minor compared to the impact for calcined clays and/or limestone to reduce CO_{2eq} at a global scale.

15.2 Life Cycle Inventory (LCI) of PLC Concrete

In this project CALTRANS is interested in increasing the amount of limestone in their portland cements to as much as 15%. The research team partnered with the University of California at Davis to implement a life cycle inventory tool recently developed for CALTRANS [176, 177]. The process flow diagram for this GHG emissions assessment tool is shown below in Figure 15-1.

This GHG emissions assessment tool was used to evaluate four example CALTRANS concrete mixtures representing bridge decks, pavements and pre-cast concrete replacement panels for transportation infrastructure. The baseline mixture data was input into the software tool and then the portland cement portion was adjusted to reflect a 10 or 15% interground limestone replacement. The overall reduction in GHG, as compared to the baseline mixtures (assuming no limestone replacement) was then calculated. A second set of calculations was done to capture the influence of supplementary cementitious material replacement in addition to the 10 or 15% interground limestone replacement, in terms of GHG savings. The mixture designs provided to the team from Caltrans for the pavement and precast panel contained 100% OPC. A third set of calculations was done to demonstrate the impact of also including SCMs in the mixture.

In this GHG emissions assessment tool, several key assumptions are of note:

- Fly ash is considered to be a waste material that is ready for use without processing. Transportation is considered in the calculation of GHG emissions. Thus, for fly ash, GHG emissions reduction are an upper bound.
- Ground granulated blast furnace slag and silica fume require additional processing before incorporation into portland cement concrete. This is captured in the EPDs and LCA documentation that supports this LCI tool. This, as well as transportation, are included in GHG emission calculations.
- Transportation distances (Table 15.1) are assumed based on market analysis [176, 177] and generally expected transportation distances for the State of California's concrete market.

The calculations shown are examples to illustrate the GHG emissions reduction potential for more sustainably designed concrete mixtures. For specific projects the referenced GHG emissions assessment tool can be used to produce data that incorporates project specific information.

In Figure 15-1, the process flow as well as boundary conditions used in the GHG emissions assessment tool are given. The raw materials acquisition, manufacturing, batching for the specific concrete mixture are included in the LCI GHG tool. The "in use" phase of the concrete is not included in this tool.

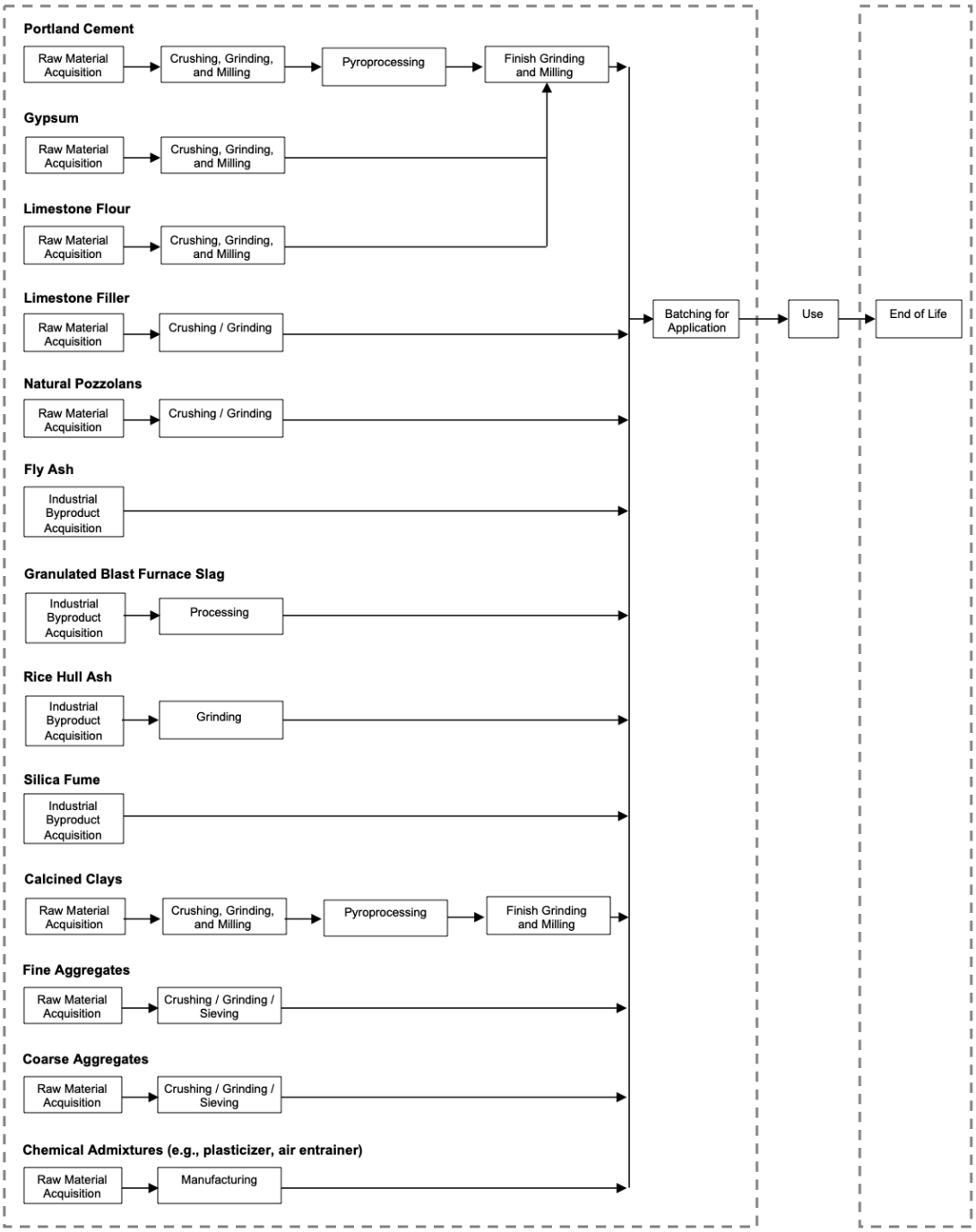

Figure 15-1. Process flow diagram for LCI greenhouse gas reduction tool [177]

Table 15.1. Transportation distances used to calculate greenhouse gas reduction in the LCI GHG tool (from [176, 177]).

Transportation Distances	
Constituent	**Distance (km)**
Portland Cement	20
Limestone, interground	20
Limestone Filler	150
Natural Pozzolans	150
Shale Ash	150
Calcined Clay	150
Silica Fume	150
Fly Ash	2000
Blast Furnace Slag	2000
Fine Aggregates	100
Coarse Aggregates	100
Superplasticizer	1000
Water	0

The example CALTRANS concrete mixture designs that were investigated are shown below in Table 15.2.

Table 15.2. Example CALTRANS concrete mixture designs evaluated using the GHG reduction in the LCI GHG tool [176]

	Cement (kg/m^3)	**w/cm**	**Water (kg/m^3)**	**Slag (kg/m^3)**	**Fly ash (kg/m^3)**	**Coarse aggregate (kg/m^3)**	**Fine aggregate (kg/m^3)**
Bridge Deck 1	334	0.38	171	-	112	979	682
Bridge Deck 2	218	0.38	168	218	-	1085	753
Precast Panel	409	0.38	154	-	-	1066	675
Jointed Plain Concrete Pavement	400	0.43	172	-	-	1075	662

In Table 15.2, four example CALTRANS concrete mixture designs are shown. It should be noted that the two bridge deck mixture designs used either a 50% replacement by slag cement or a 25% replacement by fly ash. The precast panel and jointed plain concrete pavement were 100% OPC mixtures. Those two mixtures had very similar cement contents. The cementitious materials content in bridge deck 2 was also similar but slightly higher than the previously mentioned mixtures. Bridge deck 1 had the highest cementitious materials content at 446 kg/m^3. Overall, three of the mixtures had the same w/cm at 0.38 while the joined plain concrete pavement was a bit higher at 0.43.

Figure 15-2 shows the results of the analysis on the four example CALTRANS Concrete mixture designs for potential GHG reduction.

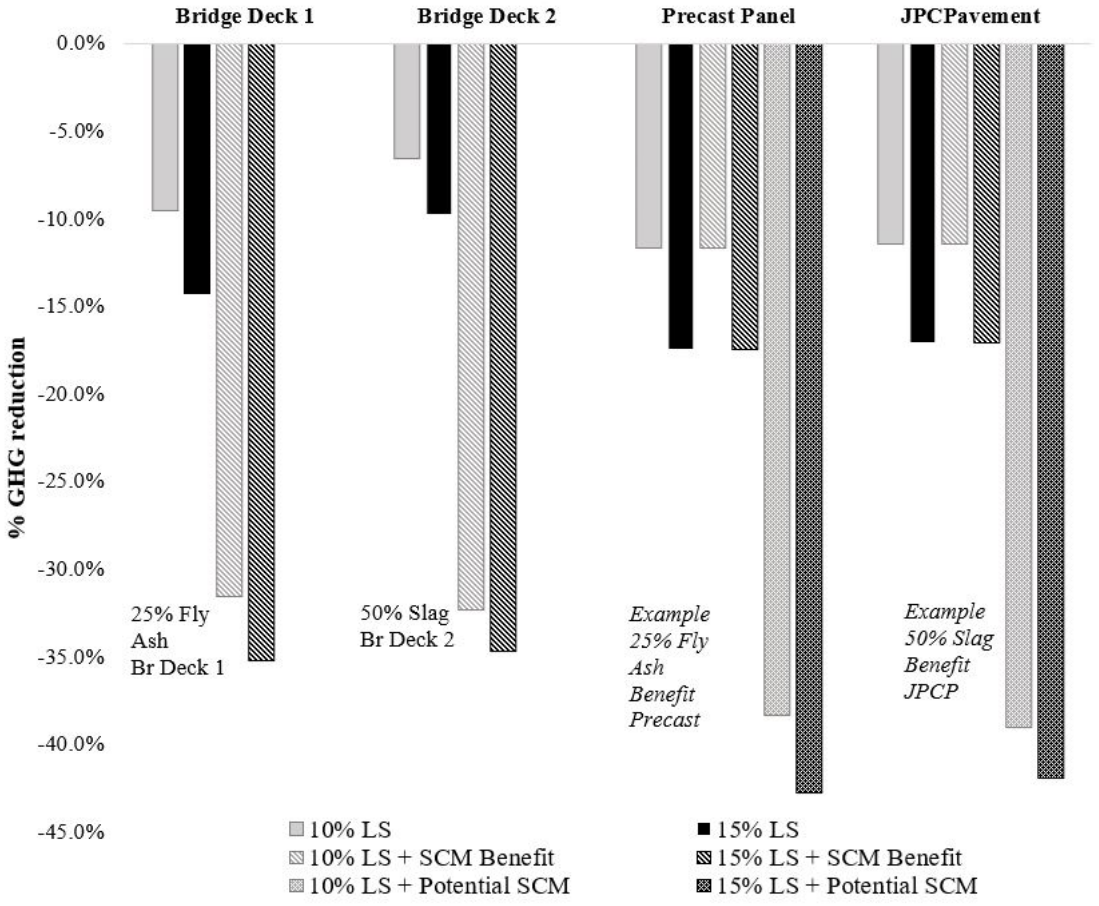

Figure 15-2. Greenhouse gas reductions compared for 10 and 15% interground limestone replacements for example CALTRANS concrete mixtures.

Figure 15-2 shows groups of bar charts where the lighter color in each pair represents 10% LS and the darker, 15%. This figure shows that there is an approximate 6.5-17% potential for greenhouse gas reduction in all the example mixtures evaluated when SCMs are not included in the analysis.

For the 10% LS replacement levels the savings ranged from 6.5-12.1%. For the 15% LS replacement levels the savings ranged from 9.8-17.5%. These variations are due to the mixture design specifics as well as associated transportation distances with the various materials in the mixtures. When SCMs are included in the analysis (e.g., compared against the same mixture design except with 100% OPC) there is a substantially higher reduction in greenhouse gas emissions, roughly around 30-35%.

It is important to note that the precast panel or jointed plain concrete pavement contained 100% OPC. To show further potential for greenhouse gas reduction in these mixtures a third set of calculations was done, and those results are shown in the last set of bars (light and dark gray dotted bars). This shows that there is a potential greenhouse gas reduction of up to 41.9% and 42.7% in the case of the jointed plain concrete pavement or the precast panel mixture, respectively, if PLC is combined with SCM in these mixtures.

15.3 Significant Findings

Overall, there is significant potential for GHG when using Portland-limestone cement to replace portland cement from 6.5% to 17.1% with an average of approximately 10%-12%. Further reductions can be realized with the incorporation of SCMs. Further, there appear to be benefits of SCM with portland-limestone cements to realize the most significant GHG reductions.

16 Thermodynamic Simulations

16.1 Research Objective

This section reports the influence of cement clinker chemistry on PLC performance. Specifically, thermodynamic simulations were performed for the clinkers used in the experimental portion of this work. The research compares the results of the model with experiments. Furthermore, the synergy between PLCs and SCMs is explored parametrically using thermodynamic modeling.

16.2 Background and Literature Review

The use of PLCs as a replacement for OPCs in concrete has been gaining momentum due to environmental benefits associated with the reduction of CO_2 emissions during production [6]. Although some consider limestone an inert material, others have shown that it can affect the reaction products of hydrated OPC systems [22, 48, 98, 150, 157, 178]. In typical OPC systems, limestone content can stabilize ettringite and result in the formation of monocarbonate instead of monosulfate [14, 22, 48, 98, 179]. This change in the phase assemblage of reaction products due to the presence of limestone can sometimes directly impact the porosity and pore volume distribution in concrete as ettringite is a more space-filling phase [6, 20, 180].

Matschei et al. [20] showed that the porosity of OPC-Limestone systems decreased (and the compressive strength increased) when the limestone content increased up to clinker replacement levels of 2%. Any further increase in limestone content led to a porosity increase (and a decrease in compressive strength). However, many have used Matschei's work as a guide for 'equivalent porosity' or 'equivalent strength' in PLC which has driven the design and proportioning of PLC-based mixtures in North America.

Several authors have experimentally studied the impact of partial replacement of clinker in OPC+SCM systems with limestone. The synergistic effect of using SCMs containing alumina (like fly ash, slag or metakaolin) with limestone has been documented on the compressive strength [14, 181] or transport properties [2]. While the synergy of limestone and alumina is noted in the literature [180, 181], there is lack of a robust recommendation on switching between OPC to PLC to exploit this synergy. For example, some have questioned how well PLC will work with SCM. Thermodynamic modeling is one such tool which can be used in a predictive capacity to study the impact of replacement of OPC with PLC in systems made with cement and SCMs.

Thermodynamic modeling is gaining popularity as a predictive tool to evaluate the solid and liquid reaction products of OPC and OPC+SCM systems [8, 22, 44, 48, 182-185]. Thermodynamic modeling has also been used in conjunction with the concepts of Power's and Brownyard's model [186, 187] to determine the pore structure of OPC [123] and OPC+SCM pastes [188, 189]. The

work on pastes has also been extended to concrete to predict the porosity, pore volumes, and service life of concrete [190]. In this work, thermodynamic modeling is used to study the impact of using PLCs as a direct replacement for OPCs.

16.3 Modeling Framework

16.3.1 Thermodynamic Modeling

The GEMS3K [191] software is used to perform thermodynamic modeling, and it is coupled with the CEMDATA thermodynamic database [48]. Thermodynamic modeling is performed by calculating the phase assemblage at equilibrium, which minimizes the system's Gibbs Free Energy. The GEMS-CEMDATA framework has been used to calculate the volumes and compositions of solids, liquid, and gaseous products at thermodynamic equilibrium. The framework has been used previously to obtain the reaction product volumes and pore solution composition of OPC [44, 182] and OPC+SCM systems [192]. While all phases are available to form in the GEMS-CEMDATA framework, siliceous hydrogarnet [123, 192, 193], hydrotalcite [123], and carbonate-ettringite phases [83, 178, 185] were blocked from forming based on empirical evidence from the literature that these phases do not form in significant quantities in cementitious systems at typical temperatures (less than 60°C) in the time frames studied (<20 years).

16.3.2 Kinetic Models

While powerful, thermodynamic models calculate only the phase assemblage of the systems studied at equilibrium (i.e., the final phases). In practice, most cementitious systems have not yet reached thermodynamic equilibrium. Kinetic models (such as the Parrot-Killoh model for OPC-clinker [194] or the Modified Parrot-Killoh Model for clinker + SCM [195]) are often used to predict the mass fraction of the clinker that reacts at a given age. Thermodynamic models are often coupled with kinetic models to predict cementitious systems' reaction products at a given age. The literature has shown that the phase assemblage of cementitious systems depends on the amount of clinker, SCM, and limestone available to react [48] and the kinetics of dissolution of the three components of the systems studied (i.e.,, clinker, SCM, limestone) are essential to understand.

16.3.2.1 Modified Parrot Killoh Model for Clinker and SCM

The Modified Parrot Killoh (MPK) model [195, 196] was used to predict the mass fraction of the clinker phases (C_3S, C_2S, C_3A, C_4AF) and oxide phases in SCMs (SiO_2, Al_2O_3, CaO) that react at a given age. The inputs to the MPK model are: (i) the chemical composition of the OPC-clinker and SCM used, (ii) the reactivity of the SCM (fraction of SCM that can react at equilibrium, usually the amorphous fraction of the SCM [196]), (iii) w/b, and, (iv) the temperature of curing.

The MPK model outputs are the degree of reaction of the clinker phases (C_3S, C_2S, C_3A, C_4AF) and pozzolanic oxide phases (SiO_2, Al_2O_3, CaO) as a function of time. The degree of reaction of

each phase at a given time ($DOR_{ph}(t)$) is the fraction of the component that is available to react at that time. The dissolution of the alkali oxide phases in the clinker (Na_2O, K_2O, MgO, SO_3) was scaled based on their distribution in the clinker phases obtained from the literature [197]. The dissolution of alkali oxide phases from the SCM were scaled with the reactivity (DOR^*) of the SCM and the degree of reaction of the SCM. The degree of reaction of the system (DOR_{sys}) is the mass averaged degree of reaction of clinker and SCM oxide phases (C_3S, C_2S, C_3A, C_4AF, SiO_2, Al_2O_3, CaO). A sample output of the MPK Model for one of the systems studied (M1, PLC+25%FA) is shown in Figure 16-1 below. The figure shows the degree of reaction of each phase as well as the degree of reaction of the whole system as a function of time from 1 day up to 365 days of hydration. Early age predictions of the model (<1 day) are not shown as they are not very accurate, which is a known issue with the Parrot and Kiloh model [194].

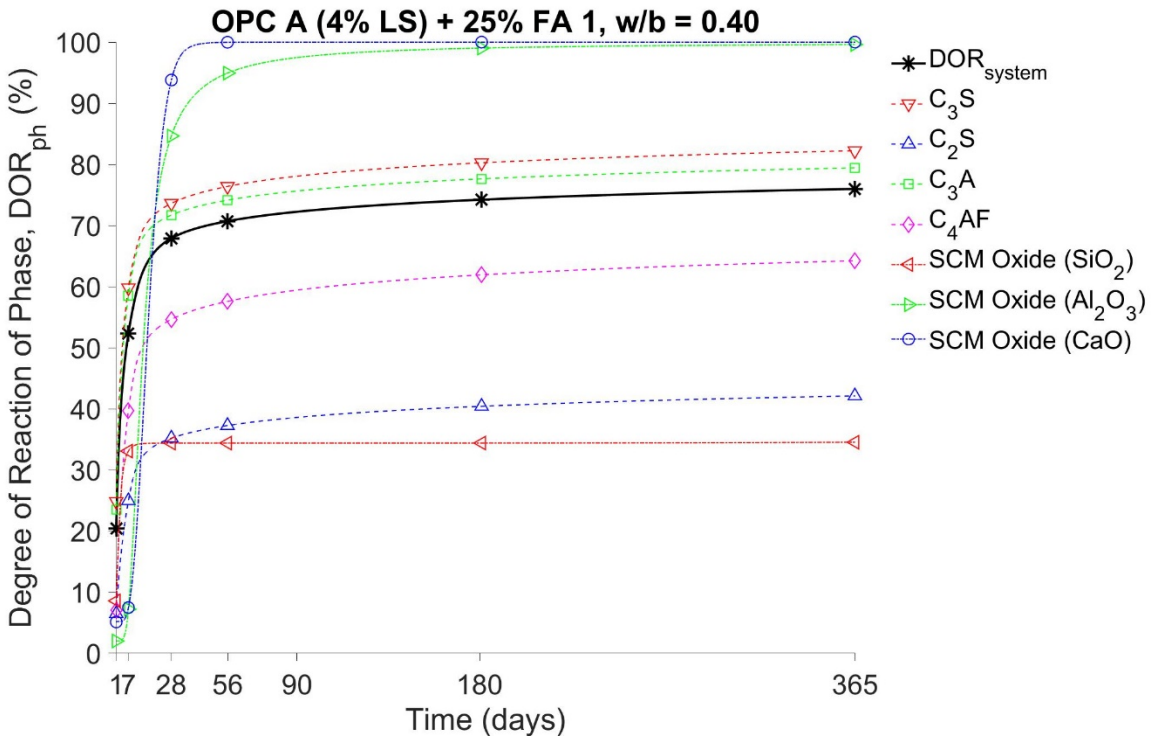

Figure 16-1. Output of the MPK model for clinker and SCM oxides

16.3.2.2 *Modeling the dissolution of limestone*

The mass of limestone available to react is an essential input parameter to thermodynamic calculations, which impacts the phase assemblage [48] and porosity [20, 22, 198] of these systems. The amount of $CaCO_3$ available to react at any given time is considered the total amount of $CaCO_3$ in the system. This is justified below.

Calcium carbonate dissolves to some extent at ambient temperature to saturate typical cementitious pore solutions with carbonate within the first few hours of mixing [14, 83, 199]. The total volume and fineness also plays only a minor role in the amount of calcium carbonate dissolved at equilibrium [200]. It has also been observed that the solubility of limestone in the pore solution of typical OPC+SCM systems is high enough to saturate the solution with carbonates within a few hours [201, 202], and often the effects of limestone dissolution kinetics disappear after the first hour of mixing [203]. Therefore, the kinetics of limestone dissolution is governed by the kinetics of product formation and not the rate at which carbonate dissolves from the limestone. In this work, since the thermodynamic models are run at ages greater than one day (typically $DOR_{sys} > 30\%$), the entire mass of calcium carbonate is considered to be available to react at all times. The material that does not react simply reforms as calcite and is considered unreacted. Preliminary studies investigated these details

While it is possible for some of the calcium carbonate to be encapsulated by reaction products rendering the rest of the calcite unable to react, it is assumed in this work that this does not occur to a significant degree in the systems studied due to the limestone being ground finely enough.

It should also be noted that the input to the thermodynamic model is the total mass of calcium carbonate, and as such, systems with inter-ground limestone (OPC+Ls) and blended limestone (PLC) are assumed to be thermodynamically equivalent.

16.4 Typical Results

Typical outputs of thermodynamic modeling at 56-days of hydration (DOR_{system}~=72%) and the Pore Partitioning Model (PPM) are shown in Figure 16-2. Figure 16-2(a) shows the phase assemblage of systems containing Type II/V clinker with varying levels of limestone addition, while Figure 16-2(b) shows the results for Type I/III clinker. It can be seen that as the limestone content increases, the volume of monosulfate decreases and is replaced by ettringite and carboaluminate phases (hemi-/monocarbonate). Above a 2% limestone content, no further limestone reacts, and unreacted calcite (limestone) remains in the system. It should be noted that the mass of alumina in Type II/V systems (which contain 4.29g alumina/100g clinker) is typically lower than the alumina in Type I/III systems (which contain 4.92g alumina/100g clinker) [204], it should be noted that the phase assemblage in these two systems are similar. It can also be noted that the relative proportions of the different types of C-S-H that form (and therefore the C/S ratio of the C-S-H) stay constant, indicating that the presence of limestone does not significantly affect the C-S-H gel chemistry.

Figure 16-2(c, d) shows a typical output of the PPM in terms of the volumes of gel solids, gel water, capillary water, and chemical shrinkage that forms in the same system. From Figure 16-2(c, d), it can be seen that the volume of gel solids increases and the volumes of capillary water

decreases when limestone content is increased from 0-2%, and at 2% the system is at the lowest porosity. Above a 2% limestone content, any further addition of limestone causes the volumes of gel solids to decrease and the volume of capillary pores to increase. This is due to the dilution of clinker with unreacted limestone.

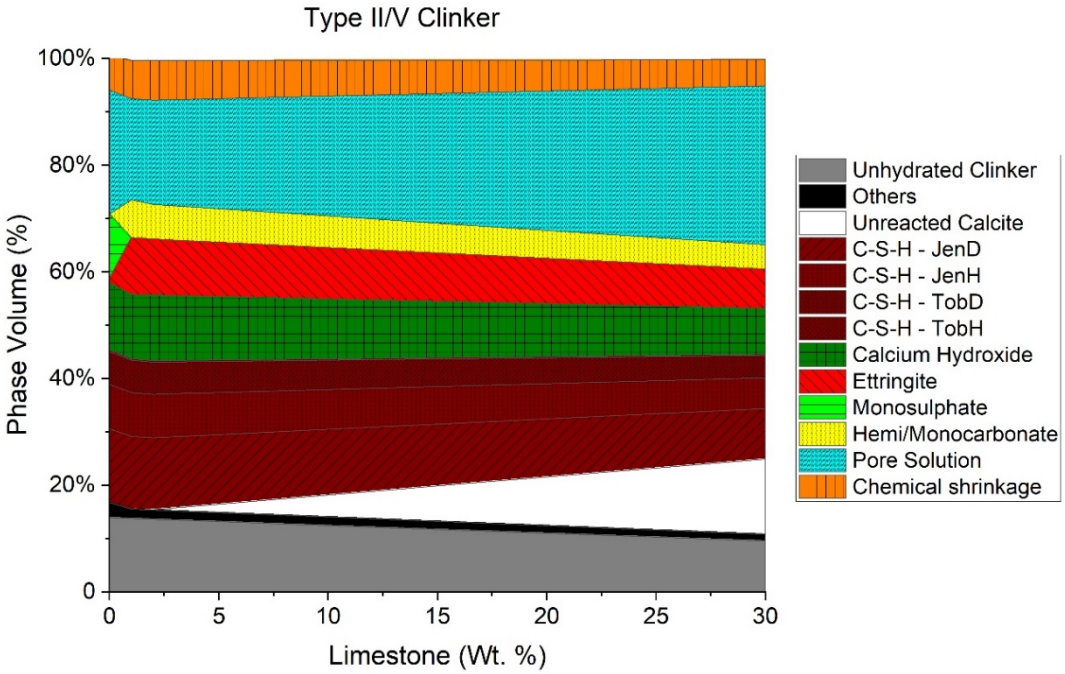

(a) The phase assemblage of Type II/V Clinker + Limestone systems

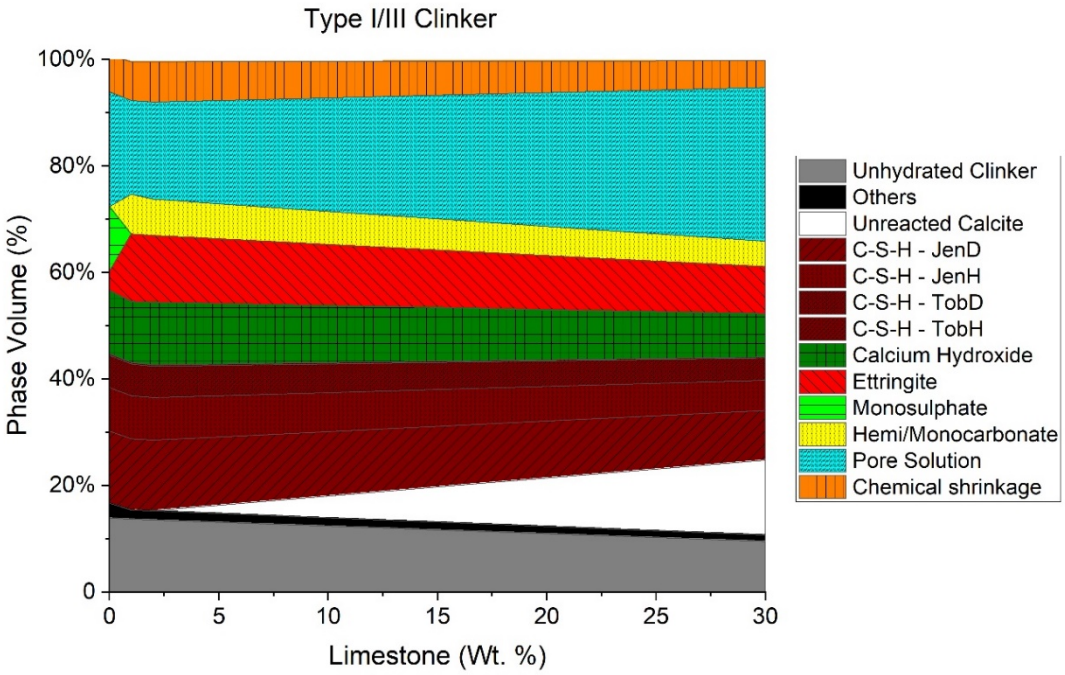

(b) The phase assemblage of Type I/III Clinker + Limestone systems

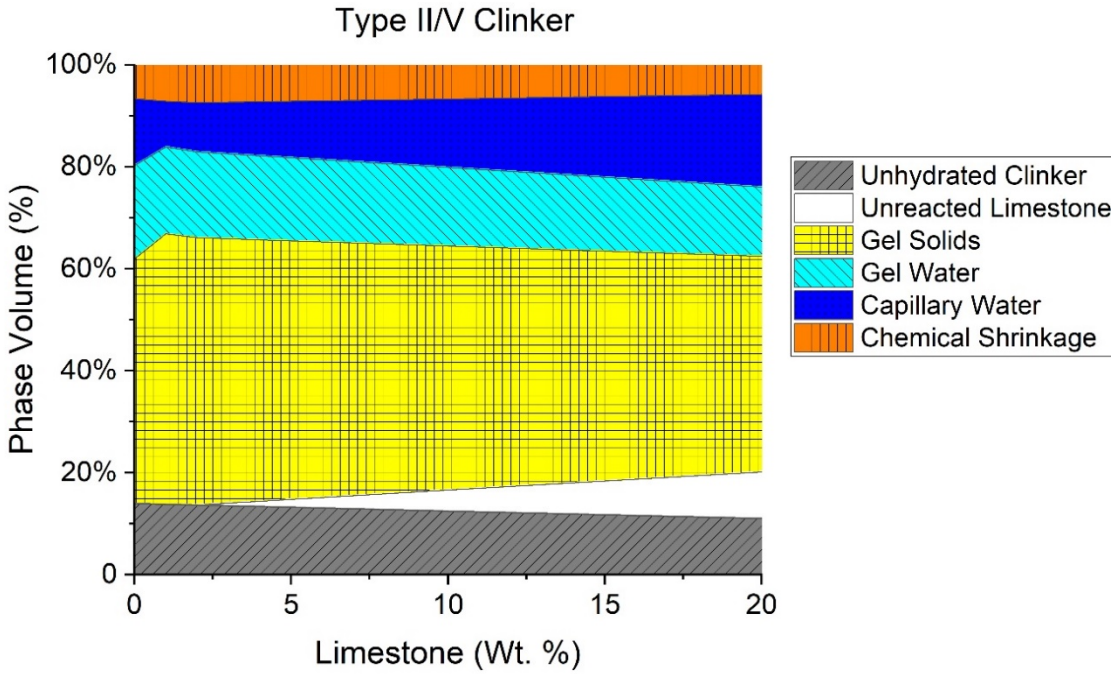

(c) Output of PPM for Type II/V clinker

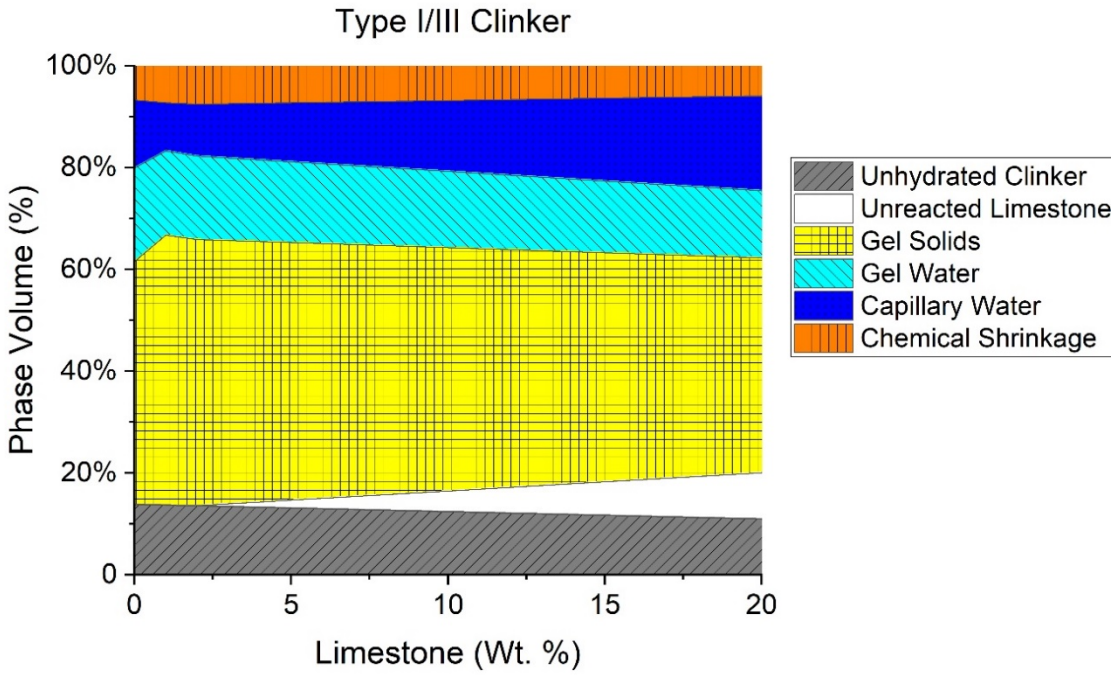

(d) Output of PPM for Type I/III clinker

Figure 16-2. Typical outputs of thermodynamic modeling showing the phase assemblage and the output of the PPM showing the different volumes of phases in the Clinker + Limestone systems

16.5 Modeling Predictions of Experimental Results

Simulations were run to predict the porosity for the experimentally tested mixtures. The results of the simulation are plotted against the results of the experiments to compare the experimentally obtained results to the theoretical values.

16.5.1 Porosity of Mortar Mixtures

The predicted porosity of the mortar mixtures (M0-M5, mixture proportions in section 3) versus the experimentally measured porosity of these mixtures is shown in Figure 16-3. The mortars were considered to have 5% entrapped air. The root mean square error between the model and the experiment is 4% for OPC systems and 4.4% for PLC systems. Most mixtures fall within ±5% porosity of the predicted value. The outlier mixtures are the mixtures made with clinker D containing 25% FA (D_OV:M1 and D_L15:M1). It is possible that this mixture was not compacted properly and had entrapped air. It can be seen that the model underpredicts the porosity of the mixtures, which is documented in the literature [123, 189]. The output data of the PPM for OPC and PLC systems is provided in the Appendix H, as Table H.2.

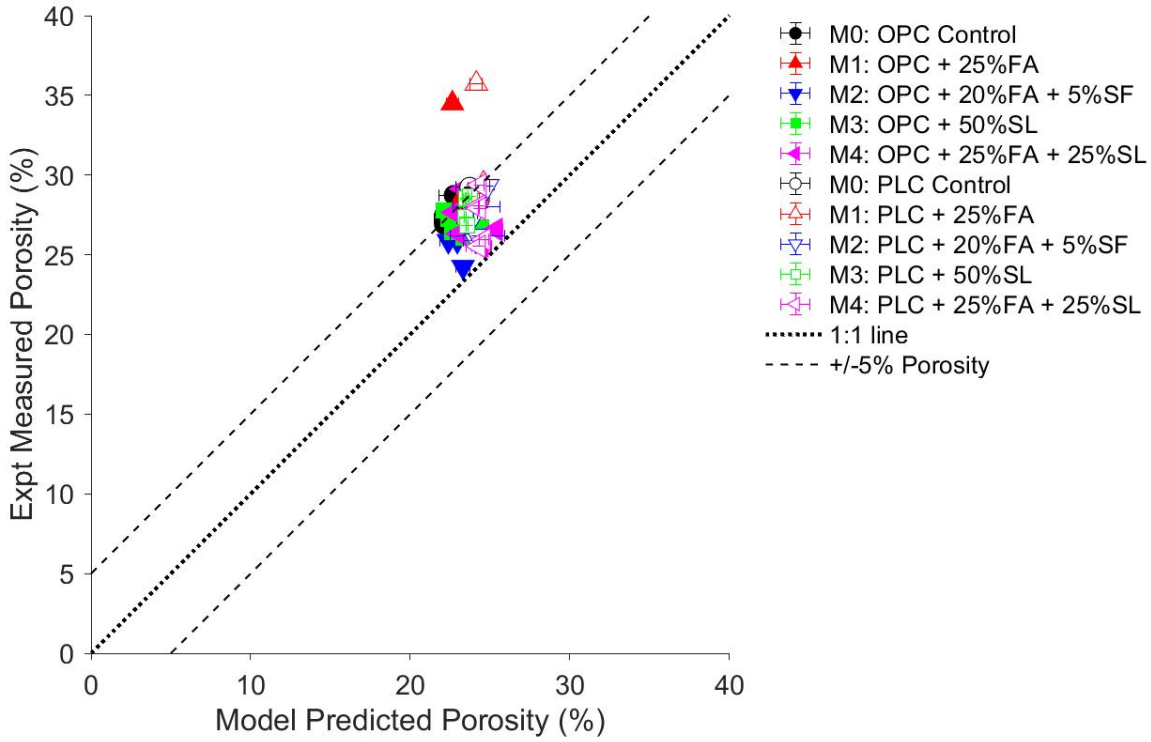

Figure 16-3. Porosity of the mortar mixtures of OPC and PLC (Model vs. Experiment)

16.6 Comparison of PLC and OPC Using Modeling

In this section, the properties of OPC and PLC systems will be directly compared against one another to compare their performance. The properties that will be studied are the paste porosity, unreacted calcite (limestone), and CH consumed. The raw data for all simulations run is available in tabular form in Appendix F.

16.6.1 Porosity

Figure 16-4 is a plot of the predicted porosity of PLC systems plotted against their corresponding OPC systems for the mixtures M0-M5 and clinkers A-E. From Figure 16-4, it can be seen that most of the results lie above the 1:1 line, indicating that the porosity of PLC pastes is slightly higher (about 2%) than the porosity of the corresponding OPC paste. This is because of the dilution of reactive clinker with unreacted limestone. The OPCs contain 3-6% limestone, which is near the optimal point of minimum porosity (2-3% Limestone), and any further limestone addition causes dilution in the system. The only exception to this observation is three mixtures (all three mixtures are M3 & M4), which contain enough reactive alumina to react with almost all the limestone in

the PLC systems, thus causing enough carboaluminate reactions to lower the porosity. The porosity difference between OPC and PLC systems is tabulated in Table 16.1. Practically, a 3% higher volume of pores in an OPC/PLC system is approximately equivalent to a 0.05 increase in the w/c or a 15% decrease in the degree of hydration.

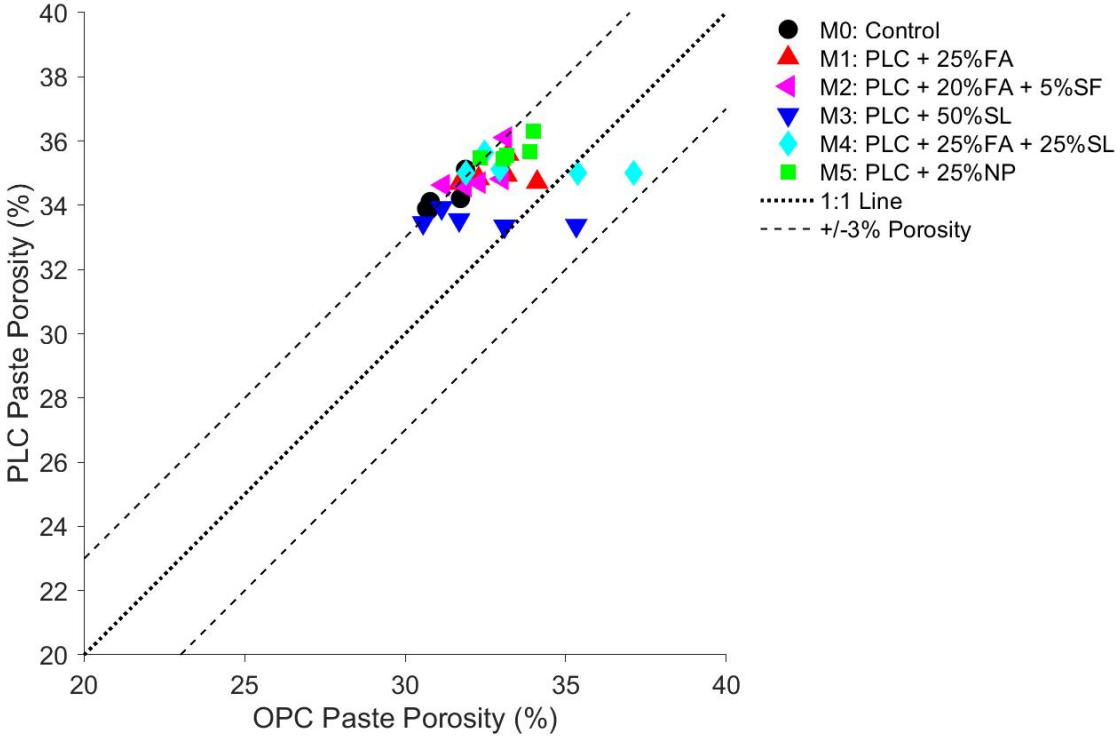

Figure 16-4. Plot of predicted porosity of PLC systems vs OPC systems.

Table 16.1. Difference in porosity between OPC and PLC systems

$\phi_{PLC} - \phi_{OPC}$	M0	M1	M2	M3	M4	M5
	PC	PC+FA	PC+FA+SF	PC+SL	PC+SL+FA	PC+NP
Clinker A	3%	3%	2%	3%	3%	2%
Clinker B	3%	1%	3%	-2%	-2%	3%
Clinker C	3%	2%	3%	3%	3%	2%
Clinker D	3%	3%	3%	0%	0%	2%
Clinker E	2%	2%	2%	2%	2%	2%
Average	*3%*	*2%*	*3%*	*1%*	*1%*	*2%*
St. Dev.	*0%*	*1%*	*1%*	*2%*	*2%*	*0%*

The synergistic effects of alumina (Al_2O_3) with limestone in PLC+Al_2O_3 systems [180] are shown in Figure 16-5 below. It can be seen in a system with no alumina that the point of minimum porosity occurs at a limestone content of 1.5%. As alumina is added to the system, it reacts with the limestone to form carboaluminate phases that reduce the porosity. Therefore, the point of minimum porosity shifts to a higher limestone content (the point of minimum porosity is 2% limestone for an Al_2O_3 content of 2.5%, 3.5% for an Al_2O_3 content of 5%, and 4% for an Al_2O_3 content of 7.5%). The value of porosity at this minimum is also lower for higher alumina contents (porosity for 0% Al_2O_3 is 34%, for 2.5% Al_2O_3 is 32%, for 5% Al_2O_3 is 29%, and for 7.5% Al_2O_3 is 27%). Beyond the point of minimum porosity, any additional limestone addition dilutes the system and increases the porosity. This however shows the synergy that can be obtained with aluminous SCMs. However, even systems with 15% limestone have a lower porosities than systems containing no limestones, demonstrating the performance improvement (in terms of porosity reduction) when limestone is used.

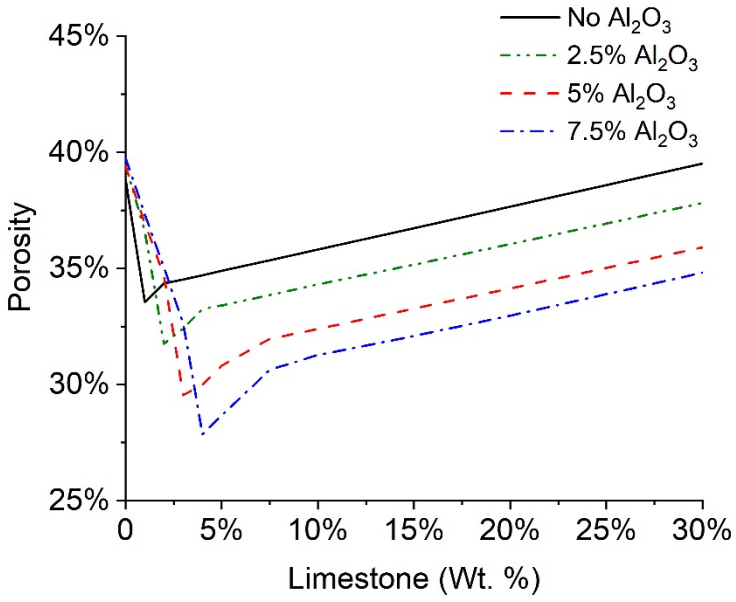

Figure 16-5. Plot of porosity of PLC+Al_2O_3 systems showing the synergy between limestone and alumina.

16.6.2 Reacted and Unreacted Calcite (From Limestone)

Figure 16-6 shows the reactive alumina in each of the mixtures and Figure 16-7 shows the amount of limestone that reacts and the unreacted limestone for each mixture. The reactive alumina is the total amount of reactive alumina from both the clinker and the SCM (calculated as the total sum of the products of degree of reactions of alumina-containing phases in the cement and SCM and

2790 the total mass of alumina in the alumina-containing compound). It must be remembered that in
2791 this section of the report the limestone is considered to be pure calcite. From Figure 16-7 it can be
2792 seen that in neat systems (M0) only up to 2g limestone reacts per 100g binder. In systems
2793 containing little reactive alumina (M1, M2, and M5), between 4g and 7g of limestone reacts per
2794 100g binder. In systems containing more reactive alumina (M3 and M4), 9g-12g of limestone
2795 reacts. A clear synergy is seen between limestone and alumina in these systems. This can also be
2796 seen in Figure 16-4, where PLC systems of M4 and M5 have a lower porosity than their OPC
2797 counterparts due to the high reaction potential of these materials with limestone.

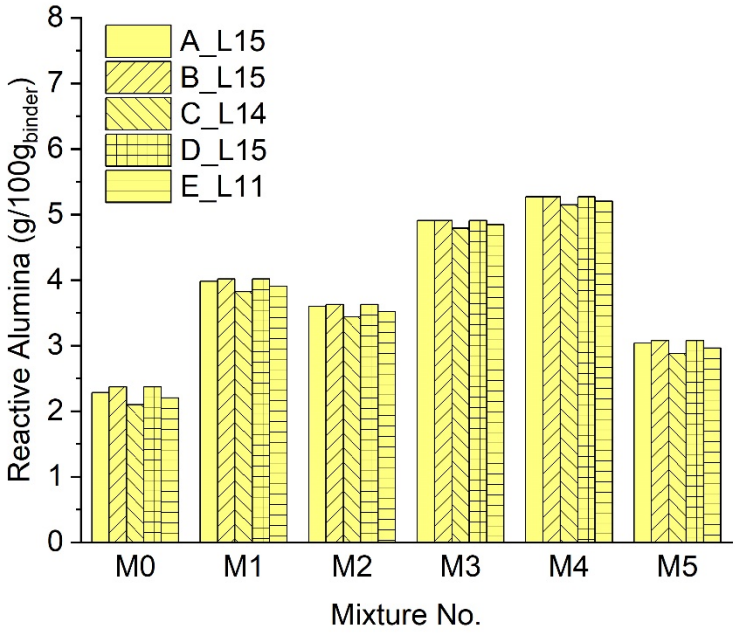

2798

2799 **Figure 16-6. Reactive alumina in all mixtures.**

2800

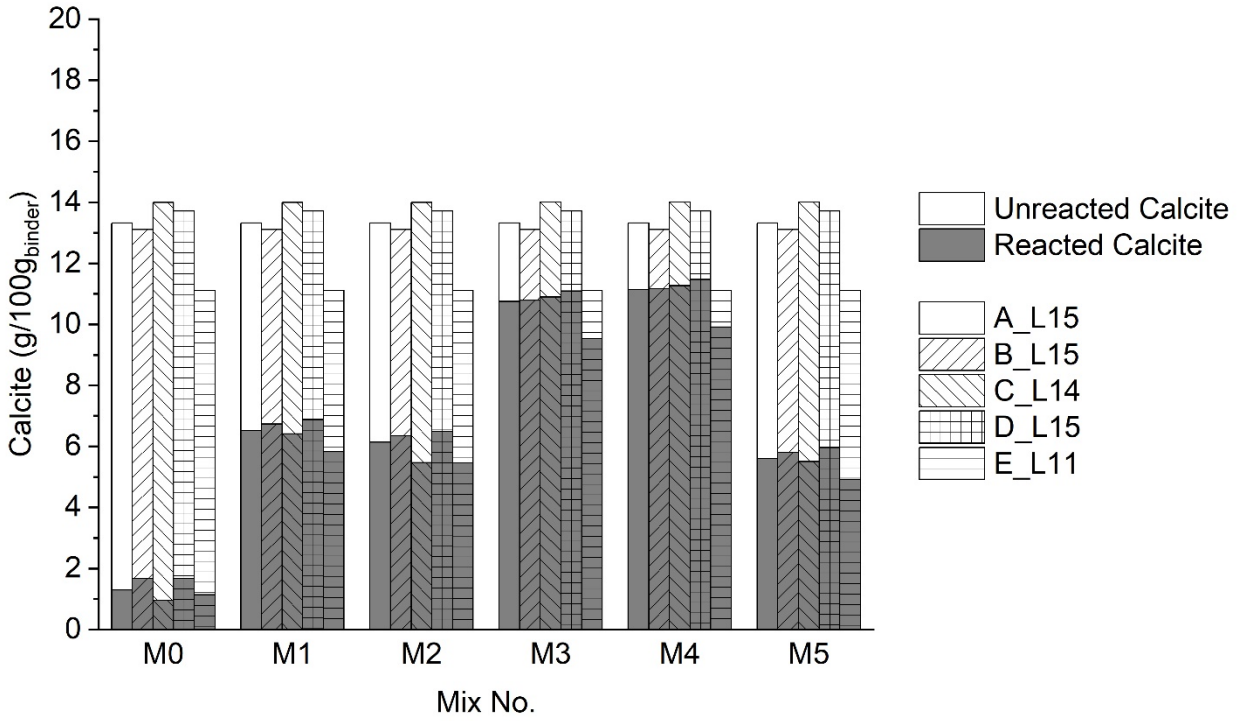

Figure 16-7. (a) Reacted calcite, and, (b) Unreacted calcite in PLC systems.

The reactive alumina in each mixture is shown in Table 16.2 and the amount of reacted limestone is shown in Table 16.3 below.

Table 16.2. Reactive alumina in each PLC mixture

Reactive Al_2O_3 (g /100g$_{binder}$)	**M0**	**M1**	**M2**	**M3**	**M4**	**M5**
	PC	**PC+FA**	**PC+FA+SF**	**PC+SL**	**PC+SL+FA**	**PC+NP**
Clinker A	2.29	3.98	3.60	4.91	5.27	3.04
Clinker B	2.37	4.02	3.63	4.91	5.27	3.07
Clinker C	2.10	3.82	3.44	4.79	5.15	2.88
Clinker D	2.37	4.02	3.63	4.91	5.27	3.07
Clinker E	2.20	3.90	3.52	4.84	5.20	2.96
Average	*2.27*	*3.95*	*3.56*	*4.87*	*5.23*	*3.01*
St. Dev.	*0.12*	*0.08*	*0.08*	*0.05*	*0.05*	*0.08*

Table 16.3. Reacted limestone in each PLC mixture

Reacted $CaCO_3$ (g /100g_{binder})	M0	M1	M2	M3	M4	M5
	PC	PC+FA	PC+FA+SF	PC+SL	PC+SL+FA	PC+NP
Clinker A	1.29	6.52	6.14	10.75	11.14	5.60
Clinker B	1.68	6.73	6.34	10.79	11.17	5.81
Clinker C	0.95	6.41	5.46	10.89	11.27	5.50
Clinker D	1.68	6.88	6.49	11.09	11.47	5.96
Clinker E	1.13	5.83	5.45	9.53	9.92	4.92
Average	*1.35*	*6.47*	*5.97*	*10.61*	*10.99*	*5.56*
St. Dev.	*0.32*	*0.40*	*0.49*	*0.62*	*0.62*	*0.40*

16.6.3 Calcium Hydroxide (CH) Consumed

Figure 16-8 is a plot of the predicted CH consumed of PLC systems plotted against their corresponding OPC systems for the mixtures M0-M5 and clinkers A-E. From Figure 16-8, it can be seen that most of the results lie above the 1:1 line, indicating that the CH consumed in PLC pastes is slightly higher (about 1-2g CH / 100g binder higher) than the CH consumed in the corresponding OPC paste. This is because of the carboaluminate reactions and the formation of different carboaluminate phases (monocarbonate forms at higher calcite contents and hemicarbonate forms at lower calcite contents [22, 48]). It can also be seen that the CH consumed in PLC+SCM systems (M1 to M5) is higher than the CH consumed in PLC systems (M0). This is due to pozzolanic reactions that take place. Recent work [189] has also shown that the CH consumed in a system is an indicator of the secondary reactions that occur in cementitious systems and can be related to the extent of pore refinement. This would indicate that PLC systems have slightly more refined pore networks than the corresponding OPC systems. This is seen in Figure 8-6. Whether this is due to the effect of finer grinding or changes to the phase assemblage needs to be investigated.

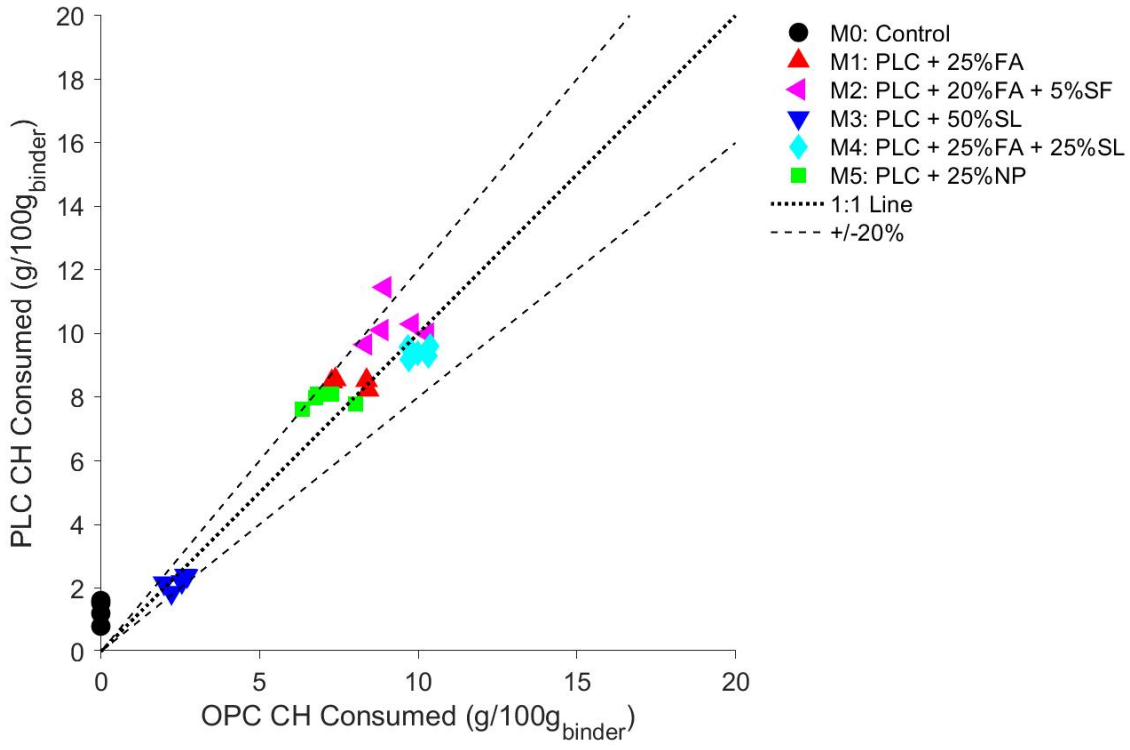

Figure 16-8. Plot of predicted CH consumed in PLC systems vs OPC systems.

16.6.4 C-S-H

Figure 16-9 is a plot of the predicted C-S-H volume fraction PLC systems plotted against their corresponding OPC systems for the mixtures M0-M5 and clinkers A-E. From Figure 16-9, it can be seen that most of the results lie below the 1:1 line, indicating that the C-S-H volume in PLC pastes is slightly lower (approximately 3% lower volume of C-S-H forms in PLC systems than OPC systems). This is because dilution of the clinker with limestone in PLC systems. It can also be seen that the C-S-H in neat systems (M0) is higher than the PLC+SCM systems (M1 to M5). This is because of the low reactivity of the SCMs in this study. This is underscored by the observation that system with a highly reactive SCM like silica fume (M2) has the closest volume of C-S-H to the neat system (M0).

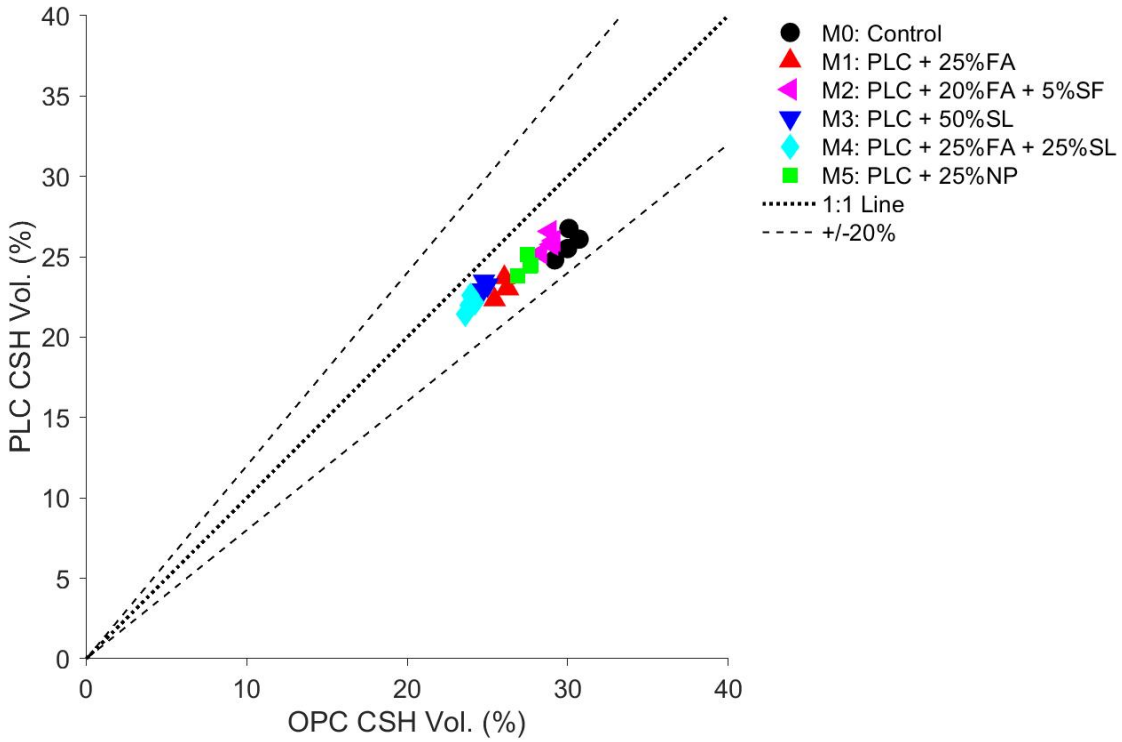

Figure 16-9. Plot of predicted C-S-H volume in PLC systems vs OPC systems.

The volume difference of C-S-H between OPC and PLC systems is tabulated in Table 16.4 below.

Table 16.4. Decrease in C-S-H volume when OPC is replaced with PLC

C-S-H Volume Difference	**M0**	**M1**	**M2**	**M3**	**M4**	**M5**
	PC	**PC+FA**	**PC+FA+SF**	**PC+SL**	**PC+SL+FA**	**PC+NP**
Clinker A	5%	3%	3%	2%	2%	3%
Clinker B	4%	3%	3%	2%	2%	3%
Clinker C	4%	3%	3%	2%	2%	3%
Clinker D	4%	3%	3%	2%	2%	3%
Clinker E	3%	2%	2%	1%	1%	2%
Average	*4%*	*3%*	*3%*	*2%*	*2%*	*3%*
St. Dev.	*1%*	*0%*	*0%*	*0%*	*0%*	*0%*

16.6.5 Carboaluminate Phases

Figure 16-10 is a plot of the predicted carboaluminate (hemi-/monocarbonate) phase volume fraction PLC systems plotted against their corresponding OPC systems for the mixtures M0-M5 and clinkers A-E. From Figure 16-10, it can be seen that most of the results except for five data points lie below the 1:1 line, indicating that the carboaluminate phase volume in PLC pastes is slightly lower (approximately 0.4% lower volume of C-S-H forms in PLC systems than OPC systems). This is because dilution of the clinker with limestone in PLC systems without significant contribution of carboaluminate reaction from the SCMs. It can also be seen that the carboaluminate in neat systems is (M0) is much lower than in the PLC+SCM systems (M1 to M5). This is because of the reactive alumina in the SCMs used, which reacts with the limestone to form carboaluminate reactions. The mixtures M3 and M4 have the highest volumes of carboaluminate as they have the highest amounts of reactive alumina. This is also noted in Figure 16-7 where it can be seen that in mixtures M3 and M4, more limestone reacts.

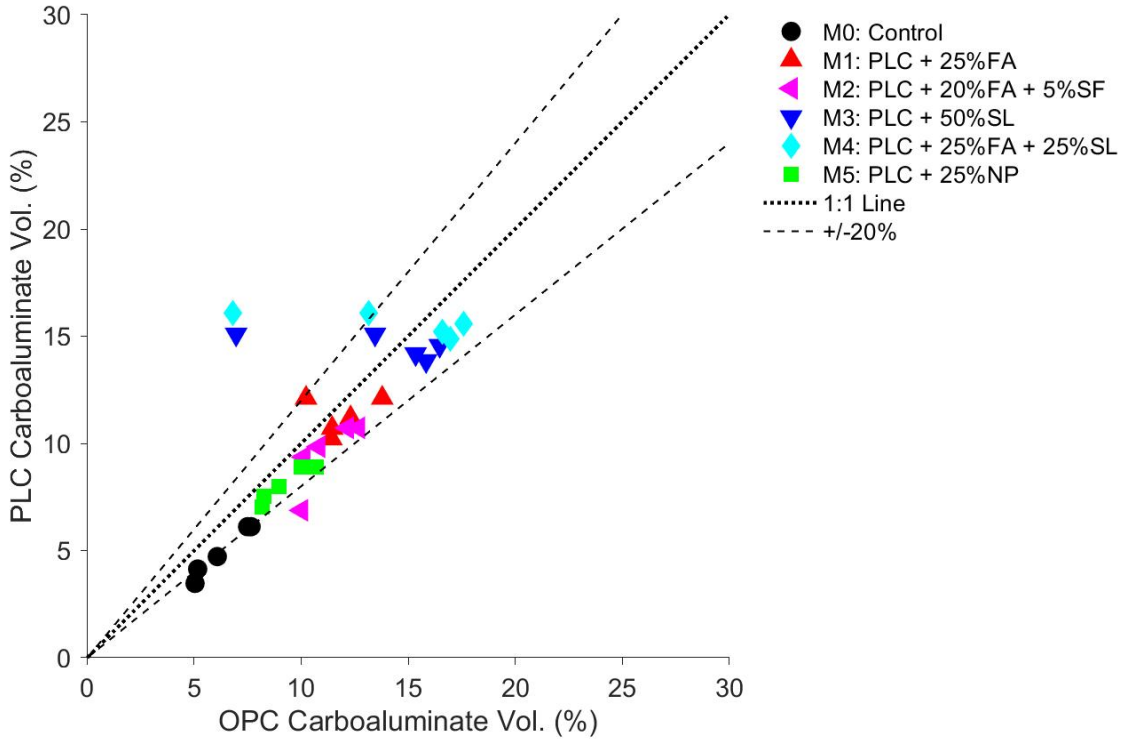

Figure 16-10. Plot of predicted volume of hemi-/monocarbonates in PLC systems vs OPC systems.

The volumes of the carboaluminate phases formed in PLC systems is shown in Table 16.5 below.

Table 16.5. Volume fraction of carboaluminate phases in the PLC systems

Carboaluminates (% Vol.)	M0	M1	M2	M3	M4	M5
	PC	PC+FA	PC+FA+SF	PC+SL	PC+SL+FA	PC+NP
Clinker A	5%	11%	10%	15%	16%	8%
Clinker B	6%	12%	11%	15%	16%	9%
Clinker C	3%	10%	7%	14%	15%	7%
Clinker D	6%	12%	11%	15%	16%	9%
Clinker E	4%	11%	9%	14%	15%	8%
Average	*5%*	*11%*	*10%*	*15%*	*16%*	*8%*
St. Dev.	*1%*	*1%*	*2%*	*1%*	*1%*	*1%*

16.6.6 The pH of Pore Solution

Figure 16-11 is a plot of the predicted pH of pore solution in pastes made of OPC and PLC for the mixtures M0-M5 and clinkers A-E. From Figure 16-11, it can be seen that most of the results lie on the 1:1 line, indicating that the pH of PLC systems is not significantly different from the pH in OPC systems (the results all lie within 0.02pH of each other). This is likely because the dilution of the clinker with limestone in PLC systems counteracts the increased hydration due to finer grinding. These competing effects combined with the alkali binding due to the C-(A)-S-H phases present cause the pH to remain nearly similar.

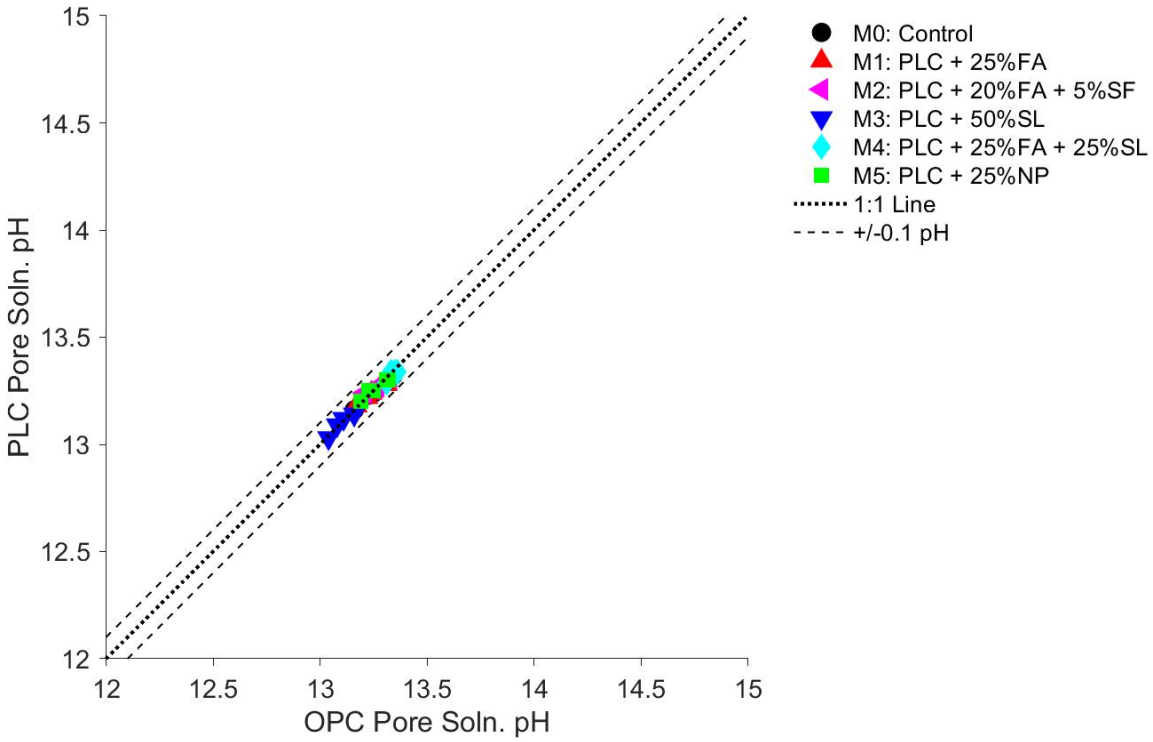

Figure 16-11. Plot of predicted pH of pore solution of PLC systems vs OPC systems.

The difference in pH of pore solution between OPC and PLC systems is tabulated in Table 16.6 below.

Table 16.6. Difference in pore solution pH when OPC is replaced with PLC

pH difference	M0	M1	M2	M3	M4	M5
	PC	PC+FA	PC+FA+SF	PC+SL	PC+SL+FA	PC+NP
Clinker A	0.00	0.00	-0.01	-0.01	-0.01	-0.02
Clinker B	0.02	0.01	0.02	0.02	0.01	0.02
Clinker C	0.00	-0.01	-0.03	0.01	0.02	-0.01
Clinker D	0.02	0.03	0.02	0.02	0.02	0.01
Clinker E	0.01	0.00	0.00	-0.01	-0.01	0.00
Average	*0.01*	*0.01*	*0.00*	*0.01*	*0.01*	*0.00*
St. Dev.	*0.01*	*0.02*	*0.02*	*0.02*	*0.02*	*0.02*

16.7 Conclusions

It is well known that the presence of limestone causes a change in the phase assemblage of cementitious systems. In the presence of limestone, ettringite is stabilized and hemi-/monocarbonate forms instead of monosulfate [21, 22, 48]. It is also known from previous experiments that SCMs containing alumina can react with the limestone in PLCs to improve performance [14, 83, 181]. In this section thermodynamic modeling was used to model experimental mixtures and it was found that the results of the model and the results of the experiment correlated well. The performance of PLC systems with respect to the heat released, porosity, quantity of limestone that reacts, Calcium Hydroxide consumed, the key phases that form (C-S-H, carboaluminates), and pH of pore solution is compared to the OPC counterparts. It is noteworthy that similar trends were obtained in both experiments and models. In general, the porosity of PLC systems is 1-3% higher than OPC systems, and the pore solution pH is not significantly different in PLC and OPC systems. When SCMs rich in alumina are used, they show synergistic behavior with the limestone in PLCs and the mass of limestone that reacts is directly proportional to the mass of reactive alumina in the SCMs. Therefore, we conclude that in typical OPC systems, PLCs can be used as a direct replacement for OPC, and in OPC+SCM systems (for typical SCM replacement levels), PLCs can be used instead of OPCs due to the synergistic behavior of limestone and alumina.

17 Conclusions

A comprehensive plan was undertaken to provide both experimental and computationally modeled results to address whether PLC may significantly impact the mechanical performance and durability of concrete materials specific to California, as compared to OPC. This work aims to provide CALTRANS with data to make informed decisions on the potential specification of PLC.

The loss on ignition, chemical composition, oxide composition, the particle size of the raw materials, and the SCMs reactivity were determined. The heat of hydration was found to be within +/-10% when the OPC, PLC, and OPC+LS systems were compared based on total cumulative heat; however, the PLC and OPC+LS systems were found to have a greater degree of reaction.

ASR testing showed that the PLCs perform similar to or better than their parent OPCs. In addition, all the SCMs reduced expansions compared to the control for most of the mixtures. This resulted in the majority of the mixtures being below the 0.10% expansion limit recommended in ASTM C1778 (AASHTO R 80) for ASTM C1567 testing with the six exceptions, as noted in Section 5.7.4.

Shrinkage measurements were performed for eighty mixtures. The majority of the samples were found to be statistically similar when comparing OPC, PLC and OPC + LS. The only exception for the OPC versus PLC system occurred for M3 and M4 at 14 and 28 days, with the PLC systems' shrinkage being 7-8% higher. It should be noted that M3 and M4 mixtures made using OPC have approximately 10% more shrinkage than M0. It is anticipated that this increase in shrinkage is due to increased reaction product. As a result, variations in shrinkage with replacing OPC with PLC or OPC with OPC + LS do not appear to be a concern as related to a potential increase in the shrinkage cracking.

The flexural strength in the PLC and OPC + LS mixtures was on average less than 5% lower than the OPC mixtures. However, the flexural strength was up to 13% greater for PLC when combined with slag. Overall, the flexural strength was consistently within the +/- 15% range compared with the parent system. In conclusion, PLC can be used as an alternative to OPC for systems made with type II/V clinker with and without SCM.

The initial or final setting times of the PLC and OPC + LS mixtures was statistically similar. In some cases, the addition of SCMs did influence the initial and final setting times.

No statistically significant difference was observed in the bound chloride contents of mixtures comparing OPC (i.e., ASTM C 150/AASHTO M 85), PLC (i.e., ASTM C 595/AASHTO M 240), and OPC+LS (provided that a specific size and quality of limestone is used). No statistically significant difference was observed in the bound chloride contents for mixtures comparing OPC, PLC, and OPC+LS with SCM (i.e., fly ash, silica fume, natural pozzolan). Mixtures containing PLC and OPC + LS mixtures made with ground granulated blast-furnace slag, which is generally

referred to as slag cement if it meets ASTM C 989, outperformed the OPC+Slag system. It should also be noted that for the calculation of the allowable chloride content for new mixtures and comparison with set limits by ACI 318, limestone should be included in the total binder content. In other words, the PLC+SCM content, or OPC+SCM+LS content be considered as binder.

The measured porosity, formation factor, and chloride apparent diffusion coefficient of PLC concrete are comparable to those obtained on OPC concrete. The OPC +LS mixture may result in excessive porosity due to insufficient consolidation and as such care should be taken to examine the PSDs when these materials are combined.

The OPC and PLC systems have comparable times to corrosion initiation. The critical chloride concentration was approximately 0.4% by weight of binder. The findings from the modified ASTM G109 test indicate that OPC and PLC specimens exhibit similar total charge passed until the time of activation and most of the specimens were observed to activate after 7 cycles. The OPC and PLC will likely exhibit similar times to corrosion.

There was no significant difference in measured air contents between OPC and PLC concrete mixtures that are not consistent with variations in the grind of the cement. As such, OPC and PLC can be used in concrete mixtures to obtain air contents that perform well in a FT environment.

The PLCs performed similar to, if not better than, their corresponding OPC mixtures when exposed to sulfate when SCMs are used. Therefore, CALTRANS can use their current SCM mixtures as is with ASTM C 150 Type II or V clinker that is then interground or interblended with PLC and expect similar external sulfate resistance to ASTM C150 Type II or V cements.

Replacement of OPC with PLC (or OPC +LS) offers the potential for a reduction of GHG of 10-12% on average (up to 15%).

Computational modeling was used to show that the presence of limestone, ettringite is stabilized, and hemi-/monocarbonate forms instead of monosulfate. SCMs containing alumina can react with the limestone in PLCs to improved performance. The performance of PLC systems with respect to the heat released, porosity, quantity of limestone that reacts, Calcium Hydroxide consumed, the key phases that form (C-S-H, carboaluminates), and pH of pore solution is compared or improved when compared to the OPC counterparts. As a result, PLCs can be used as a direct replacement for OPC, and in OPC+SCM systems (for typical SCM replacement levels). Further, when PLCs are used with SCM there can be a synergistic behavior between the limestone and alumina that improves overall performance.

The results indicate that PLCs can be used as a direct replacement for OPC. It should also be noted that PLC can replace OPC in systems containing SCM systems. Further, when PLCs are used with SCM, there can be a synergistic behavior between the limestone and reactive alumina in the SCMs

that improves overall performance. As such, we recommend that specifications that permit the use of OPC (ASTM C 150, AASHTO M 85) could also permit the use of PLC (ASTM C 595, AASHTO M 240). Specifications could also be developed to permit the use of up to 10% limestone with OPC; however, some details will be needed on the chemical and physical properties of the limestone to ensure its size (packing and reaction) and chemical purity.

18 References

1. Weiss, J.W., et al., *Impact of Use of Portland-Limestone Cement on Concrete Performance as Plain or Reinforced Material*, in *California Department of Transportation - Research Proposal*. 2017, Oregon State University: Corvallis.
2. Barrett, T.J., H. Sun, and W.J. Weiss, *Performance of portland limestone cements: Cements designed to be more sustainable that include up to 15% limestone addition.* 2013.
3. Smartz, B.W., T.S. Laker, and T. Van Dam, *Performance and Sustainability.* Concrete international, 2013. **35**(9): p. 39-43.
4. Hawkins, P., P.D. Tennis, and R.J. Detwiler, *The use of limestone in Portland cement: a state-of-the-art review*. 1996: Portland Cement Association.
5. Hooton, R., M. Nokken, and M. Thomas, *Portland-limestone cement: state-of-the-art report and gap analysis for CSA A 3000.* Cement Association of Canada. University of Toronto, 2007.
6. Tennis, P., M. Thomas, and W. Weiss, *State-of-the-Art Report on Use of Limestone in Cements at Levels of up to 15%.* PCA R&D SN3148, Portland Cement Association, Skokie, IL, 2011.
7. Chang, M.T., et al., *Using X-ray fluorescence to assess the chemical composition and resistivity of simulated cementitious pore solutions.* International Journal of Advances in Engineering Sciences and Applied Mathematics, 2017. **9**(3): p. 136-143.
8. Lothenbach, B., K. Scrivener, and R.D. Hooton, *Supplementary cementitious materials.* Cement and Concrete Research, 2011. **41**(12): p. 1244-1256.
9. Thomas, M., *Supplementary cementing materials in concrete*. 2013: CRC press.
10. Shaker, F., A. Rashad, and M. Allam, *Properties of concrete incorporating locally produced Portland limestone cement.* Ain Shams Engineering Journal, 2018. **9**(4): p. 2301-2309.
11. Dhir, R., et al., *Evaluation of Portland limestone cements for use in concrete construction.* Materials and structures, 2007. **40**(5): p. 459-473.
12. Chen, J., A. Kwan, and Y. Jiang, *Adding limestone fines as cement paste replacement to reduce water permeability and sorptivity of concrete.* Construction and Building Materials, 2014. **56**: p. 87-93.
13. Meddah, M.S., M.C. Lmbachiya, and R.K. Dhir, *Potential use of binary and composite limestone cements in concrete production.* Construction and Building Materials, 2014. **58**: p. 193-205.
14. De Weerdt, K., et al., *Synergy between fly ash and limestone powder in ternary cements.* Cement and concrete composites, 2011. **33**(1): p. 30-38.
15. Alunno-Rosetti, V. and F. Curcio. *A contribution to the knowledge of the properties of Portland-Limestone Cement concretes, with respect to the requirements of European and Italian design code*. in *Proceedings of the 10th International Congress on the Chemistry of Cement*. 1997. H. Justnes.
16. Bonavetti, V., et al., *Influence of initial curing on the properties of concrete containing limestone blended cement.* Cement and Concrete Research, 2000. **30**(5): p. 703-708.
17. Irassar, E., et al., *Mechanical properties and durability of concrete made with portland limestone cement.* ACI SPECIAL PUBLICATIONS, 2001. **202**: p. 431-450.

18. Ghrici, M., S. Kenai, and M. Said-Mansour, *Mechanical properties and durability of mortar and concrete containing natural pozzolana and limestone blended cements.* Cement and Concrete Composites, 2007. **29**(7): p. 542-549.
19. Li, W., et al., *Effects of nano-silica and nano-limestone on flowability and mechanical properties of ultra-high-performance concrete matrix.* Construction and Building Materials, 2015. **95**: p. 366-374.
20. Matschei, T., et al. *Relationships of Cement Paste Mineralogy to Porosity and Mechanical Properties*. in *International Conference on Modelling of Heterogeneous Materials with Applications in Construction and Biomedical Engineering*. 2007.
21. Hawkins, P., P.D. Tennis, and R.J. Detwiler, *The use of limestone in Portland cement: a state-of-the-art review*. ENGINEERING BULLETIN 227 ed. 2005: Portland Cement Association. 41.
22. Lothenbach, B., et al., *Influence of limestone on the hydration of Portland cements.* Cement and Concrete Research, 2008. **38**(6): p. 848-860.
23. Vuk, T., et al., *The effects of limestone addition, clinker type and fineness on properties of Portland cement.* Cement and concrete Research, 2001. **31**(1): p. 135-139.
24. Voglis, N., et al., *Portland-limestone cements. Their properties and hydration compared to those of other composite cements.* Cement and Concrete Composites, 2005. **27**(2): p. 191-196.
25. Schmidt, M., *Cement with interground additives--capabilities and environmental relief: I.* ZKG International, Edition B, 1992. **45**(2): p. 64-9.
26. Schmidt, M., *Cement with interground additives--capabilities and environmental relief: II.* ZKG International, Edition B, 1992. **45**(6): p. 296-301.
27. Seyedalhosseini Natanzi, A.S., *Improving Durability of Different Limestone Cement and Effects of it on Reinforcement*. 2013.
28. Menéndez, G., V. Bonavetti, and E. Irassar, *Strength development of ternary blended cement with limestone filler and blast-furnace slag.* Cement and Concrete Composites, 2003. **25**(1): p. 61-67.
29. Turker, P. and K. Erdogdu. *Effects of Limestone Addition on Microstructure and Hydration of Cements*. in *PROCEEDINGS OF THE INTERNATIONAL CONFERENCE ON CEMENT MICROSCOPY*. 2000. INTERNATIONAL CEMENT MICROSCOPY ASSOCIATION.
30. Ezziane, K., et al., *Effect of mineral additives on the setting of blended cement by the maturity method.* Materials and structures, 2010. **43**(3): p. 393-401.
31. Choudhary, A., V. Shah, and S. Bishnoi, *Effect of low cost fillers on cement hydration.* Construction and Building Materials, 2016. **124**: p. 533-543.
32. Sun, H., et al., *Jet mill grinding of portland cement, limestone, and fly ash: Impact on particle size, hydration rate, and strength.* Cement and Concrete Composites, 2013. **44**: p. 41-49.
33. Bentz, D.P., et al., *Relating compressive strength to heat release in mortars.* Advances in Civil Engineering Materials, 2012. **1**(1): p. 1-14.
34. Choudhary, A., et al., *Examining Factors that Influence the Measurement of Pozzolanic Reactivity of Supplementary Cementitious Materials.* In Review, 2021.
35. Glosser, D., et al., *Investigation of the Reactivity of Fly Ash and its Effect on Mixture Properties.* ACI Materials Journal, 2019. **In Press**.

36. Moradllo, M.K., et al., *Use of borosilicate glass powder in cementitious materials: Pozzolanic reactivity and neutron shielding properties.* Cement and Concrete Composites, 2020. **112**: p. 103640.
37. Suraneni, P. and J. Weiss, *Examining the pozzolanicity of supplementary cementitious materials using isothermal calorimetry and thermogravimetric analysis.* Cement and Concrete Composites, 2017. **83**: p. 273-278.
38. ASTM, *Standard Test Methods for Chemical Analysis of Hydraulic Cement*, in *C114-18*. 2018, ASTM International: West Conshohocken.
39. Alarcon-Ruiz, L., et al., *The use of thermal analysis in assessing the effect of temperature on a cement paste.* Cement and Concrete research, 2005. **35**(3): p. 609-613.
40. Pane, I. and W. Hansen, *Investigation of blended cement hydration by isothermal calorimetry and thermal analysis.* Cement and concrete research, 2005. **35**(6): p. 1155-1164.
41. Villain, G., M. Thiery, and G. Platret, *Measurement methods of carbonation profiles in concrete: Thermogravimetry, chemical analysis and gammadensimetry.* Cement and concrete research, 2007. **37**(8): p. 1182-1192.
42. McConnell, D., et al. *Cement-aggregate reaction in concrete*. in *Journal Proceedings*. 1947.
43. Kim, T. and J. Olek, *Effects of sample preparation and interpretation of thermogravimetric curves on calcium hydroxide in hydrated pastes and mortars.* Transportation research record, 2012. **2290**(1): p. 10-18.
44. Lothenbach, B. and F. Winnefeld, *Thermodynamic modelling of the hydration of Portland cement.* Cement and Concrete Research, 2006. **36**(2): p. 209-226.
45. Lothenbach, B., et al., *Effect of temperature on the pore solution, microstructure and hydration products of Portland cement pastes.* Cement and Concrete Research, 2007. **37**(4): p. 483-491.
46. Azad, V.J., et al., *A COMSOL–GEMS interface for modeling coupled reactive-transport geochemical processes.* Computers & Geosciences, 2016. **92**: p. 79-89.
47. Guo, Y., et al., *Internal Curing for Concrete Bridge Decks: Integration of a Social Cost Analysis in Evaluation of Long-Term Benefit.* Transportation Research Record, 2016. **2577**(1): p. 25-34.
48. Lothenbach, B., et al., *Cemdata 18: A chemical thermodynamic database for hydrated Portland cements and alkali-activated materials.* Cement and Concrete Research, 2019. **115**: p. 472-506.
49. Stanton, T.E., *Expansion of concrete through reaction between cement and aggregate.* Transactions of the American Society of Civil Engineers, 1942. **107**(1): p. 54-84.
50. Rajabipour, F., et al., *Alkali–silica reaction: Current understanding of the reaction mechanisms and the knowledge gaps.* Cement and Concrete Research, 2015. **76**: p. 130-146.
51. Thomas, M., *The effect of supplementary cementing materials on alkali-silica reaction: A review.* Cement and concrete research, 2011. **41**(12): p. 1224-1231.
52. Bhatty, M. and N. Greening. *Interaction of alkalies with hydrating and hydrated calcium silicates*. in *Proceedings*. 1978.
53. Hong, S.-Y. and F. Glasser, *Alkali binding in cement pastes: Part I. The CSH phase.* Cement and Concrete Research, 1999. **29**(12): p. 1893-1903.

54. Chappex, T. and K. Scrivener, *Alkali fixation of C–S–H in blended cement pastes and its relation to alkali silica reaction.* Cement and Concrete Research, 2012. **42**(8): p. 1049-1054.
55. Shi, Z., B. Ma, and B. Lothenbach, *Effect of Al on the formation and structure of alkali-silica reaction products.* Cement and Concrete Research, 2021. **140**: p. 106311.
56. Folliard, K.J., et al., *Preventing Alkali-Silica Reaction and Delayed Ettringite Formation in New Concrete.* Project Summary report 0-4085, Center for Transportation Research, University of Texas, Austin, 2006.
57. Ramezanianpour, A.A., et al., *Influence of various amounts of limestone powder on performance of Portland limestone cement concretes.* Cement and Concrete Composites, 2009. **31**(10): p. 715-720.
58. ASTM, *Standard Test Method for Determining the Potential Alkali-Silica Reactivity of Combinations of Cementitious Materials and Aggregate (Accelerated Mortar-Bar Method)*, in *C1567-13*. 2013, ASTM International: West Conshohocken.
59. ASTM, *Standard Test Method for Determination of Length Change of Concrete Due to Alkali-Silica Reaction*, in *C1293-20a*. 2020, ASTM International: West Conshohocken.
60. Thomas, M., et al., *Test methods for evaluating preventive measures for controlling expansion due to alkali–silica reaction in concrete.* Cement and Concrete Research, 2006. **36**(10): p. 1842-1856.
61. AASHTO, *Standard Method of Test for Potential Alkali Reactivity of Aggregates and Effectiveness of ASR Mitigation Measures (Miniature Concrete Prism Test, MCPT)*, in *T 380-19*. 2019, American Association of State Highway and Transportation Officials: Washington DC.
62. Chopperla, K.S.T. and e. al., *Bench-marking the miniature concrete prism test and the concrete cylinder tests to field exposure blocks for mitigation of alkali-silica reaction*, in *15th International Congreess on the Chemistry of Cement*. 2019: Prague, Czech Republic.
63. Tanesi, J., et al., *Divergence between Performance in the Field and Laboratory Test Results for Alkali-Silica Reaction.* Transportation Research Record, 2020. **2674**(5): p. 120-134.
64. Laker, T. and B. Smartz, *Evaluation of Portland limestone performance cements in Colorado and Utah transportation projects: 2007 to present*, in *Transportation Research Board*. 2012.
65. Thomas, M., et al. *Equivalent performance with half the clinker content using PLC and SCM*. in *Proc., NRMCA Concrete Sustainability Conference*. 2010.
66. Hooton, R., A. Ramezanianpour, and U. Schutz. *Decreasing the clinker component in cementing materials: performance of Portland-limestone cements in concrete in combination with supplementary cementing materials*. in *2010 Concrete Sustainability Conference, NRMCA*. 2010. Arizona State University Tempe, AZ.
67. ASTM, *Standard Test Method for Effectiveness of Pozzolans or Ground Blast-Furnace Slag in Preventing Excessive Expansion of Concrete Due to the Alkali-Silica Reaction1*, in *C441-17*. 2017, ASTM International: West Conshohocken.
68. ASTM, *Standard Guide for Reducing the Risk of Deleterious Alkali-Aggregate Reaction in Concrete*, in *C1778-20*. 2020, ASTM International: West Conshohocken.
69. Schlorholtz, S.M., *Alkali Content of Fly Ash–Measuring and Testing Strategies for Compliance.* 2015.

70. Thomas, M. and M. Shehata. *Use of blended cements to control expansion of concrete due to alkali-silica reaction*. in *Proc. 8 th CANMET/ACI Int. Conf. on Fly Ash, Silica Fume, Slag and Natural Pozzolans in Concrete*. 2004.
71. Latifee, E.R. and P.R. Rangaraju, *Miniature concrete prism test: rapid test method for evaluating alkali-silica reactivity of aggregates.* Journal of Materials in Civil Engineering, 2015. **27**(7): p. 04014215.
72. Thomson, W., *4. On the equilibrium of vapour at a curved surface of liquid.* Proceedings of the Royal Society of Edinburgh, 1872. **7**: p. 63-68.
73. Bucher, B., A. Radlinska, and J. Weiss. *Preliminary comments on shrinkage and shrinkage cracking behavior of cement systems that contain limestone*. in *Concrete Technology Forum. Focus on Sustainable DevelopmentNational Ready Mixed Concrete Association*. 2008.
74. Bucher, B.E., *Shrinkage and shrinkage cracking behavior of cement systems containing ground limestone, fly ash, and lightweight synthetic particles.* 2009.
75. Stubstad, R., D. Glauz, and D. Rufino, *Use of Raw Limestone in Portland Cement*. 2008, California Department of Transportation. p. 1-20.
76. Barrett, T., et al., *Early-age shrinkage behavior of Portland limestone cement.* Concrete international, 2014. **36**(2).
77. Adams, L.D. and R.M. Race, *Effect of limestone additions upon drying shrinkage of Portland cement mortar*, in *Carbonate additions to cement*. 1990, ASTM International.
78. Cost, T. *The Advantages of Portland Limestone Cement*. 2014; Available from: https://www.concreteconstruction.net/concrete-production-precast/the-advantages-of-portland-limestone-cement_o.
79. Piasta, W. and H. Sikora, *Effect of air entrainment on shrinkage of blended cements concretes.* Construction and Building Materials, 2015. **99**: p. 298-307.
80. Bentz, D.P., et al. *Sorptivity-based service life predictions for concrete pavements*. in *Proceedings of the 7th International Conference on Concrete pavements*. 2001. Citeseer.
81. ASTM, *Standard Test Method for Length Change of Hardened Hydraulic-Cement Mortar and Concrete*, in *C157-17*. 2017, ASTM International: West Conshohocken.
82. Pickett, G. *Effect of aggregate on shrinkage of concrete and a hypothesis concerning shrinkage*. in *Journal Proceedings*. 1956.
83. De Weerdt, K., et al., *Hydration mechanisms of ternary Portland cements containing limestone powder and fly ash.* Cement and Concrete Research, 2011. **41**(3): p. 279-291.
84. Bentz, D.P., et al., *Fine limestone additions to regulate setting in high volume fly ash mixtures.* Cement and Concrete Composites, 2012. **34**(1): p. 11-17.
85. Börger, A., P. Supancic, and R. Danzer, *The ball on three balls test for strength testing of brittle discs: stress distribution in the disc.* Journal of the European Ceramic Society, 2002. **22**(9-10): p. 1425-1436.
86. Börger, A., P. Supancic, and R. Danzer, *The ball on three balls test for strength testing of brittle discs: Part II: analysis of possible errors in the strength determination.* Journal of the European Ceramic Society, 2004. **24**(10-11): p. 2917-2928.
87. Borges, J.U.A., et al., *Length effect on ductility of concrete in uniaxial and flexural compression.* Structural Journal, 2004. **101**(6): p. 765-772.
88. Danzer, R., et al., *The ball on three balls test—Strength and failure analysis of different materials.* Journal of the European ceramic society, 2007. **27**(2-3): p. 1481-1485.

89. Fu, T. and W.J. Weiss, *The Ball-on-Three-Ball (B3B) Test–Application to Cement Paste and Mortar.* Advances in Civil Engineering Materials, 2020. **9**(1): p. 128-142.
90. AASHTO, *Standard Method of Test for Determining the Total Pore Volume in Hardened Concrete Using Vacuum Saturation*, in *AASHTO TP 135-20*. 2020, American Association of State Highway and Transportation Officials: Washington DC.
91. AASHTO, *Standard Method of Test for Electrical Resistivity of a Concrete Cylinder Tested in a Uniaxial Resistance Test*, in *TP 119-20*. 2020, American Association of State Highway and Transportation Officials: Washington DC.
92. Coyle, A.T., et al., *Comparison of linear temperature corrections and activation energy temperature corrections for electrical resistivity measurements of concrete.* Advances in Civil Engineering Materials, 2018. **7**(1): p. 174-187.
93. Ramachandran, V.S., R. Seeley, and G. Polomark, *Free and combined chloride in hydrating cement and cement components.* Matériaux et Construction, 1984. **17**(4): p. 285-289.
94. Diamond, S., *Chloride concentrations in concrete pore solutions resulting from calcium and sodium chloride admixtures.* Cement, concrete and aggregates, 1986. **8**(2): p. 97-102.
95. Beaudoin, J.J., V.S. Ramachandran, and R.F. Feldman, *Interaction of chloride and C□S□H.* Cement and Concrete Research, 1990. **20**(6): p. 875-883.
96. Zibara, H., *Binding of external chlorides by cement pastes*. 2001.
97. Hussain, S.E. and S. Al-Saadoun, *Effect of tricalcium aluminate content of cement on chloride binding corrosion of reinforcing steel in concrete.* Materials Journal, 1993. **89**(1): p. 3-12.
98. Thomas, M.D. and R.D. Hooton, *The durability of concrete produced with portland-limestone cement: Canadian studies.* PCA R&D SN3142, Portland Cement Association, Skokie, IL, 2010: p. 28.
99. Jafari Azad, V., et al., *Relating the formation factor and chloride binding parameters to the apparent chloride diffusion coefficient of concrete.* Journal of Materials in Civil Engineering, 2019. **31**(2): p. 04018392.
100. Justnes, H., *A review of chloride binding in cementitious systems.* Nordic Concrete Research-Publications-, 1998. **21**: p. 48-63.
101. Balonis, M., et al., *Impact of chloride on the mineralogy of hydrated Portland cement systems.* Cement and Concrete Research, 2010. **40**(7): p. 1009-1022.
102. Luping, T. and L.-O. Nilsson, *Chloride binding capacity and binding isotherms of OPC pastes and mortars.* Cement and concrete research, 1993. **23**(2): p. 247-253.
103. Csizmadia, J., G. Balázs, and F.D. Tamás, *Chloride ion binding capacity of tetracalcium aluminoferrite.* Periodica Polytechnica Civil Engineering, 2000. **44**(2): p. 135-150.
104. Marty, N.C., et al., *Dissolution kinetics of hydrated calcium aluminates (AFm-Cl) as a function of pH and at room temperature.* Mineralogical Magazine, 2017. **81**(5): p. 1245-1259.
105. Birnin-Yauri, U. and F. Glasser, *Friedel's salt, Ca2Al (OH) 6 (Cl, OH)· 2H2O: its solid solutions and their role in chloride binding.* Cement and Concrete Research, 1998. **28**(12): p. 1713-1723.
106. Sui, S., et al., *Quantification methods for chloride binding in Portland cement and limestone systems.* Cement and Concrete Research, 2019. **125**: p. 105864.

107. Glasser, F., A. Kindness, and S. Stronach, *Stability and solubility relationships in AFm phases: Part I. Chloride, sulfate and hydroxide.* Cement and Concrete Research, 1999. **29**(6): p. 861-866.
108. Yoon, S., et al., *Phase changes of monosulfoaluminate in NaCl aqueous solution.* Materials, 2016. **9**(5): p. 401.
109. Ipavec, A., et al., *Chloride binding into hydrated blended cements: The influence of limestone and alkalinity.* Cement and Concrete Research, 2013. **48**: p. 74-85.
110. Ben-Yair, M., *The effect of chlorides on concrete in hot and arid regions.* Cement and Concrete Research, 1974. **4**(3): p. 405-416.
111. Yuan, Q., et al., *Chloride binding of cement-based materials subjected to external chloride environment–a review.* Construction and building materials, 2009. **23**(1): p. 1-13.
112. Qiao, C., P. Suraneni, and J. Weiss, *Phase Diagram and Volume Change of the Ca (OH) 2 — CaCl 2— H 2 O System for Varying Ca (OH) 2/CaCl 2 Molar Ratios.* Journal of Materials in Civil Engineering, 2018. **30**(2): p. 04017281.
113. Qiao, C., et al., *Chloride binding of cement pastes with fly ash exposed to CaCl2 solutions at 5 and 23° C.* Cement and Concrete Composites, 2019. **97**: p. 43-53.
114. De Weerdt, K., et al., *Impact of the associated cation on chloride binding of Portland cement paste.* Cement and Concrete Research, 2015. **68**: p. 196-202.
115. De Weerdt, K., D. Orsáková, and M.R. Geiker, *The impact of sulphate and magnesium on chloride binding in Portland cement paste.* Cement and Concrete Research, 2014. **65**: p. 30-40.
116. Bu, Y., R. Spragg, and W. Weiss, *Comparison of the pore volume in concrete as determined using ASTM C642 and vacuum saturation.* Advances in Civil Engineering Materials, 2014. **3**(1): p. 308-315.
117. Jensen, O.M., et al., *Chloride ingress in cement paste and mortar.* Cement and Concrete Research, 1999. **29**(9): p. 1497-1504.
118. Kalinichev, A.G. and R.J. Kirkpatrick, *Molecular dynamics modeling of chloride binding to the surfaces of calcium hydroxide, hydrated calcium aluminate, and calcium silicate phases.* Chemistry of Materials, 2002. **14**(8): p. 3539-3549.
119. Delagrave, A., et al., *Chloride binding capacity of various hydrated cement paste systems.* Advanced Cement based materials, 1997. **6**(1): p. 28-35.
120. Bu, Y. and J. Weiss, *The influence of alkali content on the electrical resistivity and transport properties of cementitious materials.* Cement and Concrete Composites, 2014. **51**: p. 49-58.
121. Thomas, J.J., A.J. Allen, and H.M. Jennings, *Density and water content of nanoscale solid C–S–H formed in alkali-activated slag (AAS) paste and implications for chemical shrinkage.* Cement and Concrete Research, 2012. **42**(2): p. 377-383.
122. Tabachnick, B.G. and L.S. Fidell, *Experimental designs using ANOVA*. 2007: Thomson/Brooks/Cole Belmont, CA.
123. Azad, V.J., et al., *Interpreting the pore structure of hydrating cement phases through a synergistic use of the Powers-Brownyard model, hydration kinetics, and thermodynamic calculations.* Advances in Civil Engineering Materials, 2017. **6**(1): p. 1-16.
124. Shi, Z., et al., *Role of calcium on chloride binding in hydrated Portland cement–metakaolin–limestone blends.* Cement and Concrete Research, 2017. **95**: p. 205-216.

125. Ding, Z., et al., *Cementing mechanism of potassium phosphate based magnesium phosphate cement.* Ceramics International, 2012. **38**(8): p. 6281-6288.
126. Qiao, C., et al., *Prediction of chloride ingress in saturated concrete using formation factor and chloride binding isotherm.* Advances in Civil Engineering Materials, 2018. **7**(1): p. 206-220.
127. ASTM, *Standard Test Method for Determining the Apparent Chloride Diffusion Coefficient of Cementitious Mixtures by Bulk Diffusion*, in *C1556-11a*. 2016, ASTM International: West Conshohocken.
128. ASTM, *Standard Test Method for Acid-Soluble Chloride in Mortar and Concrete*, in *C1152-20*. 2020, ASTM International: West Conshohocken.
129. Trejo, D., C. Halmen, and K. Reinschmidt, *Corrosion performance tests for reinforcing steel in concrete: technical report*. 2009, Texas Transportation Institute.
130. Trejo, D., P.N. Vaddey, and C. Halmen, *Quantifying the corrosion threshold of steel in cementitious systems.* ACI Mater J, 2021. **In Review**.
131. Vaddey, P.N. and D. Trejo, *Optimizing Test parameters for quantifying critical chloride threshold.* ACI Mater J, 2021. **In Review**.
132. Andrade, C. and C. Alonso, *On-site measurements of corrosion rate of reinforcements.* Construction and building materials, 2001. **15**(2-3): p. 141-145.
133. Arya, C., N. Buenfeld, and J. Newman, *Factors influencing chloride-binding in concrete.* Cement and Concrete research, 1990. **20**(2): p. 291-300.
134. Diab, A.M., A.A. Aliabdo, and I.A. Mohamed, *Corrosion behaviour of reinforced steel in concrete with ground limestone partial cement replacement.* Magazine of Concrete Research, 2015. **67**(14): p. 747-761.
135. Elgalhud, A.A., R.K. Dhir, and G. Ghataora, *Chloride ingress in concrete: limestone addition effects.* Magazine of Concrete Research, 2018. **70**(6): p. 292-313.
136. Evgenia, Z., et al., *Effect of corrosion inhibitors in limestone cement.* Materials Sciences and Applications, 2013. **2013**.
137. Shannon, J., I.L. Howard, and V.T. Cost, *Benefits of portland-limestone cement for concrete with rounded gravel aggregates and higher fly ash replacement rates*. 2015.
138. Thomas, M., et al., *The effect of supplementary cementitious materials on chloride binding in hardened cement paste.* Cement and Concrete Research, 2012. **42**(1): p. 1-7.
139. Halmen, C. and D. Trejo, *Accelerating Standard Test Method for Assessing Corrosion of Steel in Concrete.* ACI Materials Journal, 2012. **109**(4).
140. Mazarei, V., et al., *Synergistic effects of ASR and fly ash on the corrosion characteristics of RC systems.* Construction and Building Materials, 2017. **153**: p. 647-655.
141. ACI, *ACI Committee 201: Guide to Druable Concrete*, in *ACI 201.02R-08*. 2008, American Concrete Institute.
142. Scherer, G.W., *Crystallization in pores.* Cement and Concrete research, 1999. **29**(8): p. 1347-1358.
143. Scherer, G.W., *Stress from crystallization of salt.* Cement and concrete research, 2004. **34**(9): p. 1613-1624.
144. Müllauer, W., R.E. Beddoe, and D. Heinz, *Sulfate attack expansion mechanisms.* Cement and concrete research, 2013. **52**: p. 208-215.

145. Santhanam, M., M.D. Cohen, and J. Olek, *Effects of gypsum formation on the performance of cement mortars during external sulfate attack.* Cement and concrete research, 2003. **33**(3): p. 325-332.
146. Eglinton, M., *Resistance of Concrete to Destructive.* Lea's chemistry of cement and concrete, 2003: p. 299.
147. Hobbs, D., *Thaumasite sulfate attack in field and laboratory concretes: implications for specifications.* Cement and Concrete Composites, 2003. **25**(8): p. 1195-1202.
148. Barcelo, L., et al., *A modified ASTM C1012 procedure for qualifying blended cements containing limestone and SCMs for use in sulfate-rich environments.* Cement and concrete research, 2014. **63**: p. 75-88.
149. Rahman, M. and M. Bassuoni, *Thaumasite sulfate attack on concrete: Mechanisms, influential factors and mitigation.* Construction and Building Materials, 2014. **73**: p. 652-662.
150. Hooton, R. and M. Thomas, *Sulfate Resistance of Mortar and Concrete Produced with Portland-Limestone Cement and Supplementary Cementing Materials: Recommendation for ASTM C595/AASHTO M 240*. 2016, Portland Cement Association, Skokie, IL, USA, Report SN3285a.
151. Monteiro, P.J. and K.E. Kurtis, *Time to failure for concrete exposed to severe sulfate attack.* Cement and Concrete research, 2003. **33**(7): p. 987-993.
152. Cyr, M., P. Lawrence, and E. Ringot, *Efficiency of mineral admixtures in mortars: Quantification of the physical and chemical effects of fine admixtures in relation with compressive strength.* Cement and concrete research, 2006. **36**(2): p. 264-277.
153. Irassar, E., *Sulfate attack on cementitious materials containing limestone filler—A review.* Cement and Concrete Research, 2009. **39**(3): p. 241-254.
154. Pipilikaki, P., M. Katsioti, and J. Gallias, *Performance of limestone cement mortars in a high sulfates environment.* Construction and Building Materials, 2009. **23**(2): p. 1042-1049.
155. Schmidt, T., et al., *Physical and microstructural aspects of sulfate attack on ordinary and limestone blended Portland cements.* Cement and Concrete Research, 2009. **39**(12): p. 1111-1121.
156. Lee, S.T., et al., *Effect of limestone filler on the deterioration of mortars and pastes exposed to sulfate solutions at ambient temperature.* Cement and concrete research, 2008. **38**(1): p. 68-76.
157. Ramezanianpour, A.M. and R.D. Hooton, *A study on hydration, compressive strength, and porosity of Portland-limestone cement mixes containing SCMs.* Cement and Concrete Composites, 2014. **51**: p. 1-13.
158. Ryou, J., et al., *Durability of cement mortars incorporating limestone filler exposed to sodium sulfate solution.* KSCE Journal of Civil Engineering, 2015. **19**(5): p. 1347-1358.
159. Thomas, M.D., et al., *Field trials of concrete produced with Portland limestone cement.* Concrete international, 2010. **32**(1): p. 35-41.
160. Hossack, A.M. and M.D. Thomas, *Varying fly ash and slag contents in Portland limestone cement mortars exposed to external sulfates.* Construction and Building Materials, 2015. **78**: p. 333-341.
161. Sezer, G.İ., *Compressive strength and sulfate resistance of limestone and/or silica fume mortars.* Construction and Building Materials, 2012. **26**(1): p. 613-618.

162. Ramezanianpour, A.A., *Cement replacement materials.* Springer, Berlin. doi, 2014. **10**: p. 978-3.
163. Tiburzi, N.B., et al., *Sulfate resistance of portland-limestone cement systems containing greater than 15% limestone.* Cement and Concrete Composites, 2019. **100**: p. 60-73.
164. *ASTM C1753/C1753M-15e1 Standard Practice for Evaluating Early Hydration of Hydraulic Cementitious Mixtures Using Thermal Measurements.* 2015, ASTM International: West Conshohocken, PA. p. 19.
165. Sandberg, J. and S. Liberman, *Monitoring and evaluation of cement hydration by semi-adiabatic field calorimetry.* Special Publication, 2007. **241**: p. 13-24.
166. Kosmatka, S.H., B. Kerkhoff, and W.C. Panarese, *Design and control of concrete mixtures*. Vol. 5420. 2002: Portland Cement Association Skokie, IL.
167. Environment, U., et al., *Eco-efficient cements: Potential economically viable solutions for a low-CO2 cement-based materials industry.* Cement and Concrete Research, 2018. **114**: p. 2-26.
168. Tennis, P.D., J.W. Weiss and J.H. Ideker, Editors. 2021, CALTRANS Report Comments: Corvallis.
169. Gartner, E., *Industrially interesting approaches to "low-CO2" cements.* Cement and Concrete research, 2004. **34**(9): p. 1489-1498.
170. Purnell, P. and L. Black, *Embodied carbon dioxide in concrete: Variation with common mix design parameters.* Cement and Concrete Research, 2012. **42**(6): p. 874-877.
171. Ellis, G., *Are there any practical alternatives to the manufacture of Portland cement clinker?* Journal of The Chinese Ceramic Society, 2012. **40**(1): p. 61-68.
172. Juenger, M., et al., *Advances in alternative cementitious binders.* Cement and concrete research, 2011. **41**(12): p. 1232-1243.
173. EN, B.S., *206-1 Concrete-Part 1: Specification, performance, production and conformity.* British Standards Institution, 2000.
174. Scrivener, K., et al., *Calcined clay limestone cements (LC3).* Cement and Concrete Research, 2018. **114**: p. 49-56.
175. Miller, S.A., et al., *Carbon dioxide reduction potential in the global cement industry by 2050.* Cement and Concrete Research, 2018. **114**: p. 115-124.
176. Miller, S.A., *Life Cycle Inventory Data for Caltrans TO27*. 2020: Davis, California.
177. Miller, S.A., *Personal Communication about tool for LCI*, J.W. Weiss, et al., Editors. 2021.
178. Damidot, D., et al., *Thermodynamic investigation of the CaO□Al2O3□CaCO3□H2O closed system at 25°C and the influence of Na2O.* Cement and Concrete Research, 1994. **24**(3): p. 563-572.
179. Matschei, T. and F.P. Glasser, *Temperature dependence, 0 to 40 C, of the mineralogy of Portland cement paste in the presence of calcium carbonate.* Cement and Concrete Research, 2010. **40**(5): p. 763-777.
180. Bharadwaj, K., B.O. Isgor, and J.W. Weiss, *Supplementary Cementitious Materials and Portland Limestone Cements.* ACI Materials Journal, 2021. **In Review**.
181. Antoni, M., et al., *Cement substitution by a combination of metakaolin and limestone.* Cement and Concrete Research, 2012. **42**(12): p. 1579-1589.
182. Lothenbach, B., et al., *Thermodynamic modelling of the effect of temperature on the hydration and porosity of Portland cement.* Cement and Concrete Research, 2008. **38**(1): p. 1-18.

183. Damidot, D., et al., *Thermodynamics and cement science.* Cement and Concrete Research, 2011. **41**(7): p. 679-695.
184. Matschei, T., B. Lothenbach, and F.P. Glasser, *The role of calcium carbonate in cement hydration.* Cement and concrete research, 2007. **37**(4): p. 551-558.
185. Matschei, T., B. Lothenbach, and F.P. Glasser, *Thermodynamic properties of Portland cement hydrates in the system CaO–Al2O3–SiO2–CaSO4–CaCO3–H2O.* Cement and Concrete Research, 2007. **37**(10): p. 1379-1410.
186. Powers, T.C., *Structure and physical properties of hardened Portland cement paste.* Journal of the American Ceramic Society, 1958. **41**(1): p. 1-6.
187. Powers, T.C. and T.L. Brownyard. *Studies of the physical properties of hardened Portland cement paste*. in *Journal Proceedings*. 1946.
188. Glosser, D., et al., *An extension of the Powers-Brownyard model to pastes containing SCM.* ACI Materials Journal, 2019. **in Press**.
189. Bharadwaj, K., et al., *Predicting Pore Volume, Compressive Strength, Pore Connectivity, and Formation Factor in Cementitious Pastes Containing Fly Ash.* Cement and Concrete Composites, 2021. **In Press**.
190. Bharadwaj, K., et al., *Toward the Prediction of Pore Volumes and Freeze-Thaw Performance of Concrete Using Thermodynamic Modelling.* Cement and Concrete Research, 2019. **124**: p. 105820.
191. Kulik, D.A., et al., *GEM-Selektor geochemical modeling package: revised algorithm and GEMS3K numerical kernel for coupled simulation codes.* Computational Geosciences, 2013. **17**(1): p. 1-24.
192. Deschner, F., et al., *Effect of temperature on the hydration of Portland cement blended with siliceous fly ash.* Cement and Concrete Research, 2013. **52**: p. 169-181.
193. Dilnesa, B.Z., et al., *Synthesis and characterization of hydrogarnet Ca3 (AlxFe1− x) 2 (SiO4) y (OH) 4 (3− y).* Cement and Concrete Research, 2014. **59**: p. 96-111.
194. Parrot, L.J. *Prediction of cement hydration*. in *Proceedings of the British Ceramic Society*. 1984.
195. Glosser, D., et al., *Estimating reaction kinetics of cementitious pastes containing fly ash.* Cement and Concrete Composites, 2020: p. 103655.
196. Glosser, D.B., *Equilibrium and Non-equilibrium Thermodynamic Modeling of Cement Pastes Containing Supplementary Cementitious Materials*, in *Civil Engineering*. 2020, Oregon State University: Corvallis OR.
197. Taylor, H.F., *Cement chemistry*. Vol. 2. 1997: Thomas Telford London.
198. Choudhary, A., et al., *Influence of limestone cement on the electrical and transport properties of cement mortar* ASTM, 2021. **In Preparation**.
199. Zajac, M., et al., *Influence of limestone and anhydrite on the hydration of Portland cements.* Cement and Concrete Composites, 2014. **46**: p. 99-108.
200. Schöler, A., et al., *Hydration of quaternary Portland cement blends containing blast-furnace slag, siliceous fly ash and limestone powder.* Cement and Concrete Composites, 2015. **55**: p. 374-382.
201. Zajac, M., W. Dienemann, and G. Bolte. *Comparative experimental and virtual investigations of the influence of calcium and magnesium carbonate on reacting cement*. in *Proceedings of the 13th international congress on the chemistry of cements, Madrid*. 2011.

202. Zajac, M., et al., *Influence of calcium and magnesium carbonates on hydration kinetics, hydrate assemblage and microstructural development of metakaolin containing composite cements.* Cement and Concrete Research, 2018. **106**: p. 91-102.
203. Schöler, A., et al., *Early hydration of SCM-blended Portland cements: A pore solution and isothermal calorimetry study.* Cement and Concrete Research, 2017. **93**: p. 71-82.
204. Tennis, P., *Chemical and Physical Characteristics of US Hydraulic Cements: 2014.* Portland Cement Association, Skokie, Ill, 2016.

19 APPENDIX A – Determination of ultimate Degree of Reactivity of SCM

19.1 Scope

This test method covers the procedure for quantitative determination of the ultimate Degree of reactivity of an SCM using experimental methods and thermodynamic simulations. The values stated in SI units are to be regarded as the standard. This standard does not purport to address all of the safety problems, if any, associated with its use. It is the responsibility of the user of this standard to establish appropriate safety and health practices and determine the applicability of regulatory limitations prior to use.

19.2 Terminology

DOR of a supplementary cementitious material (SCM) at a given time - the amount of SCM (in %) that has reacted with pure calcium hydroxide in an alkaline environment up to that time. DOR* of a supplementary cementitious material (SCM) - the amount of SCM (in %) that has reacted with pure calcium hydroxide in an alkaline environment at an 'infinite' time. This can be considered as the maximum amount (in %) of a SCM that is available for the pozzolanic reaction in cementitious system.

19.3 Summary of Test Method

The test method uses a combination of experimentally determined calcium hydroxide consumption and heat release values to predict DOR of SCM. The DOR* of an SCM is estimated by interpolating between the pure SiO_2 and Al_2O_3 reaction reference lines. The reference lines are theoretically determined by reacting pure SiO_2 and Al_2O_3 systems reacted from 0% to 100% in thermodynamic simulations.

The SCM is dry mixed with reagent grade calcium hydroxide (CH) such that the mass ratio of CH:SCM is 3:1. The dry blend is thoroughly mixed with 0.5 M potassium hydroxide (KOH) solution (liquid to powder (CH+SCM) mass ratio of 0.9). The wet paste is immediately transferred to an isothermal calorimeter (IC) preconditioned at 50°C ± 2°C and the heat release values are recorded for a period of 240 hours from mixing. The cumulative heat released value at the end of 240 hours are extrapolated to get the heat released after infinite reaction time. The reacted paste from the IC is subsequently tested for CH consumption using a Thermo-Gravimetric Analyzer (TGA). Further details about the test procedure, results, and analysis are presented in Section 10.

This specific standard is written for the reaction between a SCM and CH at a 3:1 mass ratio in an alkaline pore solution composed of 0.5 M potassium hydroxide (KOH) solution. The effect of varying the mass ratio of reacting species and introduction of different ions in the pore solution are still being studied.

19.4 Significance and Use

The test method is designed to allow for complete reaction of the reactive portion of the supplementary cementitious material (SCM) being tested by providing an excess of calcium hydroxide in a highly alkaline environment (to simulate the alkaline conditions in OPC- and OPC-SCM systems) at an elevated temperature of 50°C for 240 hours. The underlying principle of the reactivity test is that if the main reactive phases of SCM (amorphous SiO_2 and amorphous Al_2O_3) are thermodynamically simulated at different degrees of reaction, these values can serve as reference values against which to measure the reactivity of commercial SCMs such as fly ash. The test provides a methodology for measuring the amount of the SCM that is reactive. It should be noted that the methodology discussed in this report is designed to test SCMs which primarily react in a pozzolanic manner (where SiO2 and Al2O3 in the SCM react with calcium hydroxide in the OPC-SCM system). While this approach can be extended to SCMs that also react hydraulically (like Slag) as there is no other test method that is currently available to determine the reactivity of these materials, work is ongoing on determining a more appropriate test method to determine the reactivity of such SCMs.

19.5 Apparatus

- Paste mixer - A mixer that can be used to mix cementitious paste
- Balance—Analytical balance, Class A, conforming to the requirements of M 231 to weigh the paste. The balance shall be accurate to 0.1 mg.
- Funnel – Used to pour reactive paste into the glass ampoules to ensure that all the paste directly goes at the bottom of the ampoule (with minimum splatter on the sides and the top of the ampoules) from where the heat is measured.
- IC ampoule assembly - These are glass ampoules (20 ml volume) with aluminum lids which can be used to measure the heat released from the reacting paste mixture inside them in an Isothermal Calorimeter (IC).
- Clamping tool – A mechanical or electrical clamping tool to seal the lids on the glass ampoules to prevent leakage during the test
- Isothermal calorimeter – The IC shall conform to ASTM C1679 and should be able to operate in a temperature of 50°C ± 2°C
- Decapper tool – used to remove the sealed cap from the IC ampoules

- Spatula – used to scoop out (around 20 mg) of reacted paste from the IC ampoule
- TGA pan – This is platinum pan with a hanger assembly which is inert to the reacted paste sample and whose shape and structural integrity can withstand temperatures within the TGA machine.
- Thermo-gravimetric Analyzer (TGA) - The TGA shall conform to ASTM E1131 and shall be able to operate in a temperature range of 25°C to 1000°C.

19.6 Materials

- Reagents—Reagent grade chemicals shall be used in all tests. Unless otherwise indicated, all reagents shall conform to the specifications of the Committee on Analytical Reagents of the American Chemical Society. For this standard, reagent grade calcium hydroxide ($Ca(OH)_2$) and potassium hydroxide (KOH) is used to prepare paste mixture.
- Distilled Water— Unless otherwise indicated, water used shall be distilled water
- Pore Solution Preparation— in a small graduated cylinder, dissolve 2.805g of anhydrous KOH, in 50 mL of distilled water. Slowly, add distilled water with constant stirring to make the volume of the solution equal to 100 mL. Store the solution in a sealed plastic container with secondary containment at a temperature of 23 ± 1°C. Use this solution within 7 days of its preparation. If any precipitates are noted in the solution at any time, discard the solution and prepare a fresh one.
- Note: The dissolution of KOH in water is highly exothermic, so precautions should be taken to prevent burning when large amounts of solution are to be prepared (over 30 g).

19.7 Sample Preparation

Reactive Paste Preparation: For each test, gently dry mix the SCM and calcium hydroxide in a 1:3 mass ratio by hand for uniform distribution of SCM throughout the powder system. Prepare the paste mixture by thoroughly mixing the simulated pore solution with dry powder in 0.9:1 mass ratio.

19.8 Testing Procedure

Heat of reaction (Q) measurement: Immediately after mixing, pour approximately 7 g of the wet paste into a glass ampoule using a funnel and then seal them. Transfer the ampoules to an IC that had been preconditioned at 50°C ± 2°C for 24 hours. Allow signal stabilization (time varies depending of the instrument) and then record the heat flow for a total of 240 hours. Note down the cumulative heat at the end test period.

Calcium hydroxide measurement: After 240 hours of IC testing, remove the ampoules from the calorimeter. Take approximately 20 mg of the reacted paste from the ampoules and put it on the TGA pan. Run the following TGA method on the sample. Equilibrate the pan at 25 °C. Heat the pan from 23 °C to 1000 °C in a nitrogen purged atmosphere at a rate of 10 °C/min. (Note: Perform TGA within 12 hours of removing the samples from the isothermal calorimeter.)

19.9 Calculation and Interpretation of Results

Reference SiO_2 and Al_2O_3 reaction lines: Thermodynamic modelling can be used to provide reference reactivity range of pure silicate phases and aluminate phases. The modelling simulations calculate the heat release and calcium hydroxide consumed due to the pozzolanic reaction of pure amorphous silica and pure amorphous alumina. The simulations are run at a CH:SCM ratio of 3:1, liquid to CH+SCM ratio of 0.9, and at a temperature of 50°C at varying degrees of reactivity (0% to 100%) of SiO_2 and Al_2O_3. The calculated Q∞ vs CH consumption values for SiO_2 and Al_2O_3 of varying degrees of reactivity is shown in Figure A-1.

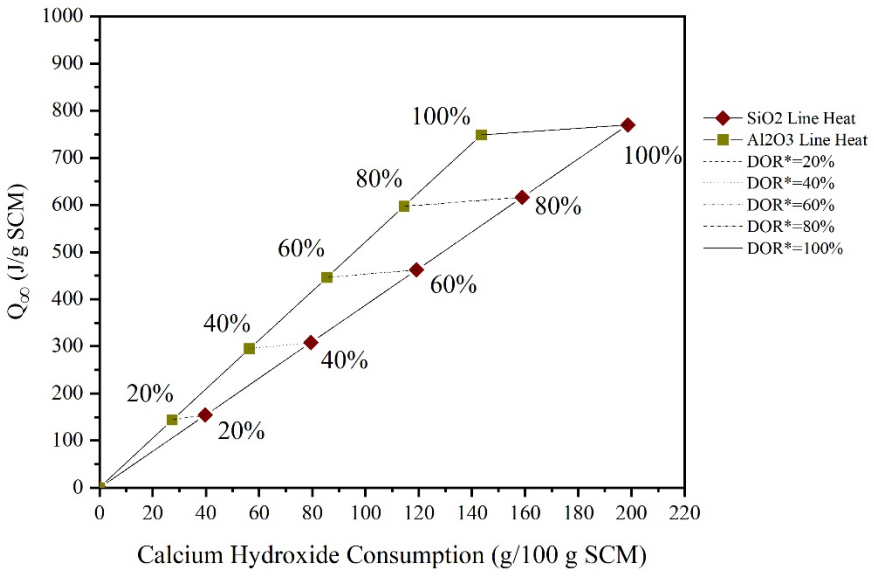

Figure A-19-1. Reference reaction lines of pure silica and pure alumina under simulated experimental condition

Note: The thermodynamic modelling is performed using GEMS3K software and the CemData v.18 database

19.9.1 Ultimate heat of hydration calculation

Normalize the heat release values by the amount of SCM in the reacted paste, which was tested in the IC. Plot the normalized heat release curves vs reaction time. If it is still evident from the plot that the reaction would continue beyond the measured 240 hours, correct them mathematically for Q∞ using either of the following two approaches mentioned in the next paragraph.

Correction for ultimate heat released (Q∞)- The heat released due to the pozzolanic reaction which takes place in the test setup starts off very rapidly in the beginning but slow down with time as the concentration of the reactants in the system start to decrease. It can be shown that a system reacting at 240 hours (10 days) at 50 °C is equivalent to a system reacting for 50 days at 23 °C. For most SCMs, this amount of time is sufficient to allow the SCM to react to completion, and the value of heat released at 240 hours of experiment is the ultimate heat released from the system (Q∞). However, in some cases, the SCM may not have reacted completely, and a correction may need to be done to estimate the ultimate value of heat released. One of the following corrections is used to provide the heat released values at reaction completion (Q∞). The comparison of the Q∞ value from the two different correction methods are presented in Table A.1.

Table A.1. Comparison of different heat released correction methods

	Heat released in 240 hours	Curve fitting approach	Inverse heat and time approach	
	Q (J/g SCM)	Q_∞ (J/g SCM)	y-intercept	Q_∞ (J/g SCM)
SCM1	223.44	223.44	0.0043	232.56
SCM2	399.73	457.6275	0.0021	476.19

19.9.2 Curve fitting approach

Fit the experimental data with a logarithmic function and extrapolate the curves till the completion of the reaction (defined as the point where instantaneous heat change per unit time approaches 0) is achieved. An example of the fitting model has been shown in Figure A-19-2. Figure A-19-2 shows that the heat release curve of SCM1 has plateaued in 240 hours (duration of experiment) implying that the reaction between SCM1 and CH is completed. On the other hand, the heat release curve of SCM2 still has a positive slope at the end of 240 hours. In order to estimate the heat released at complete reaction of SCM2,, a logarithmic model was used to fit the curve and the curve was extrapolated till slope almost became zero to get to the Q∞ value for SCM2.

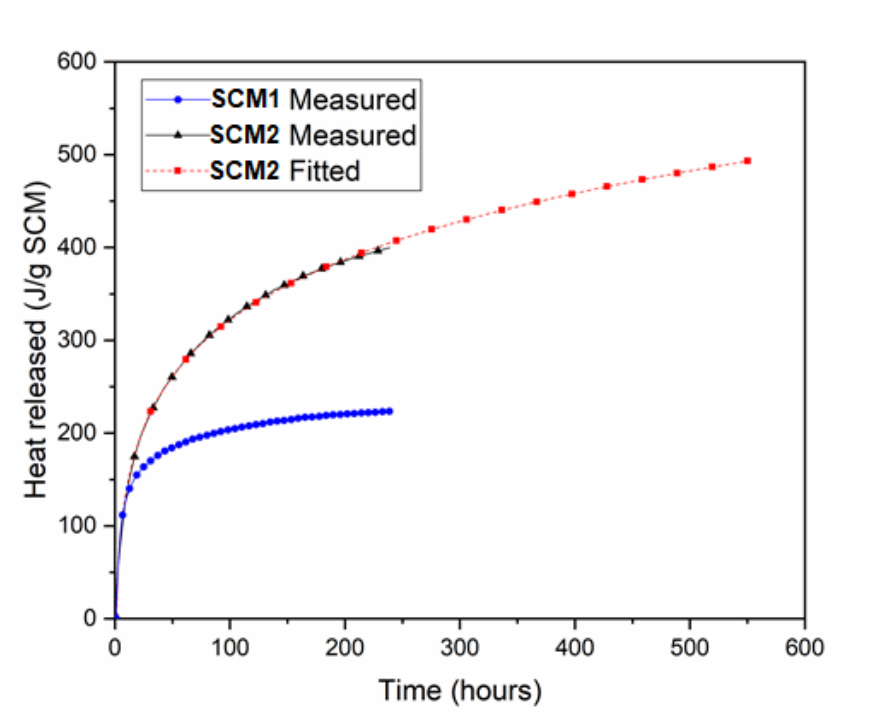

Figure A-19-2. Heat release curves determined by isothermal calorimetry for SCM1 and SCM2. The heat release data for SCM2 data was extrapolated to equilibrium to calculate the heat release correction. SCM1 did not require any extrapolation.

19.9.3 Inverse heat and time approach

Over the course of experiment, the heat release values start to plateau. This plateau is defined by the reaction rate ($\partial Q/\partial t$) being lesser than or equal to 0.05. For SCMs that still have some reactivity potential left over after 240 hours ($\partial Q/\partial t \geq 0.05$), the inverse of heat released values (1/Q) can be plotted against the inverse of time taken (1/t) for data range with $\partial Q/\partial t \leq 1$. The trend of this curve (mostly linear) is then extrapolated to intersect the y-axis. The y-intercept of 1/Q vs 1/t plot will represent 1/ $Q\infty$ for that SCM. An example of the fitting model using SCM1 and SCM2 is shown in Figure A-19-3. The figure shows 1/Q vs 1/t curve of SCM1 and SCM2. The y- intercept of the linear fit trend line on the data gives the Q_∞ value.

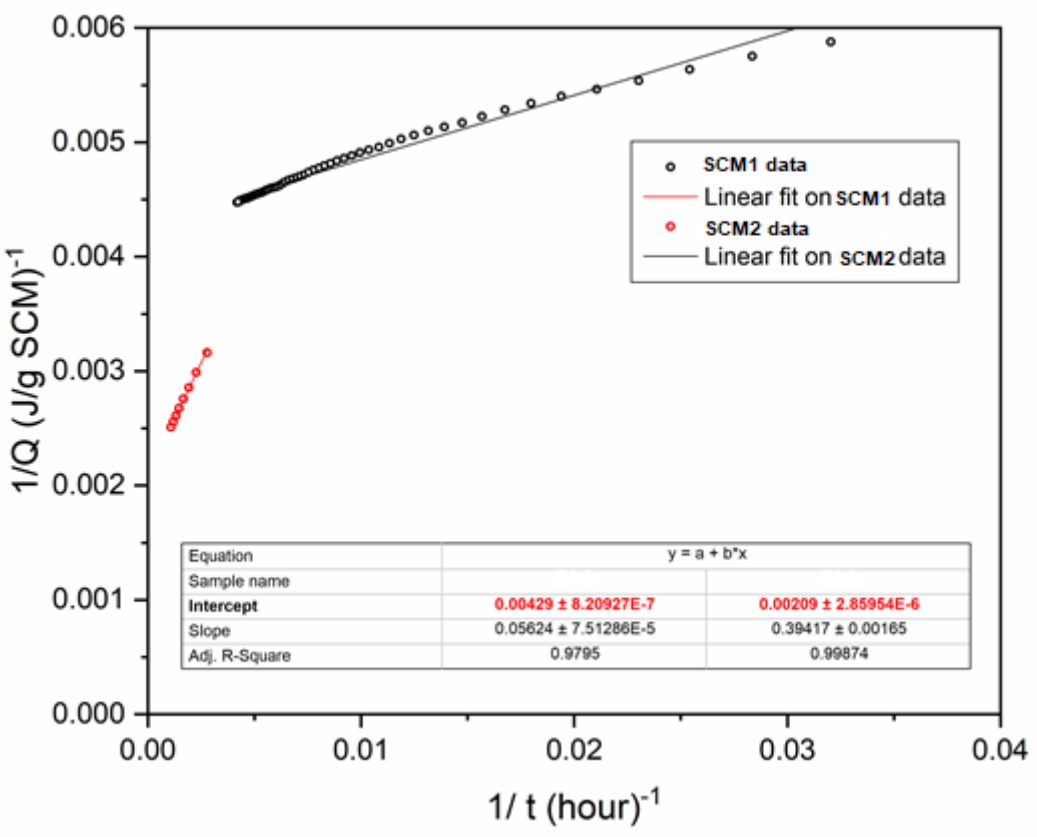

Figure A-19-3. 1/Q vs 1/t curve for SCM1 and SCM2 with their corresponding linear trendline

Calcium hydroxide consumed calculation: TGA data is reported as change in sample mass with temperature. the characteristic peak of the decomposition of certain compounds is used in quantitative analysis. In the case of $Ca(OH)_2$, decomposition typically occurs between 350-450°C. The mass loss in the sample between 350°C to 450°C corresponds to loss of water due the decomposition of $Ca(OH)_2$ present in the system as shown in Figure A-19-4. The amount of $Ca(OH)_2$ reacted (normalized per 100 g of SCM) is calculated using Equation A-1 and A-2:

$$Ca(OH)_{2\,final} = (\Delta m \times \frac{74.09}{18.01}) \times 100 \quad \text{(A-1)}$$

$$Ca(OH)_{2\,consumed} = (Ca(OH)_{2\,initial} - Ca(OH)_{2\,final}) \times \frac{100}{13.16} \quad \text{(A-2)}$$

where:

Δm = weight reduction due loss of water detected in TGA between 350 °C to 450 °C,

$Ca(OH)_{2\ initial}$ = mass of $Ca(OH)_2$ in the original paste per 100 g of paste, known to be 39.47 $g/100g_{paste}$ from the initial mixture design,

$Ca(OH)_{2\ final}$ = mass of $Ca(OH)_2$ in the remaining in the reacted paste (in $g/100g_{paste}$),

100/13.16 is the conversion factor (100g paste contains ~13.16g SCM), and,

$Ca(OH)_{2\ consumed}$= mass of $Ca(OH)_2$ consumed due to the pozzolanic reaction (in $g/100g_{SCM}$).

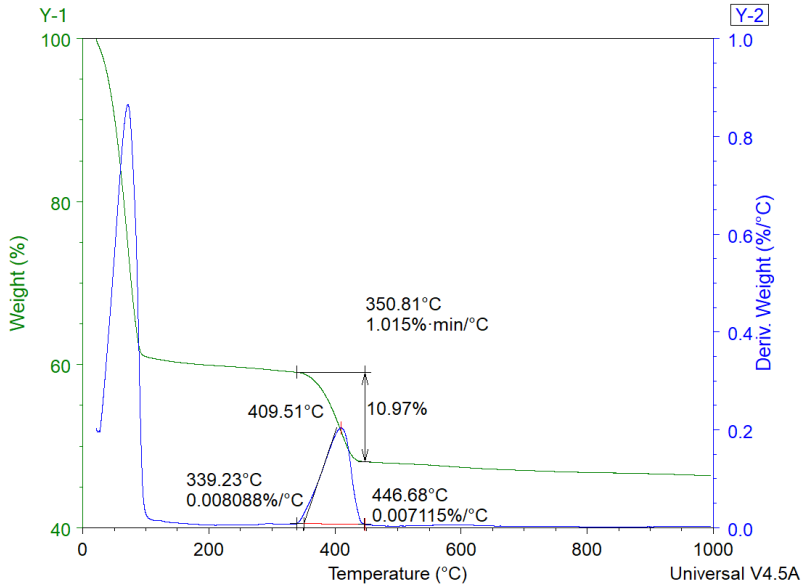

Figure A-19-4. Typical TGA plot of reacted SCM paste

19.10 Reporting

Plot the $Ca(OH)_2$ consumption vs. heat release data results in comparison with the reference lines shown in Figure A-19-1. The reactivity of the SCM is read from the plot with respect to the reference lines. This method allows for the determination of the equilibrium degree of reactivity (DOR*) of a SCM.

20 APPENDIX B – Heat of Hydration

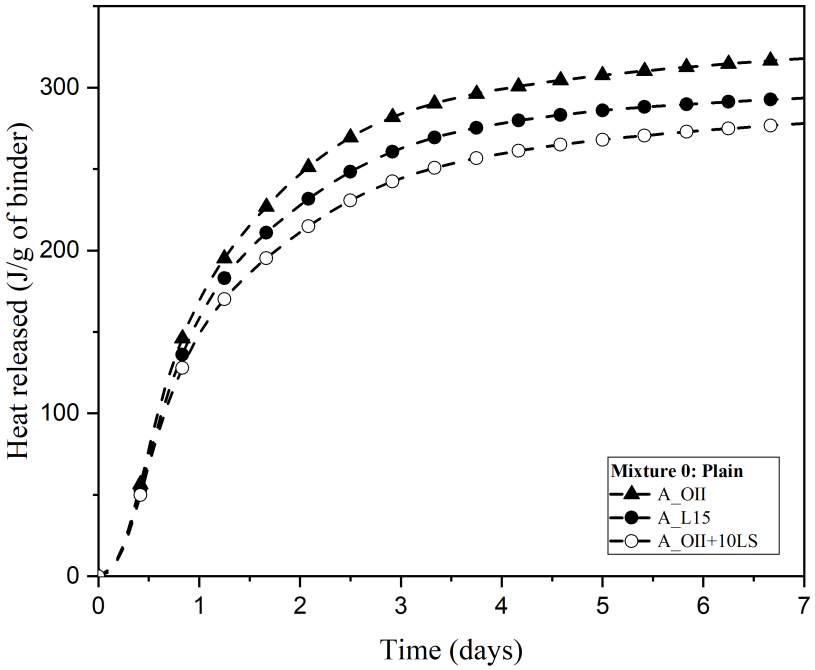

Figure B-20-1. Heat of Hydration of Cement A – M0

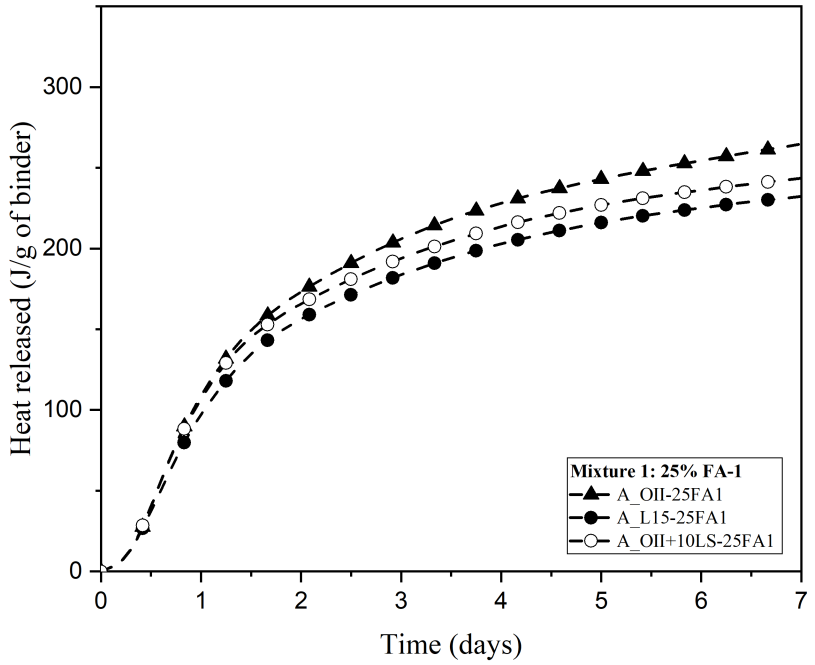

Figure B-20-2. Heat of Hydration of Cement A – M1

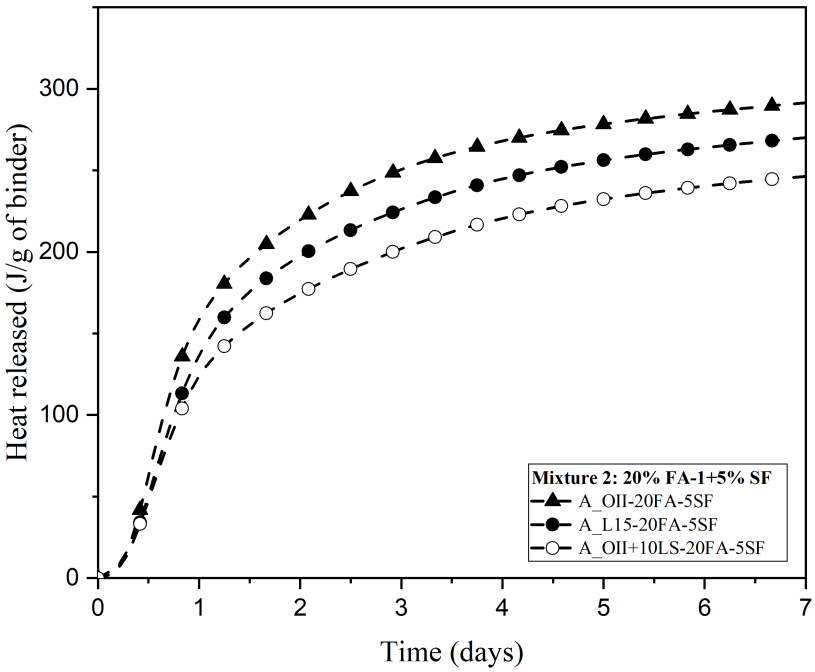

3665

3666 **Figure B-20-3. Heat of Hydration of Cement A – M2**

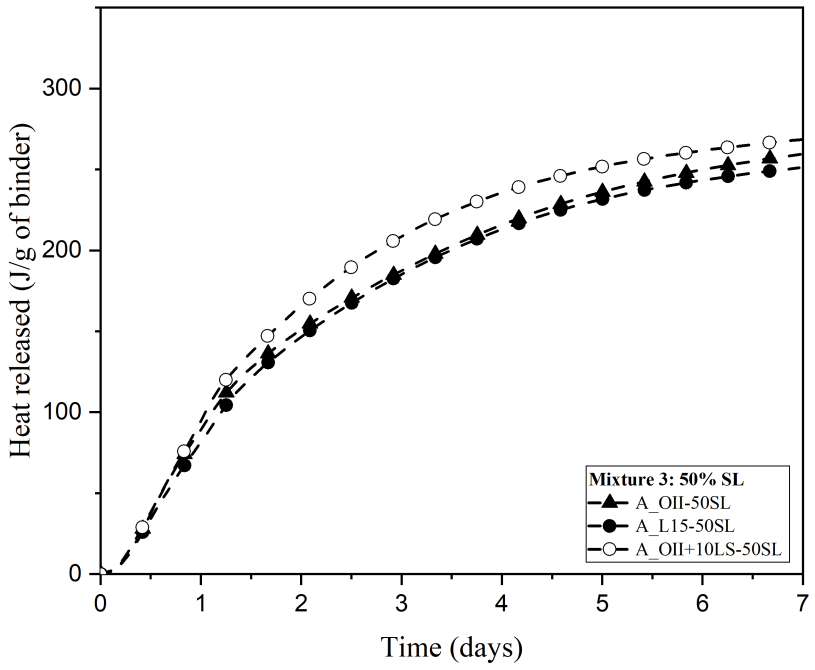

3667

3668 **Figure B-20-4. Heat of Hydration of Cement A – M3**

3669

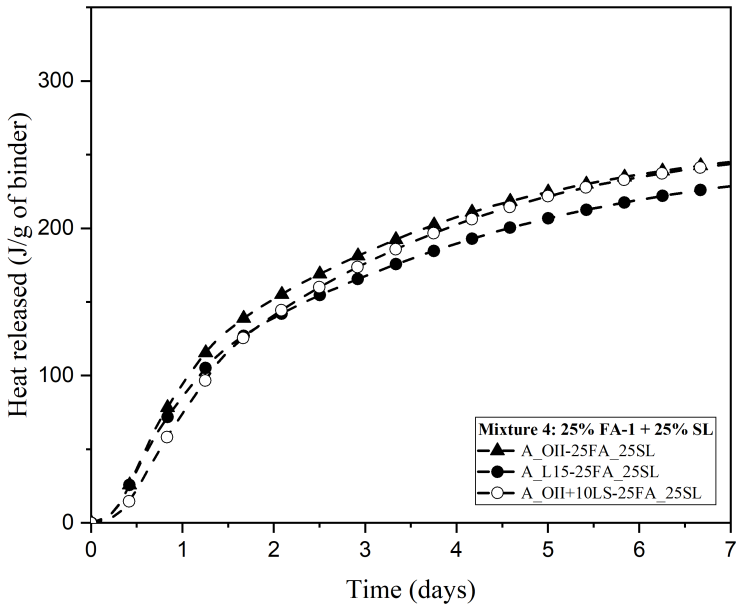

3670

3671 **Figure B-20-5. Heat of Hydration of Cement A – M4**

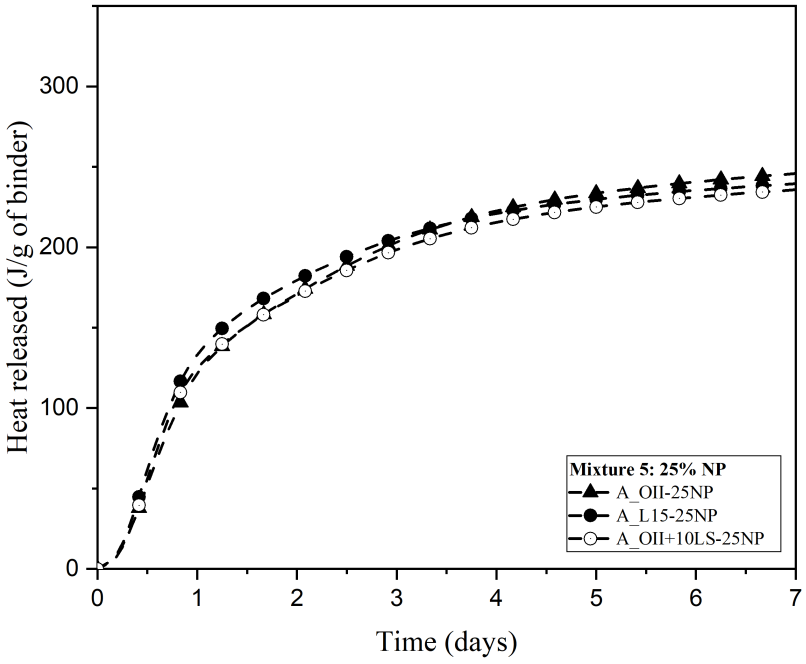

3672

3673 **Figure B-20-6. Heat of Hydration of Cement A – M5**

3674

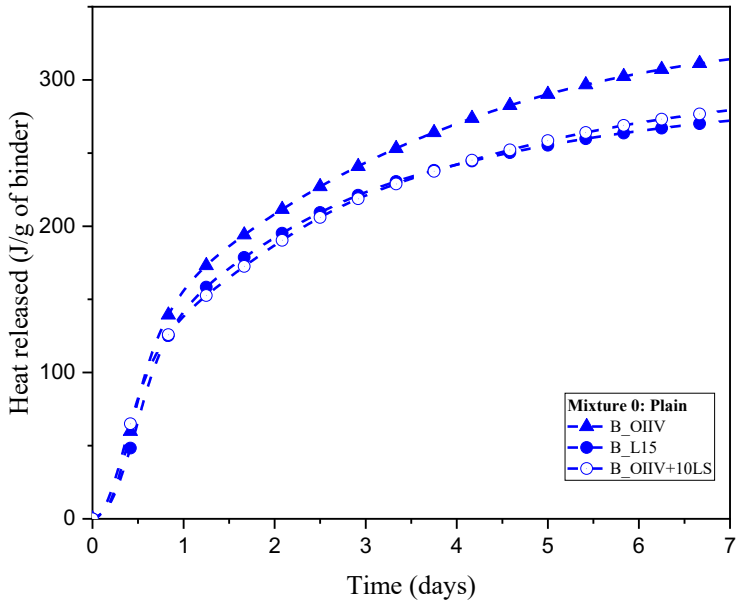

3675

3676 **Figure B-20-7. Heat of Hydration of Cement B – M0**

3677

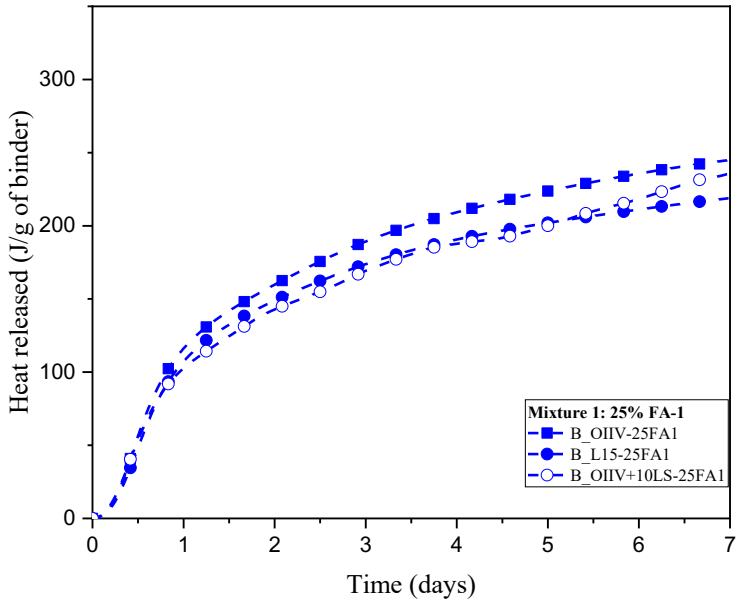

3678

3679 **Figure B-20-8. Heat of Hydration of Cement B – M1**

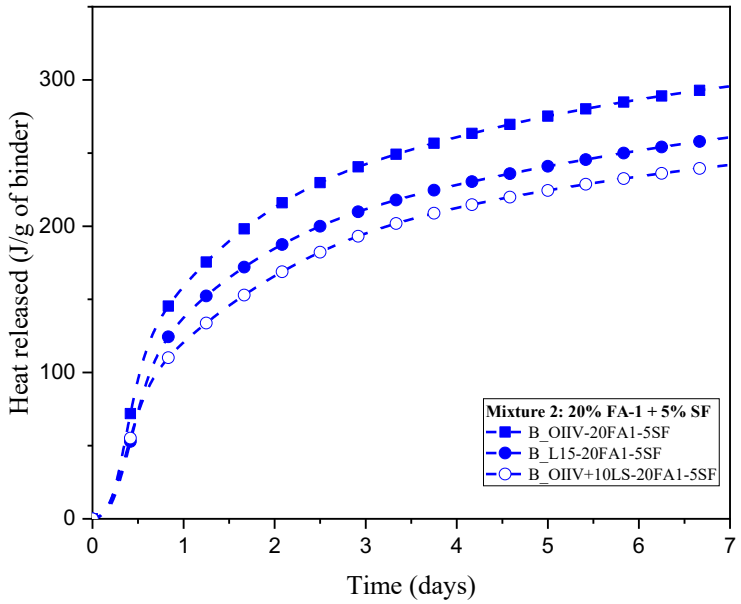

Figure B-20-9. Heat of Hydration of Cement B – M2

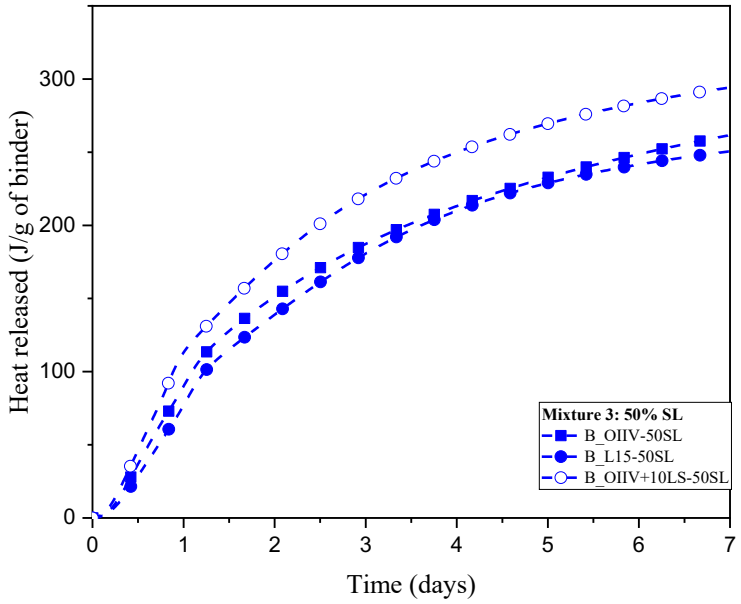

Figure B-20-10. Heat of Hydration of Cement B – M3

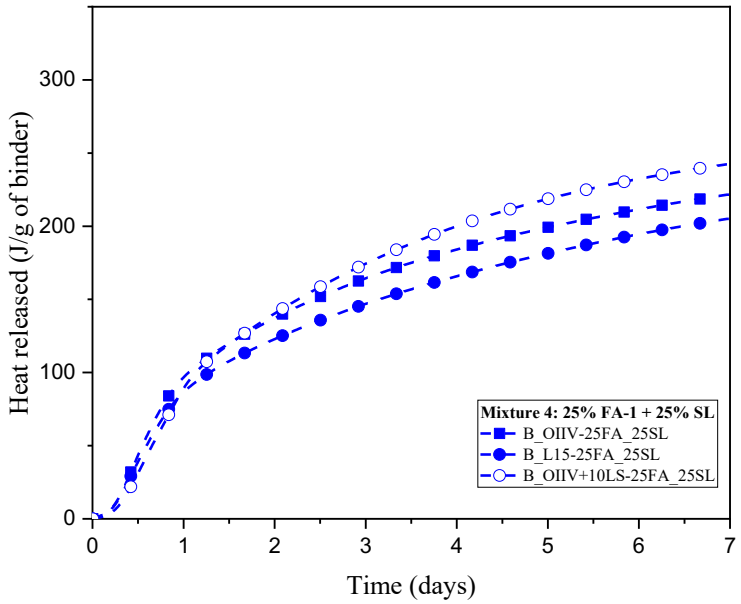

3685

3686 **Figure B-20-11. Heat of Hydration of Cement B – M4**

3687

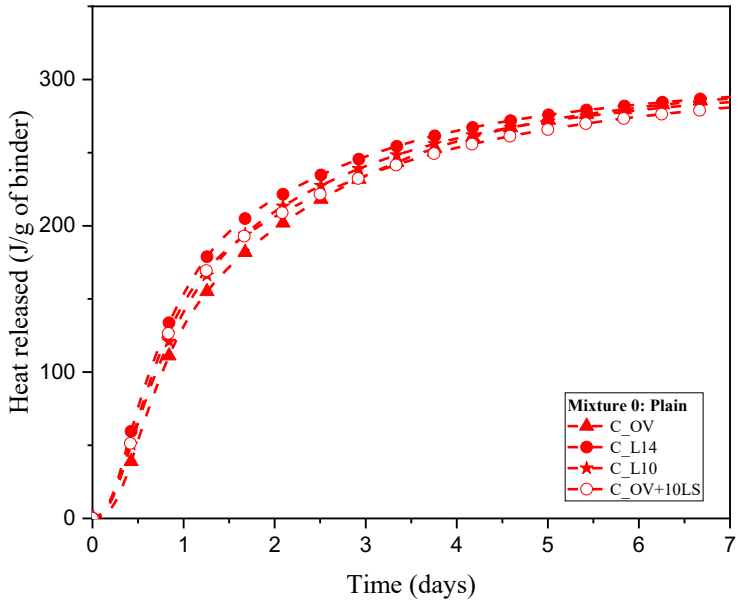

3688

3689 **Figure B-20-12. Heat of Hydration of Cement C – M0**

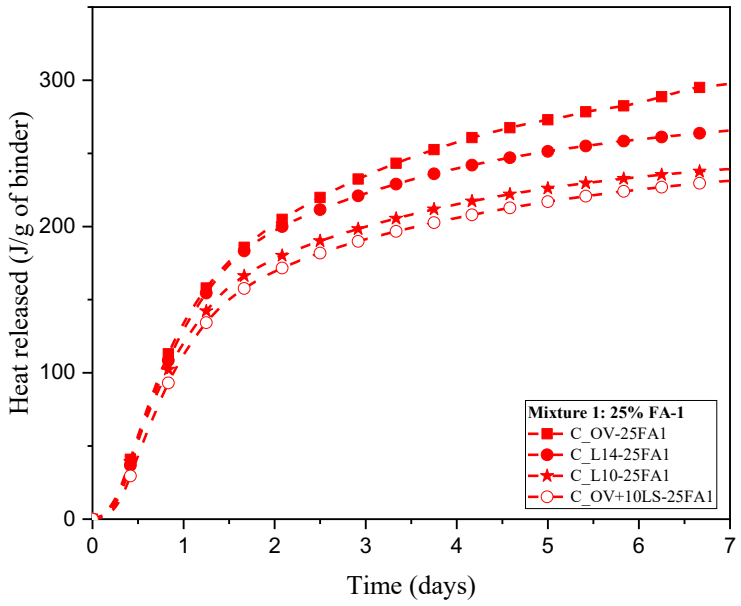

Figure B-20-13. Heat of Hydration of Cement C – M1

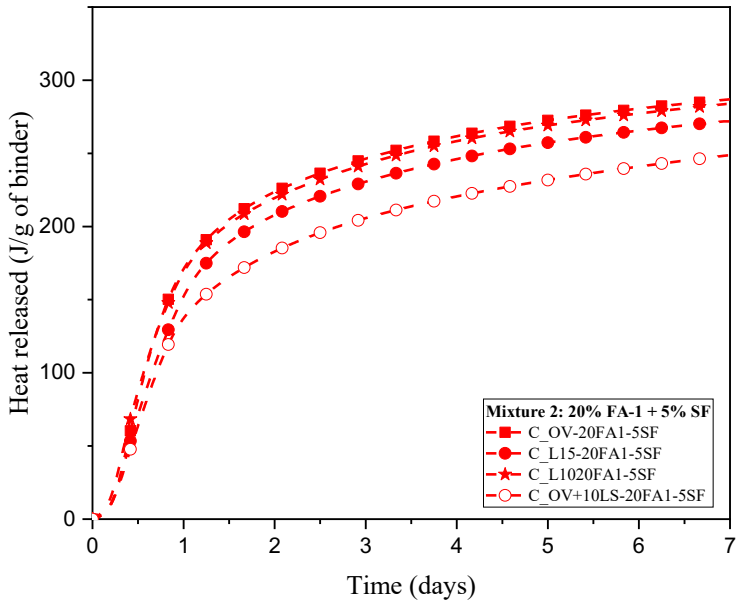

Figure B-20-14. Heat of Hydration of Cement C – M2

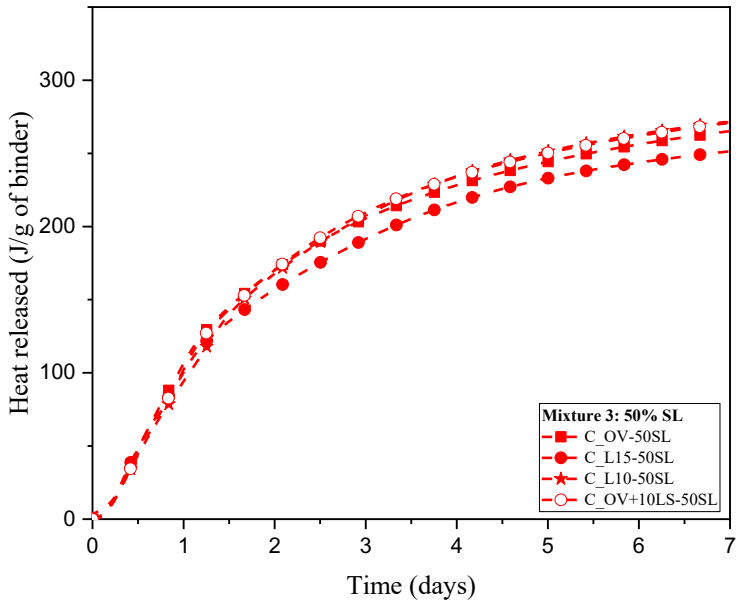

Figure B-20-15. Heat of Hydration of Cement C – M3

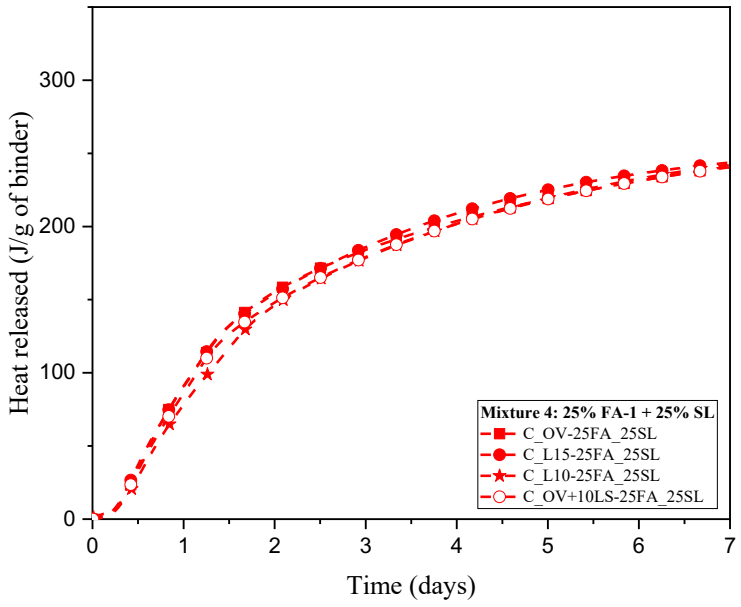

Figure B-20-16. Heat of Hydration of Cement C – M4

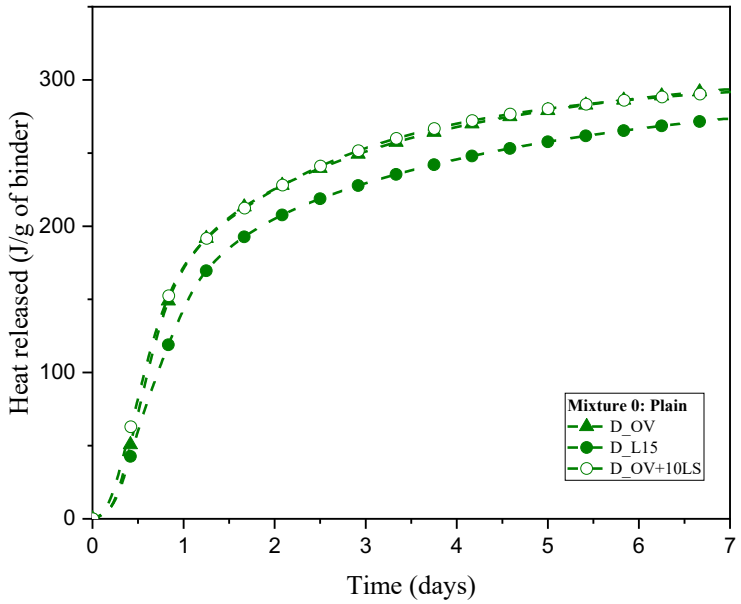

3700

3701 **Figure B-20-17. Heat of Hydration of Cement D – M0**

3702

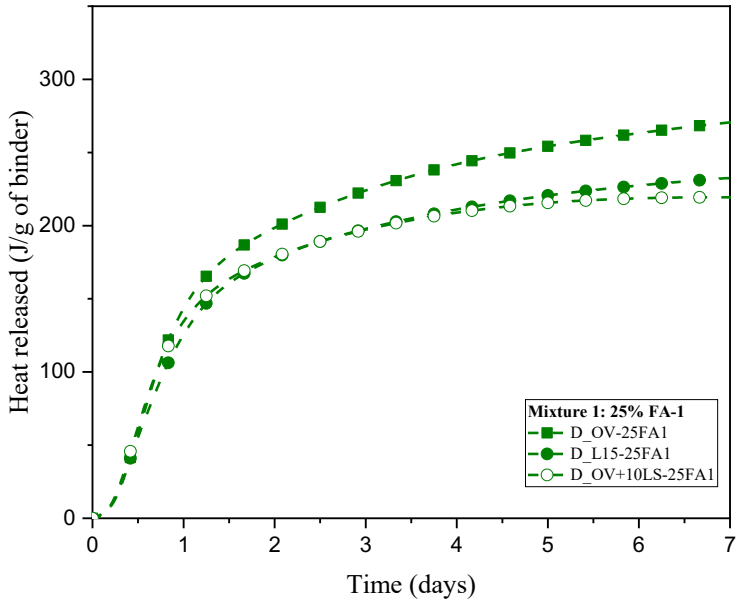

3703

3704 **Figure B-20-18. Heat of Hydration of Cement D – M1**

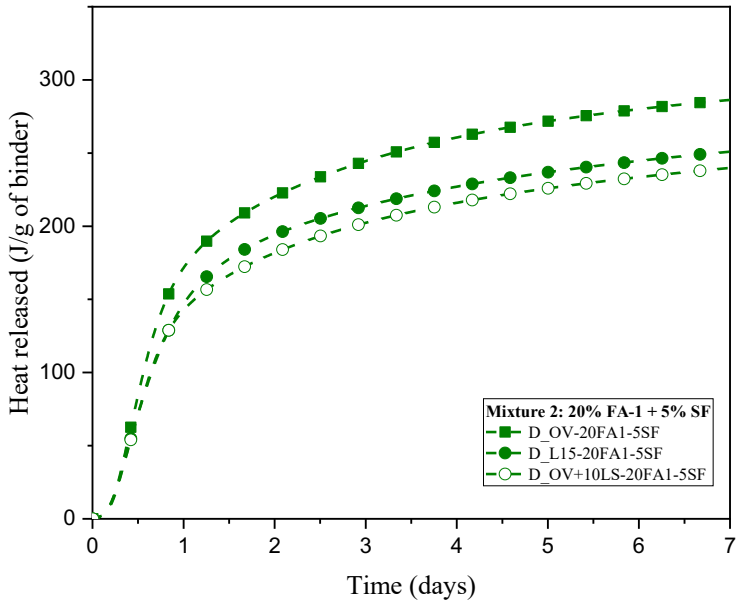

3705

3706 **Figure B-20-19. Heat of Hydration of Cement D – M2**

3707

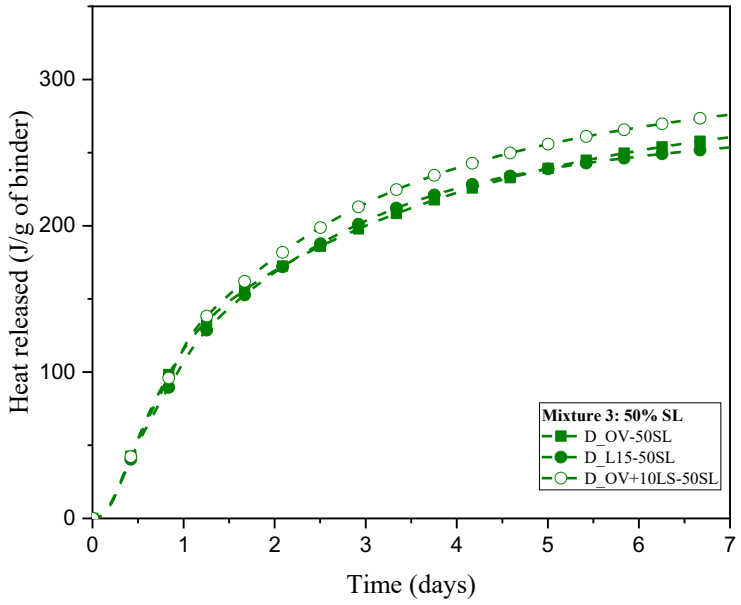

3708

3709 **Figure B-20-20. Heat of Hydration of Cement D – M3**

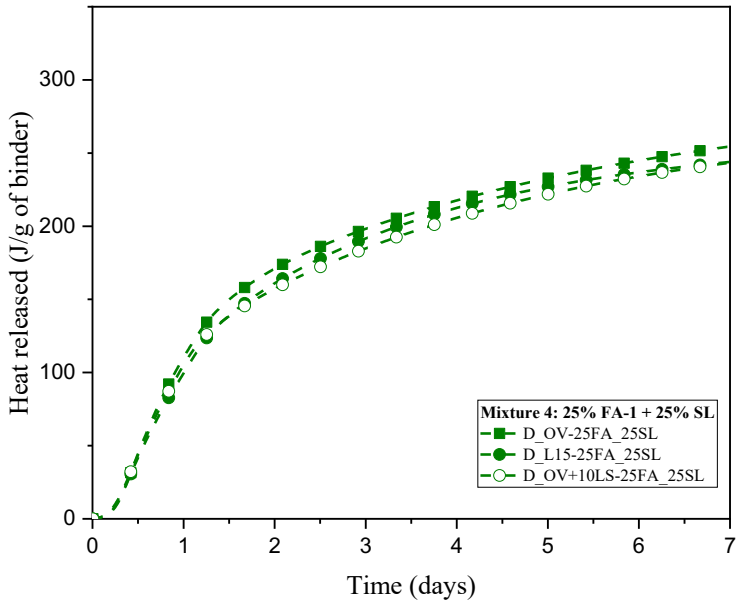

Figure B-20-21. Heat of Hydration of Cement D – M4

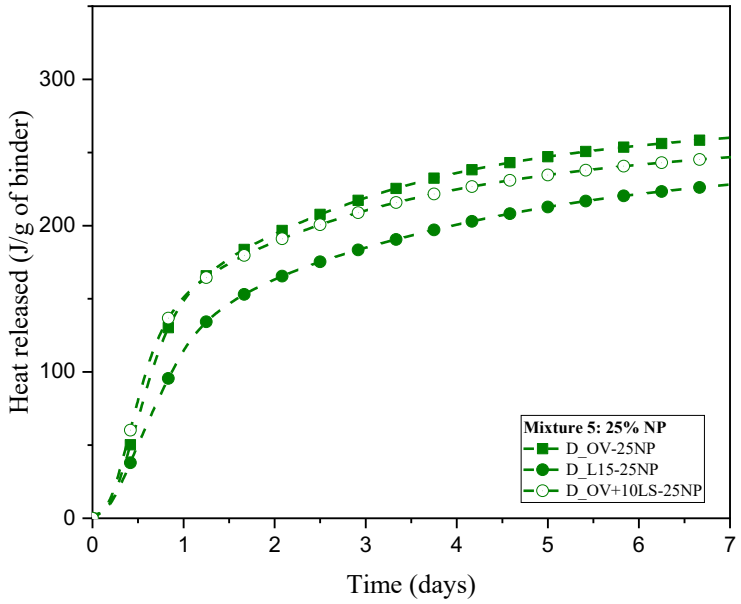

Figure B-20-22. Heat of Hydration of Cement D – M5

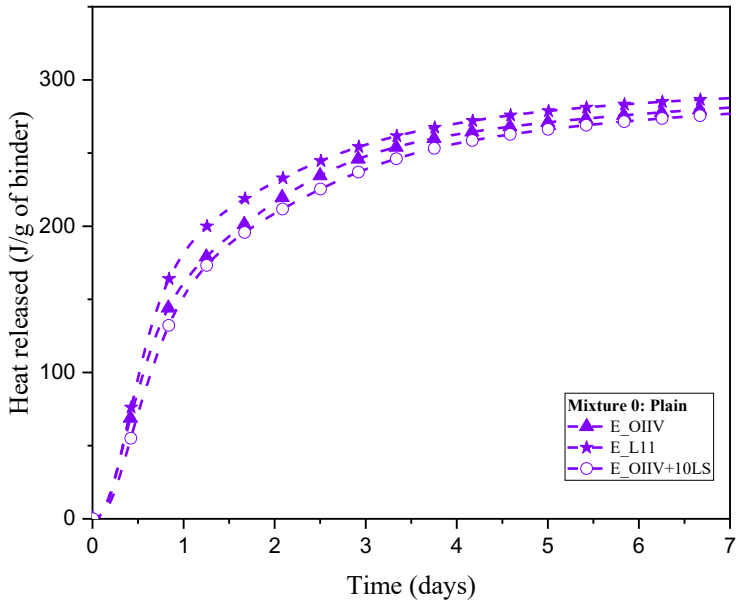

3715

3716 **Figure B-20-23. Heat of Hydration of Cement E – M0**

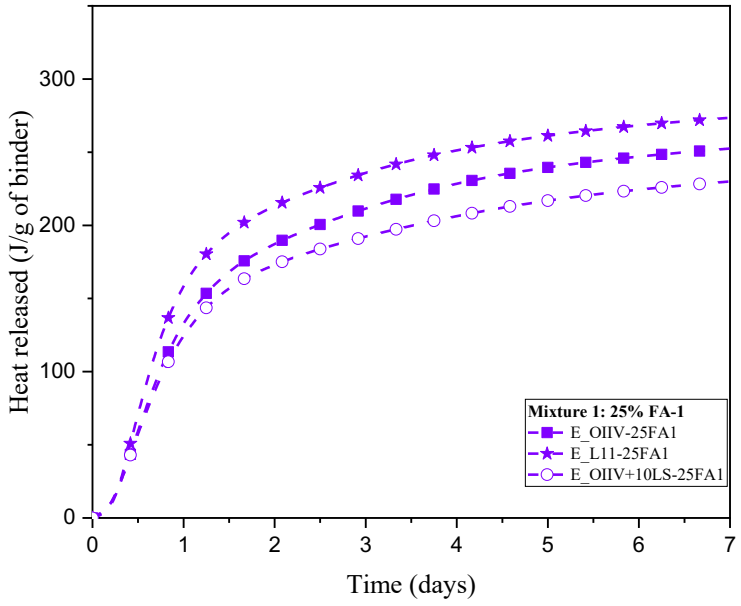

3717

3718 **Figure B-20-24. Heat of Hydration of Cement E – M1**

3719

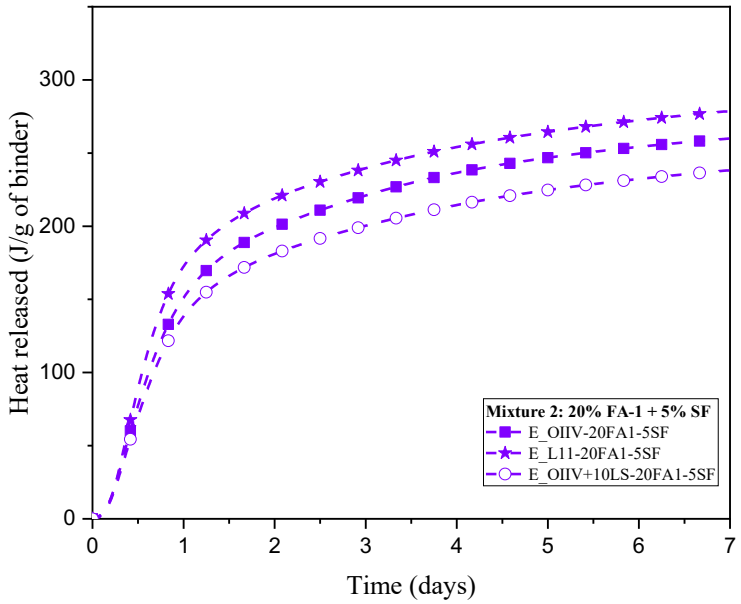

Figure B-20-25. Heat of Hydration of Cement E – M2

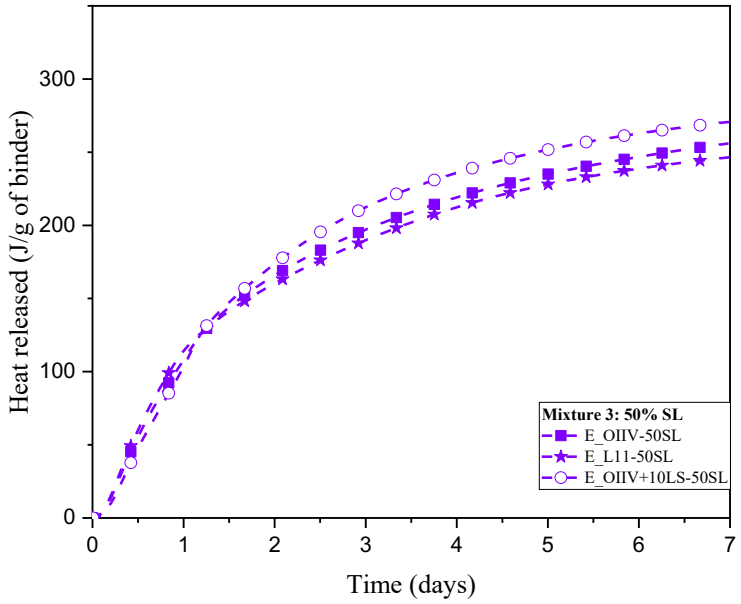

Figure B-20-26. Heat of Hydration of Cement E – M3

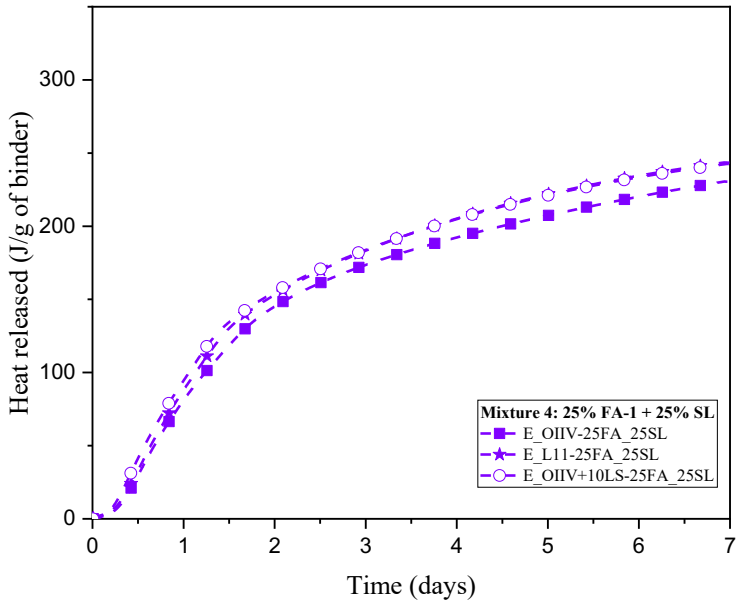

Figure B-20-27. Heat of Hydration of Cement E – M4

21 APPENDIX C – Drying Shrinkage Results

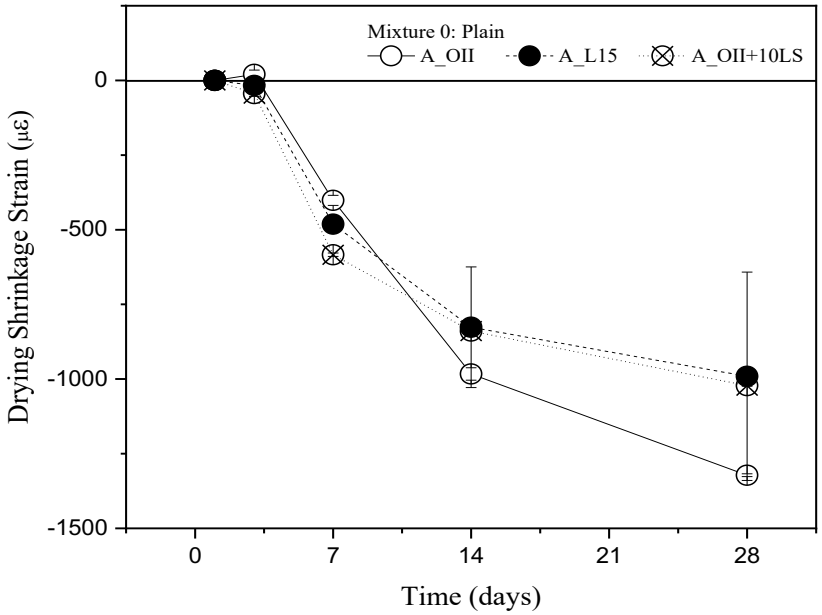

Figure C-21-1. Drying Shrinkage of Cement A – M0

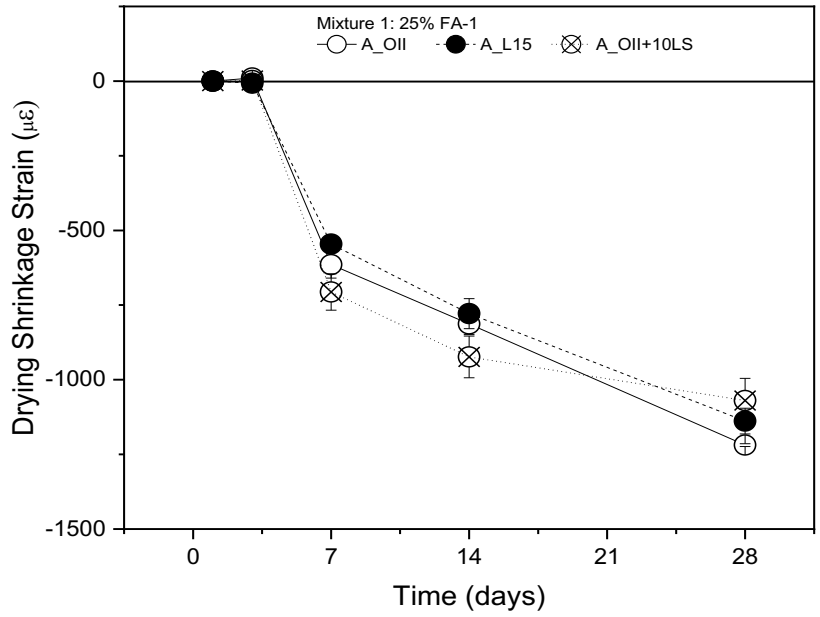

3734

3735 **Figure C-21-2. Drying Shrinkage of Cement A – M1**

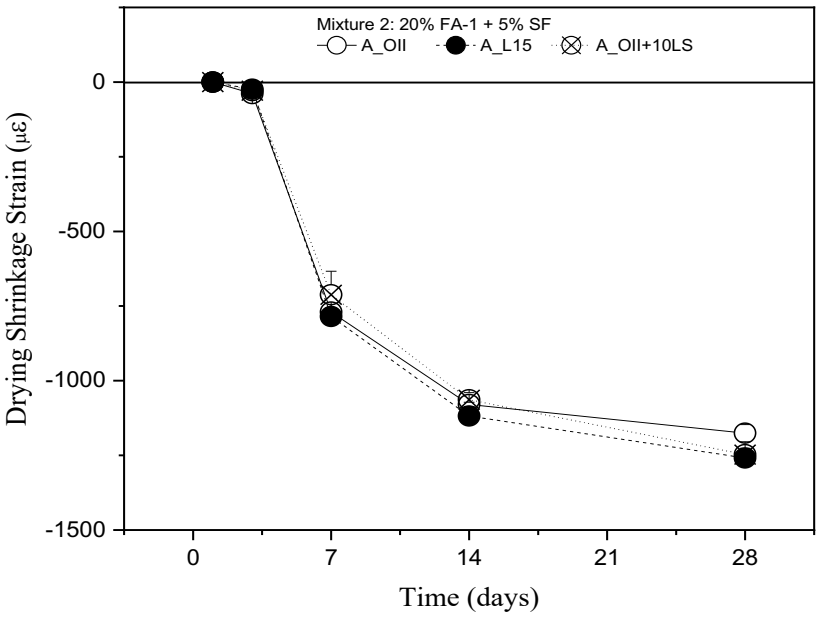

3736

3737 **Figure C-21-3. Drying Shrinkage of Cement A – M2**

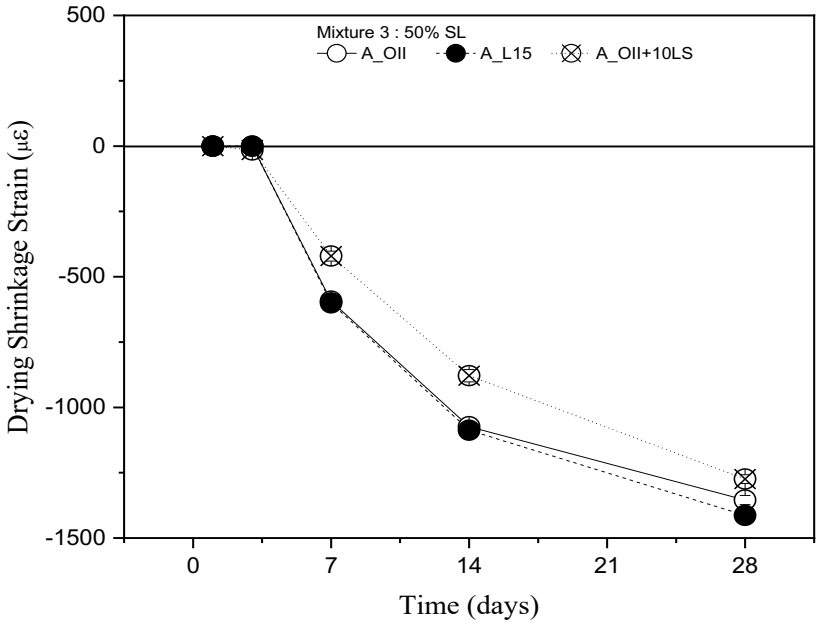

3738

3739 **Figure C-21-4. Drying Shrinkage of Cement A – M3**

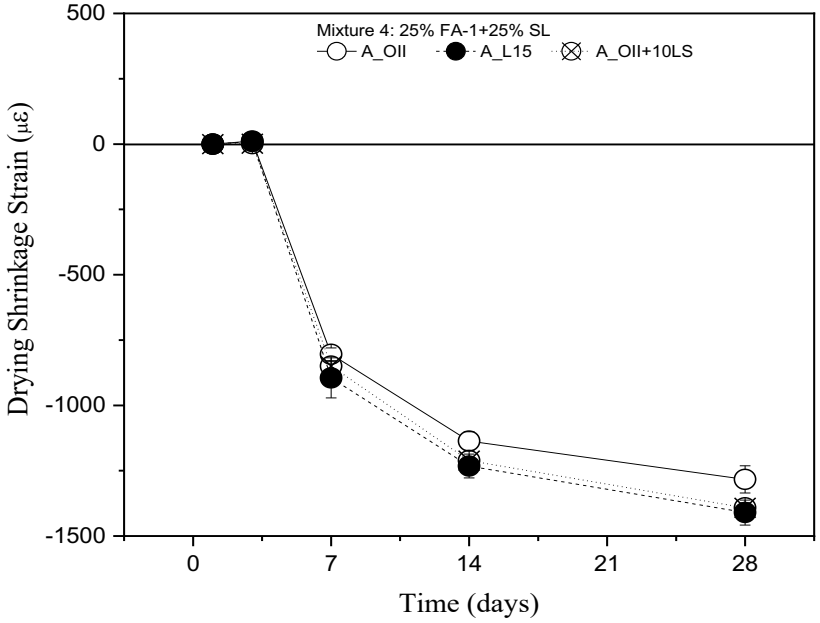

3740

3741 **Figure C21-5. Drying Shrinkage of Cement A – M4**

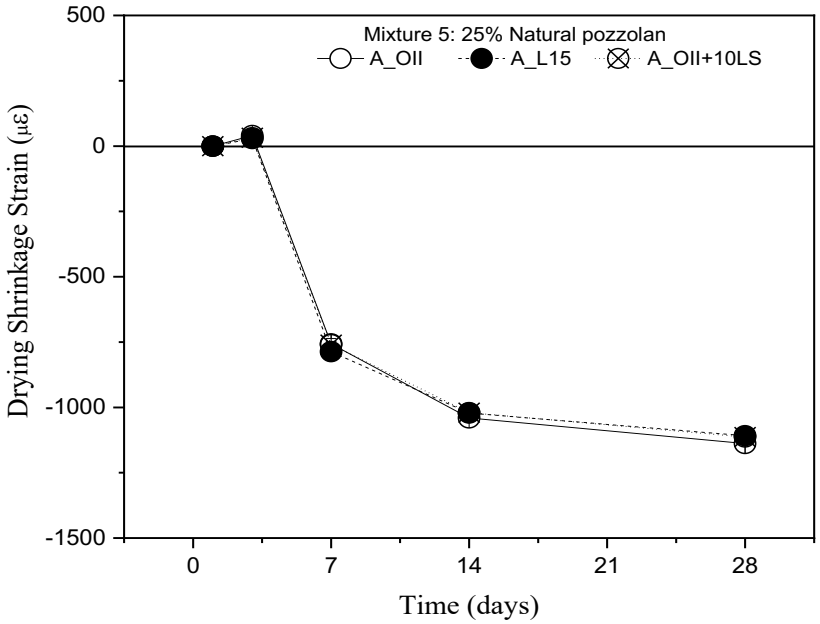

3742

3743 **Figure C-21-6. Drying Shrinkage of Cement A – M5**

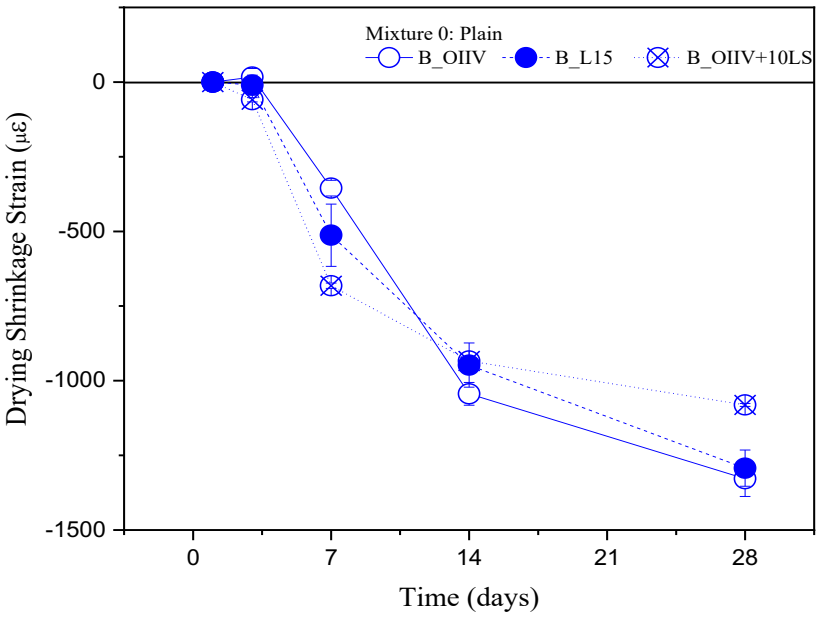

3744

3745 **Figure C-21-7. Drying Shrinkage of Cement B – M0**

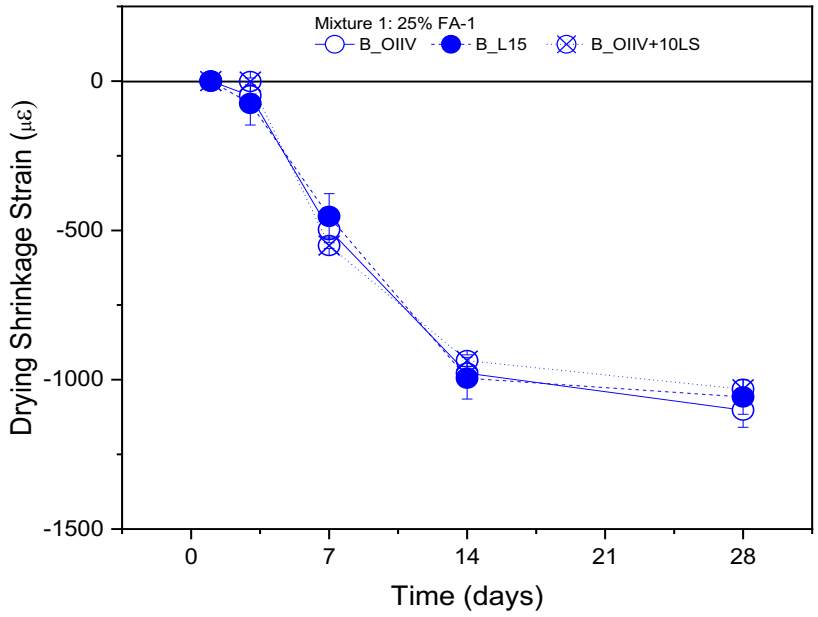

3746

3747 **Figure C-21-8. Drying Shrinkage of Cement B – M1**

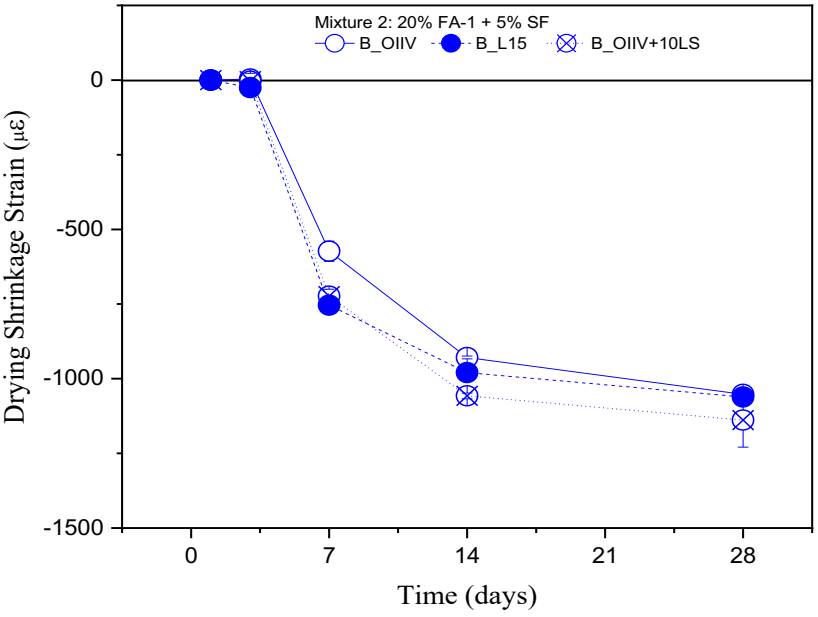

3748

3749 **Figure C-21-9. Drying Shrinkage of Cement B – M2**

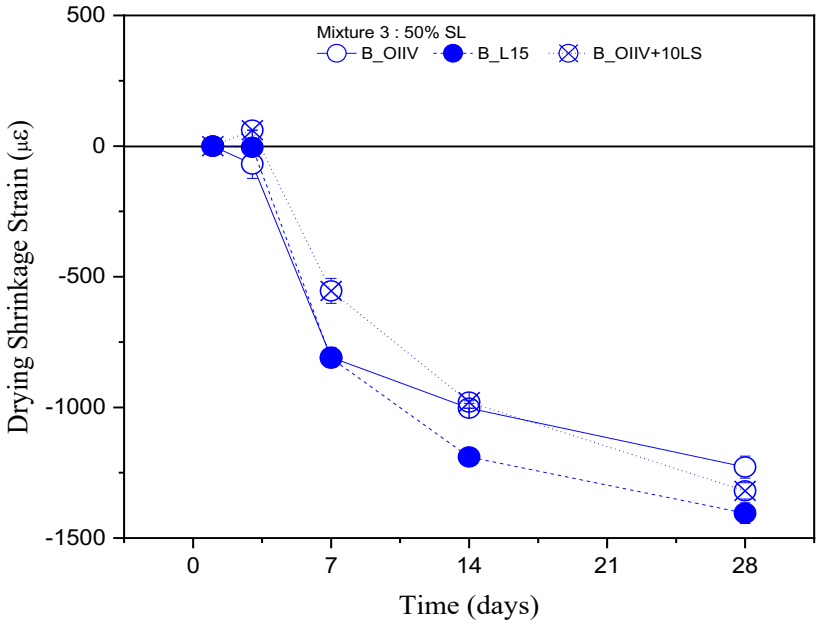

3750

3751 **Figure C-21-10. Drying Shrinkage of Cement B – M3**

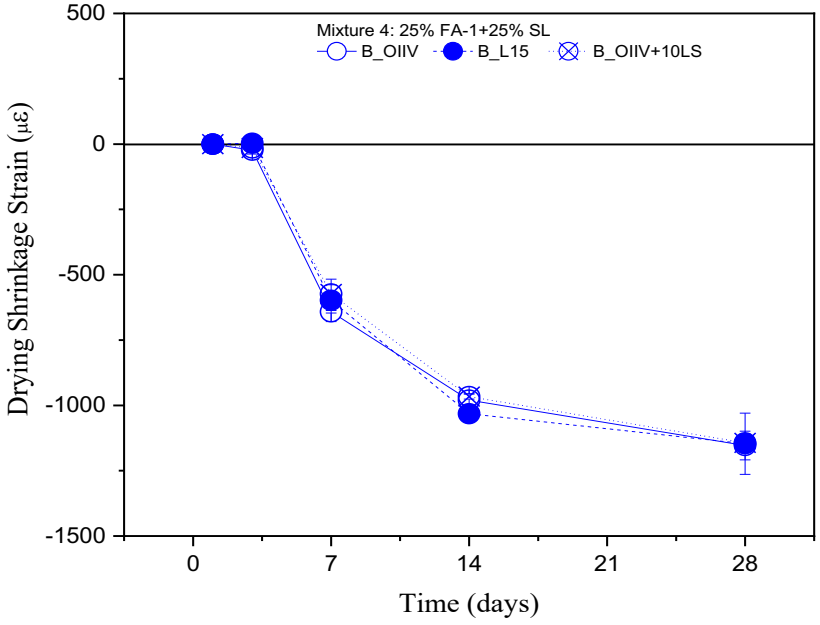

3752

3753 **Figure C-21-11. Drying Shrinkage of Cement B – M4**

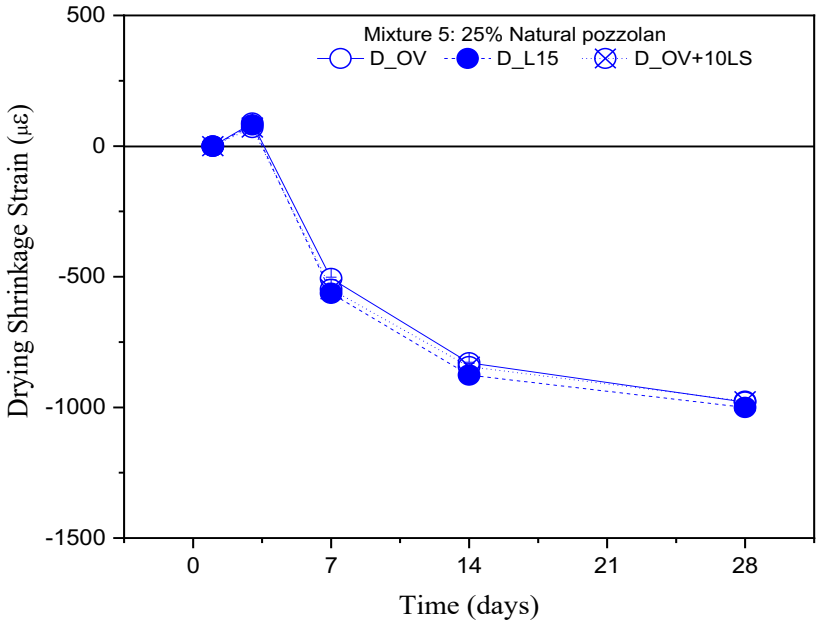

3754

3755 **Figure C-21-12. Drying Shrinkage of Cement B – M5**

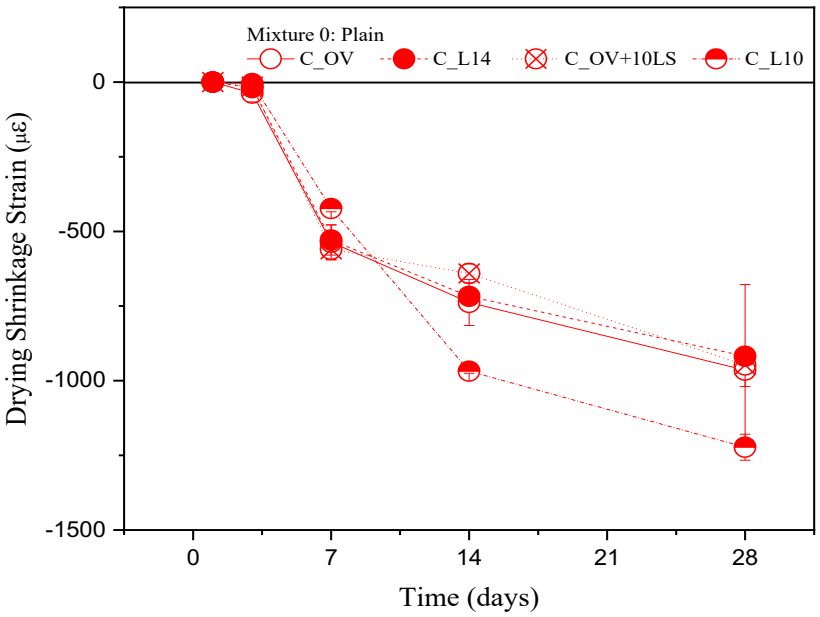

3756

3757 **Figure C-21-13. Drying Shrinkage of Cement C – M0**

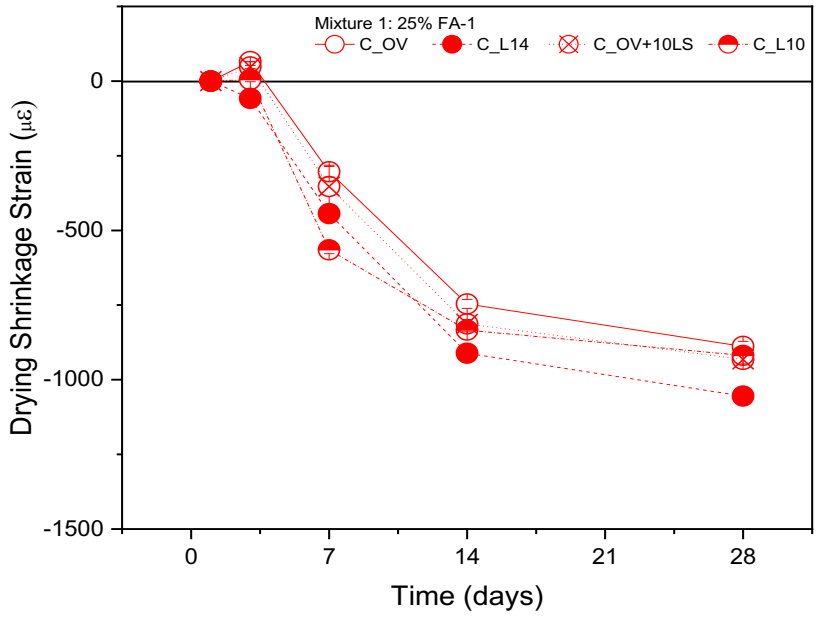

3758

3759 **Figure C-21-14. Drying Shrinkage of Cement C – M1**

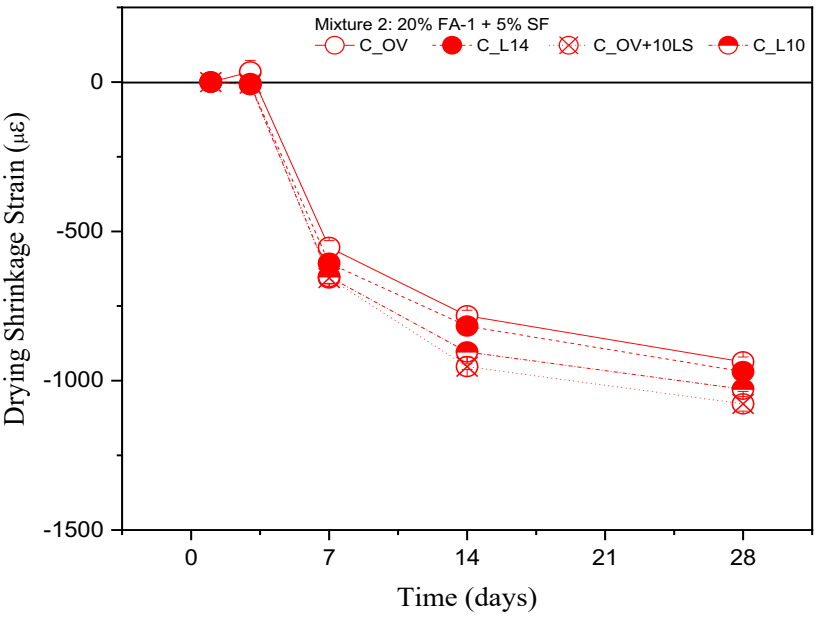

3760

3761 **Figure C-21-15. Drying Shrinkage of Cement C – M2**

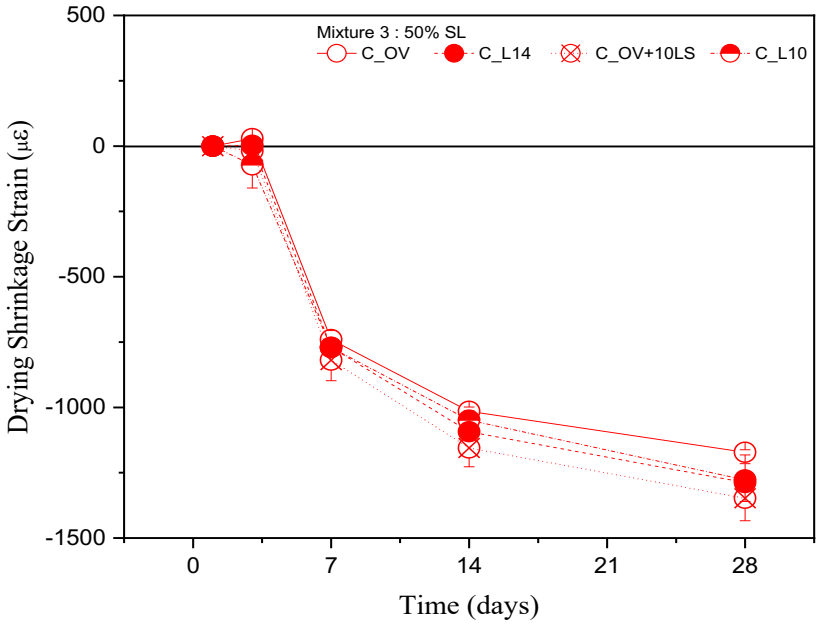

3762

3763 **Figure C-21-16. Drying Shrinkage of Cement C – M3**

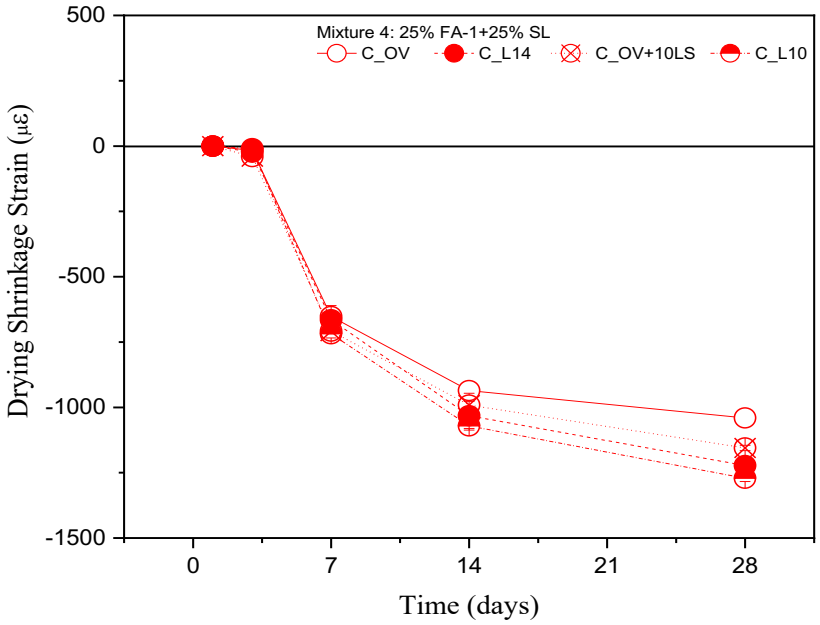

3764

3765 **Figure C-21-17. Drying Shrinkage of Cement C – M4**

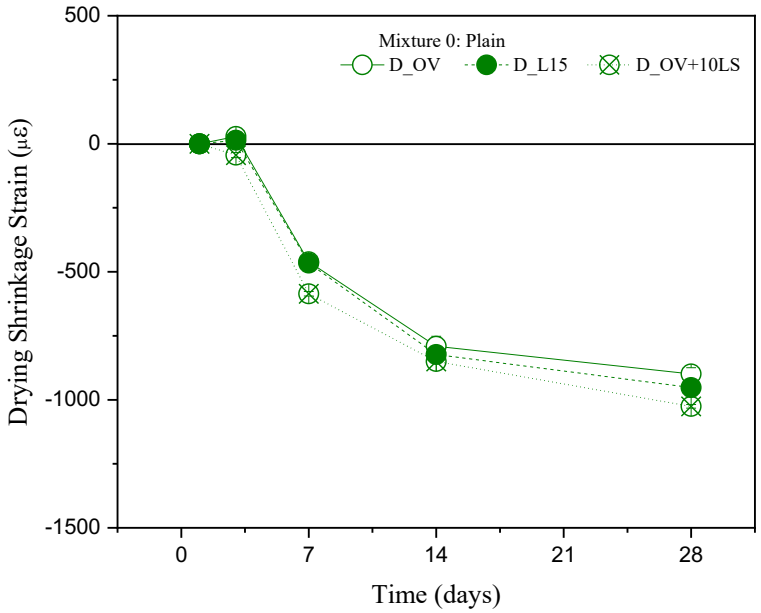

3766

3767 **Figure C-21-18. Drying Shrinkage of Cement D – M0**

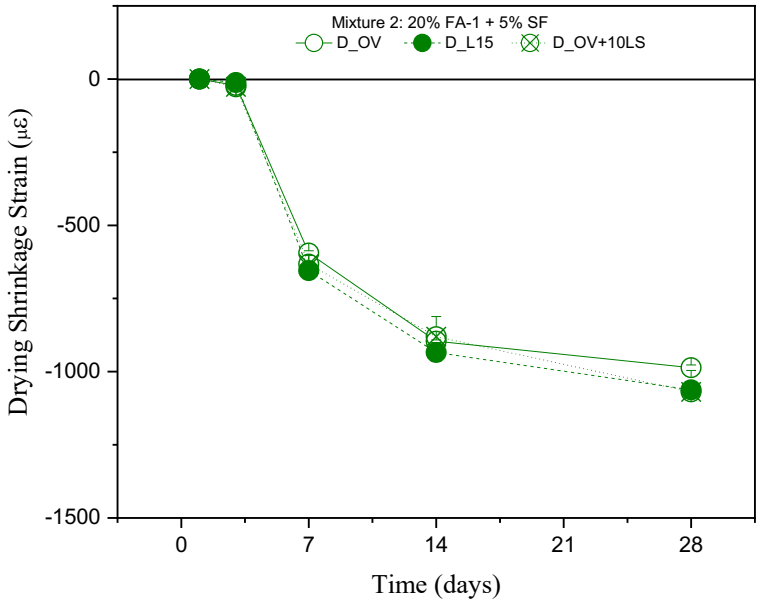

3768

3769 **Figure C-21-19. Drying Shrinkage of Cement D – M1**

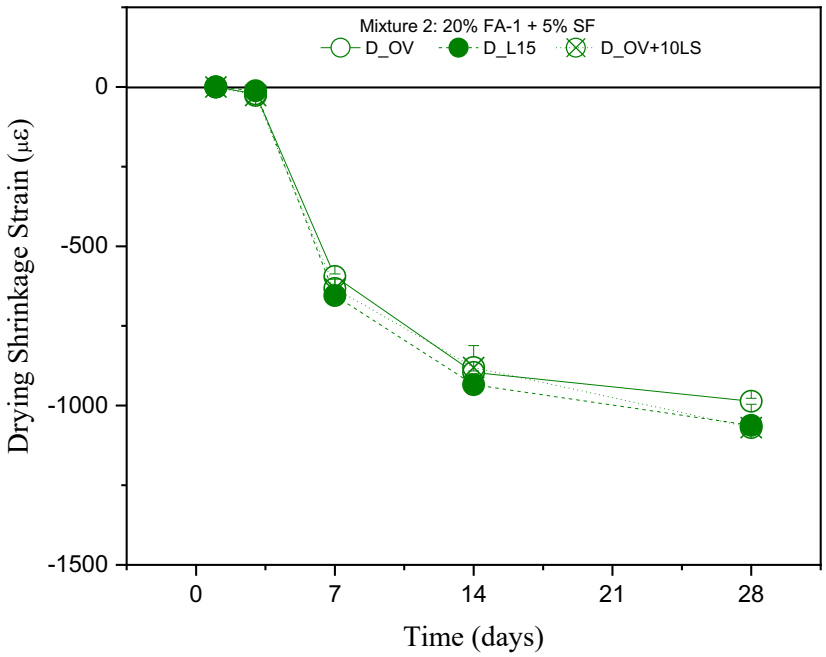

3770

3771 **Figure C-21-20. Drying Shrinkage of Cement D – M2**

3772

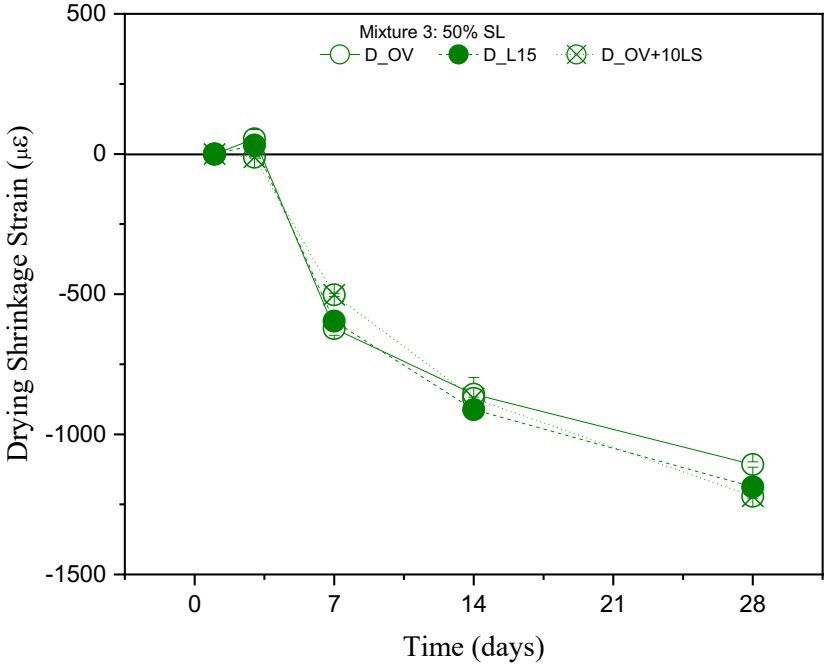

3773

3774 **Figure C-21-21. Drying Shrinkage of Cement D – M3**

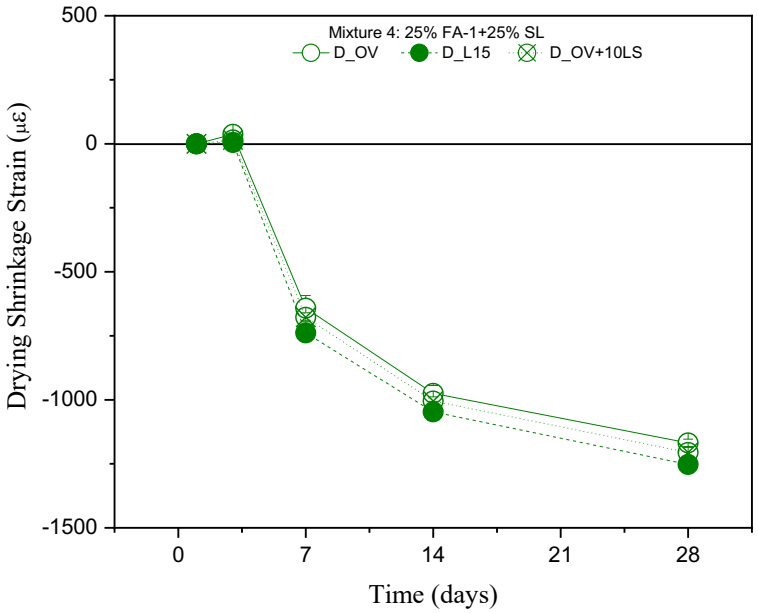

3775

3776 **Figure C-21-22. Drying Shrinkage of Cement D – M4**

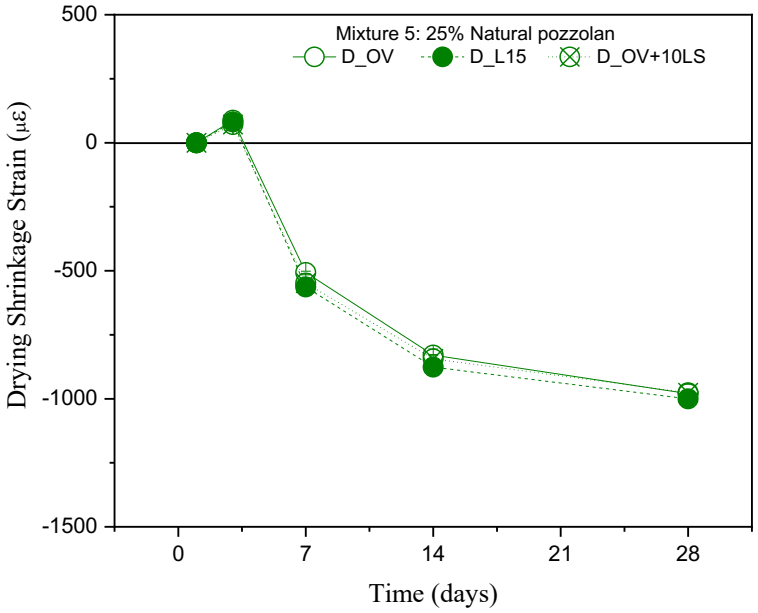

3777

3778 **Figure C-21-23. Drying Shrinkage of Cement D – M5**

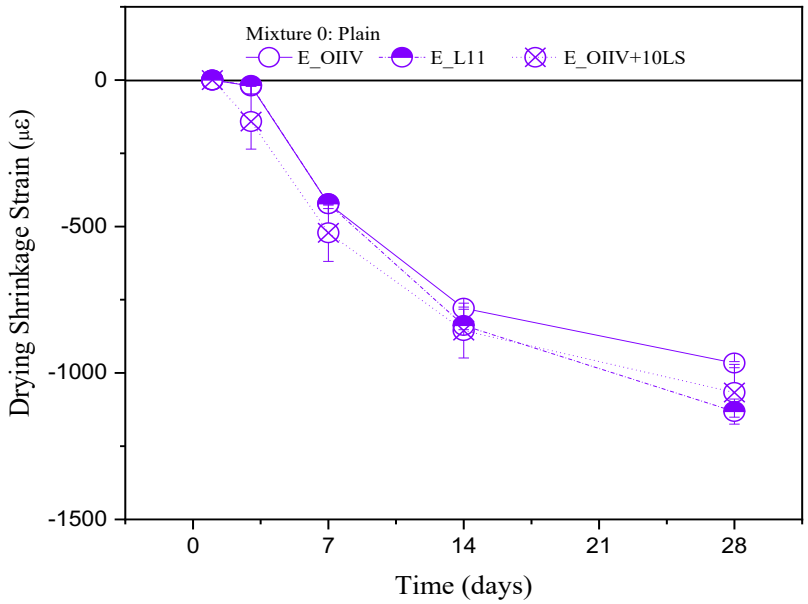

Figure C-21-24. Drying Shrinkage of Cement E – M0

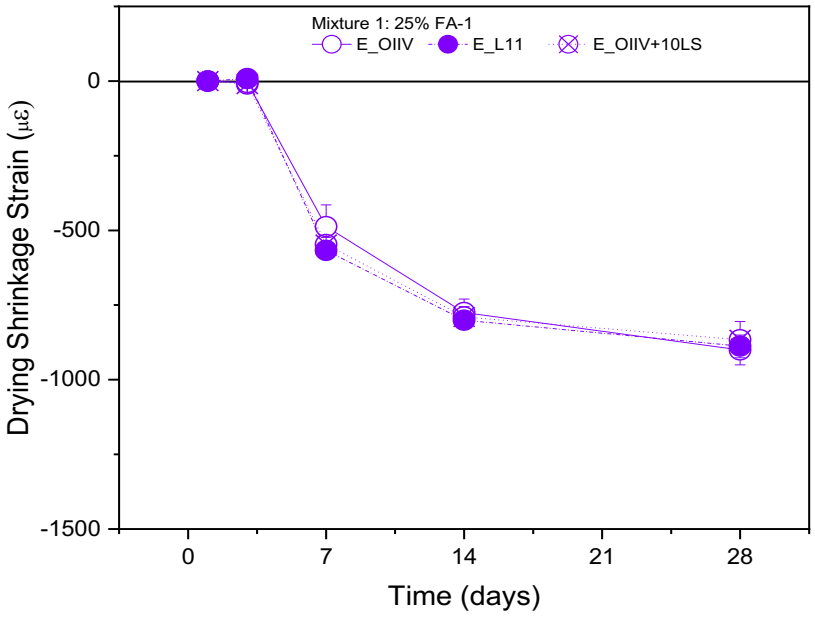

Figure C-21-25. Drying Shrinkage of Cement E – M1

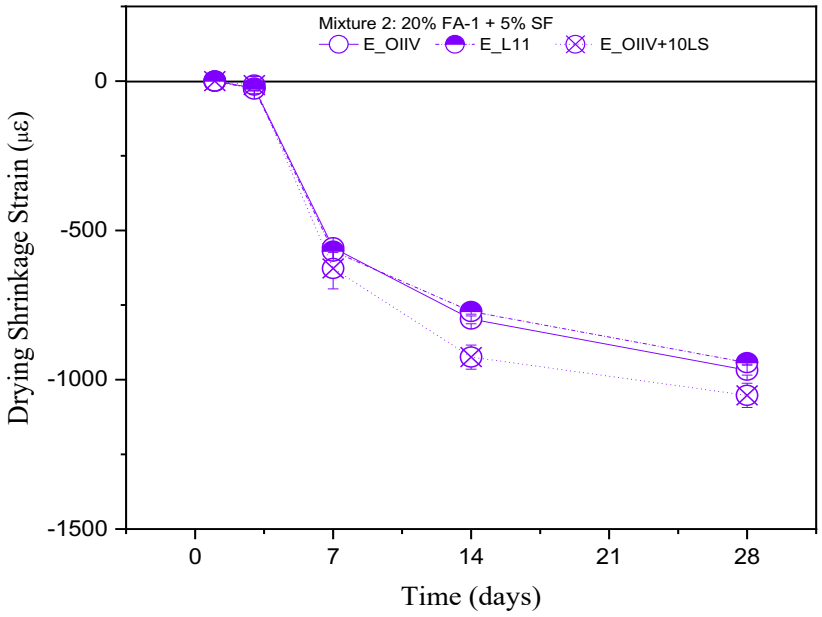

3783

3784 **Figure C-21-26. Drying Shrinkage of Cement E – M2**

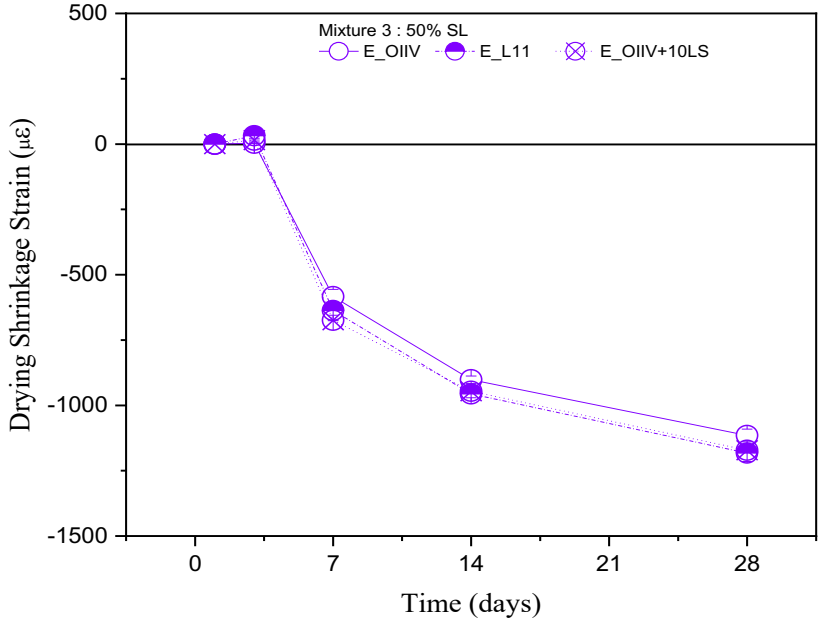

3785

3786 **Figure C-21-27. Drying Shrinkage of Cement E – M3**

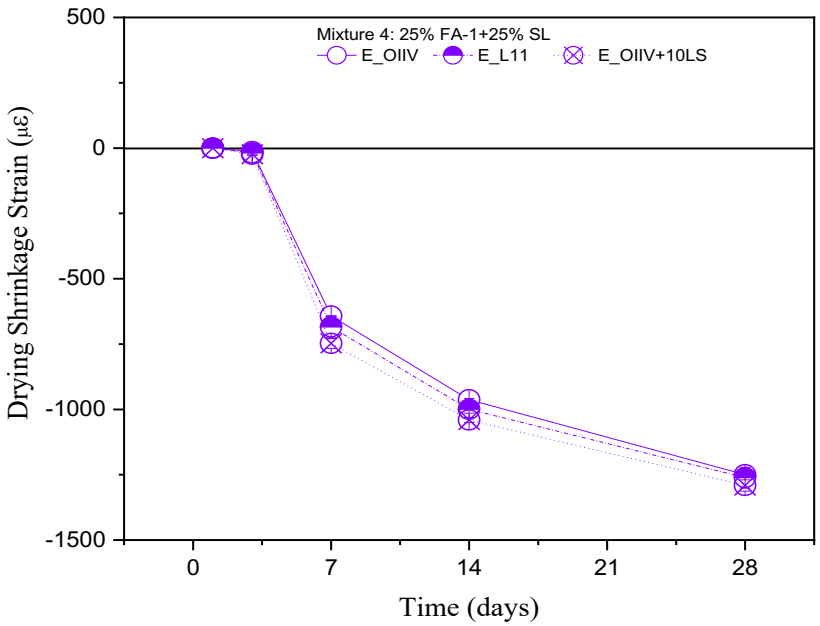

3787

3788 **Figure C-21-28. Drying Shrinkage of Cement E – M4**

22 APPENDIX D - Flexural Strength Results

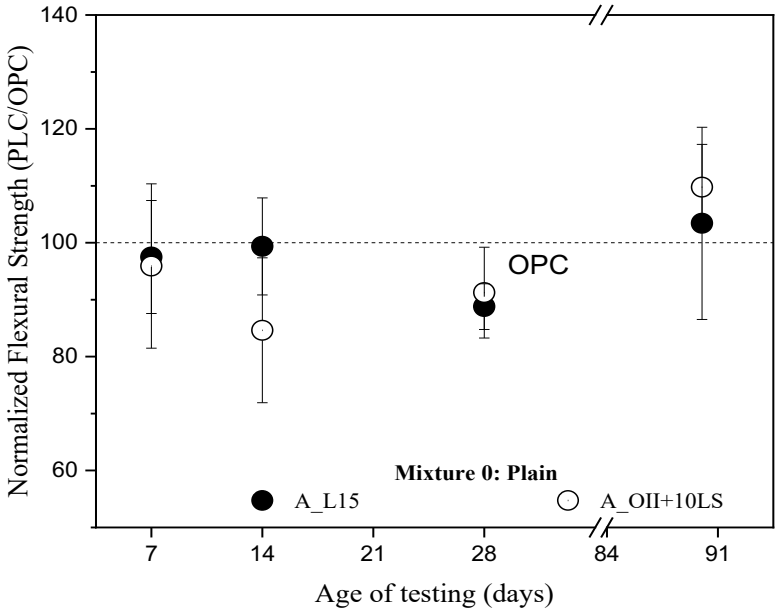

Figure D-22-1. Flexural Strength of Cement A – M0

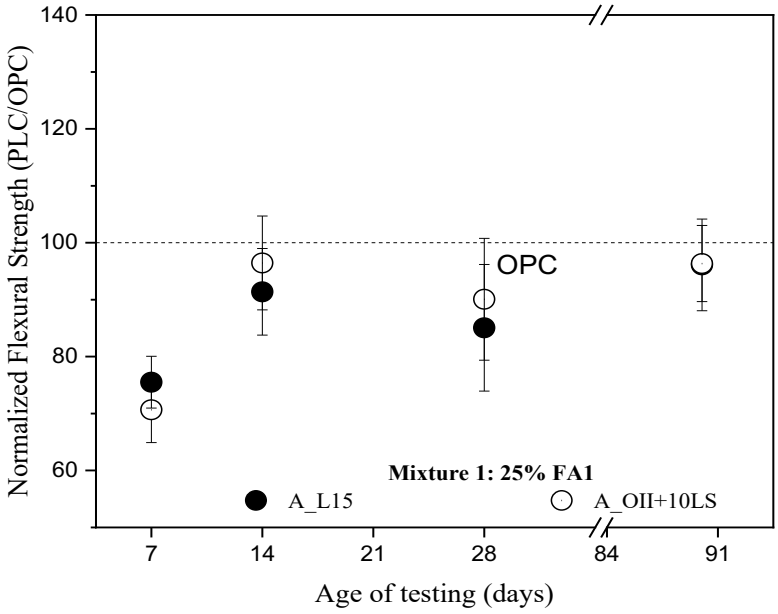

Figure D-22-2. Flexural Strength of Cement A – M1

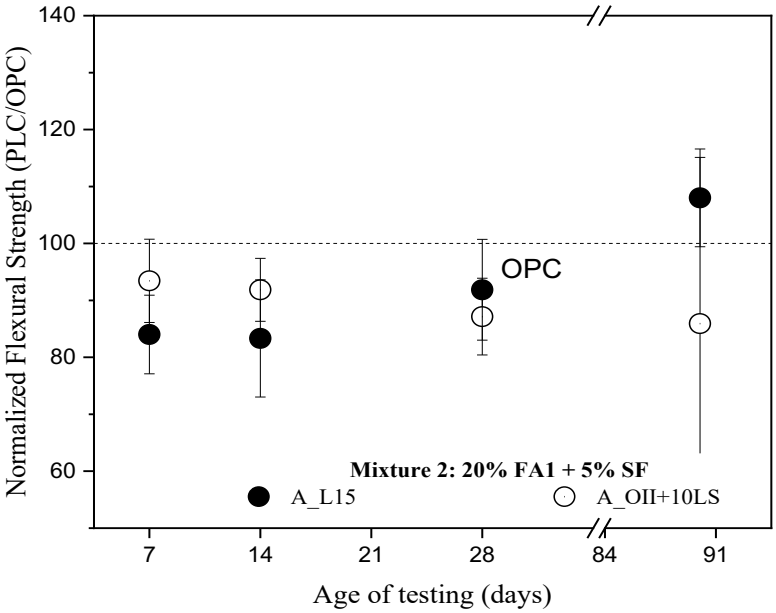

3794

3795 **Figure D-22-3. Flexural Strength of Cement A – M2**

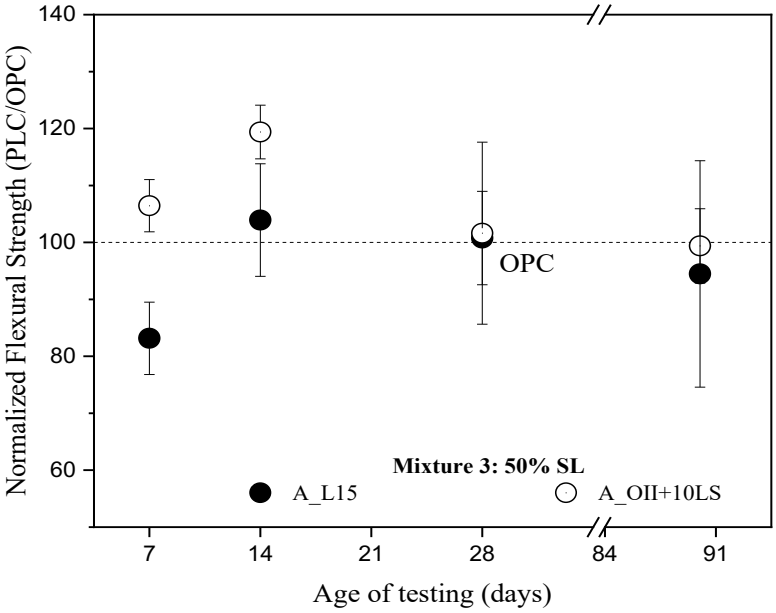

3796

3797 **Figure D-22-4. Flexural Strength of Cement A – M3**

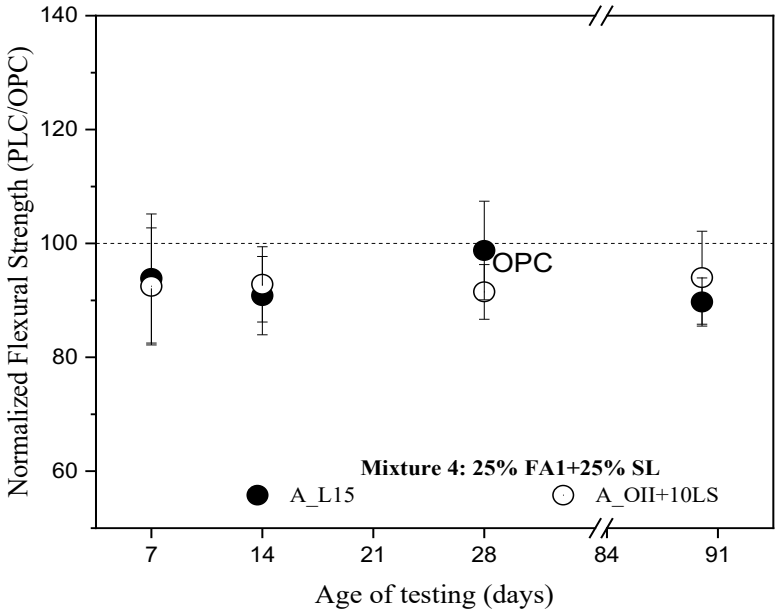

3798

3799 **Figure D-22-5. Flexural Strength of Cement A – M4**

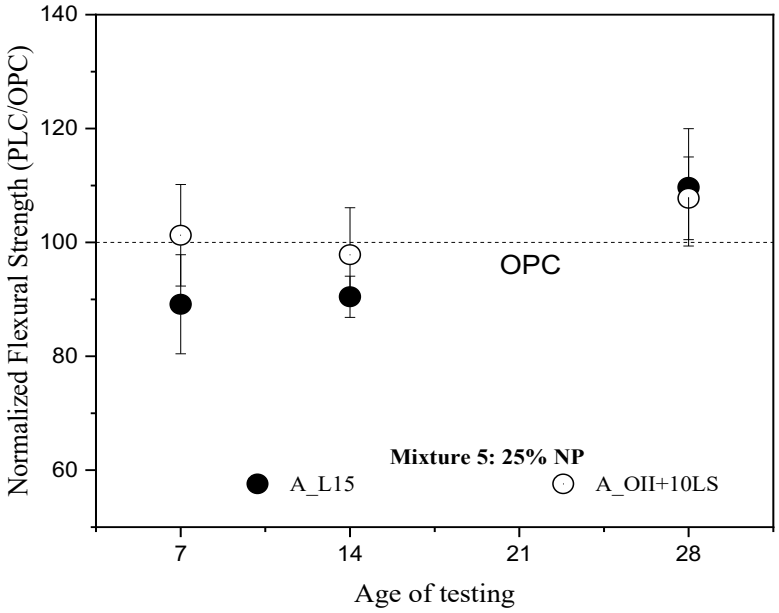

3800

3801 **Figure D-22-6. Flexural Strength of Cement A – M5**

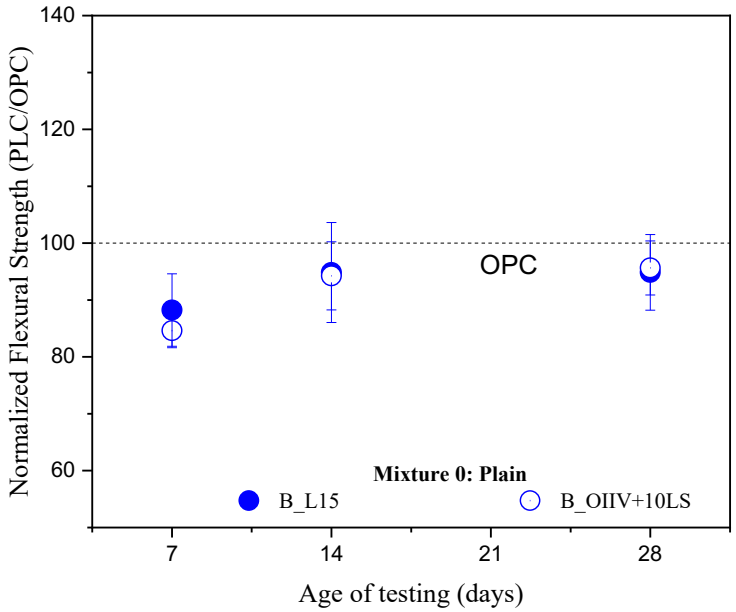

3802

3803 **Figure D-22-7. Flexural Strength of Cement B – M0**

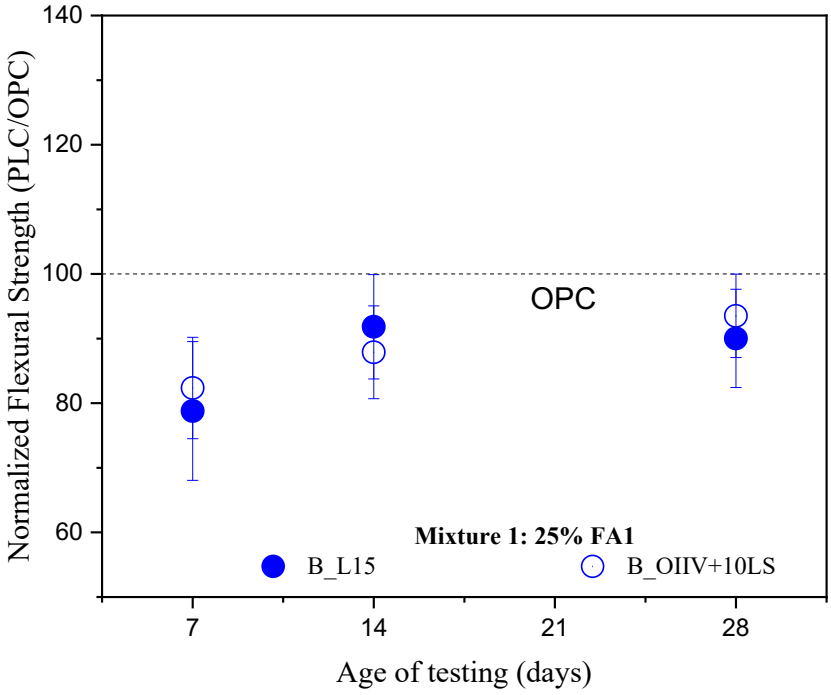

3804

3805 **Figure D-22-8. Flexural Strength of Cement B – M1**

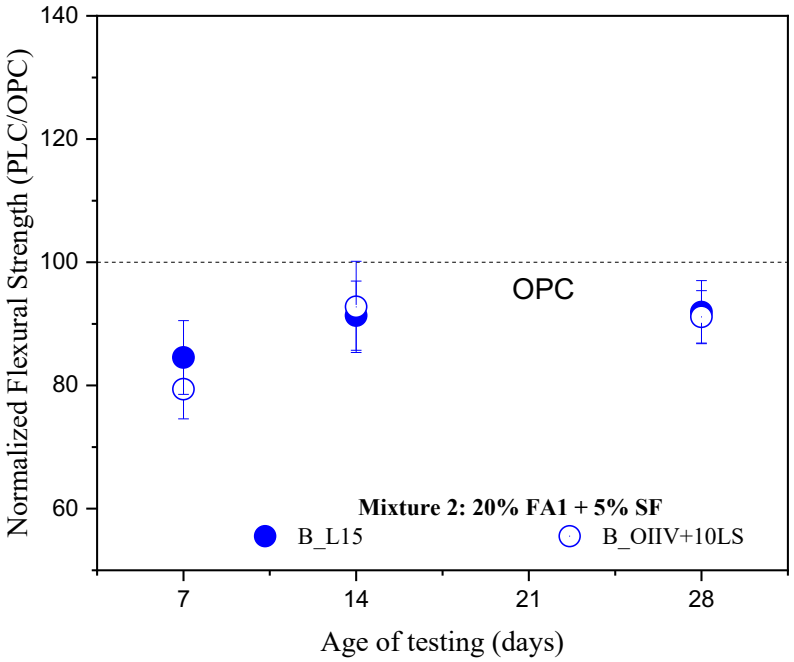

3806

3807 **Figure D-22-9. Flexural Strength of Cement B – M2**

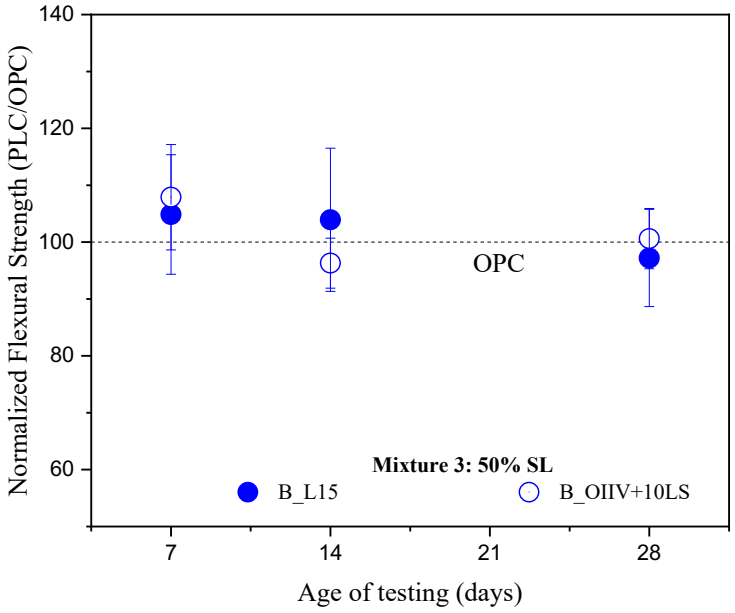

3808

3809 **Figure D-22-10. Flexural Strength of Cement B – M3**

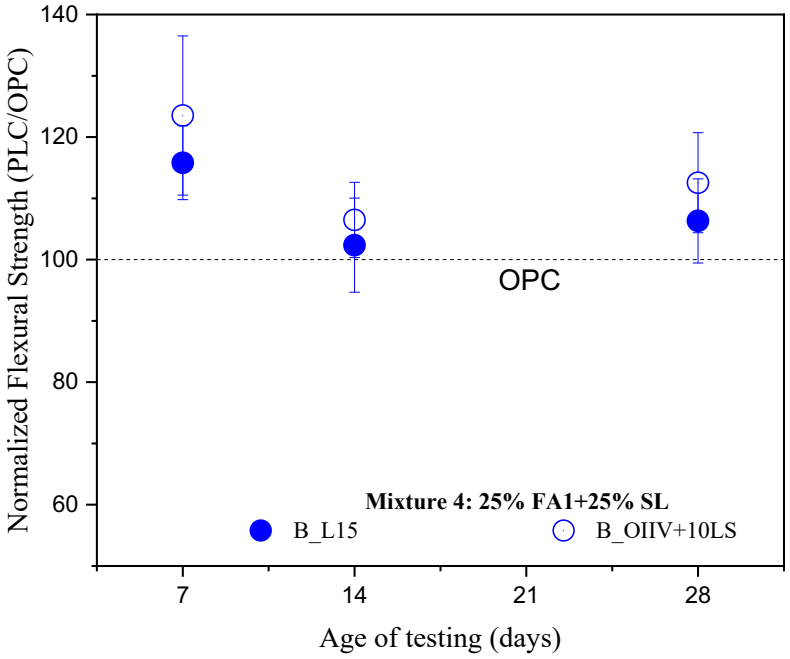

3810

3811 **Figure D-22-11. Flexural Strength of Cement B – M4**

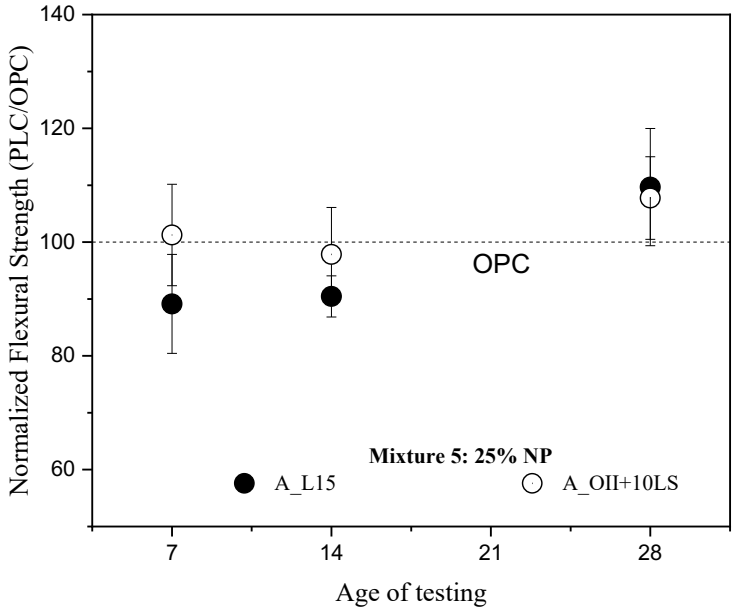

3812

3813 **Figure D-22-12. Flexural Strength of Cement B – M5**

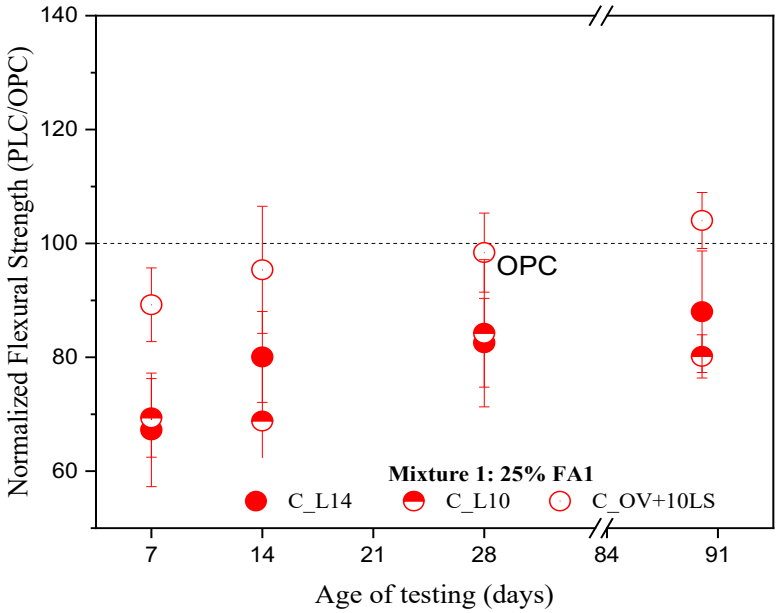

3814

3815 **Figure D-22-13. Flexural Strength of Cement C – M0**

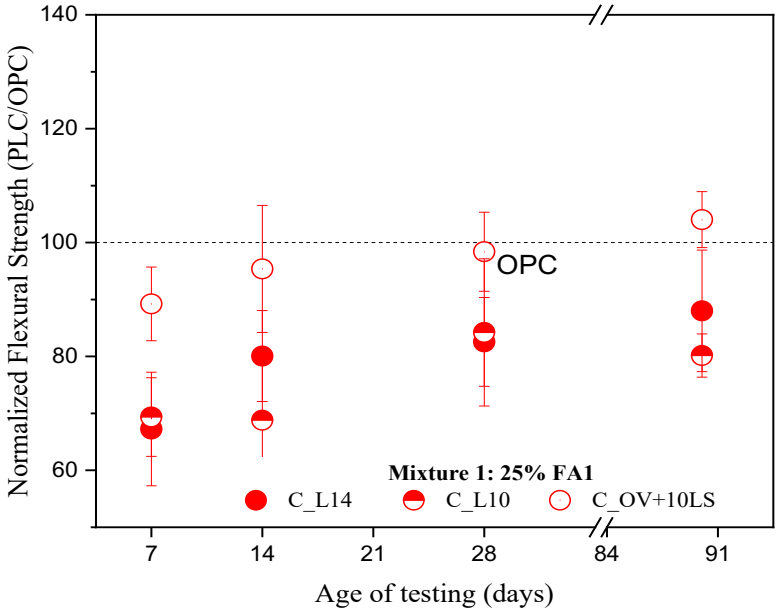

3816

3817 **Figure D-22-14. Flexural Strength of Cement C – M1**

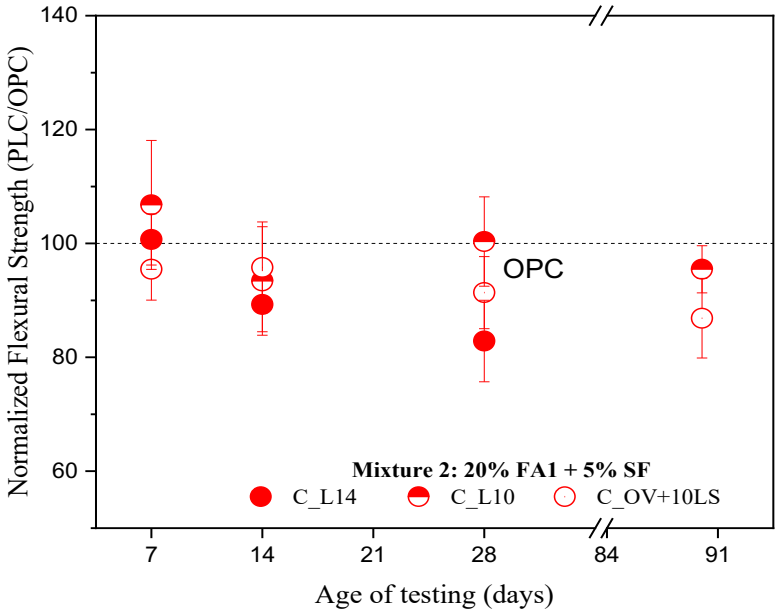

3818

3819 **Figure D-22-15. Flexural Strength of Cement C – M2**

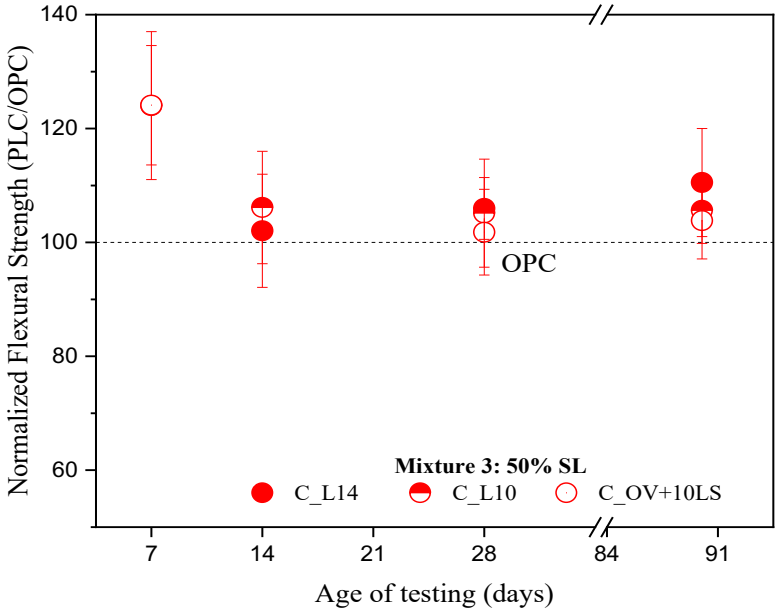

3820

3821 **Figure D-22-16. Flexural Strength of Cement C – M3**

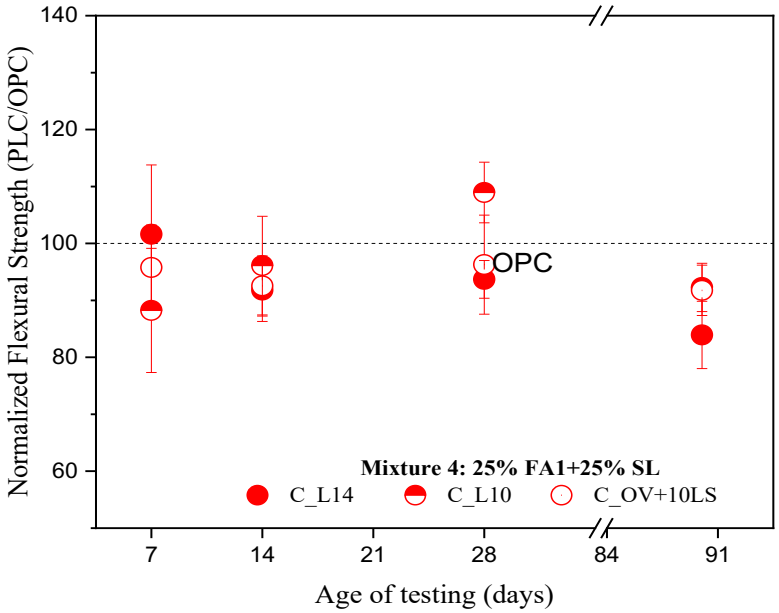

3822

3823 **Figure D-22-17. Flexural Strength of Cement C – M4**

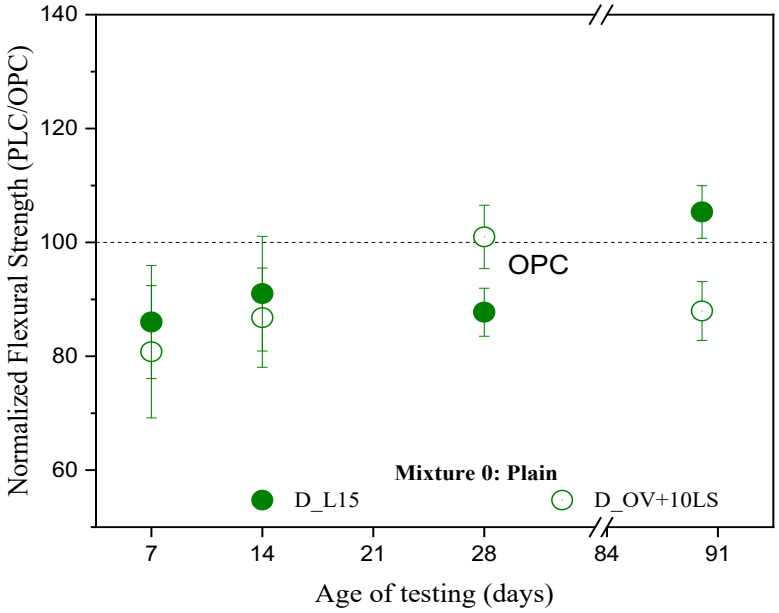

3824

3825 **Figure D-22-18. Flexural Strength of Cement D – M0**

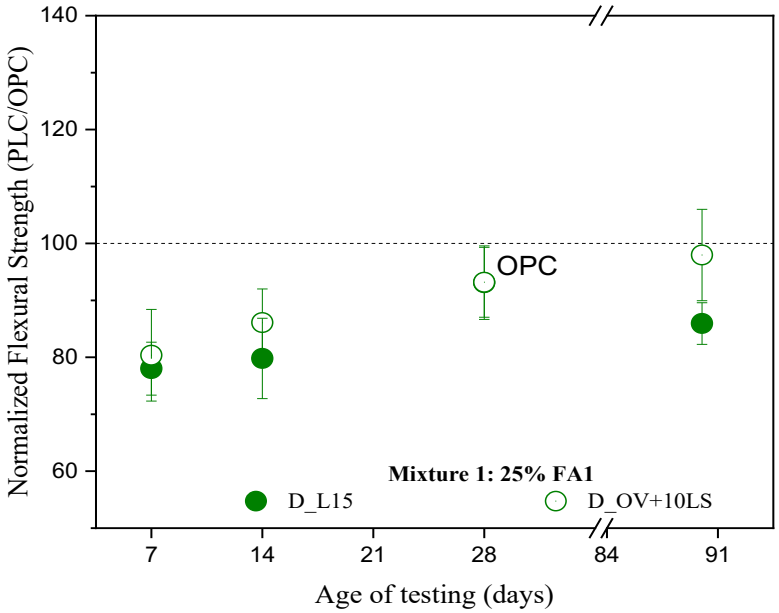

3826

3827 **Figure D-22-19. Flexural Strength of Cement D – M1**

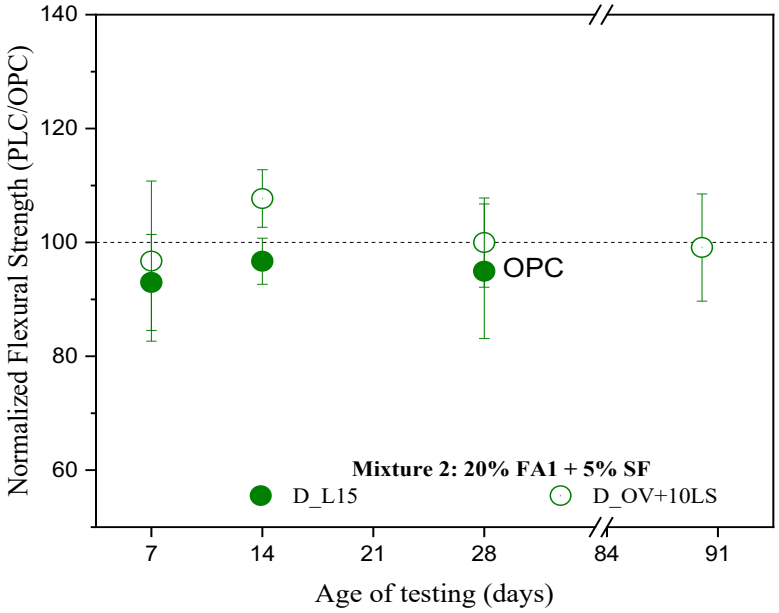

3828

3829 **Figure D-22-20. Flexural Strength of Cement D – M2**

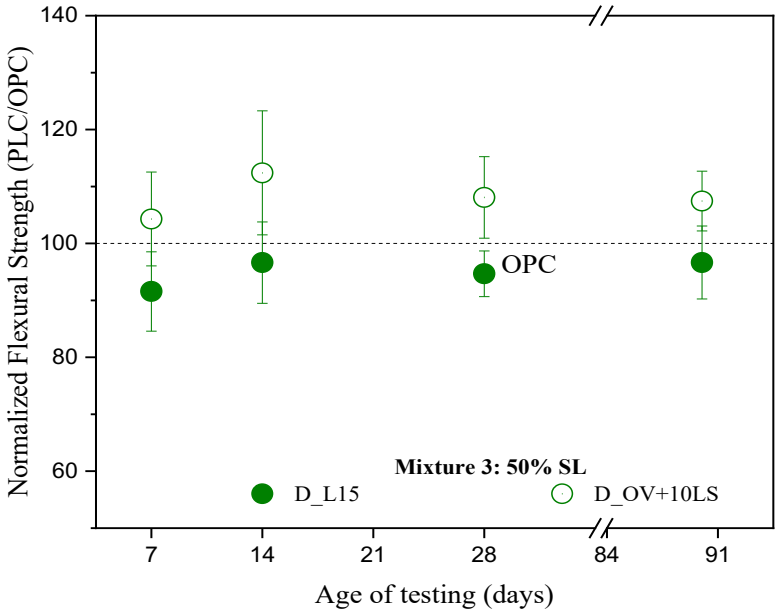

3830

3831 **Figure D-22-21. Flexural Strength of Cement D – M3**

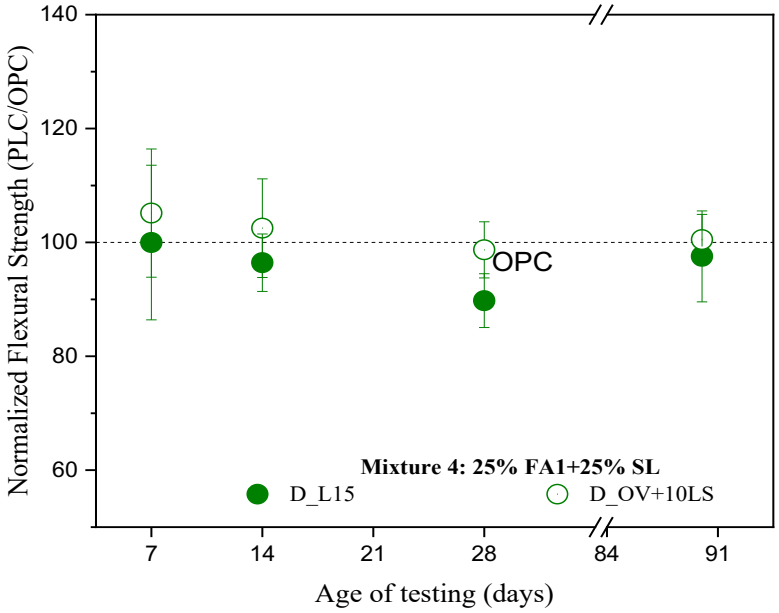

3832

3833 **Figure D-22-22. Flexural Strength of Cement D – M4**

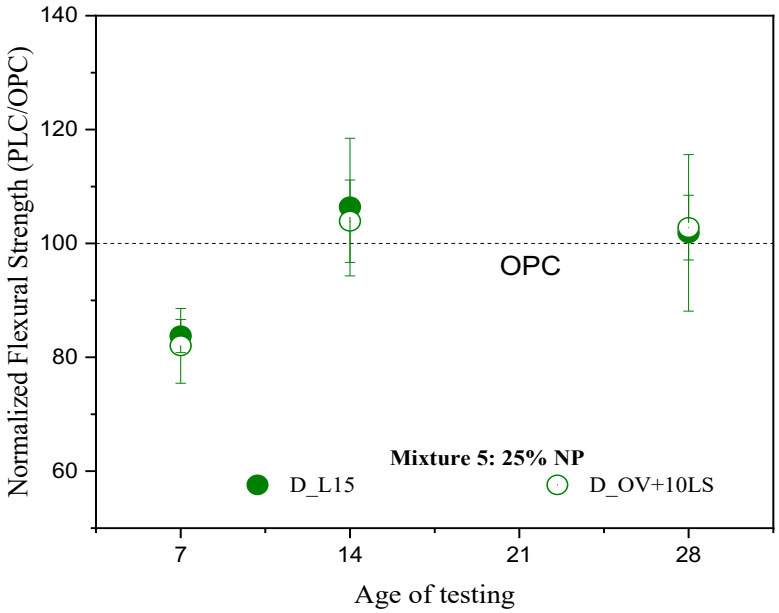

3834

3835 **Figure D-22-23. Flexural Strength of Cement D – M5**

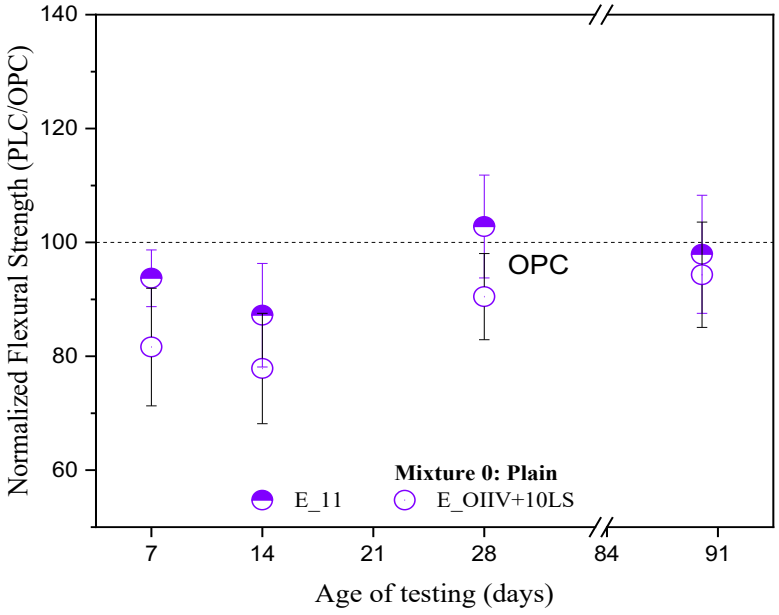

3836

3837 **Figure D-22-24. Flexural Strength of Cement E – M0**

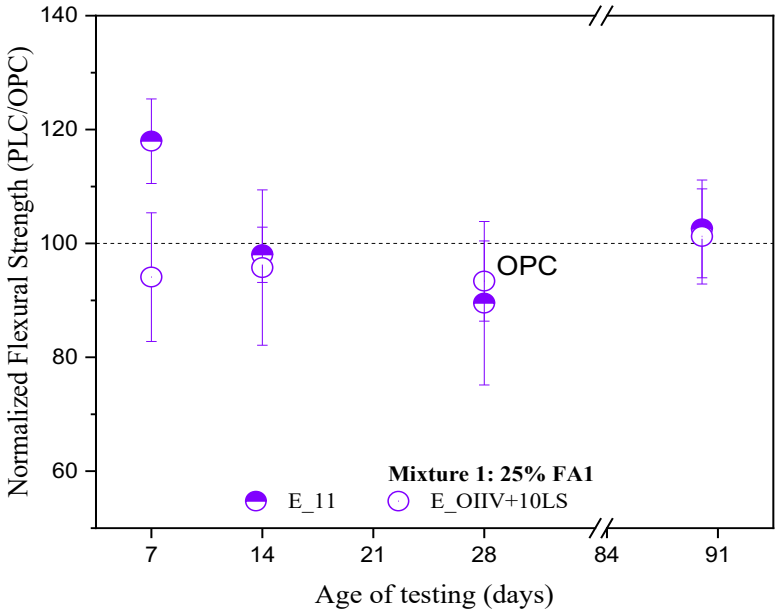

3838

3839 **Figure D-22-25. Flexural Strength of Cement E – M1**

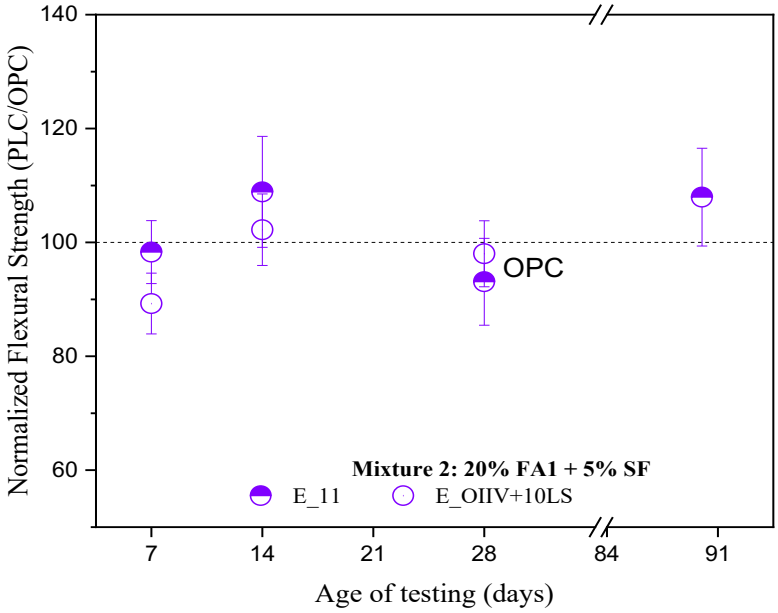

3840

3841 **Figure D-22-26. Flexural Strength of Cement E – M2**

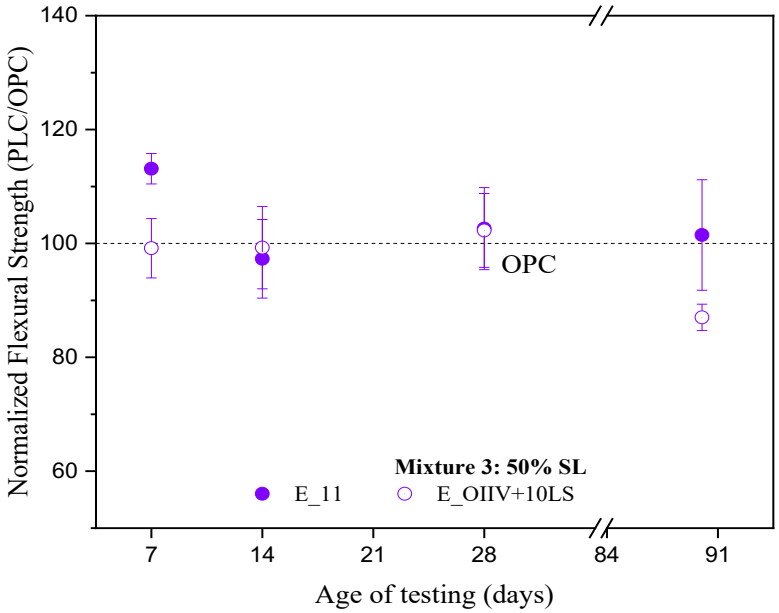

3842

3843 **Figure D-22-27. Flexural Strength of Cement E – M3**

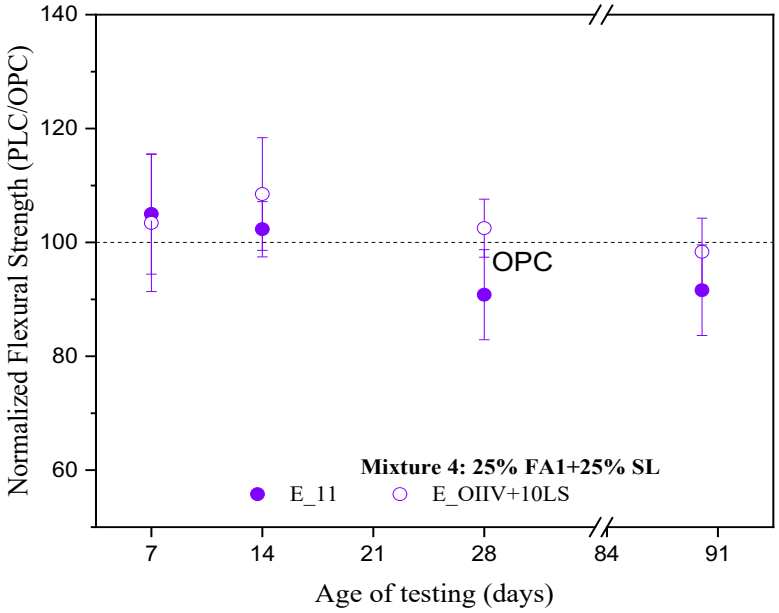

3844

3845 **Figure D-22-28. Flexural Strength of Cement E – Mixture**

3846

23 APPENDIX E – Transport Properties Results

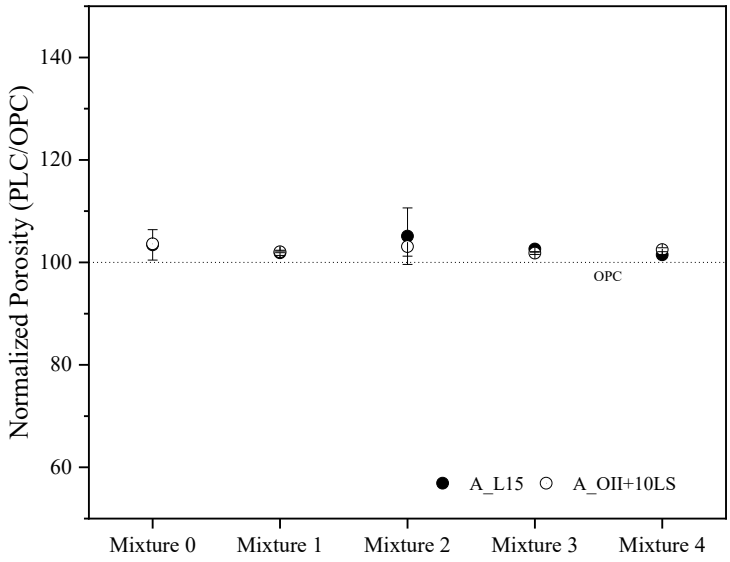

Figure E-23-1. Porosity of Cement A

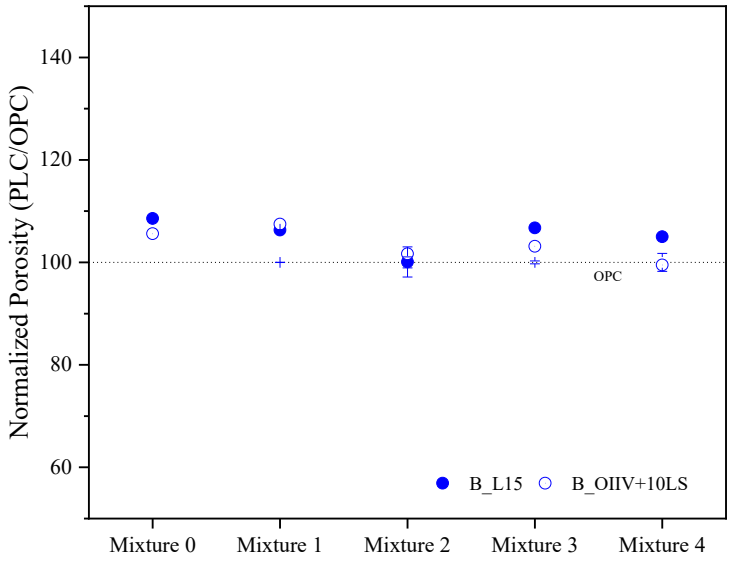

Figure E-23-2. Porosity of Cement B

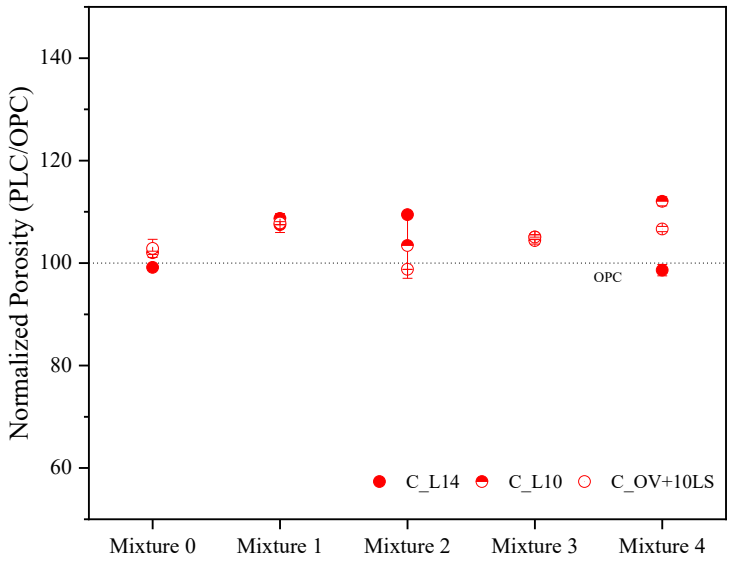

3852

3853 **Figure E-23-3. Porosity of Cement C**

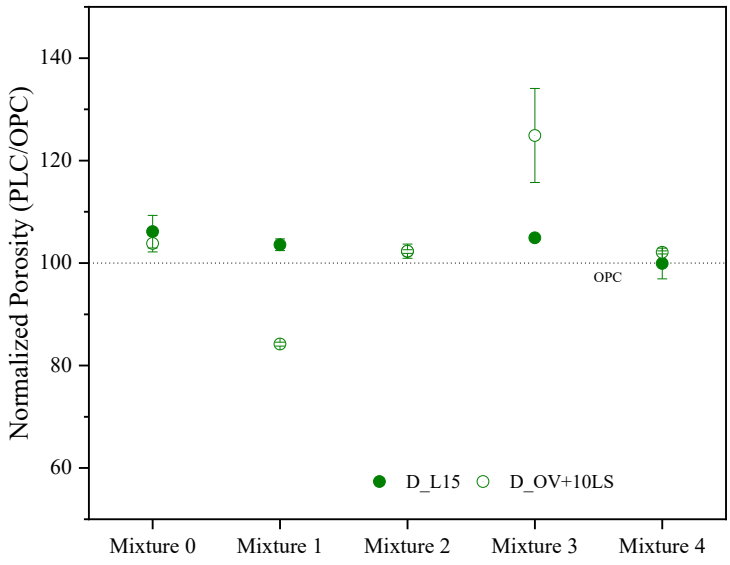

3854

3855 **Figure E-23-4. Porosity of Cement D**

3856

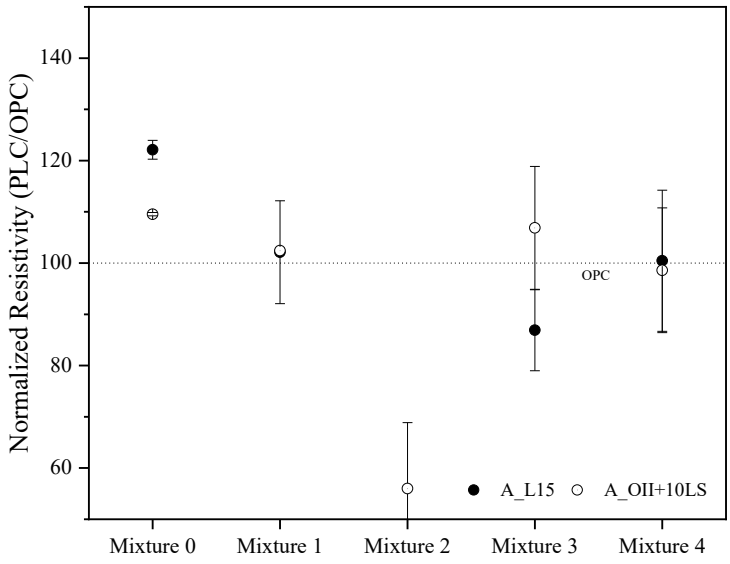

3857

3858 **Figure E-23-5. Electrical resistivity of Cement A**

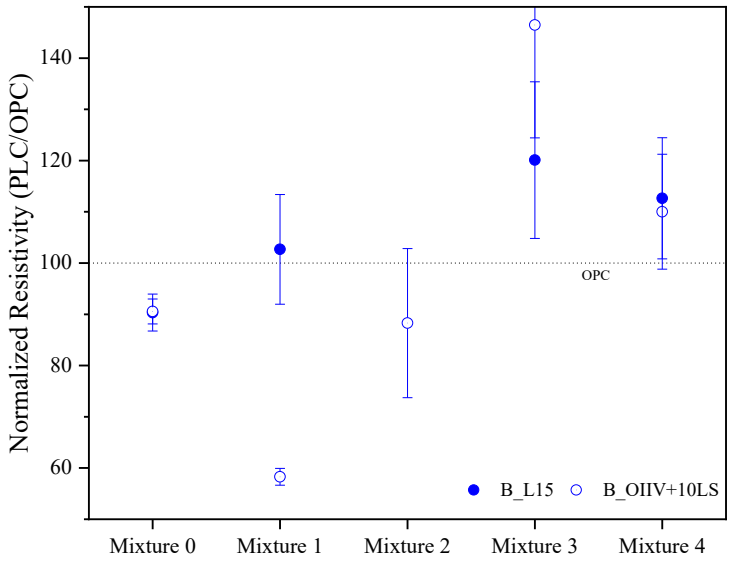

3859

3860 **Figure E-23-6. Electrical resistivity of Cement B**

3861

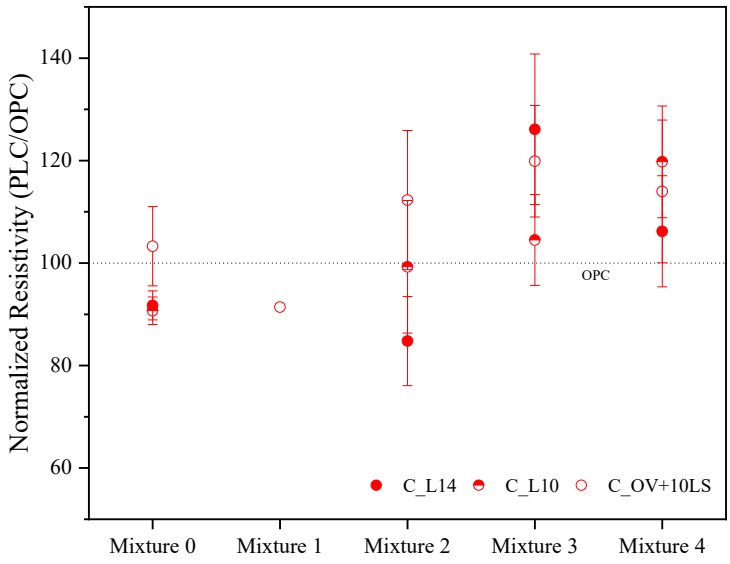

3862

3863 **Figure E-23-7. Electrical resistivity of Cement C**

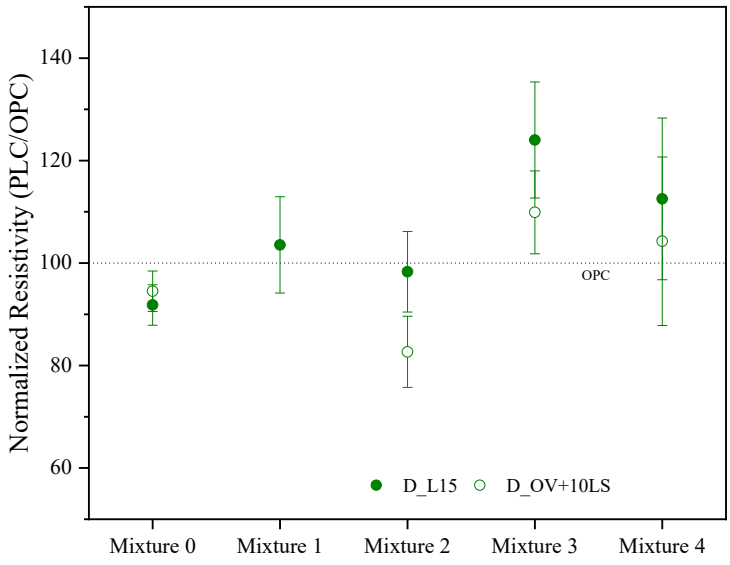

3864

3865 **Figure E-23-8. Electrical resistivity of Cement D**

3866

24 APPENDIX F – Chloride Binding Results

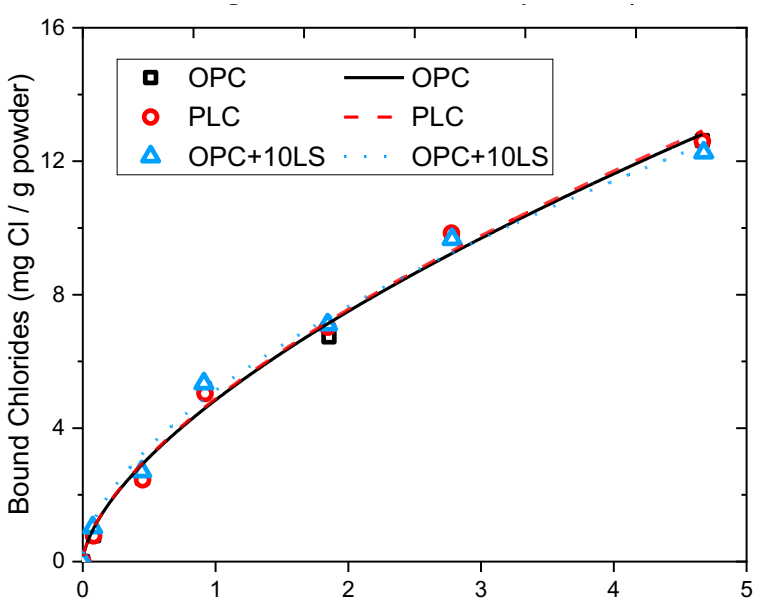

Figure F-24-1 : Binding Isotherm of Cement A – M0 (NaCl)

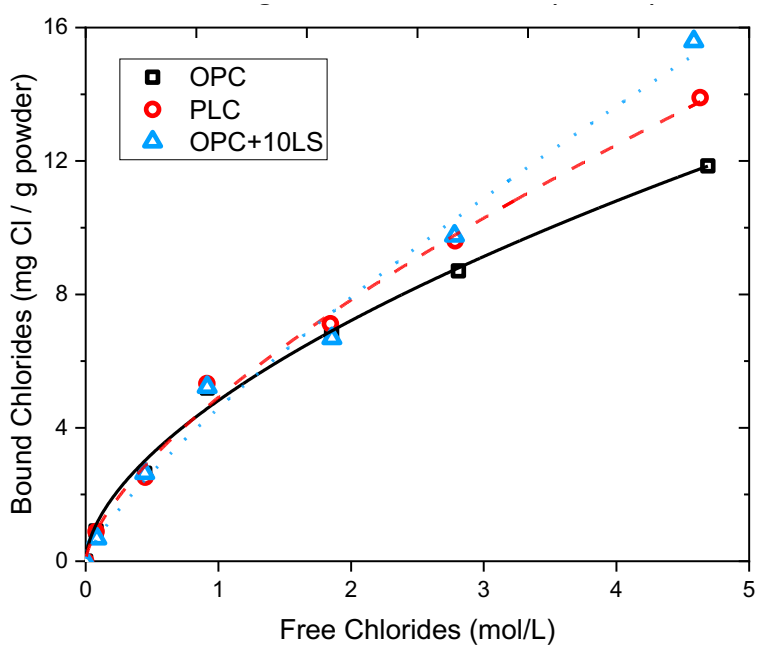

Figure F-24-2. Binding Isotherm of Cement A – M1 (NaCl)

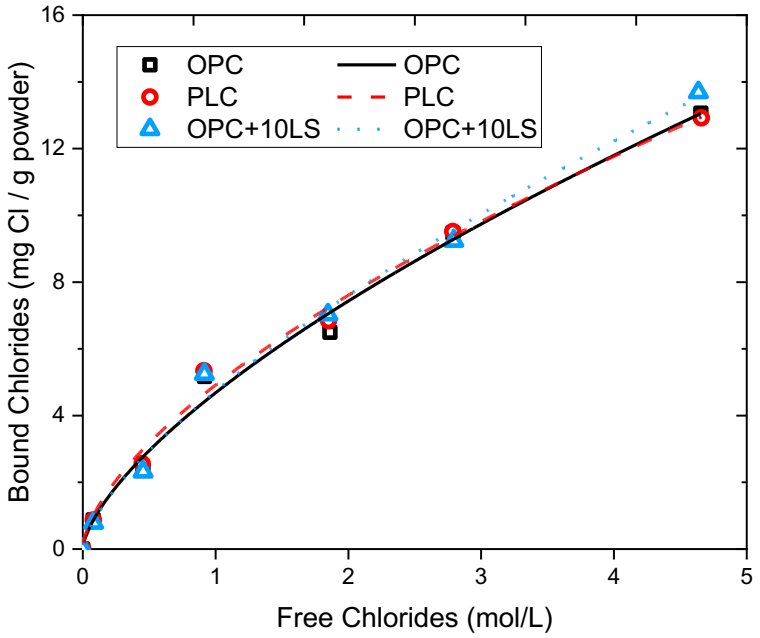

Figure F-24-3. Binding Isotherm of Cement A – M2 (NaCl)

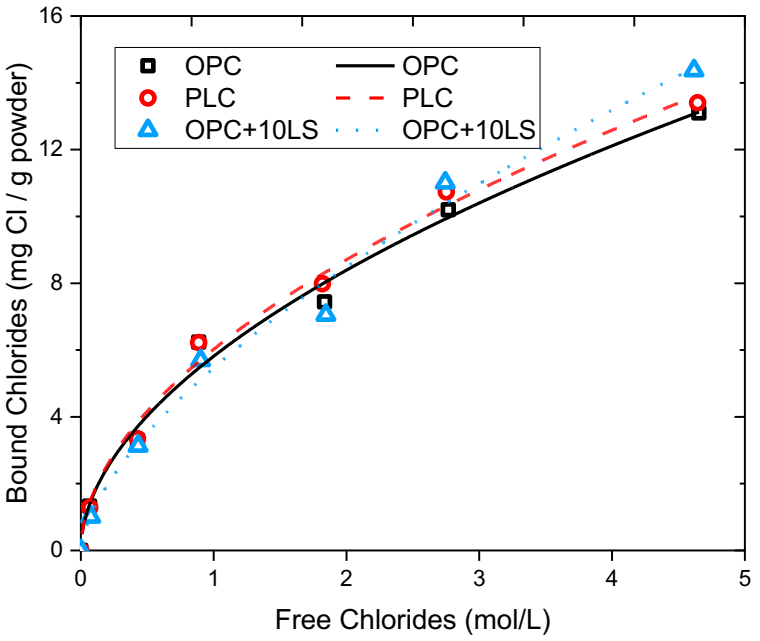

Figure F-24-4. Binding Isotherm of Cement A – M3 (NaCl)

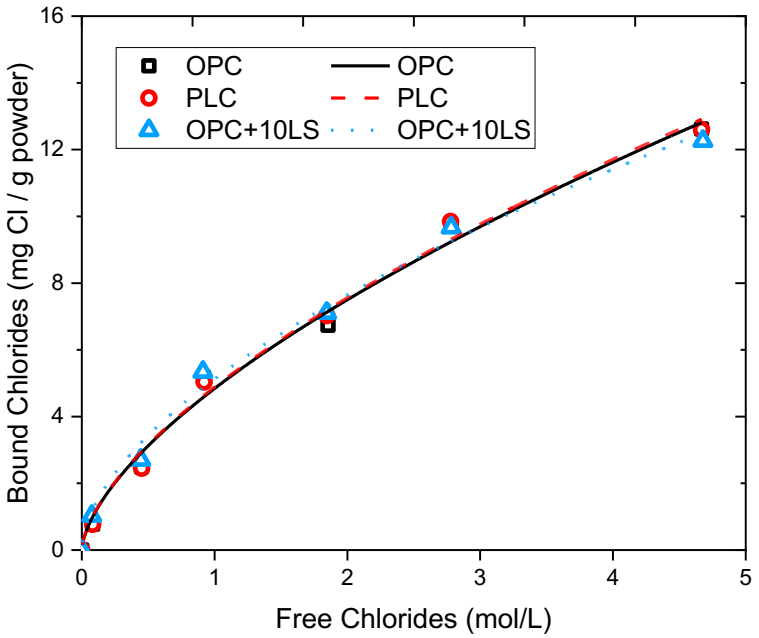

Figure F-24-5. Binding Isotherm of Cement A – M4 (NaCl)

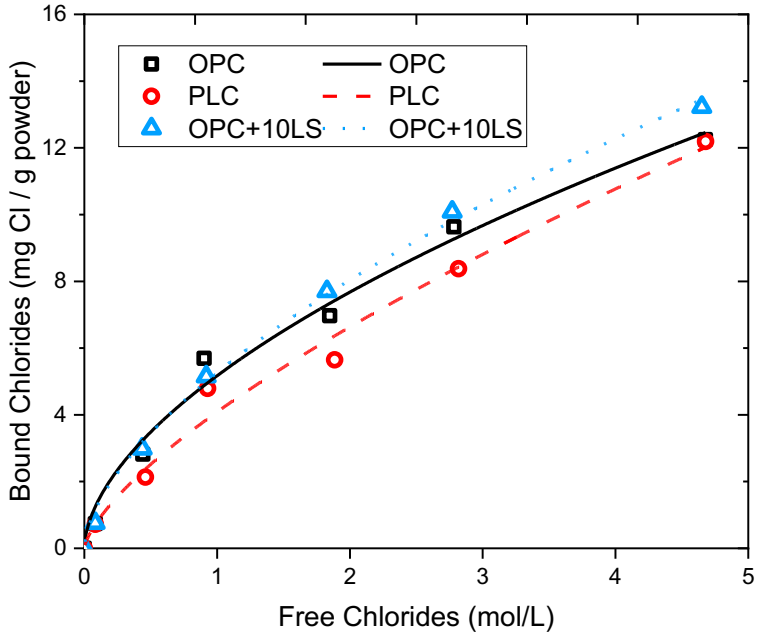

Figure F-24-6. Binding Isotherm of Cement A – M5 (NaCl)

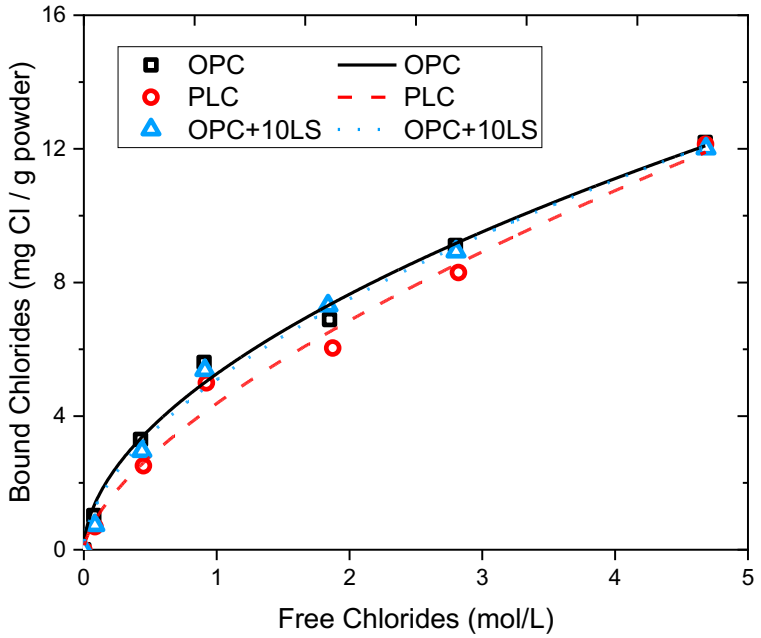

3884

3885 **Figure F-24-7. Binding Isotherm of Cement B – M0 (NaCl)**

3886

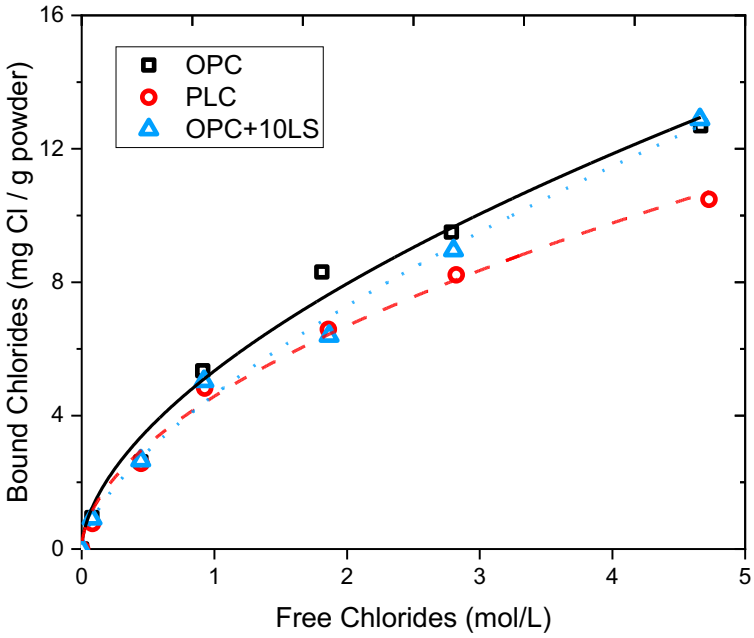

3887

3888 **Figure F-24-8. Binding Isotherm of Cement B – M1 (NaCl)**

3889

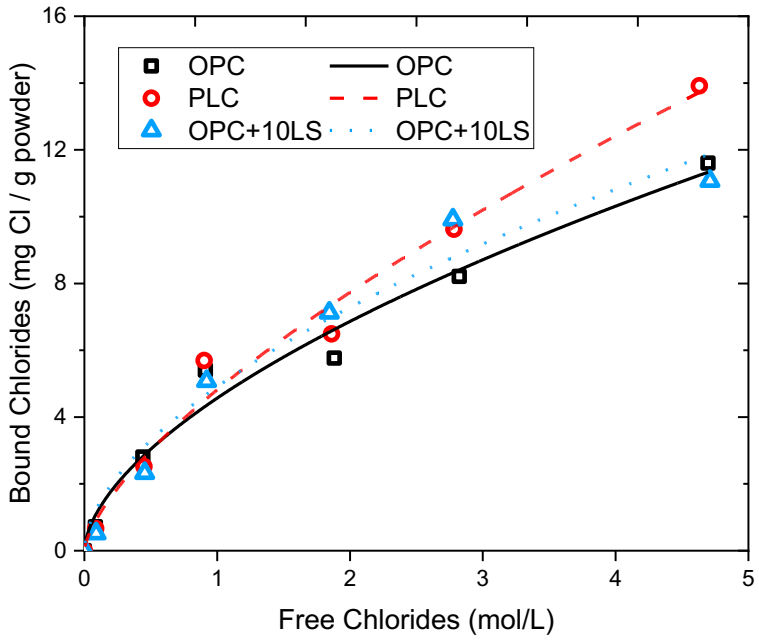

Figure F-24-9. Binding Isotherm of Cement B – M2 (NaCl)

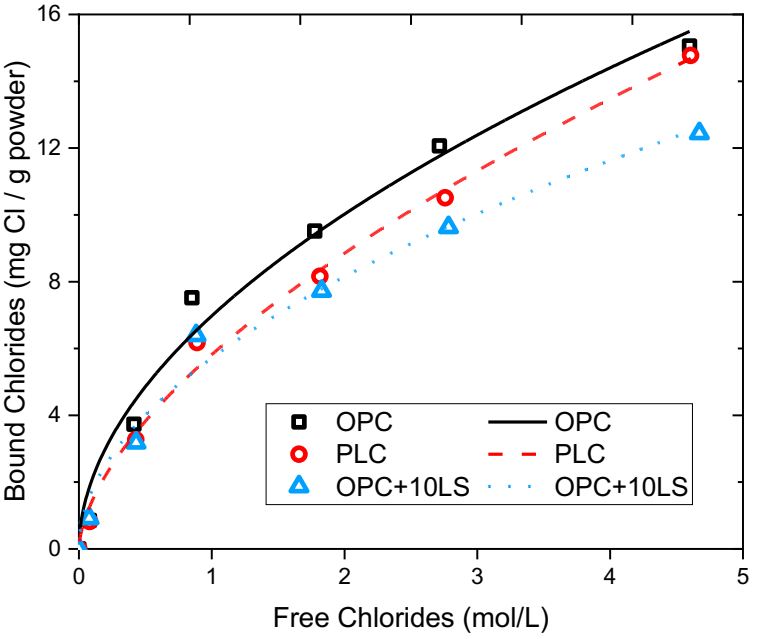

Figure F-24-10. Binding Isotherm of Cement B – M3 (NaCl)

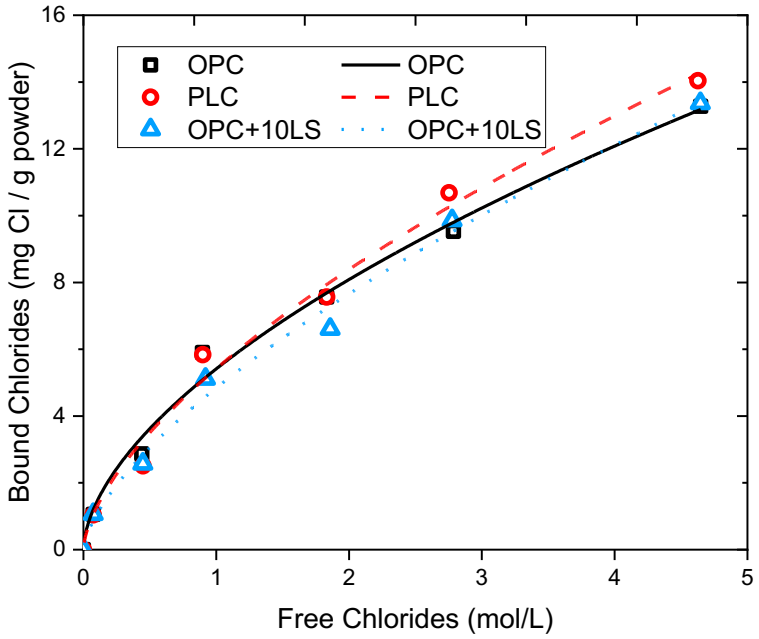

Figure F-24-11. Binding Isotherm of Cement B – M4 (NaCl)

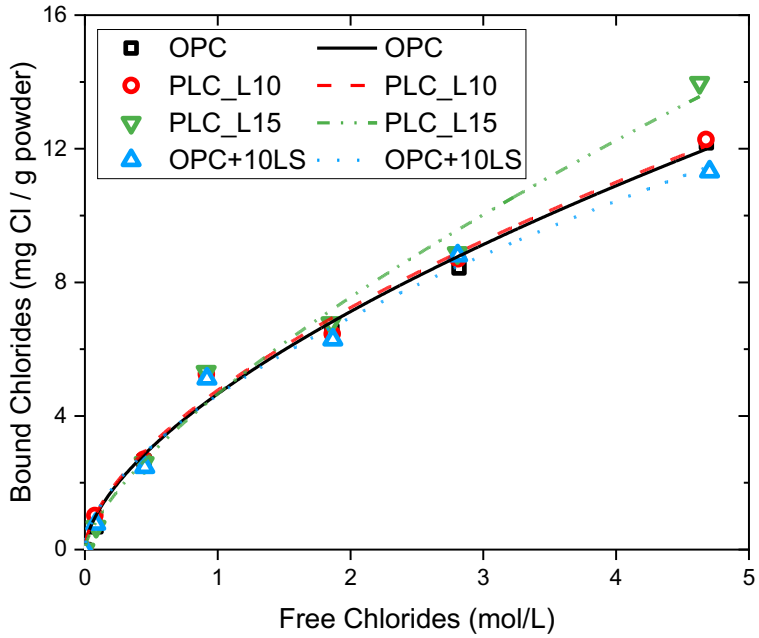

Figure F-24-12. Binding Isotherm of Cement C – M0 (NaCl)

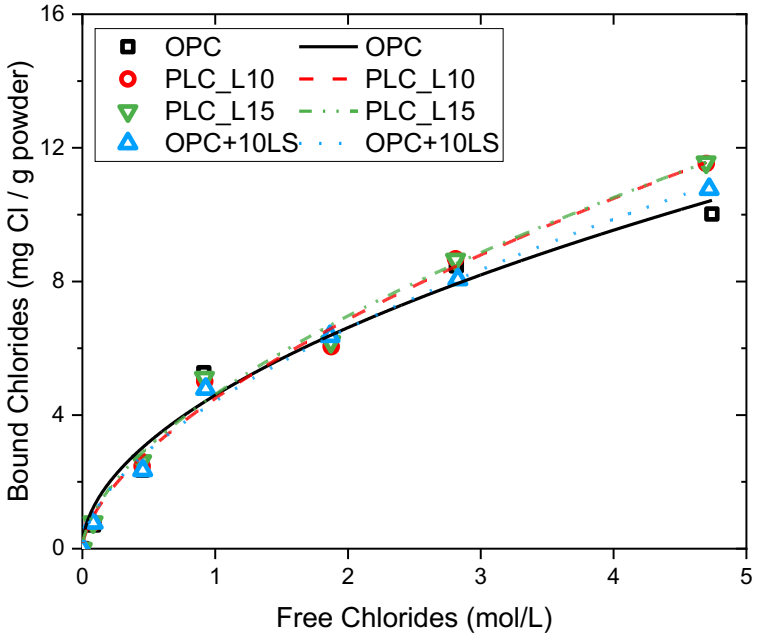

3901

3902 **Figure F-24-13. Binding Isotherm of Cement C – M1 (NaCl)**

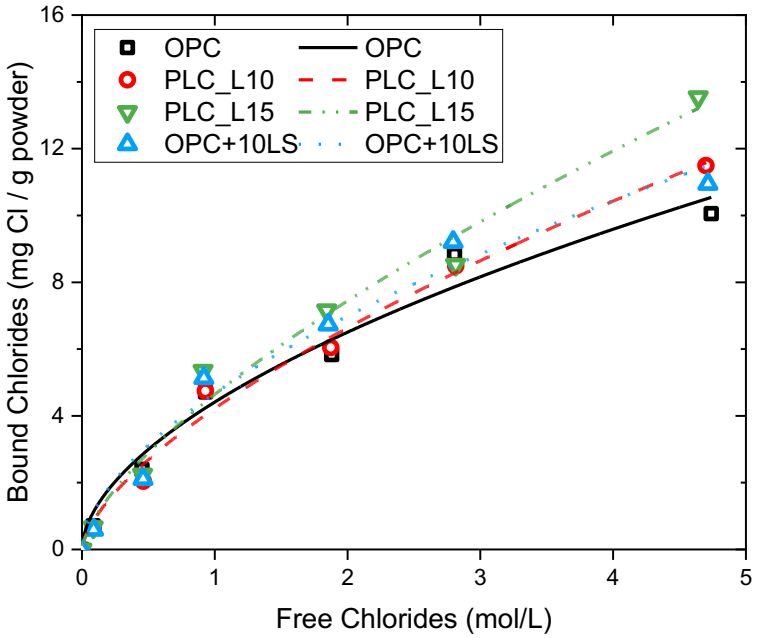

3903

3904 **Figure F-24-14. Binding Isotherm of Cement C – M2 (NaCl)**

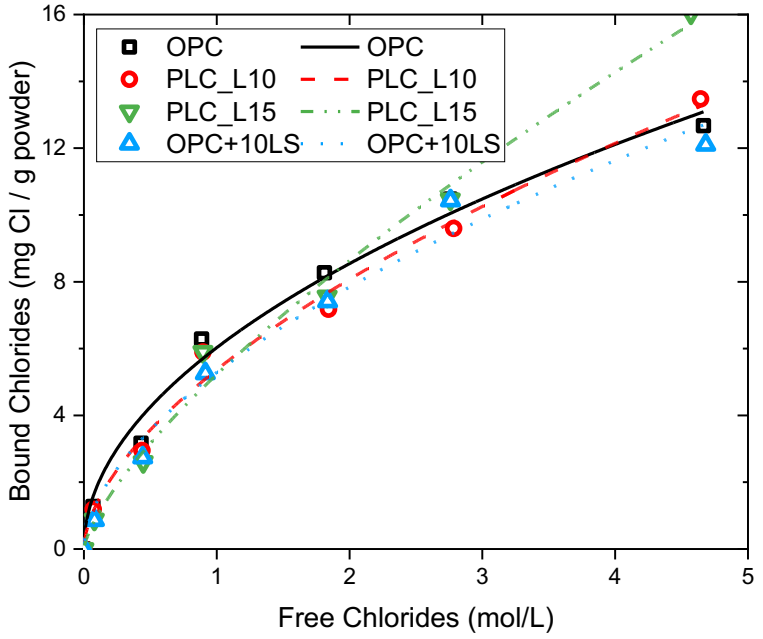

Figure F-24-15. Binding Isotherm of Cement C – M3 (NaCl)

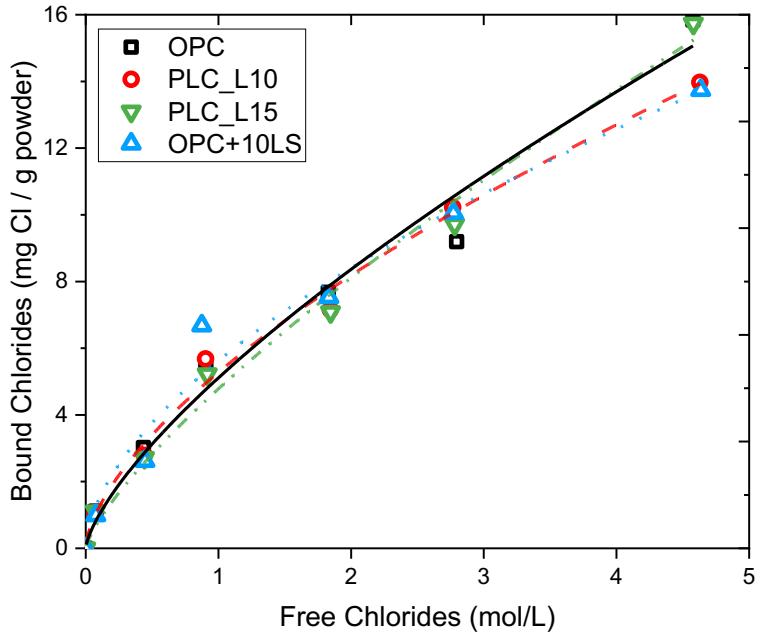

Figure F-24-16. Binding Isotherm of Cement C – M4 (NaCl)

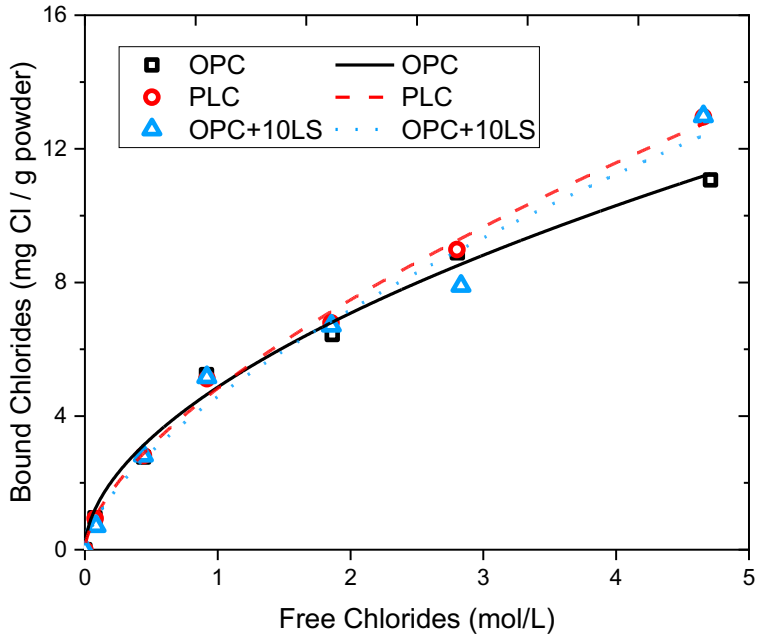

3912

3913 **Figure F-24-17. Binding Isotherm of Cement D – M0 (NaCl)**

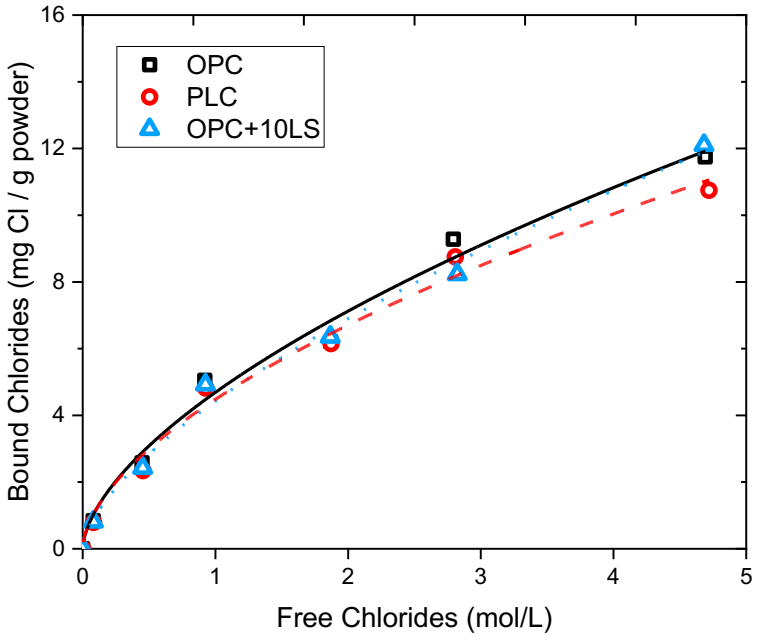

3914

3915 **Figure F-24-18. Binding Isotherm of Cement D – M1 (NaCl)**

3916

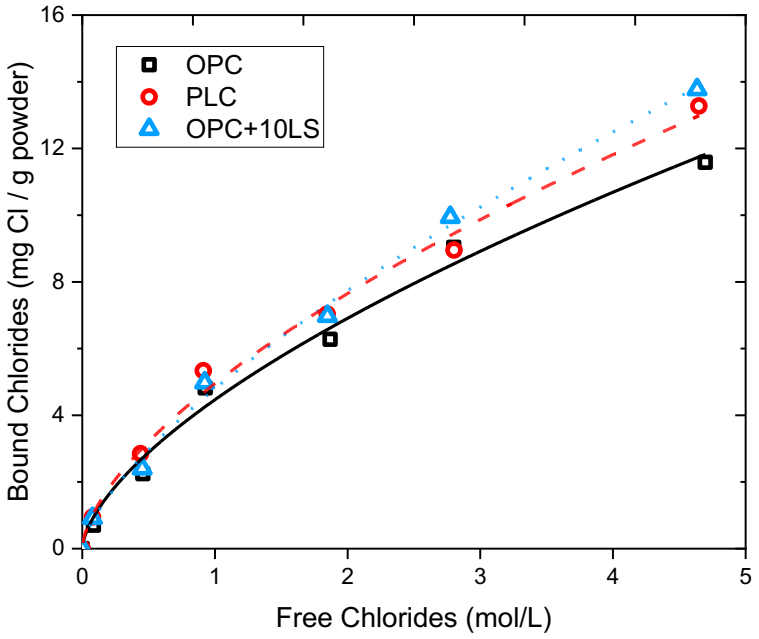

Figure F-24-19. Binding Isotherm of Cement D – M2 (NaCl)

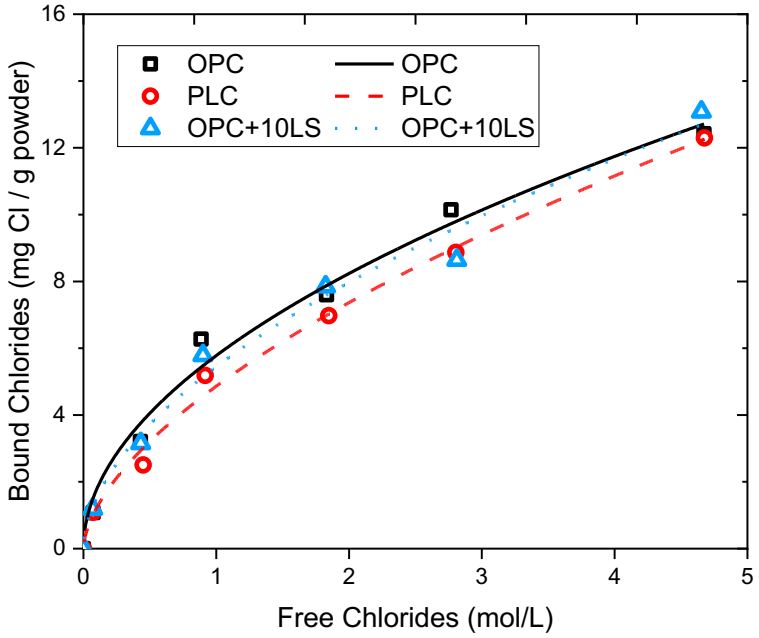

Figure F-24-20. Binding Isotherm of Cement D – M3 (NaCl)

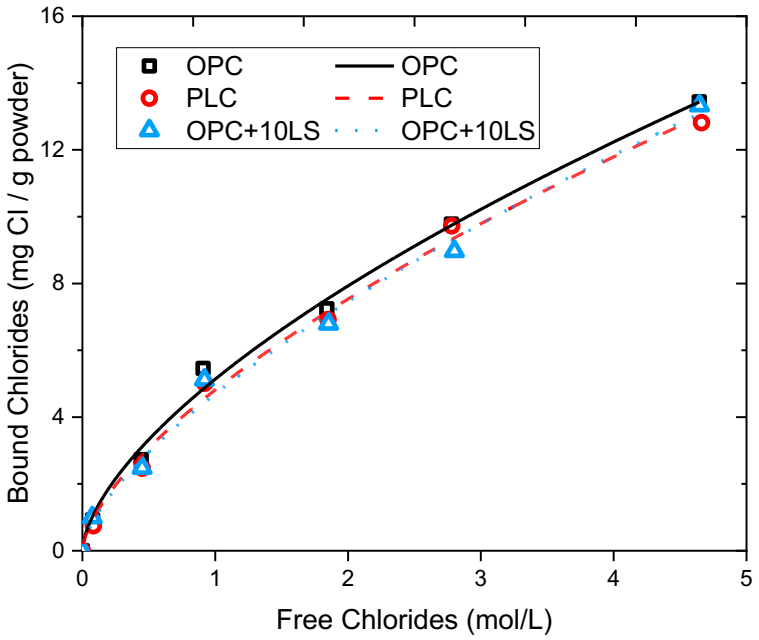

Figure F-24-21. Binding Isotherm of Cement D – M4 (NaCl)

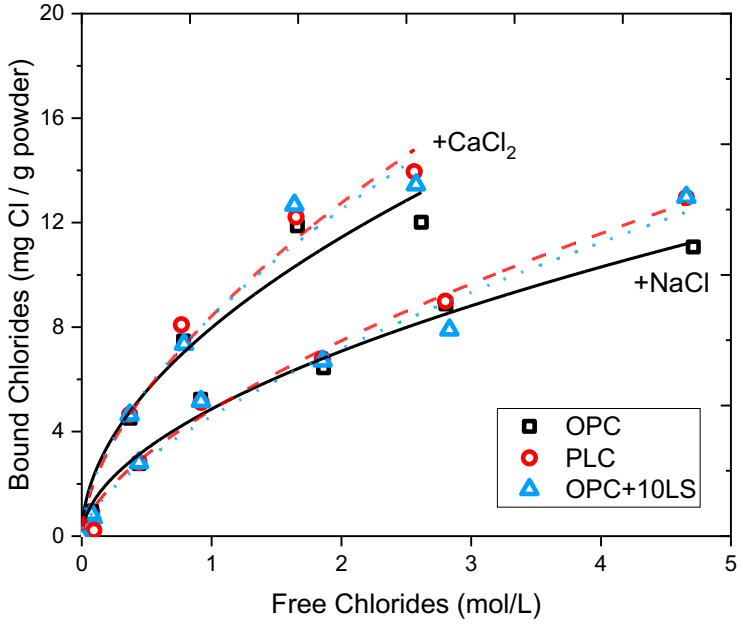

Figure F-24-22. Binding Isotherm of Cement D – M0 (NaCl, $CaCl_2$)

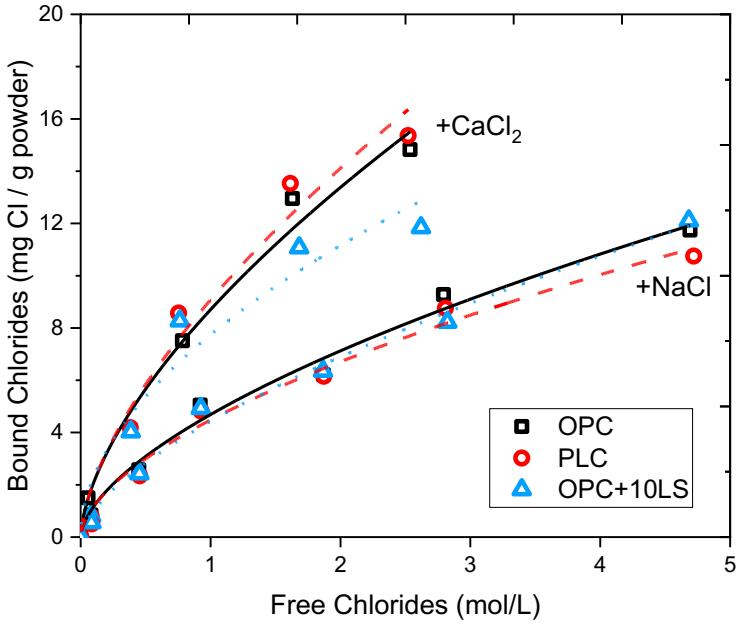

Figure F-24-23. Binding Isotherm of Cement D – M1 (NaCl, $CaCl_2$)

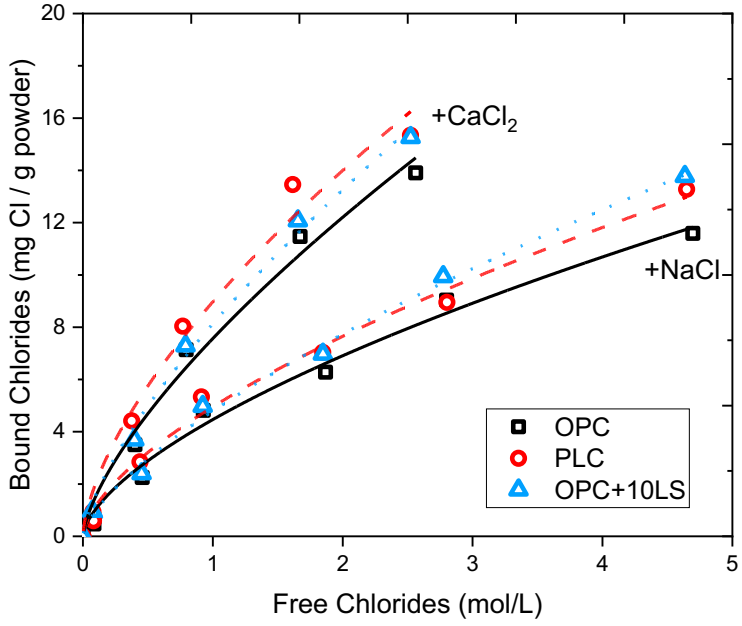

Figure F-24-24. Binding Isotherm of Cement D – M2 (NaCl, $CaCl_2$)

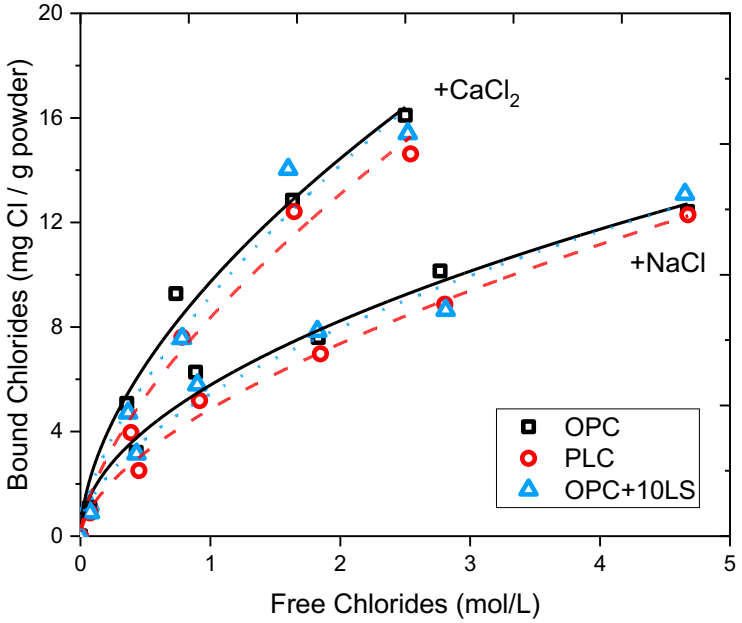

3932

3933 **Figure F-24-25. Binding Isotherm of Cement D – M3 (NaCl, $CaCl_2$)**

3934

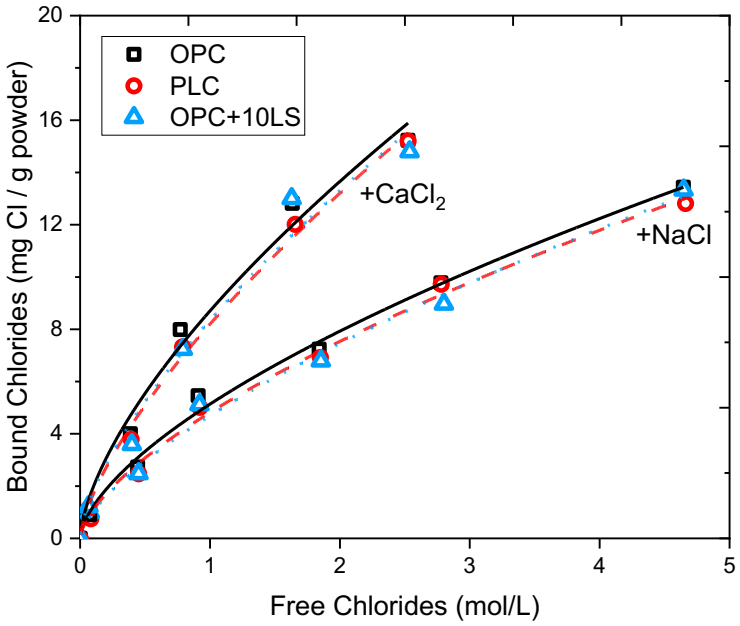

3935

3936 **Figure F-24-26. Binding Isotherm of Cement D – M4 (NaCl, $CaCl_2$)**

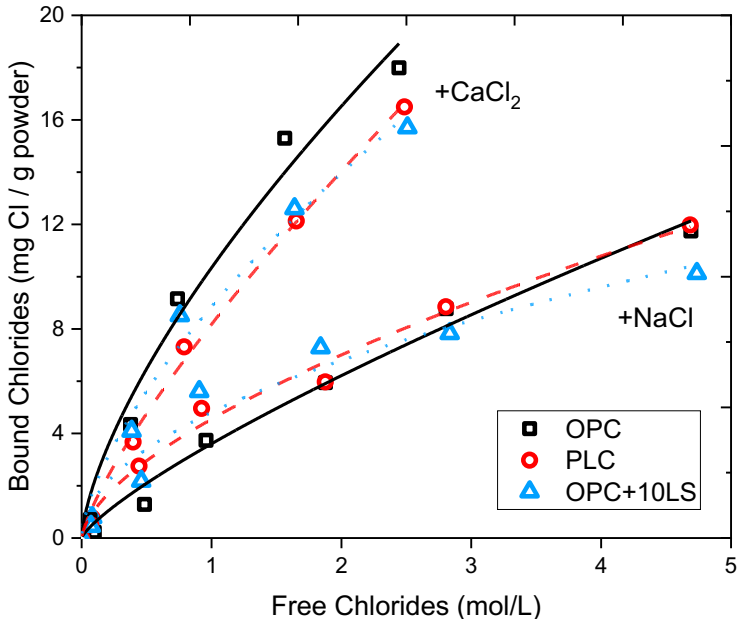

3937

3938 **Figure F-24-27. Binding Isotherm of Cement D – M5 (NaCl, $CaCl_2$)**

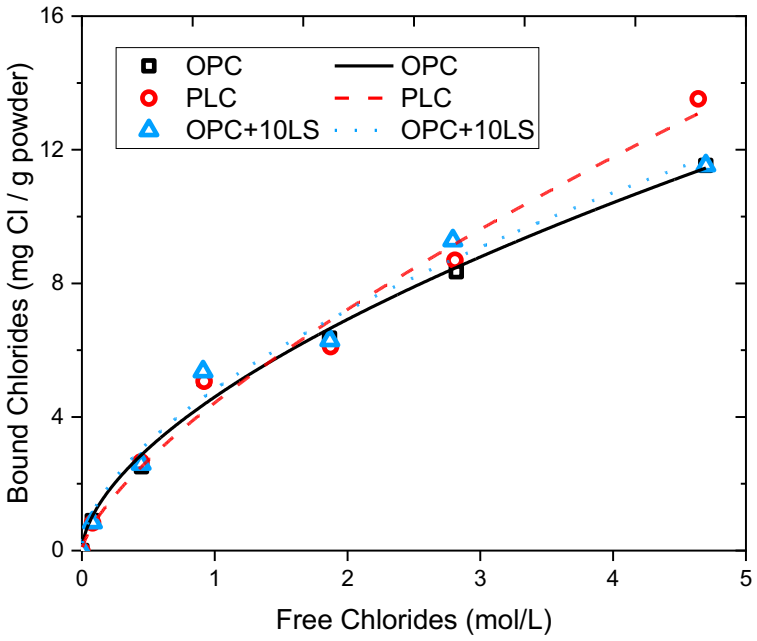

3939

3940 **Figure F-24-28. Binding Isotherm of Cement E – M0 (NaCl)**

3941

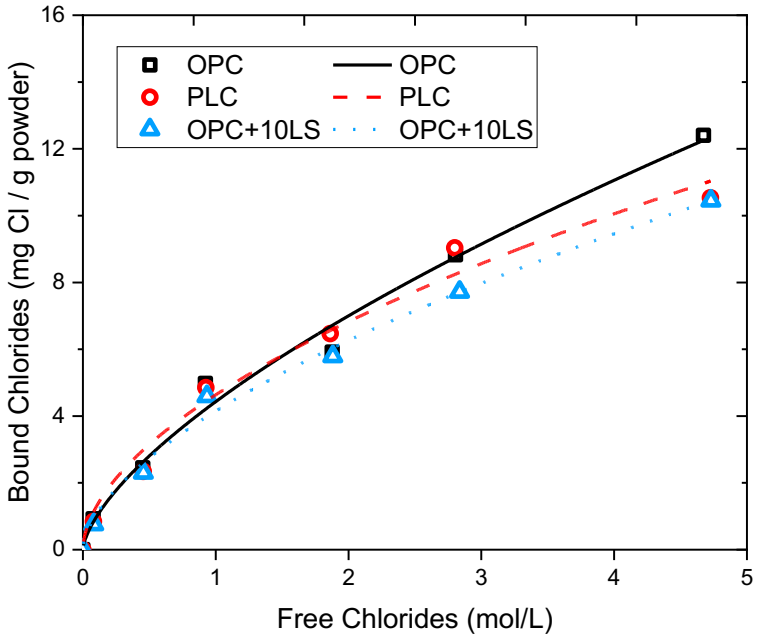

3942

3943 **Figure F-24-29. Binding Isotherm of Cement E – M1 (NaCl)**

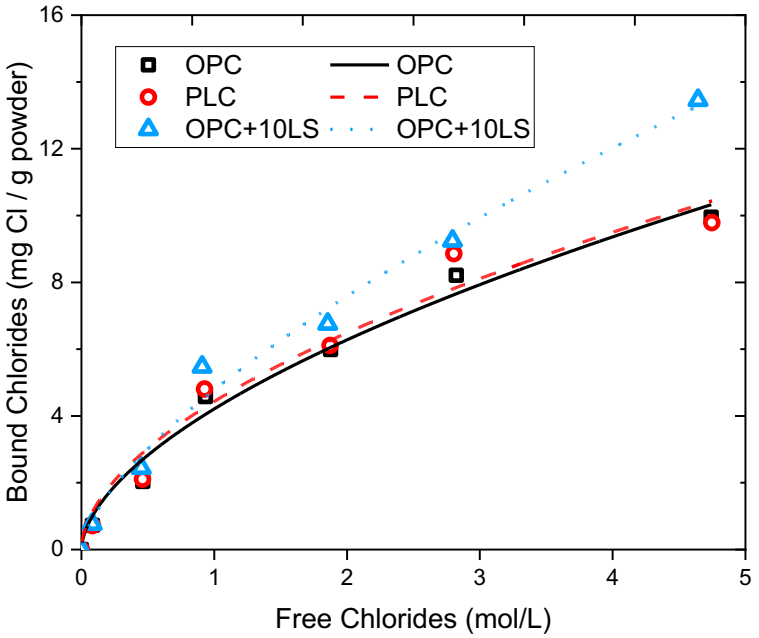

3944

3945 **Figure F-24-30. Binding Isotherm of Cement E – M2 (NaCl)**

3946

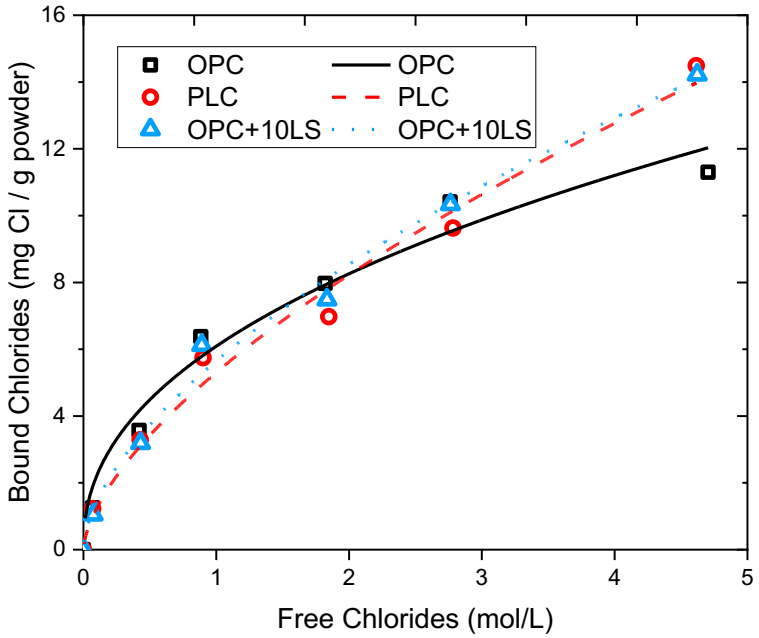

Figure F-24-31. Binding Isotherm of Cement E – M3 (NaCl)

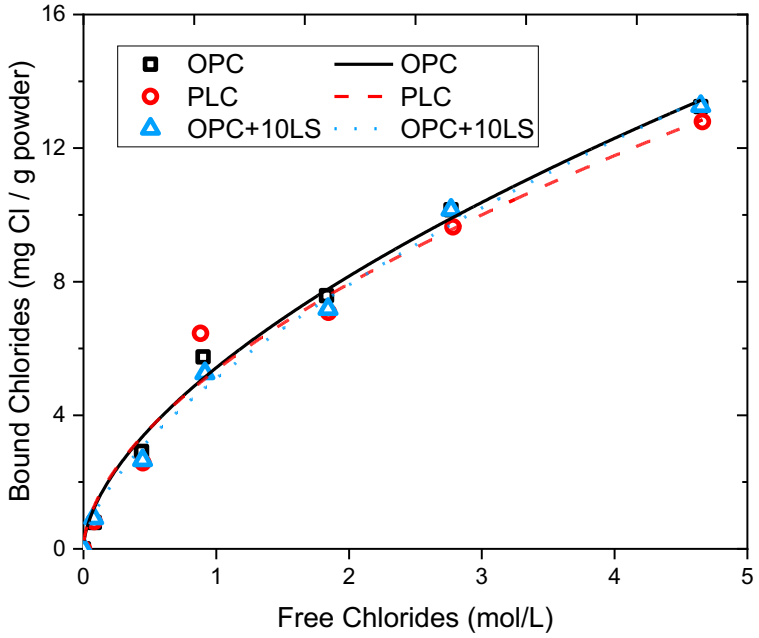

Figure F-24-32. Binding Isotherm of Cement E – M4 (NaCl)

3953 **Table F.1. Binding Parameters of Cement A – Mixtures 0 to 5 (NaCl)**

A OPC						
Sample	**M0**	**M1**	**M2**	**M3**	**M4**	**M5**
α	5.29	4.82	4.68	5.81	4.84	5.17
β	0.60	0.58	0.67	0.53	0.63	0.57
R^2	0.992	0.991	0.986	0.985	0.987	0.980

A PLC_L15						
Sample	**M0**	**M1**	**M2**	**M3**	**M4**	**M5**
α	5.11	4.91	4.92	6.02	4.89	4.09
β	0.65	0.67	0.63	0.53	0.63	0.70
R^2	0.982	0.992	0.989	0.989	0.989	0.980

A OPC+10LS						
Sample	**M0**	**M1**	**M2**	**M3**	**M4**	**M5**
α	5.00	4.79	4.73	5.46	5.13	5.27
β	0.64	0.69	0.69	0.64	0.58	0.61
R^2	0.984	0.989	0.989	0.982	0.989	0.996

3954

3955

Table F.2. Binding Parameters of Cement B – Mixtures 0 to 4 (NaCl)

M5 was not cast for Cement B

B OPC						
Sample	**M0**	**M1**	**M2**	**M3**	**M4**	**M5***
α	5.26	5.28	4.57	6.97	5.41	~
β	0.54	0.55	0.59	0.52	0.58	~
R^2	0.990	0.975	0.964	0.973	0.987	~

B PLC_L15						
Sample	**M0**	**M1**	**M2**	**M3**	**M4**	**M5***
α	4.38	4.58	4.82	5.82	5.42	~
β	0.65	0.55	0.68	0.61	0.63	~
R^2	0.983	0.989	0.974	0.991	0.984	~

B OPC+10LS						
Sample	**M0**	**M1**	**M2**	**M3**	**M4**	**M5***
α	5.09	4.63	4.91	5.71	4.84	~
β	0.56	0.66	0.57	0.51	0.66	~
R^2	0.990	0.989	0.953	0.975	0.988	~

Table F.3. Binding Parameters of Cement C – Mixtures 0 to 4 (NaCl)

M5 was not cast for Cement C

C OPC						
Sample	**M0**	**M1**	**M2**	**M3**	**M4**	**M5***
α	4.66	4.59	4.41	6.03	5.39	~
β	0.61	0.53	0.56	0.50	0.54	~
R^2	0.984	0.960	0.962	0.981	0.992	~

C PLC_L10						
Sample	**M0**	**M1**	**M2**	**M3**	**M4**	**M5***
α	4.77	4.50	4.22	5.37	5.28	~
β	0.60	0.61	0.65	0.59	0.63	~
R^2	0.987	0.984	0.985	0.985	0.988	~

C PLC_L14						
Sample	**M0**	**M1**	**M2**	**M3**	**M4**	**M5***
α	4.66	4.62	4.64	5.23	4.78	~
β	0.70	0.59	0.68	0.72	0.76	~
R^2	0.981	0.985	0.975	0.985	0.984	~

C OPC+10LS						
Sample	**M0**	**M1**	**M2**	**M3**	**M4**	**M5***
α	4.63	4.41	4.67	5.29	5.62	~
β	0.59	0.58	0.58	0.57	0.58	~
R^2	0.983	0.989	0.963	0.974	0.963	~

Table F.4. Binding Parameters of Cement D – Mixtures 0 to 5 (NaCl)

D OPC						
Sample	**M0**	**M1**	**M2**	**M3**	**M4**	**M5**
α	4.87	4.69	4.47	5.78	5.10	3.61
β	0.54	0.60	0.63	0.51	0.63	0.78
R^2	0.985	0.982	0.985	0.979	0.993	0.983

D PLC_L15						
Sample	**M0**	**M1**	**M2**	**M3**	**M4**	**M5**
α	4.83	4.95	4.48	4.86	4.81	4.55
β	0.63	0.63	0.58	0.60	0.65	0.62
R^2	0.993	0.989	0.981	0.991	0.992	0.984

D OPC+10LS						
Sample	**M0**	**M1**	**M2**	**M3**	**M4**	**M5**
α	4.59	4.43	4.79	5.45	4.69	4.81
β	0.65	0.64	0.69	0.55	0.67	0.50
R^2	0.969	0.988	0.994	0.977	0.989	0.934

Table F.5. Binding Parameters of Cement D – Mixtures 0 to 5 ($CaCl_2$)

D OPC						
Sample	**M0**	**M1**	**M2**	**M3**	**M4**	**M5**
α	7.97	8.70	7.57	9.72	8.70	10.34
β	0.52	0.62	0.69	0.57	0.65	0.68
R^2	0.926	0.976	0.974	0.977	0.976	0.968

D PLC_L15						
Sample	**M0**	**M1**	**M2**	**M3**	**M4**	**M5**
α	8.42	9.08	8.97	8.36	8.20	8.18
β	0.74	0.64	0.64	0.65	0.69	0.78
R^2	0.941	0.949	0.963	0.977	0.993	0.995

D OPC+10LS						
Sample	**M0**	**M1**	**M2**	**M3**	**M4**	**M5**
α	8.40	7.74	8.13	9.17	8.35	8.86
β	0.57	0.53	0.71	0.63	0.67	0.66
R^2	0.948	0.897	0.991	0.957	0.966	0.971

Table F.6. Binding Parameters of Cement E – Mixtures 0 to 4 (NaCl)

M5 was not cast for Cement E

E OPC						
Sample	**M0**	**M1**	**M2**	**M3**	**M4**	**M5**
α	4.60	4.43	4.21	6.09	5.42	~
β	0.59	0.66	0.58	0.44	0.59	~
R^2	0.987	0.982	0.975	0.960	0.989	~

E PLC_L11						
Sample	**M0**	**M1**	**M2**	**M3**	**M4**	**M5**
α	4.42	4.64	4.43	5.31	5.36	~
β	0.71	0.56	0.55	0.63	0.57	~
R^2	0.977	0.972	0.949	0.978	0.958	~

E OPC+10LS						
Sample	**M0**	**M1**	**M2**	**M3**	**M4**	**M5**
α	4.83	4.15	4.79	5.65	5.10	~
β	0.57	0.59	0.66	0.60	0.63	~
R^2	0.974	0.989	0.983	0.987	0.992	~

Table F.7. Bound chloride content for OPCs immersed in NaCl – Cements A to E, Mixtures 0 to 5 (NaCl)

M5 was cast only for cements A and D

A OPC						
Sample	**M0**	**M1**	**M2**	**M3**	**M4**	**M5**
0.1M	0.86	0.90	0.88	1.33	0.77	0.74
0.5M	2.97	2.64	2.37	3.30	2.49	2.82
1M	5.53	5.19	5.17	6.23	5.18	5.69
2M	7.27	6.80	6.50	7.44	6.73	6.97
3M	10.02	8.71	9.47	10.20	9.70	9.63
5M	13.17	11.85	13.06	13.10	12.62	12.24

D OPC						
Sample	**M0**	**M1**	**M2**	**M3**	**M4**	**M5**
0.1M	0.96	0.84	0.70	1.08	0.93	0.22
0.5M	2.77	2.58	2.25	3.21	2.73	1.28
1M	5.24	5.05	4.82	6.27	5.46	3.74
2M	6.44	6.21	6.28	7.60	7.24	5.94
3M	8.89	9.28	9.03	10.14	9.78	8.77
5M	11.07	11.75	11.59	12.42	13.44	11.75

B OPC						
Sample	**M0**	**M1**	**M2**	**M3**	**M4**	**M5**
0.1M	1.03	0.94	0.72	0.85	1.05	~
0.5M	3.30	2.61	2.80	3.73	2.87	~
1M	5.61	5.34	5.40	7.52	5.90	~
2M	6.89	8.30	5.77	9.51	7.56	~
3M	9.11	9.50	8.21	12.07	9.53	~
5M	12.19	12.69	11.60	15.06	13.28	~

E OPC						
Sample	**M0**	**M1**	**M2**	**M3**	**M4**	**M5**
0.1M	0.90	0.92	0.73	1.25	0.79	~
0.5M	2.51	2.45	2.04	3.57	2.91	~
1M	5.11	4.98	4.58	6.38	5.75	~
2M	6.36	5.91	5.99	7.97	7.58	~
3M	8.35	8.83	8.21	10.41	10.16	~
5M	11.53	12.40	9.95	11.30	13.24	~

C OPC						
Sample	**M0**	**M1**	**M2**	**M3**	**M4**	**M5**
0.1M	0.68	0.71	0.70	1.27	1.11	~
0.5M	2.66	2.35	2.40	3.17	3.02	~
1M	5.23	5.27	4.72	6.29	5.58	~
2M	6.55	6.20	5.83	8.27	7.68	~
3M	8.43	8.46	8.83	10.48	9.19	~
5M	12.17	10.02	10.05	12.67	15.84	~

Table F.8. Bound chloride content for PLCs immersed in NaCl – Cements A to E, Mixtures 0 to 5 (NaCl)

M5 was cast only for cements A and D

A PLC_L15						
Sample	**M0**	**M1**	**M2**	**M3**	**M4**	**M5**
0.1M	0.97	0.89	0.87	1.28	0.77	0.72
0.5M	2.85	2.52	2.56	3.35	2.45	2.13
1M	5.71	5.33	5.34	6.22	5.04	4.79
2M	7.12	7.12	6.85	7.98	7.02	5.65
3M	9.38	9.60	9.51	10.73	9.85	8.38
5M	14.17	13.90	12.92	13.40	12.60	12.19

C PLC_L14						
Sample	**M0**	**M1**	**M2**	**M3**	**M4**	**M5**
0.1M	0.68	0.79	0.67	0.88	1.11	~
0.5M	2.59	2.62	2.24	2.60	2.71	~
1M	5.32	5.12	5.35	5.90	5.22	~
2M	6.78	6.19	7.16	7.56	7.08	~
3M	8.87	8.65	8.52	10.46	9.71	~
5M	13.97	11.57	13.54	16.03	15.73	~

B PLC_L15						
Sample	**M0**	**M1**	**M2**	**M3**	**M4**	**M5**
0.1M	0.69	0.77	0.66	0.82	1.04	~
0.5M	2.51	2.57	2.52	3.27	2.51	~
1M	4.99	4.82	5.69	6.18	5.84	~
2M	6.04	6.58	6.49	8.16	7.56	~
3M	8.30	8.22	9.62	10.51	10.68	~
5M	12.14	10.48	13.92	14.77	14.04	~

D PLC_L15						
Sample	**M0**	**M1**	**M2**	**M3**	**M4**	**M5**
0.1M	0.93	0.79	0.95	1.09	0.75	0.77
0.5M	2.82	2.34	2.85	2.51	2.47	2.75
1M	5.12	4.82	5.33	5.18	5.01	4.96
2M	6.79	6.15	7.04	6.98	6.92	5.97
3M	8.99	8.75	8.95	8.87	9.72	8.85
5M	12.96	10.75	13.28	12.30	12.81	11.98

C PLC_L10						
Sample	**M0**	**M1**	**M2**	**M3**	**M4**	**M5**
0.1M	1.02	0.77	0.86	1.19	1.07	~
0.5M	2.70	2.47	2.44	2.95	2.79	~
1M	5.25	5.01	4.99	5.90	5.68	~
2M	6.46	6.04	6.53	7.18	7.15	~
3M	8.70	8.68	8.58	9.60	10.23	~
5M	12.28	11.53	11.50	13.47	13.97	~

E PLC_L11						
Sample	**M0**	**M1**	**M2**	**M3**	**M4**	**M5**
0.1M	0.83	0.84	0.72	1.23	0.81	~
0.5M	2.65	2.34	2.11	3.29	2.58	~
1M	5.07	4.85	4.80	5.75	6.45	~
2M	6.10	6.47	6.11	6.98	7.08	~
3M	8.69	9.03	8.86	9.63	9.64	~
5M	13.52	10.54	9.79	14.49	12.80	~

Table F.9. Bound chloride content for OPC+10LS mixtures immersed in NaCl – Cements A to E, Mixtures 0 to 5 (NaCl)

M5 was cast only for cements A and D

A OPC+10LS						
Sample	**M0**	**M1**	**M2**	**M3**	**M4**	**M5**
0.1M	0.86	0.68	0.78	1.01	1.02	0.76
0.5M	2.81	2.64	2.32	3.13	2.70	2.98
1M	5.52	5.22	5.24	5.69	5.34	5.15
2M	6.66	6.69	7.03	7.05	7.11	7.71
3M	9.75	9.76	9.24	11.01	9.66	10.08
5M	13.49	15.59	13.69	14.37	12.26	13.22

D OPC+10LS						
Sample	**M0**	**M1**	**M2**	**M3**	**M4**	**M5**
0.1M	0.71	0.81	0.91	1.19	1.00	0.79
0.5M	2.82	2.42	2.40	3.15	2.48	2.18
1M	5.16	4.92	4.98	5.79	5.12	5.61
2M	6.71	6.35	6.98	7.84	6.79	7.28
3M	7.90	8.23	9.94	8.64	8.97	7.83
5M	12.97	12.10	13.77	13.08	13.33	10.13

B OPC+10LS						
Sample	**M0**	**M1**	**M2**	**M3**	**M4**	**M5**
0.1M	0.73	0.91	0.52	0.91	1.06	~
0.5M	2.95	2.65	2.32	3.18	2.57	~
1M	5.37	5.03	5.08	6.39	5.11	~
2M	7.31	6.39	7.12	7.72	6.61	~
3M	8.93	8.95	9.91	9.63	9.86	~
5M	12.01	12.88	11.07	12.44	13.36	~

E OPC+10LS						
Sample	**M0**	**M1**	**M2**	**M3**	**M4**	**M5**
0.1M	0.84	0.75	0.77	1.04	0.91	~
0.5M	2.59	2.30	2.44	3.19	2.65	~
1M	5.36	4.59	5.47	6.12	5.26	~
2M	6.29	5.79	6.76	7.49	7.18	~
3M	9.28	7.72	9.24	10.34	10.16	~
5M	11.53	10.45	13.45	14.22	13.26	~

C OPC+10LS						
Sample	**M0**	**M1**	**M2**	**M3**	**M4**	**M5**
0.1M	0.77	0.77	0.59	0.87	0.99	~
0.5M	2.47	2.35	2.11	2.74	2.62	~
1M	5.12	4.78	5.13	5.26	6.68	~
2M	6.29	6.37	6.73	7.41	7.53	~
3M	8.80	8.06	9.21	10.43	10.05	~
5M	11.32	10.77	10.94	12.10	13.74	~

Table F.10. Bound chloride content for Cement D mixtures immersed in $CaCl_2$ – Mixtures 0 to 5 ($CaCl_2$)

Cement D + $CaCl_2$						
OPC						
Sample	**M0**	**M1**	**M2**	**M3**	**M4**	**M5**
0.1M	0.91	1.50	0.47	1.08	0.90	0.70
0.5M	4.51	4.10	3.51	5.08	4.00	4.34
1M	7.47	7.51	7.14	9.28	7.99	9.15
2M	11.88	12.95	11.47	12.85	12.82	15.30
3M	12.01	14.82	13.90	16.10	15.23	17.99

PLC_L15						
Sample	**M0**	**M1**	**M2**	**M3**	**M4**	**M5**
0.1M	0.22	0.50	0.59	0.89	1.14	0.51
0.5M	4.66	4.18	4.42	3.96	3.78	3.67
1M	8.09	8.57	8.04	7.61	7.33	7.31
2M	12.21	13.53	13.45	12.42	12.01	12.13
3M	13.95	15.36	15.34	14.62	15.20	16.50

OPC+10LS						
Sample	**M0**	**M1**	**M2**	**M3**	**M4**	**M5**
0.1M	0.84	0.56	0.96	0.90	1.22	0.46
0.5M	4.64	4.03	3.69	4.72	3.59	4.09
1M	7.35	8.28	7.29	7.57	7.24	8.51
2M	12.68	11.07	12.08	14.04	13.00	12.61
3M	13.45	11.84	15.26	15.41	14.80	15.70

3997 **25 APPENDIX G – Transport Properties of Concrete**

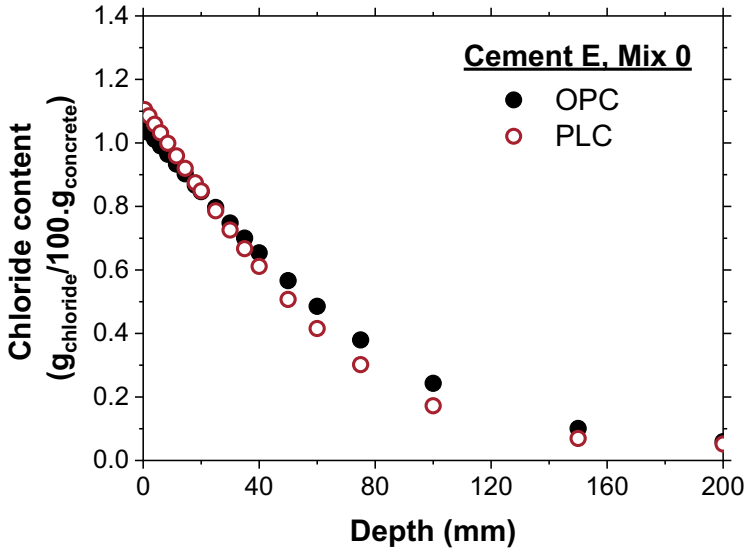

(a)

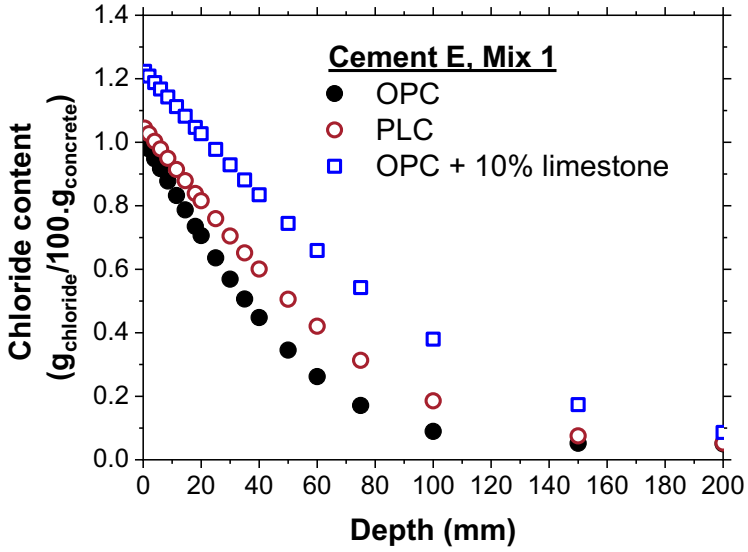

(b)

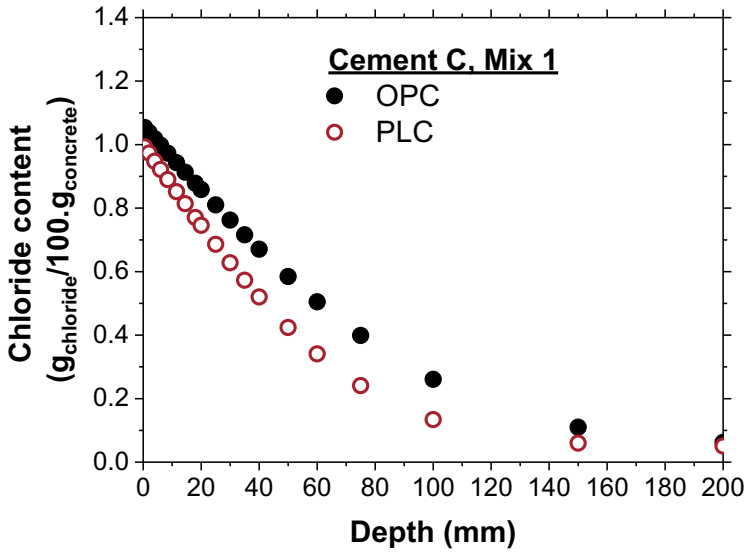
Cement C, Mix 1
OPC
PLC
Chloride content
(g chloride/100.g concrete)
Depth (mm)
0.0
0.2
0.4
0.6
0.8
1.0
1.2
1.4
0
20
40
60
80
100
120
140
160
180
200

(c)

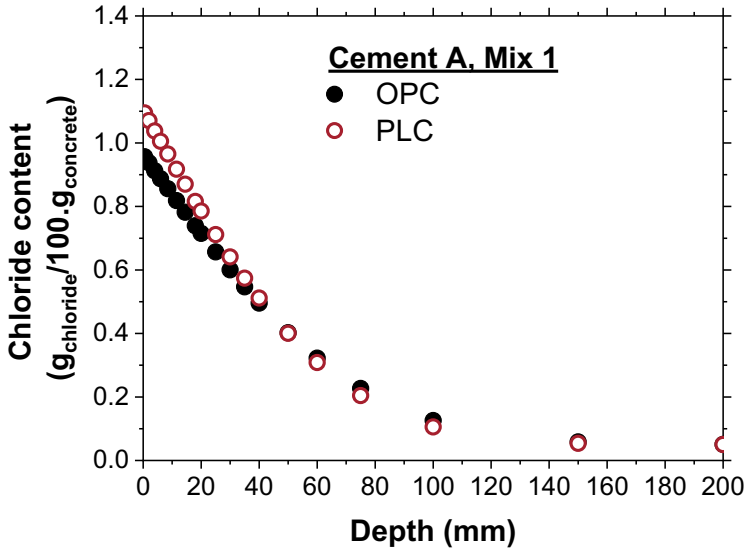
Cement A, Mix 1
OPC
PLC
Chloride content
(g chloride/100.g concrete)
Depth (mm)
0.0
0.2
0.4
0.6
0.8
1.0
1.2
1.4
0
20
40
60
80
100
120
140
160
180
200

(d)

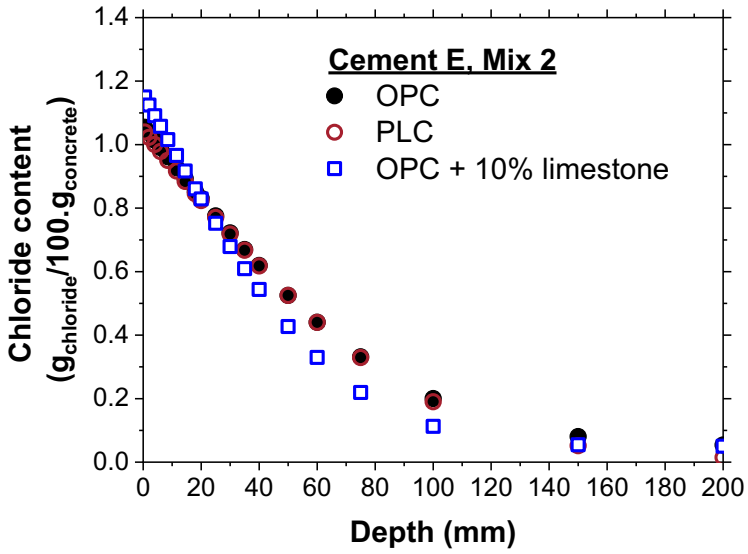
Cement E, Mix 2
OPC
PLC
OPC + 10% limestone
Chloride content
(g_chloride/100.g_concrete)
Depth (mm)
0.0
0.2
0.4
0.6
0.8
1.0
1.2
1.4
0
20
40
60
80
100
120
140
160
180
200

(e)

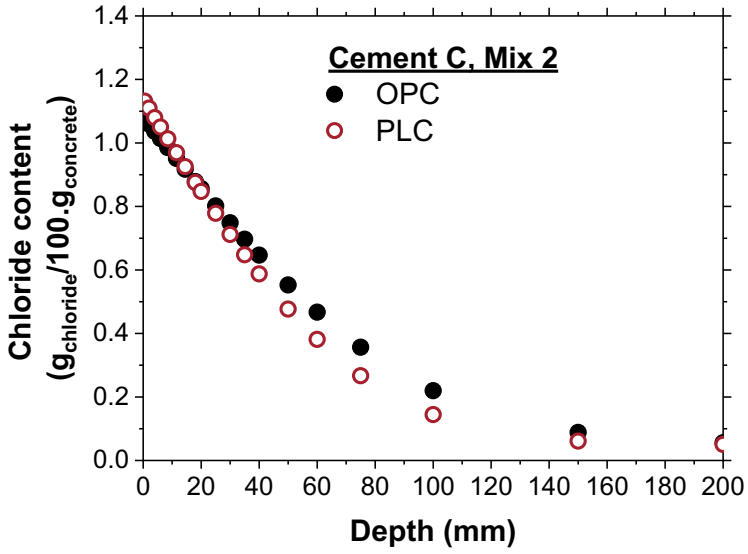
Cement C, Mix 2
OPC
PLC
Chloride content
(g_chloride/100.g_concrete)
Depth (mm)
0.0
0.2
0.4
0.6
0.8
1.0
1.2
1.4
0
20
40
60
80
100
120
140
160
180
200

(f)

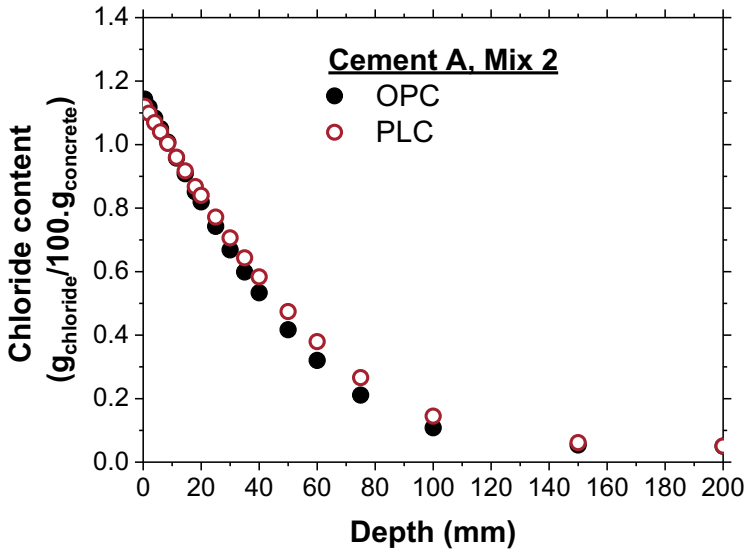
Cement A, Mix 2
OPC
PLC
Chloride content
(g chloride/100.g concrete)
Depth (mm)
0.0
0.2
0.4
0.6
0.8
1.0
1.2
1.4
0
20
40
60
80
100
120
140
160
180
200

(g)

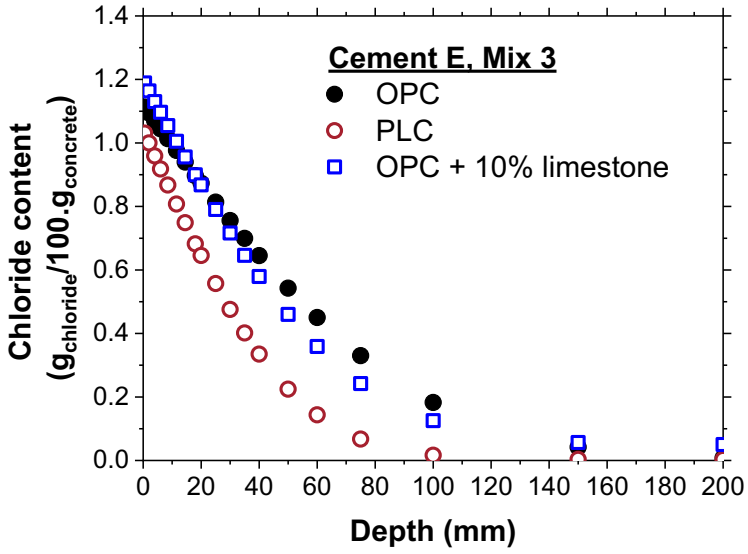
Cement E, Mix 3
OPC
PLC
OPC + 10% limestone
Chloride content
(g chloride/100.g concrete)
Depth (mm)
0.0
0.2
0.4
0.6
0.8
1.0
1.2
1.4
0
20
40
60
80
100
120
140
160
180
200

(h)

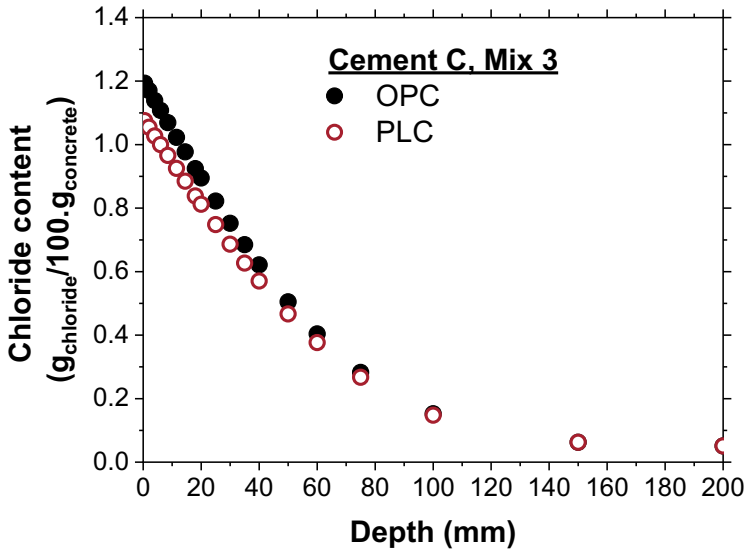
Cement C, Mix 3
OPC
PLC
Chloride content
(g_chloride/100.g_concrete)
Depth (mm)
0.0
0.2
0.4
0.6
0.8
1.0
1.2
1.4
0
20
40
60
80
100
120
140
160
180
200

(i)

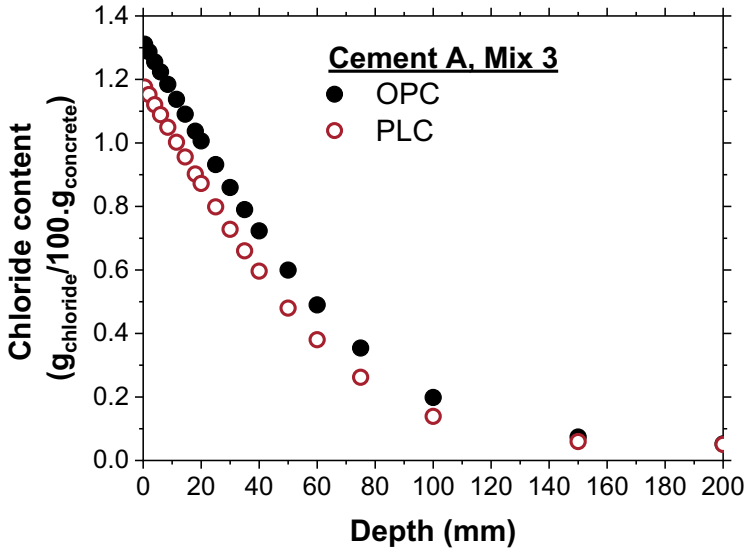
Cement A, Mix 3
OPC
PLC
Chloride content
(g_chloride/100.g_concrete)
Depth (mm)
0.0
0.2
0.4
0.6
0.8
1.0
1.2
1.4
0
20
40
60
80
100
120
140
160
180
200

(j)

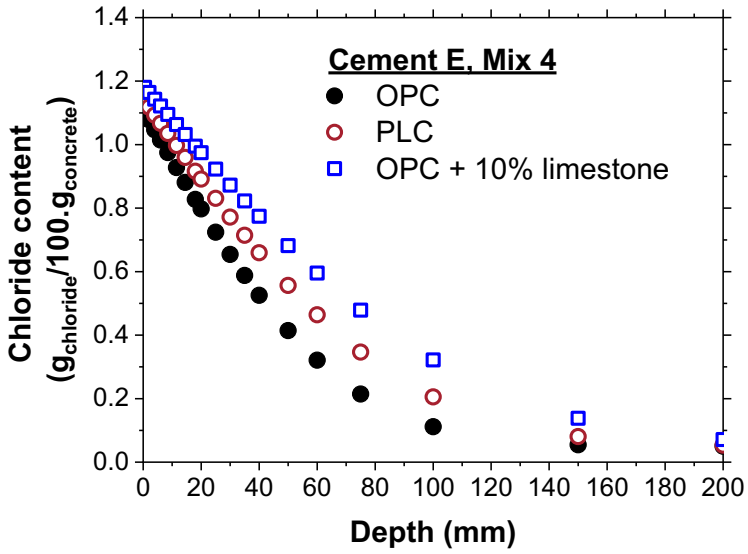
Cement E, Mix 4
OPC
PLC
OPC + 10% limestone
Chloride content
(g chloride/100.g concrete)
Depth (mm)
0.0
0.2
0.4
0.6
0.8
1.0
1.2
1.4
0
20
40
60
80
100
120
140
160
180
200

(k)

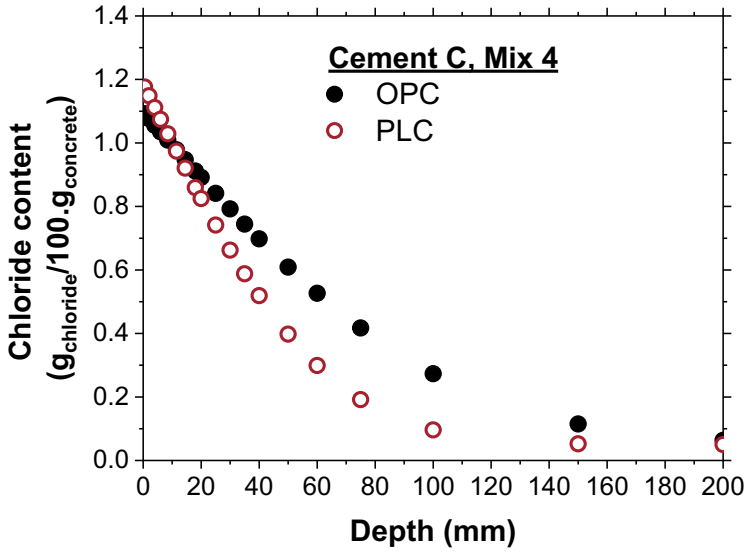
Cement C, Mix 4
OPC
PLC
Chloride content
(g chloride/100.g concrete)
Depth (mm)
0.0
0.2
0.4
0.6
0.8
1.0
1.2
1.4
0
20
40
60
80
100
120
140
160
180
200

(l)

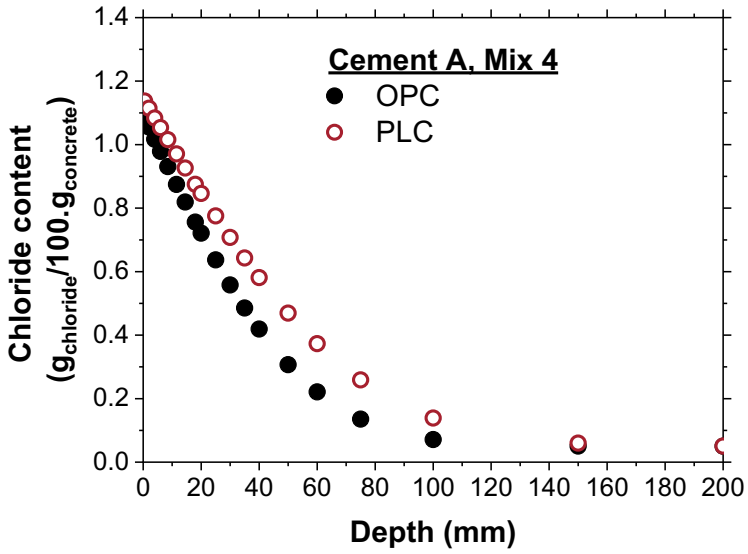

(m)

Figure Appendix G- Acid soluble profiles for all mixtures determined using the calculated values of D_a, and C_{s-a} (from formation factor and porosity) for an exposure time of 20 years: (a) cement E, Mix 0; (b) cement E, Mix 1; (c) cement C, Mix 1; (d) Cement A, Mix 1; (e) cement E, Mix 2; (f) cement C, Mix 2; (g) Cement A, Mix 2; (h) cement E, Mix 3; (i) cement C, Mix3; (j) cement A, Mix3; (k) cement E, Mix 4; (l) cement C, Mix4; (m) cement A, Mix4.

26 APPENDIX H - Additional Data from Thermodynamic Modeling

H.1 Porosity Data

H.1.1 Total Porosity

The porosity of the paste as determined from thermodynamic modeling and the PPM is shown below in Table H.1.

Table H.1. Total porosity of paste from thermodynamic modeling

Paste Porosity (in %)	Mix. Long Name	Control	PLC + 25% FA	PLC + 20%FA + 5% SF	PLC + 50% SL	PLC + 25% SL + 25% FA	PLC + 25% NP
	Mix No.	M0	M1	M2	M3	M4	M5
OPC (<5.99% Ls)	A	31%	32%	32%	31%	32%	33%
	B	31%	34%	31%	35%	37%	32%
	C	32%	33%	33%	31%	32%	34%
	D	31%	32%	32%	33%	35%	33%
	E	32%	33%	33%	32%	33%	34%
PLC (13-15% Ls)	A	34%	35%	35%	33%	35%	36%
	B	34%	35%	35%	33%	35%	35%
	C	35%	36%	36%	34%	36%	36%
	D	34%	35%	35%	33%	35%	35%
	E	34%	35%	35%	34%	35%	36%

The total porosity of mortar consisting of 50% paste, 45% fine aggregates (of 3.7% absorption capacity), and 5% entrapped air is shown in Table H.2.

Table H.2. Total porosity of mortar calculated from the PPMC

Mortar Porosity (in %)	Mix. Long Name	Control	PLC + 25% FA	PLC + 20%FA + 5% SF	PLC + 50% SL	PLC + 25% SL + 25% FA	PLC + 25% NP
	Mix No.	**M0**	**M1**	**M2**	**M3**	**M4**	**M5**
OPC (<5.99% Ls)	**A**	22.1%	22.8%	22.8%	21.9%	22.6%	23.2%
	B	22.0%	23.7%	22.3%	24.3%	25.2%	22.8%
	C	22.6%	23.3%	23.2%	22.2%	22.9%	23.7%
	D	22.0%	22.5%	22.6%	23.2%	24.4%	23.2%
	E	22.5%	23.2%	23.2%	22.5%	23.1%	23.6%
PLC (13-15% Ls)	**A**	23.7%	24.1%	24.0%	23.4%	24.2%	24.4%
	B	23.6%	24.0%	24.0%	23.3%	24.2%	24.4%
	C	24.2%	24.5%	24.7%	23.6%	24.5%	24.8%
	D	23.6%	24.0%	24.0%	23.3%	24.2%	24.4%
	E	23.8%	24.1%	24.1%	23.4%	24.2%	24.5%

H.1.2 Phase Volumes (including Pore Volume Distribution)

Table H.3. Phase volumes determined from thermodynamic modeling (output of the PPM)

Phase Volumes in Paste	Mix. Long Name		Control	PLC + 25% FA	PLC + 20%FA + 5% SF	PLC + 50% SL	PLC + 25% SL + 25% FA	PLC + 25% NP
		Mix No.	**M0**	**M1**	**M2**	**M3**	**M4**	**M5**
OPC (<5.99% Ls)	**A**	**v_ub**	12%	20%	19%	19%	22%	20%
		v_gs	57%	48%	49%	51%	46%	47%
		v_gw	19%	16%	17%	15%	14%	16%
		v_cw	4%	9%	7%	8%	9%	10%
		v_cs	7%	8%	8%	8%	8%	7%
	B	**v_ub**	14%	21%	20%	19%	22%	21%
		v_gs	55%	45%	49%	45%	40%	47%
		v_gw	17%	15%	16%	16%	15%	15%
		v_cw	6%	12%	8%	12%	14%	11%
		v_cs	7%	7%	8%	8%	8%	7%
	C	**v_ub**	13%	20%	19%	19%	22%	20%
		v_gs	55%	47%	48%	50%	46%	46%
		v_gw	19%	16%	17%	15%	15%	16%
		v_cw	6%	10%	8%	8%	9%	11%

		v_cs	7%	8%	8%	8%	8%	7%
	D	**v_ub**	13%	20%	19%	19%	22%	21%
		v_gs	56%	48%	49%	48%	43%	46%
		v_gw	17%	14%	16%	15%	15%	15%
		v_cw	6%	10%	8%	10%	12%	11%
		v_cs	7%	8%	8%	8%	8%	7%
	E	**v_ub**	12%	19%	19%	18%	22%	20%
		v_gs	56%	47%	48%	50%	45%	46%
		v_gw	19%	16%	17%	15%	15%	16%
		v_cw	6%	9%	8%	8%	10%	11%
		v_cs	7%	8%	8%	8%	9%	7%
PLC (13-15% Ls)	**A**	**v_ub**	13%	20%	19%	19%	22%	20%
		v_gs	53%	45%	46%	48%	43%	44%
		v_gw	17%	14%	15%	14%	14%	15%
		v_cw	12%	14%	12%	11%	13%	15%
		v_cs	5%	7%	7%	8%	9%	6%
	B	**v_ub**	13%	20%	20%	19%	22%	21%
		v_gs	53%	45%	46%	48%	43%	44%
		v_gw	15%	13%	14%	13%	13%	13%
		v_cw	13%	15%	13%	12%	13%	16%
		v_cs	6%	7%	7%	8%	9%	6%
	C	**v_ub**	13%	20%	19%	19%	22%	20%
		v_gs	52%	45%	45%	48%	43%	43%
		v_gw	18%	15%	19%	15%	14%	15%
		v_cw	12%	14%	10%	11%	13%	15%
		v_cs	5%	7%	6%	8%	9%	6%
	D	**v_ub**	13%	20%	19%	19%	22%	20%
		v_gs	53%	45%	46%	48%	43%	44%
		v_gw	15%	13%	14%	13%	13%	13%
		v_cw	13%	15%	13%	12%	13%	16%
		v_cs	6%	7%	7%	8%	9%	6%
	E	**v_ub**	13%	20%	19%	19%	22%	20%
		v_gs	53%	45%	46%	48%	43%	44%
		v_gw	18%	15%	16%	15%	14%	15%
		v_cw	10%	13%	12%	11%	12%	14%
		v_cs	6%	7%	7%	8%	9%	6%

4019

H.2 Reacted and Unreacted Limestone Data

Table H.4. Reacted calcite (limestone) in the systems as determined from thermodynamic modeling

Reacted calcite (in $g/100g_{binder}$)	Mix. Long Name	Control	PLC + 25% FA	PLC + 20%FA + 5% SF	PLC + 50% SL	PLC + 25% SL + 25% FA	PLC + 25% NP
	Mix No.	M0	M1	M2	M3	M4	M5
OPC (<5.99% Ls)	A	1.67	4.31	4.17	4.31	4.31	3.63
	B	1.79	1.79	1.79	1.79	1.79	1.79
	C	1.38	4.20	3.91	4.20	4.20	3.37
	D	2.05	3.48	3.48	3.48	3.48	3.48
	E	1.41	4.76	4.39	5.99	5.99	3.85
PLC (13-15% Ls)	A	1.29	6.52	6.14	10.75	11.14	5.60
	B	1.68	6.73	6.34	10.79	11.17	5.81
	C	0.95	6.41	5.46	10.89	11.27	5.50
	D	1.68	6.88	6.49	11.09	11.47	5.96
	E	1.13	5.83	5.45	9.53	9.92	4.92

Table H.5. Unreacted calcite (limestone) that remains in the systems as determined from thermodynamic modeling

Unreacted calcite (in $g/100g_{binder}$)	Mix. Long Name	Control	PLC + 25% FA	PLC + 20%FA + 5% SF	PLC + 50% SL	PLC + 25% SL + 25% FA	PLC + 25% NP
	Mix No.	M0	M1	M2	M3	M4	M5
OPC (<5.99% Ls)	A	2.64	0.00	0.14	0.00	0.00	0.68
	B	0.00	0.00	0.00	0.00	0.00	0.00
	C	2.82	0.00	0.29	0.00	0.00	0.83
	D	1.43	0.00	0.00	0.00	0.00	0.00
	E	4.58	1.23	1.60	0.00	0.00	2.14
PLC (13-15% Ls)	A	12.03	6.80	7.18	2.57	2.18	7.72
	B	11.43	6.38	6.77	2.32	1.94	7.30
	C	13.05	7.59	8.54	3.11	2.73	8.50
	D	12.03	6.83	7.22	2.62	2.24	7.75
	E	9.98	5.28	5.66	1.58	1.19	6.19

H.3 CH Consumed Data

Table H.6. CH Consumed in the systems as determined from thermodynamic modeling

CH Consumed (in g/100g_{binder})	Mix. Long Name	Control	PLC + 25% FA	PLC + 20%FA + 5% SF	PLC + 50% SL	PLC + 25% SL + 25% FA	PLC + 25% NP
	Mix No.	M0	M1	M2	M3	M4	M5
OPC (<5.99% Ls)	A	0.00	7.14	2.23	6.34	8.34	9.70
	B	0.00	8.43	2.55	8.02	10.29	9.99
	C	0.00	7.39	2.72	6.83	8.95	10.32
	D	0.00	8.37	2.67	7.28	9.81	10.38
	E	0.00	7.28	1.99	6.78	8.86	9.68
PLC (13-15% Ls)	A	1.61	8.24	1.85	7.63	9.66	9.20
	B	0.80	8.23	2.19	7.79	10.00	9.39
	C	1.55	8.56	2.38	8.09	11.46	9.31
	D	1.20	8.53	2.40	8.09	10.30	9.60
	E	1.53	8.49	2.16	7.99	10.11	9.57

27 APPENDIX I - Additional Mixture Proportions for GHG Modeling

I.1 Jointed Plain Concrete Mix Design

STATE OF CALIFORNIA—BUSINESS, TRANSPORTATION AND HOUSING AGENCY ARNOLD SCHWARZENEGGER, Governor

DEPARTMENT OF TRANSPORTATION
TRUCKEE CONSTRUCTION FIELD OFFICE
12047 DONNER PASS ROAD, SUITE B-4
TRUCKEE, CA 96161
PHONE (530) 587-9827; FAX (530) 587-9829

Flex your power!
Be energy efficient!

May 13, 2010

03-0A6314
03-Nev-080-R14.6/24.9 (KP)
ACIM-080-4(184)E
DONNER 1 – REHAB. & WIDENING

CT Ref. No. 088

Mr. Chris Fallbeck, Project Manager
Teichert Construction
P.O. Box 276830
Sacramento, CA 95827-6830

Dear Mr. Purvis:

Jointed Plain Concrete Pavement

Reference Teichert Construction's letter No. DOT-101, "PCC Mix Design," dated April 29, 2010.

JPCP mix design No. 07-0010-2 (R3) designed by Coffman Specialties has been reviewed and is approved in accordance with Section 10-1.56, "Jointed Plain Concrete Pavement," of the Special Provisions.

If there are any questions regarding this letter feel free to contact me at your convenience.

Sincerely,

DAVID F.CATANIA, P.E.
Senior Resident Engineer

cc: NRCO, CT 5.3, 36.93.1
Attachment: Yes

"Caltrans improves mobility across California"

Project Number: 07-0010

CONCRETE MIX DESIGN

Date: 4/28/2010

Job:	Route 10
Address:	Donner Lake UC to Trout Creek UC
Contractor:	Coffman Specialties, Inc
Mix Design use:	Slipform Pavement
Concrete Supplier:	Coffman Specialties, Inc
Coarse Agg Source:	Martin Marietta, Spanish Springs
Fine Agg Source:	Teichert, Hallwood
Cement Source:	Cemex, Victorville
Fly Ash Source:	N/A
Total Cementitious, lb/yd^3 (kg/m^3):	675 (400 kg/m3)
Water / Cementitious Ratio (lb./lb.):	0.43

Mix Design No.:	07-0010-2 (R3)
Design Strength:	3.9 @ 28 Days 4.5 @ 42 Days
Spec. Slump (in.):	2.0

ADMIXTURES	
No. 1:	Master Pave @ 22 oz/cu.yd. (851 ml/m3)
No. 2:	PaveAir @ 8.4 oz/cu.yd. (325 ml/m3)
No. 3:	
No. 4:	

GRADING ANALYSIS: PERCENT PASSING U.S. STANDARD SIEVE

SIEVE SIZE, mm	50	37.5	25	19	12.5	9.5	4.75	2.36	1.18	0.600	0.300	0.150	0.075	F.M.
WC Sand	100	100	100	100	100	100	96	81	66	49	27	8	1.8	2.73
1" x #4	100	100	100	91	44	28	4	1						
1-1/2" x 3/4"	100	97	38	7	2	1								
COMBINED	100	99	86	75	56	49	38	31	25	19	10	3	0.7	
"x" Values			35	85		25			68	46	25			

Combined % passing 3/8" sieve and retained on #8 sieve =17.8

DESIGN FOR ONE CUBIC YARD OF CONCRETE (SATURATED AND SURFACE DRY)

ABSOLUTE VOLUME OF AGGREGATE IN ONE CUBIC YARD, CUBIC FEET: 17.70

SPECIFIC GRAVITY OF COMBINED AGGREGATES: 2.68

WEIGHT OF AGGREGATES IN ONE CUBIC YARD BATCH, LBS. 2958.4

MATERIAL	PERCENT	BATCH LBS.	SP. GR.	ABSOLUTE VOLUME (ft 3)	SACK WEIGHTS (lbs)
WC Sand	38.0	1116	2.66	6.726	
1" x #4 (#57)	39.0	1159	2.69	6.903	
1-1/2" x 3/4" (#4)	23.0	683	2.69	4.071	
WATER (gal) 34.8		290	1.00	4.651	
FLY ASH (sks)					
CEMENT (sks) 7.2	100.0	675	3.15	3.434	
ESTIMATED ENTRAINED AIR	4.5			1.215	
TOTALS		3924		27.00	

Calculated Wet Weight (pcf): 145.3

DESIGN FOR ONE CUBIC METER OF CONCRETE (SATURATED AND SURFACE DRY)

ABSOLUTE VOLUME OF AGGREGATE IN ONE CUBIC METER: 0.66

SPECIFIC GRAVITY OF COMBINED AGGREGATES: 2.68

WEIGHT OF AGGREGATES IN ONE CUBIC METER BATCH, Kg: 1753.3

MATERIAL	PERCENT	BATCH (kg)	SP. GR.	ABSOLUTE VOLUME (m^3)	SACK WEIGHTS (kg)
WC Sand	38.0	661.64	2.66	0.2493	
25mm x 4.75mm	39.0	686.71	2.69	0.2558	
37.5mm x 19mm	23.0	404.98	2.69	0.1509	
WATER (lit) 172.0		172.02	1.00	0.1720	
FLY ASH (kg)					
CEMENT (kg) 400.05	100.0	400.05	3.15	0.1270	
ESTIMATED ENTRAINED AIR	4.5			0.0450	
TOTALS		2325		1.000	

Calculated Wet Weight (kg/m^3): 2325.4

Light Weight Agg.: _____ C.F. Loose Vo. At: _____ pcf.

Prepared By: _____
John Inlow, QA Manager

Approved
DFC 5/13/10

I.2 Concrete Deck containing Slag – Mix Design

FOLSOM READY MIX

Concrete Mix Design Submittal

Date : 02/05/2021 **No. 21–000069 Version 3**
Mix Code : **C78A9S1** Description : **7000 PSI @ 28 DAYS**

Customer	MYERS & SONS CONSTRUCTION, LP
Contact	BIANCA MEDINA
Office Phone	916-283-9950
Project Name	#111234 AB219 CDOT 03-0H4604
Project Contact	BROOKE
Usage/ Placement	BRIDGE DECK WITH FIBERS

	Design	Tolerance
Air Content	1.5	
Slump	5	+/-1
Design Strength	7000	psi
Unit Weight	152.5	lb/ft3
W/C Ratio	0.38	

Admixtures may be adjusted to meet field conditions.

Please consult pump company prior to placement.

The following mix additions, if required, are to be requested by customer when placing order

SikaFiber Novomesh CAL-51 fibers with a 3 to 1 macro to micro blend added at 4 lbs per yard

Material Type	Description	Source Supplier	<ASTM>	Design Quantity	Specific Gravity	Volume (ft3)
Coarse Aggregate	1" ROCK	Western Aggregate-Marysville, CA	ASTM C33	1828 lb	2.77	10.58
Fine Aggregate	SAND	Teichert Materials-Marysville, CA	ASTM C33	1270 lb	2.68	7.59
Cement	CEMENT	Lehigh Southwest-Type II-V	ASTM C150	368 lb	3.15	1.87
Slag	SLAG	Cemex Victorville-Cemex Rizhao	ASTM C989	368 lb	2.92	2.02
Water	WATER	Municipal-Municipal	ASTM 1602	33.9 gal	1.00	4.53
Admixture	MASTERLIFE SRA	BASF Corporation-BASF USA	ASTM C494	96 lq oz	-	-
Admixture	MASTERPOZZOLITH 322	BASF Corporation-BASF USA	ASTM C494	44 lq oz	-	-
Admixture	MASTERPOLYHEED	BASF Corporation-BASF USA	ASTM C494	40 lq oz	-	-
			Air Content	**1.50 %**	**–**	**0.41**
			Yield	**4117 lb**	**–**	**27.00**

CONDITIONALLY
AUTHORIZED
Pursuant to Section 5-1.23
of the Standard Specifications

State of California
DEPARTMENT OF TRANSPORTATION
Division of Engineering Services
Offices of Structure Construction
Signed Joseph R. Harline
Structure Representative
Date 10 February 2021

PREQUALIFY UNDER 90-1.01D(5)(b).

SUBMIT SHRINKAGE TEST DATA PER SECTION 90-1.02A.

FOLSOM READY MIX

Concrete Mix Design Submittal

Date : 02/05/2021 **No. 21–000069** **Version 3**

Mix Code : **C78A9S1** Description : **7000 PSI @ 28 DAYS**

Sieve Size	1ROCK % Passing	SAND % Passing	Combined % Passing
2"	100.0	100.0	100.0
1-1/2"	100.0	100.0	100.0
1"	99.0	100.0	99.4
3/4"	86.0	100.0	91.7
1/2"	42.0	100.0	65.8
3/8"	17.0	100.0	51.0
No. 4	2.0	96.0	40.5
No. 8	1.0	81.0	33.8
No. 16		67.0	27.5
No. 30		47.0	19.3
No. 50		17.0	7.0
No. 100		5.0	2.0
No. 200		2.1	0.9

	1ROCK	SAND	Combined
DRUW lb/ft3			
% Agg	**59.0**	**41.0**	
% Coarse Agg	**100.0**		
% Fine Agg		**100.0**	
SG	**2.77**	**2.68**	
FM	**8.53**	**3.85**	**6.61**

Prepared By :

Jon Jackson QC Manager

4037

4038 **I.3 Concrete Deck containing Fly Ash – Mix Design**

SYAR CONCRETE LLC
P.O. BOX 2700 NAPA, CA 94558
(877) SYARMIX

Concrete Mix Design Submittal

DATE: 04/09/2020 **No. 042013 Version 1**

Mix Design Code: AE075CC5WA

Customer	COD - FLATIRON WEST INC	Design Strength	5000 PSI @ 42 DAYS	
		W/CM Ratio	0.38	
Project Name	CT 03-0H3414 REPLACE BRIDGE - POLLOCK P	Slump	5.00"	+/- 1"
		Air Content	6.00	+/- 1.5%
Usage/Placement	BRIDGE DECK	Unit Weight	142.15	lb/ft3

SYAR CONCRETE LLC has no authority regarding the appropriate application of the mix design. It is the responsibility of the owner's representative and or contractor to insure that this mix design is appropriate for the intended use and environmental conditions for the intended application of the mix. This concrete mix design will meet design strengths when tested in strict compliance with current ASTM Standard and evaluated in accordance with ACI standard practices. Approval of the mix design carries the inclusion of SYAR CONCRETE LLC on the distribution list for all concrete test results.Cementitious content is expressed as a minimum and SYAR CONCRETE LLC reserves the right to increase the total cementitious content. Admixtures are dosed as per manufactures recommendations and may be adjusted to maintain mix design properties. Aggregate weights may be adjusted to maintain proper yield and to comply with grading specifications.
It is the responsibility of the contractor to verify pumpability with the pumping contractor.

Material Type	Description	Design Quantity (SSD)	Specific Gravity	Volume (ft3)
Cement	CEMENT TYPE II / V MODIFIED	562.5 lb	3.15	2.86
Fly Ash	FLY ASH / CLASS F	188 lb	2.30	1.31
Coarse Aggregate	ASTM C33 #57 CONCRETE AGGREGATE	1650 lb	2.73	9.69
Fine Aggregate	ASTM C33 CONCRETE SAND	1150 lb	2.67	6.91
Water	WATER	34.5 gal	1.00	4.61
Admixture	POLYHEED 1025 - TYPE A & F WATER REDUCER	50 lq oz	-	-
Admixture	AE 200 / AIR ENTRAINING ADMIXTURE	2 lq oz	-	-
Admixture	MASTERLIFE SRA 35 SHRINKAGE REDUCING ADM	128 lq oz	-	-
	Air Content	**6.00 %**	**–**	**1.62**
	Yield	**3838 lb**	**–**	**27.00**

Contingent on acceptable prequalification and shrinkage test results.

AUTHORIZED
Pursuant to Section 5-1.23
of the Standard Specifications

State of California
DEPARTMENT OF TRANSPORTATION
Division of Engineering Services
Offices of Structure Construction

Signed Joseph R Harline
Structure Representative

Date 13 APRIL 2020

NOTES
BASF MASTERFIBER F70 (MICRO) FIBERS TO BE ADDED @ 1.0 LB/CYD
BASF MASTERFIBER MACMATRIX (MACRO) FIBERS TO BE ADDED @ 3.0 LBS/CYD

Prepared By :

Connor Clay Technical Services Rep.

4039

SYAR CONCRETE LLC
P.O. BOX 2700 NAPA, CA 94558
(877) SYARMIX

Concrete Mix Design Combined Aggregate Grading

Date : 04/09/2020 Mix Code : **AE075CC5WA** **No. 042013** **Version1**

Sieve Size	Coarse 011110 % Passing	Fine 041200 % Passing	Combined % Passing	Caltrans 1" Combined Min % Passing	Caltrans 1" Combined Max % Passing
1 1/2	100.0	100.0	100.0	100.0	100.0
1	100.0	100.0	100.0	90.0	100.0
3/4	85.0	100.0	91.2	55.0	100.0
1/2	50.0	100.0	70.5	50.0	88.0
3/8	27.0	100.0	57.0	45.0	75.0
No. 4	2.0	100.0	42.3	35.0	60.0
No. 8	1.0	84.0	35.1	27.0	45.0
No. 16		69.0	28.3	20.0	35.0
No. 30		45.0	18.5	12.0	25.0
No. 50		17.0	7.0	5.0	15.0
No. 100		4.0	1.6	1.0	8.0
No. 200		1.1	0.5	0.0	4.0

	Coarse 011110	Fine 041200	Combined
DRUW lb/ft3			
% Agg	**58.9**	**41.1**	
% Coarse Agg	**100.0**		
% Fine Agg		**100.0**	
SG	**2.73**	**2.67**	
FM	**7.35**	**2.81**	**5.49**

4040

4041